ANALYSIS OF A REACTION-DIFFUSION
SYSTEM WITH LOCAL AND NONLOCAL DIFFUSION TERMS

by

Richard D. Tatum
A Dissertation
Submitted to the
Graduate Faculty
of
George Mason University
In Partial fulfillment of
The Requirements for the Degree
of
Doctor of Philosophy
Computational and Data Sciences

Committee:

_____	Dr. Evelyn Sander, Dissertation Director
_____	Dr. Thomas Wanner, Committee Member
_____	Dr. David F. Walnut, Committee Member
_____	Dr. John Wallin, Committee Member
_____	Dr. Dimitrios Papaconstantopoulos, Department Chair
_____	Richard Diecchio, Associate Dean for Graduate Programs, College of Science
_____	Dr. Vikas Chandhoke, Dean, College of Science

Date: _____ Summer Semester 2010
George Mason University
Fairfax, VA

Analysis of a Reaction-diffusion System with Local and Nonlocal Diffusion Terms

A dissertation submitted in partial fulfillment of the requirements for the degree of Doctor of Philosophy at George Mason University

By

Richard D. Tatum
Master of Applied Mathematical Science
University of Georgia, 1999
Bachelor of Arts, Mathematics
Albany State University, 1996

Director: Dr. Evelyn Sander, Professor
Department of Mathematical Sciences

Summer Semester 2010
George Mason University
Fairfax, VA

Dedication

I dedicate this dissertation to my wife and son, Jamie and Christian. Their love means everything to me.

Acknowledgments

Let me first acknowledge God for being with me and for blessing me with the tenacity and abilities necessary to complete this thesis. I thank Dr. Sander as she has guided me and instructed me in the ways of mathematical research. Furthermore, she also demonstrated great patience by reading the most technical portions of this thesis for what seemed to be an uncountable number of times. I also want to thank her for her style of mathematical prose, which I have tried to adopt and emulate. Let me also thank Dr. Wanner, Dr. Walnut and Dr. Wallin who gave their time and insightful comments that have helped me to produce a better thesis.

I also want to thank my parents, Chester and Louise Tatum. I especially want to thank my mother for teaching me her love of numbers. I owe much to my wife and son, Jamie and Christian, for their patience, encouragement, and their gifts of silence when required. I also want to thank Debbie and Kenny Truitt, as well as Mike Lane who are my sister, brother-in-law and father-in-law, respectively. The offered many kind words of encouragement that always seemed appropriately timed. Let me also give many thanks to Janet Lane, my mother-in-law, as well as Debbie and Kenny for watching Christian during the critical weeks prior to my pre-defense.

Table of Contents

List of Tables

List of Figures

Abstract

ANALYSIS OF A REACTION-DIFFUSION SYSTEM WITH LOCAL AND NONLOCAL DIFFUSION TERMS

Richard D. Tatum, PhD

George Mason University, 2010

Dissertation Director: Dr. Evelyn Sander

Reaction-diffusion describes the process in which multiple participating chemicals or agents react with each other, while simultaneously diffusing or spreading through a liquid or gaseous medium. Typically, these processes are studied for their ability to produce nontrivial patterns that evolve over time. These patterns, often referred to as Turing structures or Turing patterns, are diffusion driven. In the presence of diffusion, the Turing patterns are observable, but are not present in the absence of diffusion. It is important for reaction-diffusion models to replicate the behavior that is experimentally observed. That is to say that the models must be able to produce solutions with traits, such as pattern type, that are similar to experimentally observed traits. Mathematically, we seek to explain certain aspects of the models such as pattern selection in the hope of broadening our understanding of the underlying process for which the model represents.

I analyze a mixed reaction-diffusion system containing an instability that results in nontrivial Turing structures. This system uses a homotopy parameter β to vary the effect of both local ($\beta = 1$) and nonlocal ($\beta = 0$) diffusion. Furthermore, I consider $\epsilon-$scaled kernels J such that $\epsilon^{\theta}J$ is $\epsilon-$independent for $\theta \in \mathbb{R}$. For $\theta < 1$ and $0 < \beta \leq 1$, I show that the generated Turing patterns are explained using only finite number of eigenfunctions

corresponding to the most unstable eigenvalues of the linearization. However, for $\theta = 1$ and $\beta < 1$, I show how the nonlinearity is no longer bounded above by an $\epsilon-$dependent bound that ensures the smallness of the nonlinearity as in the $\theta < 1$ case. The lack of this critical bound allows for a greater influence of the nonlinearity. Consequently, the unstable eigenfunctions of the linearization do not describe the solutions as well as they do for the solutions of the $\theta < 1$ case. The numerics provided show little agreement between the solutions and their nonlinearized counterparts as a consequence of greater influence of the nonlinearity.

The thesis is concluded with numerical pattern studies of the local and nonlocal reaction-diffusion systems. The patterns are studied as the values of various parameters of the reaction-diffusion system are changed. These numerical experiments reveal typical patterns such as stripes and spots, as well as irregular snakelike patterns. Furthermore, solutions for the local system subject to homogeneous Neumann boundary conditions are compared to the solutions of the local system subject to periodic boundary conditions. For some cases, the solutions for both systems are quite similar.

Chapter 1: Introduction

Reaction-diffusion describes the process in which multiple participating chemicals or agents react with each other, while simultaneously diffusing or spreading through a liquid or gaseous medium. Typically, these processes are studied for their ability to produce nontrivial patterns that evolve over time. These patterns, often referred to as Turing structures or Turing patterns, are diffusion driven. In the presence of diffusion, the Turing patterns are observable, but are not present in the absence of diffusion. It is important for reaction-diffusion models to replicate the behavior that is experimentally observed. That is to say that the models must be able to produce solutions with traits, such as pattern type, that are similar to experimentally observed traits. Mathematically, we seek to explain certain aspects of the models such as pattern selection in the hope of broadening our understanding of the underlying process for which the model represents.

Therefore, the overall emphasis of this thesis is to study reaction-diffusion models, with a particular emphasis upon the pattern formation process. A reaction-diffusion model is a system of mathematical equations that describe how the concentration of one or more substances are affected by reaction and diffusion processes. Specifically, the types of reaction-diffusion models that are considered by this research are reaction-diffusion models subject to periodic boundary conditions and homogeneous Neumann boundary conditions. Subject to periodic boundary conditions, the mixed local and nonlocal equations are considered of the more general form

$$\begin{aligned} u_t &= (\beta\Delta u + (1-\beta)(J * u - \hat{J}_0)) + \gamma f(u,v), \\ v_t &= d(\beta\Delta v + (1-\beta)(J * v - \hat{J}_0)) + \gamma g(u,v), \end{aligned} \tag{1.1}$$

where$\Omega \subset \mathbb{R}^n$ for $n \in \{1,2,3\}$ is rectangular, $J * u(x,t) = \int_\Omega J(x-y)u(y,t)dy$, $\hat{J}_0 = \int_\Omega J(x)dx$, and $J : \mathbb{R}^n \to \mathbb{R}$ is periodic with respect toΩ . Subject to homogeneous Neumann boundary conditions, the local equations are considered of the form

$$u_t = \Delta u + \gamma f(u,v),$$

$$v_t = d\Delta v + \gamma g(u,v). \tag{1.2}$$

The next section provides motivation for both models, beginning with a derivation of local diffusion.

1.1 Local, nonlocal and mixed reaction-diffusion models

To derive the local reaction-diffusion system, perhaps the simplest explanation involves diffusion in the classical sense. This derivation can be found in [45, Volume 1] and is given for three spatial dimensions. Furthermore, only two participating species are assumed whose concentrations are given by the vector $U = (u,v)^T \in \mathbb{R}^2$. The idea is to write a mass conservation equation that describes the reaction-diffusion process. Suppose that the reaction-diffusion process is occurring in a volume V that is enclosed by an arbitrary surface S. The total amount of material in V is given as

$$\int_V U \; dv. \tag{1.3}$$

The assumption is made such that there are only two processes that affect the concentration U. When material moves across the boundary S, there is a change in U. Denote the flux of material across S as P_{flux}. For classical diffusion,

$$P_{flux} = -D\nabla U, \tag{1.4}$$

where D is a constant diagonal matrix whose entries represent the coefficients of diffusion for each species. The minus sign indicates that the diffusion transports matter from high to low levels of concentration. By integrating over the surface S, we get that the total flow of material across S is

$$-\int_S P_{flux} \cdot ds = D \int_S \nabla U \cdot ds. \tag{1.5}$$

The remaining source of change in the concentration U comes from the creation of new material from the reactions. If we denote this as $F = (f(U,t), g(U,t))$, the total contribution of material from the reaction is

$$\int_V F dv. \tag{1.6}$$

The observation that the rate of change of the total concentration must equal to the rate of flow of material across S plus the material created in V gives the general mass conservation equation

$$\frac{\partial}{\partial t} \int_V U dv = D \int_S \nabla U \cdot ds + \int_V F dv. \tag{1.7}$$

By the Divergence Theorem, we have

$$D \int_S \nabla U ds = D \int_V \Delta U dv. \tag{1.8}$$

Combining Equations (1.7) with (1.8) gives

$$\int_V (U_t - D\Delta U - F) dv = 0.$$

Since V is arbitrary, we have the nonlocal reaction diffusion system as

$$U_t = D\Delta U + F. \tag{1.9}$$

Local existence and uniqueness results for reaction-diffusion equations with homogeneous Neumann boundary conditions can be found in works by Pazy [47] and Friedman [20]. More recent global existence results can be attributed to Kouachi [36]. For existence results for the local reaction-diffusion system subject to periodic boundary conditions, again see Pazy [47].

Reaction-diffusion processes that are modeled with equations of the form of (1.9) include the light sensitive Belousov-Zhabotinsky (BZ) reaction, the chlorite-iodide-malonic acid (CIMA) reaction, and the (chlorine dioxide-iodine-malonic acid) CDIMA reaction. In the typical BZ reaction, an organic substrate such as malonic acid in the presence of a redox-active catalyst like cerrium ion or ferroin is oxidized and undergoes bromination in sulphuric acid. Field and Noyes devised the well-known Oregonator reaction-diffusion equation for the BZ reaction [18]. In the both the CIMA and CDIMA reactions, chlorite oxidizes iodide while malonic acid undergoes iodination. However, one of the main differences of the two reactions is that the CDIMA reaction is photosensitive and can be regulated by light [43]. This trait possibly gives the CDIMA reaction an advantage over the CIMA reaction in that stationary Turing patterns can be controlled experimentally [51]. Models for the CIMA and closely related CDIMA reaction have also been developed and analyzed [37, 38]. Predator-prey problems [7, 22], the spread of infectious diseases [8, 63] and mammalian pattern formation [45, Volumes II, pg. 141-252], are examples of some biological problems for which reaction-diffusion models are used. More examples can be found in [45, Volumes I and II].

The local models capture the short range effects of a physical process such as diffusion. In doing so, local models only approximate longer range effects. To model the longer range effects, a better choice than the PDE formulation involves the use of integro-differential equations since they sum up all activity in the spatial domain. We now discuss nonlocal

models and their relationship to local models in the context of the diffusion of a single species over one spatial dimension. Hutt [28] suggests the more general evolution equation

$$\hat{T}u(x,t) = f[u(x,t)] + \int_{\Omega} J(x-y) \cdot h_1[u(y,t-\tau(x-y))]dy$$

$$+ \int_{\Omega} K(x-y)h_2 \cdot [u(y,t-\tau(x-y))]dy, \tag{1.10}$$

with the scalar field variable $u(x,t)$ and a large spatial domain$\Omega \subset \mathbb{R}$. The temporal operator $\hat{T} = \hat{T}(\partial/\partial t)$ represents the temporal linear dynamics of an uncoupled element at the spatial location x. The term $f[u(x,t)]$ represents the nonlinear driving term. The kernels $J(x-y)$ and $K(x-y)$ represent two different types of coupling functions between elements at spatial locations x and y. As an example, Hutt points to models of neural nets neurons that have an excitatory net and inhibitory net with $J(x-y) > 0$ and $K(x-y) < 0$, respectively. The functionals $h_1[u]$ and $h_2[u]$ allow for various nonlinear interaction types f the corresponding spatial interactions. The propagation delay $\tau(x-y) = |x-y|/c$ with the propagation speed c account for the finite time it takes for a signal to propagate from one spatial location x to another location y. For our purposes, the standard scalar nonlocal reaction-diffusion system is obtained by choosing $\hat{T} = \partial/\partial t$, $h_1[u] = d_1 u$, $h_2[u] = 0$ and $\tau = 0$. Here, d_1 represents the diffusivity of the species u. Thus, the nonlocal system is given as

$$u_t = f[u(x,t)] + d_1 \int_{\Omega} J(x-y)u(x,t)dy. \tag{1.11}$$

However, the nonlocal reaction-diffusion system is a generalization of the local reaction-diffusion system in the following sense. Hutt noted the following identity that shows how integro-differential equations generalize PDEs [29]

$$\int_{\Omega} J(x-y)S[u(y)]dy = \sum_{n=0}^{\infty} (-1)^n J_n \frac{\partial^n S[u(x)]}{\partial x^n}. \tag{1.12}$$

For this identity, S is a nonlinear functional and $J_n = \int_\Omega J(\eta)\eta^n/n!d\eta$ are the moments of the kernel J. The expansion includes spatial interactions whose order n represents the spatial interaction range. For kernels whose odd moments are zero and that exhibit short-ranged spatial interactions with $J_n \to 0$, a good approximation of the convolution term is achieved by truncating identity 1.12 so that $n \leq 2$. In this case, we recover the local system.

Depending upon the natural process that is being considered, it is appropriate to consider models that include both local and nonlocal diffusion terms. As an example, consider the BZ reaction. The earlier Oregonator model did not include any nonlocal terms. Using a nonlocal feedback illuminating source, Hildebrand, Skødt an Showalter [27] experimentally showed the existence of novel spatiotemporal patterns in the BZ reaction. To account for the nonlocal effects, they added nonlocal operators to the original Oregonator model. We therefore consider the more general model, given as System 1.1.

1.2 Research Focus

This thesis contains the results of three primary research goals. Broadly stated, they include a description of the behavior of the solutions of System 1.1, a study of the patterns of System 1.1 and a study of the similarity of solutions of the local System 1.1 ($\beta = 0$) to the solutions of System 1.2. The remainder of this section provides more context for these tasks, as well as descriptions of the contributions made towards these objectives.

1.2.1 Early Pattern Selection

In [55], Sander and Wanner analyzed the behavior of solutions of the local reaction-diffusion system subject to homogeneous Neumann boundary conditions. Scale time as $\tilde{t} = t/\gamma$, let $\epsilon = 1/\gamma$, set the time variable $\tilde{t}$ back to t, and consider the scaled local system given by

$$\begin{aligned} u_t &= \epsilon\Delta u + f(u,v), \\ v_t &= d\epsilon\Delta v + g(u,v). \end{aligned} \tag{1.13}$$

Using this system, Sander and Wanner provided a result that described the early pattern formation process in the following way. Consider solutions that have initial conditions that are near to a homogeneous equilibrium. Using the theory developed in [40, 41], they showed that with a high probability and within a certain distance from the homogeneous equilibrium, $(\bar{u}_0, \bar{v}_0)$, nonlinear patterns that form are similar to patterns of corresponding solutions in a dominating subspace. This dominating subspace consists of eigenfunctions corresponding to a finite range of the most unstable eigenvalues of the linearization of the local system at the homogeneous equilibrium. The use of "most nonlinear patterns" is made precise by using the approach used by Maier-Paape and Wanner [40]. In a small neighborhood of the homogeneous equilibrium, there exists a finite-dimensional inertial manifold of the local reaction-diffusion system which exponentially attracts all nearby orbits. The orbit can be projected onto this finite-dimensional manifold, where the standard probability measure is induced by the finite-dimensional Lebesgue measure. Sander and Wanner were able to show that the linear description of the nonlinear patterns could be extended to regions of the phase space that were far away from the homogeneous equilibrium.

A description of the major analytical result is now given. As with the local case, we scale System 1.1 and consider

$$\begin{aligned} u_t &= \epsilon(\beta\Delta u + (1-\beta)(J * u - \hat{J}_0)) + f(u,v), \\ v_t &= d\epsilon(\beta\Delta v + (1-\beta)(J * v - \hat{J}_0)) + g(u,v), \end{aligned} \tag{1.14}$$

subject to periodic boundary conditions. On certain regions surrounding the homogeneous equilibrium, the size of the nonlinearity is small far from the homogeneous equilibrium. Let (u, v) and (u_{lin}, v_{lin}) be the solutions to the system and its linearized counterpart, respectively. For solutions that begin within an arbitrarily small $\epsilon-$dependent distance r_ϵ

to $(\bar{u}_0, \bar{v}_0)$ and exit the neighborhood at a distance of $R_\epsilon > r_\epsilon$, the relative distance

$$\frac{||(u(t), v(t)) - (\bar{u}_0, \bar{v}_0) - (u_{lin}(t), v_{lin}(t))||_{**}}{||(u_{lin}(t), v_{lin}(t))||_{**}},$$

is proportional to an $\epsilon-$dependent threshold. The $||\cdot||_{**}$-norm is equivalent to the standard Sobolev norm. For a description of the norm, see Section 4.3. In particular, r_ϵ and the relative distance decrease to zero as $\epsilon \to 0$, whereas R_ϵ grows as $\epsilon \to 0$. This behavior is called **almost linear behavior**.

Adapting the same techniques as in [40, 41, 55], the major result shows that the mixed system given by System 1.14 possesses almost linear behavior for $0 < \beta \leq 1$ for the following assumptions. We assume that $\epsilon^\theta J$ is $\epsilon-$independent and smoothly periodic , where $\theta \in \mathbb{R}$. We also assume that the eigenvalues of $J_c - \hat{J}_0$ are less than or equal to zero. Furthermore, we assume that J has an even periodic extension, which ensures that $J_c - \hat{J}_0$ is self-adjoint. For multivariate functions, we define even in a natural way. See Section 4.1. With a self-adjoint operator $J_c - \hat{J}_0$ and $\theta < 1$, we extend the almost linear results in [55] to the more general System 1.14. The major analytical result is given by the following theorem. The full version of this theorem appears in Section 4.3 as Theorems 4.3.1 and 4.3.2. The combination of both theorems leads to a complete proof of Theorem 1.2.1.

Theorem 1.2.1. *Let $\epsilon <\epsilon_0$. Consider System 1.14, where $0 < \beta \leq 1$. Assume that the domain Ω is a rectangular domain of $\mathbb{R}^n$, where $n = \{1, 2, 3\}$. The kernel function $\epsilon^\theta J$ is $\epsilon-$independent with $\theta < 1$, $\epsilon J \in C^1(\bar{\Omega})$ is smoothly periodic with respect Ω, the periodic extension of J is even and the eigenvalues of $J_0 - \hat{J}_c$ are nonnegative. Suppose that the nonlinearities f and g are sufficiently smooth and that the homogeneous equilibrium $(\bar{u}_0, \bar{v}_0)$ is unstable for ϵ_0. Finally, let (u, v) and (u_{lin}, v_{lin}) be the solutions to System 1.14 and its linear approximation at the homogeneous equilibrium, respectively. The solution (u, v) possesses almost linear behavior.*

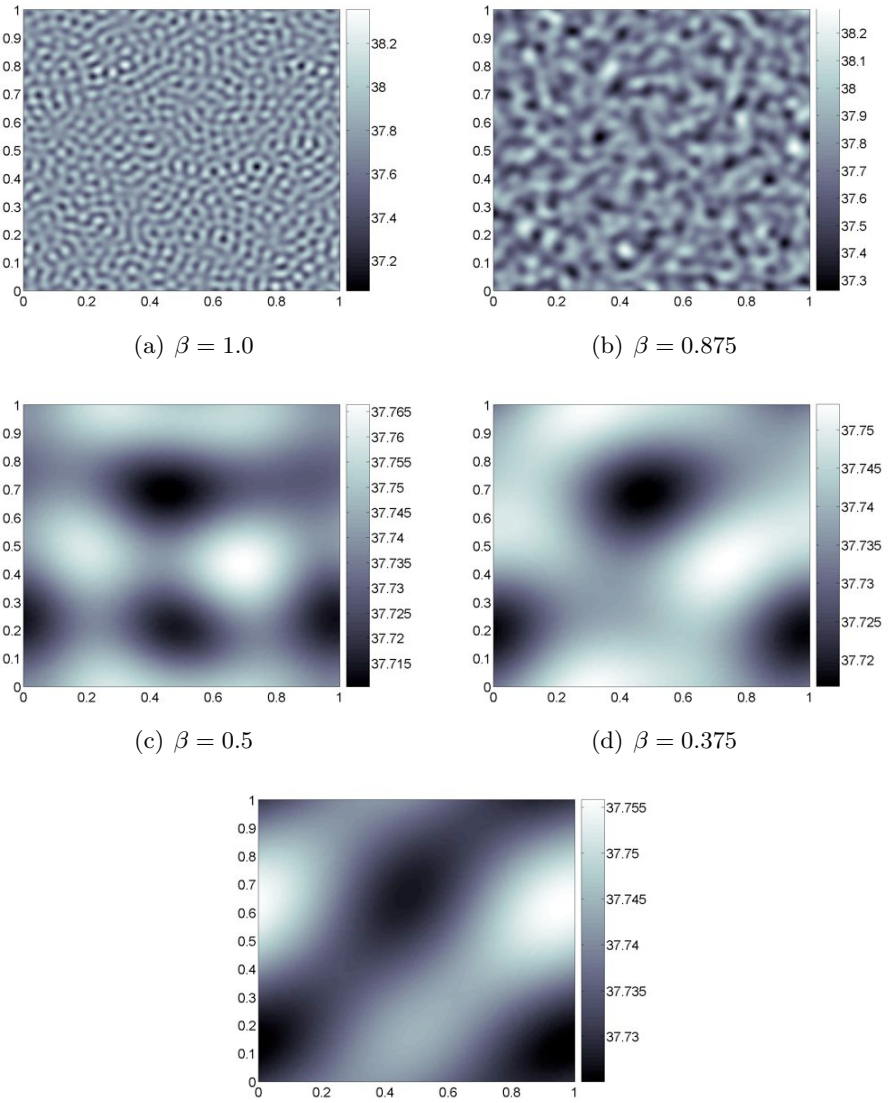

(a) $\beta = 1.0$

(b) $\beta = 0.875$

(c) $\beta = 0.5$

(d) $\beta = 0.375$

(e) $\beta = 0.00$

Figure 1.1: Examples of the patterns produced using various β values and $\epsilon = 1 \times 10^{-5}$ over the domain $[0, 1]^2$. These patterns occur when the $time = 4 \times 10^{-4}$. As β increases, the patterns become much more pronounced and well-defined.

This theorem is the first result that generalizes the almost linear behavior results obtained in [55] for the nonlocal reaction-diffusion systems. Hartley [24] numerically observed a similar effect described by Theorem 1.2.1 for the phase field model with a similar type of homotopy between purely local and purely nonlocal terms. For $\theta = 1$ and and $0 < \beta < 1$, the same techniques for $\theta < 1$ are applied. However, we show that the nonlinearity is no longer ensured to be small for large distances away from the homogeneous equilibrium. This is critical for almost linear behavior. If the nonlinearity is not small in norm, then it can greatly influence the initial pattern selection. Consider the distance for which the solutions and the solutions of the linearized system separate. We show that upon separation, the distance from the solution to the homogeneous equilibrium is bounded above by an $\epsilon-$independent constant. For large values of the standard deviation of the Gaussian kernel, which is denoted as σ, the numerics indicate that the almost linear results are diminished for small β values due to an increase of the influence of the nonlinearity. It appears that nonlinear effects dominate initial pattern selection in this case. See Figure 1.2. The distance of the solution to the homogeneous equilibrium was measured when an $\epsilon-$dependent threshold of $.25\epsilon^{1/4}$ was reached. Upon reaching the threshold for fixed ϵ, there is a significant increase in the distance from the solution to the homogeneous equilibrium as $\beta \to 1$. However, as $\beta \to 0$, there is very little agreement between the solutions and their linearized counterparts, suggesting that the nonlinearity of the system dominates the solutions for these β values. These results are also further supported in Figure 4.4. For the case of $\theta > 1$, we show that the homogeneous equilibrium becomes stable for arbitrarily small ϵ.

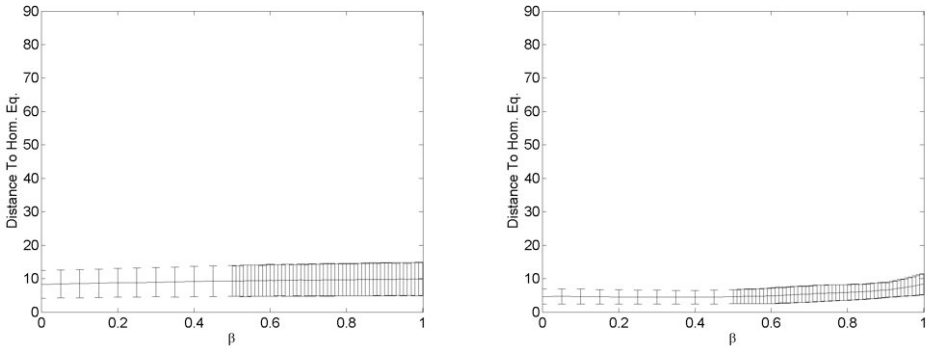

(a) $\epsilon = .01$ (b) $\epsilon = .001$

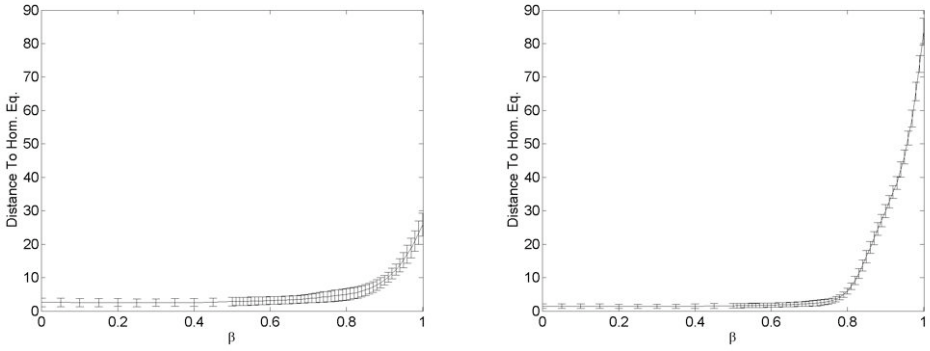

(c) $\epsilon = .0001$ (d) $\epsilon = .00001$

Figure 1.2: A plot of the distance between the nonlinear solution and the homogeneous equilibrium when the linear and nonlinear solutions deviate from each other. For these results, $\theta = 1$. As $\beta \to 0$, the measured values are smaller, meaning that the behavior of solutions is determined by nonlinear effects. This is more pronounced for smaller ϵ values. The term "deviation" means that the distance between the linear and nonlinear solutions relative to the norm of the linear solution reached the ϵ-dependent threshold of $.25\epsilon^{1/4}$. For each β and ϵ value depicted 20 simulations were performed. Shown here are the mean and standard deviation of these values. For each simulation, random initial conditions were used that were within a distance $\epsilon^{1/2}$ of the homogeneous equilibrium. Distances are measured in the $||\cdot||_{**}$ norm, as defined in Section 4.3. To capture the rapid change in the graph, a refined grid is used near $\beta = 1$.

1.2.2 Pattern Studies

Turing [59] first suggested a mechanism in which chemicals through the process of diffusion could form highly developed patterns. These patterns are referred to as Turing structures or Turing patterns. Since Turing first posed his remarkable theory, several well-known reaction-diffusion systems have been experimentally shown to produce these Turing patterns. Patterns such as spots and stripes have been experimentally observed in the CIMA reaction in a gel reactor [9, 46] and the CDIMA reaction [23]. For most conditions, the BZ reaction exhibits spirals, traveling waves and antiwaves [17]. More recently the BZ reaction dispersed in a water-in-oil microemulsion system [42, 60] has been shown to produce stripes and spots as well. Corresponding models for the CIMA reaction [32, 38], CDIMA reaction [62] and BZ reaction [33] have all been shown to produce both spots and stripes. Other types of interesting patterns, such as antisymmetric waves have been observed in he Brusselator model [49] and the Gray-Scott model [50]. The Brusselator model is a reaction-diffusion system that is closely related to thermodynamically closed systems and the Gray-Scott model is an autocatalytic model of glycolysis. These types of patterns have been explained as the result of the interaction between stationary periodic and propagating wavelike patterns [49]. This type of interaction has been described in detail [39] and conditions were given which describe when solutions can become spatiotemporally chaotic.

For a range of γ and d values, solutions of System 1.1 are numerically generated and their patterns are studied. Numerically, I demonstrate that if the positive portion of the dispersion relations for the local and nonlocal systems are close, then the solutions for the local, nonlocal and mixed systems will all have similar solutions. As this motivates the idea that the same patterns for the local case are also available for $0 \leq \beta < 1$, the analysis is only concerned with the local system. The results presented in this thesis show that for a fixed γ, the patterns become less complex as d is increased. On the other hand, for fixed d, the patterns increase in complexity as γ is increased.

The final objective is to numerically investigate how solutions of System 1.1 with $\beta = 1$ and System 1.2 compare. To accomplish this, the γ and d values from the same set of γ and

d values used for the prior task are fixed for System 1.2. The corresponding γ and d values for the local periodic system are determined so that positive dispersion relation for the Neumann system is very close to a subset of the dispersion relation of the periodic system. Section 5.4 contains more details on how the subset was chosen. For the 1d system, the results indicate that solutions are similar in appearance for both periodic and homogeneous Neumann systems. However, the patterns generated for the 2d case of both systems tend to bear little resemblance to each other.

1.3 Outline of thesis

A large portion of this thesis relies upon numerical calculations. These calculations involve numerically estimating solutions of large systems of ODEs. The background for the numerical methods used can be found in Chapter 2. The background containing the prior theoretical results for the almost linear behavior of System 1.13 is found in Chapter 3. Chapter 4 extends the results presented in Chapter 3 to System 1.14. A study of the patterns for System 1.1 is located in Chapter 5. Furthermore, Chapter 5 contains the results of comparing System 1.1, $\beta = 1$, with System 1.2. The final chapter is a summary of the results presented here and future work.

Chapter 2: Numerical Methods

As a significant portion of this research relies upon estimating the solutions of reaction-diffusion systems, an efficient and accurate method is required. For the purpose of this research, spectral methods are used. Many excellent references about the general theory of spectral methods exist. See [19, 21, 58]. This chapter provides the details for the spectral method known as the Galerkin method. The Galerkin method is applied to the mixed reaction-diffusion system with periodic boundary conditions and the local reaction-diffusion system subject to homogeneous Neumann boundary conditions. To understand the Galerkin method, consider the general reaction-diffusion system

$$u_t(x) = F(x), x \in \Omega \subset \mathbb{R}^n,$$

where $u \in L^2(\Omega)$ and $F : L^2(\Omega) \to L^2(\Omega)$ subject to a boundary condition. The F operator incorporates all of the diffusion and reaction terms. The most common types of methods used to estimate solutions for such a system are finite element methods, finite difference methods and spectral methods. Due to the increased accuracy of spectral methods compared to finite element and finite difference methods on rectangular domains, spectral methods are used for the this research [19]. One of the main reasons for the accuracy is that the spectral method uses a complete set of trial functions whose derivatives can be computed exactly.

A good numerical solution gives a small value for the residual R, given as

$$R = u_t - F.$$

Spectral methods begin with a complete family of trial functions that are globally smooth

and are denoted as $\{\chi_k\}_{k=0}^{\infty}$. The idea is then to express u as

$$u \approx \sum_{k=0}^{N} \hat{u}_k \chi_k,$$

and then determine the values for $\hat{u}_k$. The coefficients could be determined through direct substitution into the governing equation. However, spectral methods determine the coefficients so that

$$(R, \chi_k) = 0,$$

where $(\cdot, \cdot)$ represents the inner product of two functions that belong to $L^2(\Omega)$. The value of R depends upon the type test functions used. The Galerkin method uses basis functions $\{\phi_k\}_{k=0}^{\infty}$ that satisfy the boundary conditions as the test functions so that $\chi_k = \phi_k$ for $0 \leq k \leq N$. Since we are using the Galerkin method, computing (R, ϕ_k) so that the value is equal to zero will result in a solving a system of finite ODEs. To estimate the solutions, a semi-implicit numerical integration method is used. The information pertaining to semi-implicit methods presented in this thesis can be found in several texts. See [48]. These numerical methods are used later in Chapter 4 to compare solutions of the periodic system with their linearized counterparts. Furthermore, Chapter 5 uses these methods to explore more intermediate pattern formation that occurs in both System 1.1 and System 1.2.

This chapter is organized as follows. We begin with necessary background. This includes background information about numerical ODEs, followed by a description of the kernel functions used in this thesis. All of the numerical simulations for this research are done with respect to $\Omega = [0, 1]$ or $\Omega = [0, 1]^2$. Since the derivation is less tedious and more illuminating for the 1d case, all of the spectral derivations are given with respect to $\Omega = [0, 1]$. However, the methods for $\Omega = [0, 1]^2$ are given without derivation. This chapter concludes with proofs about the convergence, order of convergence, and a description of the stability of the numerical integration technique used to estimate the resulting system of ODEs.

2.1 Numerical Methods for ODEs

The most important aspect of a numerical method is its ability to converge to solutions. For convergent methods, the step size can be made arbitrarily small so that an approximate solution gets arbitrarily close to an actual solution. If the method does not converge for any step size, then the method is useless. In the case of a bounded solution, we want to know for which step sizes the numerical method produces unbounded approximations. In other words, we want to know if and which step sizes of the method produce a blow-up. This refers to the stability of the method. This section summarizes these concepts found in Iserles [31].

We begin by considering the system of ODEs given by

$$y' = f(t, y),\ t \geq t_0,\ y(t_0) = y_0, \tag{2.1}$$

where $f : [t_0, \infty) \times \mathbb{R}^d \to \mathbb{R}^d$ and $y_0 \in \mathbb{R}^d$. Let

$$y^{k+1} = \mathcal{F}^k(f, h, y_0, y_1, ..., y^k) \tag{2.2}$$

be an arbitrary time-stepping method for System 2.1. Denote that the $k-$th iterate of y as y^k. For the numerical method to be of value, it must converge and be numerically stable. Let the error be given as

$$e^k = y(t_k) - y^k, \tag{2.3}$$

where y^k again denotes the approximate solution and $y(t_k)$ represents the exact solution. For convergence, the error between the actual solution and the approximate solution must go to 0 over arbitrarily finer grids. This is indicated by the following convergence definition.

Definition 2.1.1 (Convergence of Numerical Method)**.** *Consider the time-stepping method given by Equation 2.2. For every system of ODEs of this form with a Lipschitz function f,*

a method is said to be convergent if for every $t^* > 0$, it is true that

$$\lim_{h \to 0+} \max_{k=0,1,\ldots \lfloor (t^*/h) \rfloor} \left|\left| e^k \right|\right| = 0,$$

where $h = t_{k+1} - t_k$ is the time step size.

How quickly the method converges to a solution is characterized by the order of the method. This concept is defined in the following definition.

Definition 2.1.2. *Consider System 2.1. A numerical method $\mathcal{F}$ as given in (2.2) is order p if*

$$y(t_{n+1}) - \mathcal{F}^k(f, h, y(t_0), y(t_1), ..., y(t_k)) = O(h^{p+1}).$$

If the underlying solution is stable and the method does not produce estimates whose values increase arbitrarily, then the method is considered stable. In other words, the method gives values that do not approach infinity when approximating bounded solutions.

Definition 2.1.3. *Consider the time-stepping method given by Equation 2.2 for System 2.1 where $f(t, y)$ is given by the constant matrix $A \in \mathbb{R}^d \times \mathbb{R}^d$. If $\lim_{t \to \infty} ||y(t)|| \to 0$, then the method is stable for step size h if $\lim_{k \to \infty} \left|\left| y^k \right|\right| \to 0$.*

Note that a convergent numerical method is not necessarily stable for any step size h. For example, consider the convergent explicit Euler method [31, p. 6] given as

$$y^{k+1} = y^k + hf(t_n, y^k), \tag{2.4}$$

and apply it to the scalar ODE given as

$$y' = -y, \; y(0) = 1. \tag{2.5}$$

Repeated application of Euler's method to System 2.5 gives the approximate solution as

$$y^k = (1-h)^k.$$

The actual solution given as $y = e^{-t} \to 0$ as $t \to \infty$. However, if $h > 2$, then $\left|y^k\right| \to \infty$ as $k \to \infty$. Thus, Euler's method is not stable for any h. Now consider the same problem, but with the trapezoidal method as given by

$$y^{k+1} = y^k + \frac{h}{2}(f(t_k, y^k) + f(t_{k+1}, y^{k+1})). \tag{2.6}$$

Repeated application of the convergent trapezoidal method [31, p. 8] to System 2.5 gives the approximate solution as

$$y^k = \left(\frac{1-\frac{h}{2}}{1+\frac{h}{2}}\right)^k.$$

Since we get bounded estimates when

$$\left(\frac{1-\frac{h}{2}}{1+\frac{h}{2}}\right)^k < 1,$$

we see that if for any $h > 0$, $y^k \to 0$ as $k \to \infty$. In other words, we are free to choose the step size h solely based upon accuracy considerations. Stability and accuracy both constrain the step size of a numerical method. Some methods, such as the trapezoidal method, allow for the step size to be adjusted for accuracy purposes to minimize the local error, without regard to step size. Implicit methods tend to accomplish this very well, but at a cost. As they are implicit, they require information about future approximations. This usually means employing a nonlinear solver to find the solutions of a set of algebraic equations. Explicit methods, such as the explicit Euler method, do not require such techniques. As the name implies, everything that is required to compute the next step is explicitly available.

However, as we demonstrated with Euler's method, explicit methods have costs in terms of step size constraints. Between implicit and explicit methods are methods known as semi-implicit or linear implicit methods. These methods, as their names imply, are not full implicit methods. Rather, they are hybrids of both implicit and explicit methods. The semi-implicit method applies an explicit method to the nonlinear portion of the right hand side of the ODE, while an implicit method is used for the linear piece. Methods of this type have been used in a variety of problems, such as the more recent work by Hartley and Wanner on the stochastic phase field model with nonlocal extensions [25]. To motivate the utility of semi-implicit methods a bit further, let us rewrite System 2.5 as

$$y' = -\frac{1}{2}y - \frac{1}{2}y,\ y(0) = 1,$$

and apply a semi-implicit method that uses the explicit Euler and trapezoidal methods. Thus,

$$y^{k+1} = y^k - \frac{h}{2}y^k + \frac{h}{2}\left(-\frac{1}{2}y^k - \frac{1}{2}y^{k+1}\right).$$

Collecting like terms, we have

$$y^{k+1} = \left(\frac{4-3h}{4+h}\right)y^k.$$

Repeated application of this method yields

$$y^{k+1} = \left(\frac{4-3h}{4+h}\right)^k.$$

Thus, if $h < 4$, we avoid any blow-ups in the approximations. Note that although the stability is not nearly as good as the trapezoidal method, we have achieved a greater range of stable h values when compared to Euler's method. Unfortunately, the simplicity of the System 2.5 obscures one important benefit of semi-implicit methods. We will avoid having

to use any nonlinear solvers since we use an explicit method for the nonlinear part of the right hand side of the ODE system.

For the general systems that we will encounter such as,

$$y' = f = f_1(t, y) + f_2(t, y), \tag{2.7}$$

again where f_1 is linear, we will use a hybrid of Euler's method and the midpoint method. Note that since f_1 is linear, the midpoint and trapezoid methods are equivalent. The midpoint method was chosen over the backward Euler method due to its higher order of accuracy. The backward Euler method has an order of accuracy of 1, while the midpoint method has an order of 2. However, we show that the semi-implicit method combining the midpoint and Euler methods remains as an order 1 method. Thus, the backward Euler method could have been used, as it attains the same order of convergence when combined with the explicit Euler method. Applying both the midpoint method and Euler's method to the linear and nonlinear functions yields

$$\begin{aligned} y^{k+1} - y^k &= \frac{h}{2}\left(f_1(y^k) + f_1(y^{k+1})\right) + hf_2(y^k), \\ y^{k+1} - \frac{h}{2}f_1(y^{k+1}) &= y^k + \frac{h}{2}f_1(y^k) + hf_2(y^k). \end{aligned} \tag{2.8}$$

One more important stability issue about numerically solving systems of ODEs involves the concept of *stiffness*. Consider the system given by

$$y_1' = -1000y_1,$$

$$y_2' = -y_2,$$

where $y_1(0) = 1$ and $_2(0) = 1$. Of course, the solution is given as $y_1 = e^{-1000t}$ and $y_2 = e^{-t}$. Contributions to the solution from y_1 will be very negligible compared to those of y_2, since

the associated mode of y_1, given as -1000, is several orders smaller than the mode of y_2. Furthermore, if an explicit scheme such as Euler's method is used, then the restriction on h for both y_1 and y_2 is $0 < h < 1/500$ and $0 < h < 2$, respectively. From this, we see that even though the contributions from y_1 are small, it provides the smallest constraint on the step size. As we have seen earlier, applying the trapezoidal method will not result in stability constraints upon h. If the numerical method being used requires a significant constraint in the step size, then we say that the system is *stiff*. From this example, we see that stiffness is more of a feature of the numerical method that is used and not really a problem of the underlying system.

2.2 Kernels

Specifically, we consider a kernel that is similar to the kernel used in [25]. Let the Gaussian kernel g_1 be defined as

$$g_1(x) = \frac{c}{\epsilon^\theta} \cdot exp\left(\frac{-x^2}{\sigma^2}\right) \cdot \eta(x), \tag{2.9}$$

where $c > 0$, $\theta \in \mathbb{R}$ and $\eta(x)$ is a smooth cutoff function. The function η is 1 on $B_{1/3}(0)$, but vanishes outside of $B_{1/2}(0)$. On the domain $\Omega = [0, 1]$, the kernel G_1 is given as

$$G_1(x) = g_1(x) + g_1(x + 1). \tag{2.10}$$

Since $g_1(x)$ and $g_1(x + 1)$ are smooth, then $G_1(x)$ is also smooth. The use of the smooth cutoff function allows us to smoothly extend $G_1(x)$ periodically outside of $\Omega = [0, 1]^2$. $J_1(x)$ is given as the smooth periodic extension of $G_1(x)$, denoted as

$$J_1(x) = G_{1,per}(x). \tag{2.11}$$

The 2d kernel is defined analogously. For this case, we begin with the 2d Gaussian function given as

$$g_2(x,y) = \frac{c}{\epsilon^\theta} \cdot exp\left(\frac{-x^2-y^2}{\sigma^2}\right) \cdot \eta(x,y), \tag{2.12}$$

where $c > 0$, $\theta \in \mathbb{R}$ and $\eta(x,y)$ is a smooth cutoff function. The function η is 1 on $B_{1/3}(0,0)$, but vanishes outside of $B_{1/2}(0,0)$. On the domain $\Omega = [0,1]^2$, the kernel G_2 is given as

$$G_2(x,y) = g_2(x,y) + g_2(x+1,y) + g_2(x,y+1) + g_2(x+1,y+1). \tag{2.13}$$

Outside of $\Omega = [0,1]^2$, $J_2(x,y)$ is given as the smooth periodic extension of $G_2(x,y)$, denoted as

$$J_2(x,y) = G_{2,per}(x,y). \tag{2.14}$$

See Figures 2.1 - 2.2.

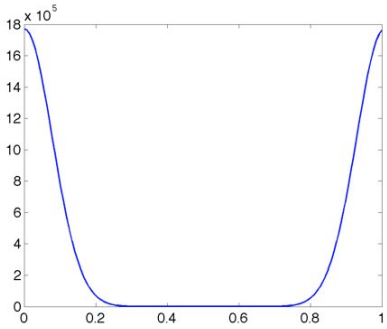

Figure 2.1: 1d periodically extended Gaussian kernel

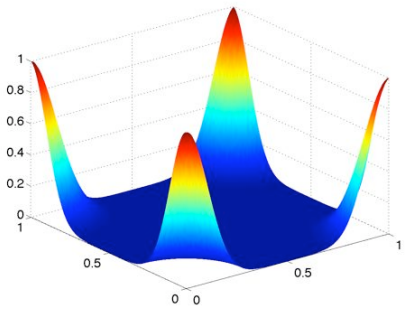

Figure 2.2: 2d periodically extended Gaussian kernel

2.3 Method for Periodic Boundary Conditions

We are now in position to derive the Galerkin method subject to periodic boundary conditions using the 1d kernel J_1. As previously stated, we need to use a complete set of functions that satisfy the boundary conditions. A good choice is supplied by the Fourier basis functions given as

$$\phi_n(x) = e^{-2\pi inx},$$

since these functions are globally smooth and form a complete set in $L^2([0,1])$ [3]. The analogous 2d Fourier basis functions are given as

$$\phi_{m,n}(x,y) = e^{-2\pi inx}e^{-2\pi imy}.$$

Before we continue with the Galerkin derivation, two necessary calculations that we need to make are$\Delta\ \phi_n$ and $J_c(\phi_n)$, where J_c is defined in the following definition.

Definition 2.3.1. *For $J \in L^2(\Omega)$, where Ω is a rectangular domain of $\mathbb{R}^n$ with $n = \{1,2,3\}$, the convolution of J and u is defined as*

$$J_c(u) = J * u = \int_\Omega J_{per}(x-y)u(y)dy,$$

where $J_c : L^2_{per}(\Omega) \to L^2_{per}(\Omega)$ and J_{per} is the periodic extension of J.

For$\Delta\ \phi_n(x)$, we have

$$\Delta\phi_n(x) = -4\pi^2 n^2 \cdot \phi_n(x), \tag{2.15}$$

and for$\Delta\ \phi_{m,n}(x,y)$, we have

$$\Delta\phi_n = -4\pi^2(m^2+n^2) \cdot \phi_n(x), \tag{2.16}$$

For $J_c(\phi_n)$, we have that

$$J_c(\phi_n(x)) = \int_0^1 J_1(y-x) \cdot \phi_n(x) dx.$$

Since $J_1 \in C^1([0,1])$ and periodic, we can write the Fourier series of J_1 as

$$J_1 = \sum_{n=-\infty}^{\infty} \hat{J}_n \phi_n,$$

where

$$\hat{J}_n = \int_0^1 J(x)\phi_n(x) dx.$$

Thus, for $J_c(\phi_n)$, we have

$$\begin{aligned} J_c(\phi_n) &= \int_0^1 \left(\sum_{k=-\infty}^{\infty} \hat{J}_k \phi_k(y-x) \right) \phi_n(x) dx, \\ &= \sum_{k=-\infty}^{\infty} \hat{J}_k \phi_k(y) \int_0^1 \phi_{-k}(x)\phi_n(x) dx. \end{aligned}$$

We are able to move the sum from under the integral and integrate each term of the sum individually due to the uniform convergence with respect to its Fourier series [35]. Since the ϕ_k form an orthonormal basis, we have that $\int_0^1 \phi_n(x)\phi_k(x)dx = 0$ if $k \neq n$ and 1 if $k = n$. Thus,

$$J_c(\phi_n(x)) = \hat{J}_n \cdot \phi_n(x). \tag{2.17}$$

The same computation for the 2d version using $J_2(x,y)$ in (2.14) shows that

$$J_c(\phi_n(x,y)) = \hat{J}_{m,n} \cdot \phi_{m,n}(x,y). \tag{2.18}$$

Therefore, we see that the $\phi_n(x)$ and $\phi_{m,n}(x,y)$ are eigenfunctions of both $\Delta$and J_c using J_1 and J_2, respectively.

Returning to 1d Galerkin method derivation, we approximate u and v with the Fourier basis functions to give

$$u \approx \sum_{n=-N/2+1}^{N/2} \hat{u}_n \phi_n, \tag{2.19}$$

and

$$v \approx \sum_{n=-N/2+1}^{N/2} \hat{v}_n \phi_n, \tag{2.20}$$

As the computations involving u and v are similar, we only present the derivations involving u. Using the expansion for u given in (2.19), the residual R is computed as

$$\begin{aligned}
R &= u_t - \beta\Delta u - (1-\beta)(J_c(u) - \hat{J}_0 u) - \gamma f(u,v), \\
&= \sum_{n=-N/2+1}^{N/2} \hat{u}_n' \phi_n + \beta \sum_{n=-N/2+1}^{N/2} 4\pi^2 n^2 \hat{u}_n \phi_n - (1-\beta)\left(\sum_{n=-N/2+1}^{N/2} \hat{J}_n \hat{u}_n \phi_n - \hat{J}_0 \hat{u}_n \phi_n \right) \\
&\quad - \gamma \sum_{n=-N/2+1}^{N/2} \hat{f}_n \phi_n, \\
&= \sum_{n=-N/2+1}^{N/2} \left(\hat{u}_n' + \left(4\pi^2 n^2 \beta - (\hat{J}_n - \hat{J}_0)(1-\beta) \right) \hat{u}_n - \gamma \hat{f}_n \right) \phi_n
\end{aligned}$$

The Galerkin method enforces the residuals to be orthogonal to the chosen set of trial functions. That is to say that $(R,\phi_j) = 0$ for $-N/2+1 \leq j \leq N/2$. To accomplish this, we have

$$(R,\phi_j) = \left(\hat{u}_n' + \left(4\pi^2 n^2 \beta - (\hat{J}_n - \hat{J}_0)(1-\beta)\right)\hat{u}_n - \gamma \hat{f}_n\right) \int_0^1 \phi_j(x)\phi_j(x)dx = 0.$$

Again, the ϕ_n are orthonormal, which implies that $\int_0^1 \phi_j(x)\phi_n(x)dx = 0$ if $n \neq j$ and 1 if $n = j$. Therefore, for $-N/2+1 \leq n \leq N/2$, we need to solve the following system of ODEs

$$\hat{u}_n' = -K_n \cdot \hat{u}_n + \gamma \hat{f}_n, \tag{2.21}$$

$$\hat{v}_n' = -d \cdot K_n \cdot \hat{v}_n + \gamma \hat{g}_n, \tag{2.22}$$

where

$$K_n = 4\beta\pi^2 n^2 - (1-\beta)(\hat{J}_n - \hat{J}_0). \tag{2.23}$$

To complete the derivation for the method, we must now numerically estimate solutions for the resulting finite system of ODEs. To integrate this system, we choose the semi-implicit method that uses Euler's method for the nonlinear portion and the implicit midpoint method for the linear portion. This method was given by Equation (2.8). To use this method, note that $f_1 = -K_n \cdot \hat{u}_n$ and $f_2 = \gamma \cdot \hat{f}_n$. Application of the method and a rearrangement of terms gives

$$\hat{u}_n^{k+1} = \frac{2 - K_n \cdot h}{2 + K_n \cdot h}\hat{u}_n^k + \frac{2\gamma h}{2 + K_n \cdot h}\hat{f}_n^k, \tag{2.24}$$

$$\hat{v}_n^{k+1} = \frac{2 - d \cdot K_n \cdot h}{2 + d \cdot K_n \cdot h}\hat{v}_n^k + \frac{2\gamma h}{2 + d \cdot K_n \cdot h}\hat{g}_n^k. \tag{2.25}$$

For $-N/2+1 \leq n \leq N/2$ and $-M/2+1 \leq m \leq M/2$ over $\Omega = [0,1]^2$, we get the analogous system as

$$\hat{u}'_{m,n} = -K_{m,n} \cdot \hat{u}_{m,n} + \gamma \hat{f}_{m,n}, \tag{2.26}$$

$$\hat{v}'_{m,n} = -d \cdot K_{m,n} \cdot \hat{v}_{m,n} + \gamma \hat{g}_{m,n}, \tag{2.27}$$

where

$$K_{m,n} = 4\beta(n^2 + m^2)\pi^2 - (1-\beta)(\hat{J}_{m,n} - \hat{J}_{0,0}). \tag{2.28}$$

and its accompanying numerical method as

$$\hat{u}^{k+1}_{m,n} = \frac{2 - K_{m,n} \cdot h}{2 + K_{m,n} \cdot h} \hat{u}^k_{m,n} + \frac{2\gamma h}{2 + K_{m,n} \cdot h} \hat{f}^k_{m,n}, \tag{2.29}$$

$$\hat{v}^{k+1}_{m,n} = \frac{2 - d \cdot K_{m,n} \cdot h}{2 + d \cdot K_{m,n} \cdot h} \hat{v}^k_{m,n} + \frac{2\gamma h}{2 + d \cdot K_{m,n} \cdot h} \hat{g}^k_{m,n}. \tag{2.30}$$

Note that the methods that we have derived are nice in the following sense. In order to continue to the next iteration, only information about the current step is required. Information about future iterations are not required and as such, we avoid having to solve systems of nonlinear algebraic equations that often accompany the use of purely implicit methods.

2.3.1 Estimating the Fourier coefficients of f and g

Until now, we have avoided the discussion on how to compute the coefficients $\hat{f}_n$ and $\hat{g}_n$. In the method at the $k-$th iteration, estimates are required for $\hat{f}_n$ and $\hat{g}_n$, respectively. To compute estimates for $\hat{f}_n$ and $\hat{g}_n$, we observe that we have known estimates for the Fourier coefficients of both u and v at each iteration. Using the Inverse Discrete Fourier Transform, which is described below, $\hat{u}_n$ and $\hat{v}_n$ are transformed to obtain estimates of u

and v. These approximations for u and v are then used to compute estimates for both f and g. Application of the Discrete Fourier Transform to the estimates for f and g yields estimates for the Fourier coefficients for $\hat{f}_n$ and $\hat{g}_n$, respectively.

The description of how to compute the Fourier coefficients of both f and g require two potentially numerically intensive steps. Given a series of discrete function values, we have to compute approximations for the Fourier coefficients. Also, given the Fourier coefficients, we have to compute approximations for the corresponding function values. These steps are accomplished using the DFT (Discrete Fourier Transform) and IDFT (Inverse Discrete Fourier Transform).

For the 1d DFT, consider a sequence of $\{u(x_j)\}$, where $-N/2+1 \leq j \leq N/2$. The DFT is given as

$$\hat{u}_n = \frac{1}{N} \sum_{j=-N/2+1}^{N/2} u(x_j) e^{-2i\pi nj/N},$$

where $-N/2+1 \leq n \leq N/2$. The IDFT is given as

$$u(x_j) = \sum_{n=-N/2+1}^{N/2} \hat{u}_n e^{2i\pi nj/N}.$$

To implement both the DFT and IDFT, the Fast Fourier transform (FFT) is used. The FFT is an algorithm original to Gauss and rediscovered by Cooley and Tukey [10]. For N data values, they showed that the computational time of *O(N log N)* is possible if $N = 2^m$ for $m \in \mathbb{N}$.

Using the DFT and IDFT can have the unintentional effect of introducing errors due to aliasing. Aliasing occurs when higher order modes become indistinguishable from lower order modes, due to discretization. However, for smooth functions, the higher order modes tend to decrease very quickly and reduce the errors associated with aliasing [19, 56, 58]. Figure 2.3 shows that the Fourier coefficients quickly go to 0 as n increases, suggesting that

the errors due to aliasing are in fact small for our situation.

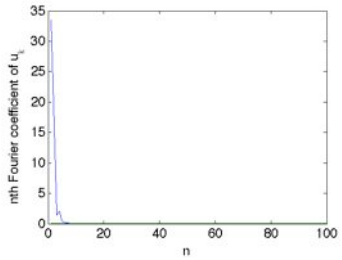

Figure 2.3: Fourier coefficients u for a sample run. Note that as n increases, the Fourier coefficients quickly approach 0, showing that for sufficiently large N, the errors from aliasing are small.

Once the spectral method generates approximations for (u, v), we can validate these values using finite differences to estimate the value of the left hand side and right hand side of System 1.1. For an accurate method, we would expect this difference between the left and right hand sides to be small. Furthermore, as we increase the value of N, this difference should also decrease. This difference between the left hand side and right hand side of System 1.1 with $\beta = 1$ was estimated using the maximum absolute value or supremum norm of the differences. Table 2.3.1 gives the average difference using 10 different random initial conditions for each value of N. As the size of the system increases, the difference between the left and right hand side of System 1.1 gets very small with respect to the supremum norm. For the numerical simulations of this thesis, we use $N \geq 128$, where $N = 2^m$ as previously explained.

2.3.2 Method for Homogeneous Neumann Boundary Conditions

In this section, we use the same techniques as those used for deriving the spectral system for the reaction-diffusion equations subject to periodic boundary conditions. As before, we provide the 1d derivation for this system. As pointed out in the section for periodic boundary conditions, we need to select trial functions that are complete and satisfy the

Table 2.1: Using the supremum norm, this table shows the difference of the left hand side and right hand side of System 1.1 when *time* reaches $T_{max} = .015$. The values (d,γ) are given as $(100, 100)$. Using the (u, v) value generated by the periodic spectral method of this section, finite differences were employed to estimate the left and right hand sides of System 1.1. The values in the table are the means of solutions from 10 separate runs. As the size of the system N increases, we see that the difference between the left and right hand side decreases, suggesting a more accurate estimate of the solution is obtained with higher values of N. The left hand side was estimated using the finite difference $(y^{k+1} - y^k)/\Delta t$.

N	$\|\|LHS - RHS\|\|_\infty$
32	2.58×10^{-2}
64	1.32×10^{-2}
128	6.96×10^{-4}

homogeneous Neumann boundary conditions. For $f \in C^1[0, 1]$, define the scalar product as

$$< f, g >= \int_0^1 f(x)\bar{g}(x)dx,$$

and the accompanying L^2-norm as

$$||f||_2 = \left(\int_0^1 |f(x)|^2 \, dx \right)^{.5}.$$

With respect to the standard L^2-norm over $[0, 1]$, the set of cosine functions, $\{\cos(n\pi x)\}_{n=0}^{\infty}$, forms a complete set in the set of functions belonging to $C^1([0, 1]) \cap S_N([0, 1])$, where $S_N([0, 1])$ is the set of functions that satisfy the homogeneous Neumann boundary conditions on $[0, 1]$. The following lemma shows this.

Lemma 2.3.1. *The set of functions,* $\{\cos(n\pi x)\}_{n=0}^{\infty}$, *is a complete set in* $C^1([0, 1]) \cap S_N([0, 1])$.

Proof. Let $u \in C^1[0,1]$ such that u satisfies the homogeneous Neumann boundary conditions. Now define the even extension U over $[-1,1]$ of u as

$$U(x) = \begin{cases} u(x), \text{ for } x \in [0,1] \\ u(-x), \text{ for } x \in [-1,0) \end{cases}.$$

Since u obeys the homogeneous Neumann boundary conditions, we see that

$$\lim_{x \to 0^+} U'(x) = \lim_{x \to 0^-} U'(x),$$

showing that $U \in C^1[-1,1]$. The Fourier series of a function $U : [-1,1] \to \mathbb{R}$ is given as

$$U(x) = \frac{1}{2}a_0 + \sum_{n=1}^{\infty}(a_n \cos(n\pi x) + b_n \sin(n\pi x)), \tag{2.31}$$

where

$$a_n = \int_{-1}^{1} U(x)\cos(n\pi x)dx, \tag{2.32}$$

$$b_n = \int_{-1}^{1} U(x)\sin(n\pi x)dx. \tag{2.33}$$

Note that the convergence is uniform with respect to the L^2-norm over $[-1,1]$. See [56]. The observation that U is even and that $\sin(n\pi x)$ is odd for all n is used to show that

$b_n = 0$ for all n. Computing the b_n, we get

$$\begin{aligned} b_n &= \int_{-1}^{1} U(x)\sin(n\pi x)dx, \\ &= \int_{-1}^{0} U(x)\sin(n\pi x)dx + \int_{0}^{1} U(x)\sin(n\pi x)dx, \\ &= -\int_{0}^{1} u(x)\sin(n\pi x)dx + \int_{0}^{1} u(x)\sin(n\pi x)dx = 0. \end{aligned}$$

Using the fact that both U and $\cos(n\pi x)$ are even functions, we can compute the a_n as

$$a_n = \int_{-1}^{1} U(x)\cos(n\pi x)dx = 2\int_{0}^{1} U(x)\cos(n\pi x)dx.$$

Therefore,

$$u(x) = \frac{1}{2}a_0 + \sum_{n=1}^{\infty} a_n \cos(n\pi x),$$

where

$$a_n = 2\int_{0}^{1} U(x)\cos(n\pi x)dx.$$

Since this expansion can be found for arbitrary $u \in C^1[0,1] \cap S_N[0,1]$, the proof is complete.

□

Since each cosine satisfies the homogeneous Neumann boundary conditions, we choose this set as an appropriate set of trial functions. Thus,

$$\phi_n = cos(\pi n x).$$

With the trial functions selected, we write the approximations of u and v as

$$u \approx \sum_{n=0}^{N-1} \hat{u}_n \phi_n,$$

and

$$v \approx \sum_{n=0}^{N-1} \hat{v}_n \phi_n.$$

As we have already demonstrated with the periodic system, the Galerkin method results in a finite system of ODEs. Since the details of the derivation for this method are the same as for the periodic system, we omit them and give the systems. For $0 \leq n \leq N-1$, the system for the Neumann case is given as

$$\hat{u}_n' = -L_n \cdot \hat{u}_n + \gamma \cdot \hat{f}_n, \tag{2.34}$$

$$\hat{v}_n' = -d \cdot L_n \hat{v}_n + \gamma \cdot \hat{g}_n, \tag{2.35}$$

where

$$L_n = n^2 \cdot \pi^2. \tag{2.36}$$

By similar reasoning, for $\Omega = [0,1]^2$, $0 \leq m \leq M-1$ and $0 \leq n \leq N-1$, we have

$$\hat{u}_{m,n}' = -L_{m,n} \cdot \hat{u}_{m,n} + \gamma \cdot \hat{f}_{m,n}, \tag{2.37}$$

$$\hat{v}_{m,n}' = -d \cdot L_{m,n} \cdot \hat{v}_{m,n} + \gamma \cdot \hat{g}_{m,n}, \tag{2.38}$$

where

$$L_{m,n} = (n^2 + m^2) \cdot \pi^2. \tag{2.39}$$

Using the semi-implicit scheme used for the mixed diffusion system with periodic boundaries yields the 1d spectral method given as

$$\hat{u}_n^{k+1} = \frac{2 - L_n \cdot h}{2 + L_n \cdot h}\hat{u}_n^k + \frac{2 \cdot \gamma \cdot h}{2 + L_n \cdot h}\hat{f}_n^k, \tag{2.40}$$

$$\hat{v}_n^{k+1} = \frac{2 - d \cdot L_n \cdot h}{2 + d \cdot L_n \cdot h}\hat{v}_n^k + \frac{2 \cdot \gamma \cdot h}{2 + L_n \cdot h}\hat{g}_n^k. \tag{2.41}$$

Analogously, the 2d spectral method is given as

$$\hat{u}_{m,n}^{k+1} = \frac{2 - L_{m,n} \cdot h}{2 + L_{m,n} \cdot h}\hat{u}_{m,n}^k + \frac{2 \cdot \gamma \cdot h}{2 + L_{m,n} \cdot h}\hat{f}_{m,n}^k, \tag{2.42}$$

$$\hat{v}_{m,n}^{k+1} = \frac{2 - d \cdot L_{m,n} \cdot h}{2 + d \cdot L_{m,n} \cdot h}\hat{v}_{m,n}^k + \frac{2 \cdot \gamma \cdot h}{2 + d \cdot L_{m,n} \cdot h}\hat{g}_{m,n}^k. \tag{2.43}$$

As with the mixed system with periodic boundary conditions, we will handle the computation of $\hat{f}_n$ and $\hat{g}_n$ using discrete Fourier transforms and discrete inverse transforms. However, as we only need the cosines for these computations, we will use the discrete cosine transform (DCT) and the inverse discrete cosine transform (IDCT). The DCT of a set of data $\{u(x_n)\}_{n=0}^N$ is given as

$$\hat{u}_n = w_n \sum_{j=0}^{N-1} u(x_j) \cos\left(\frac{\pi(2j-1)(n-1)}{2N}\right), 0 \leq n \leq N-1,$$

where

$$w_n = \begin{cases} \frac{1}{\sqrt{N}} & \text{for } n = 0 \\ \sqrt{\frac{2}{N}} & \text{for } n \geq 1 \end{cases}$$

and its inverse is given by

$$u(x_j) = \sum_{n=0}^{N-1} w_n \hat{u}_n \cos\left(\frac{\pi(2j-1)(n-1)}{2N}\right), 0 \leq j \leq N-1.$$

The DCT and IDCT achieve a computational time of $O(NlogN)$ as the algorithms make use of the FFT.

2.4 Convergence of Semi-Implicit Integration Scheme

All of the previous work relies upon the convergence of the semi-implicit method. Rather than show convergence for the semi-implicit method for each system, we show that for a more general system, the spectral method is convergent.

Consider the system of autonomous ODEs given by

$$y' = f(y),\ y(t_0) = y_0, \tag{2.44}$$

where $f : \mathbb{R}^d \to \mathbb{R}^d$, and $y, y_0 \in \mathbb{R}^d$. Further suppose that

$$f(y) = f_1(y) + f_2(y), \tag{2.45}$$

where f_1 is linear and f_2 is Lipschitz continuous. For convenience, method (2.8), is given as

$$y^{k+1} - y^k = \frac{h}{2}\left(f_1(y^k) + f_1(y^{k+1})\right) + hf_2(y^k). \tag{2.46}$$

We begin by showing that the method is order 1. In other words, it gives exact values for linear solutions, but inexact estimates for solutions that are polynomials of degree ≥ 2.

Lemma 2.4.1. *The numerical method given in 2.46 is order 1.*

Proof. We will show this result by computing the error term resulting from the difference

of the exact and approximate solutions. By the definition of order given in Definition 2.1.2, we evaluate the following expression

$$O(h^{p+1}) = y(t_{k+1}) - y(t_k) - \frac{h}{2}f_1(y(t_k)) - \frac{h}{2}f_1(y(t_{k+1})) - hf_2(y(t_k)).$$

Using the Taylor series expansion of $y(t_{k+1})$ and $f_1(y(t_{k+1}))$, we get

$$\begin{aligned} O(h^{p+1}) &= y(t_k) + hy'(t_k) + \frac{h^2}{2}y''(t_k) + O(h^3) \\ &\quad - \left(y(t_k) + \frac{h}{2}f_1(y(t_k)) + \frac{h}{2}[f_1(y(t_k) + O(h))] + hf_2(y(t_k)) \right) \\ &= hy'(t_k) - h[f_1(y(t_k)) + f_2(y(t_k))] + \frac{h^2}{2}y''(t_k) - \frac{h^2}{2}f_1'(y(t_k)) + O(h^2) \end{aligned}$$

Since $y'(t_k) = h(f_1(y(t_k)) + f_2(y(t_k))\ )$, we have that

$$\begin{aligned} O(h^{p+1}) &= \frac{h^2}{2}y''(t_k) - \frac{h^2}{2}f_1'(y(t_k)) + O(h^2), \\ &= O(h^2). \end{aligned}$$

Thus, the order of the method is 1. □

Using the order result, we now proceed with the proof for convergence.

Theorem 2.4.1. *The numerical method given in 2.46 converges.*

Proof. Evaluating the numerical method with the exact value of $y(t_n)$ gives

$$y(t_{k+1}) = y(t_k) + \frac{h}{2}f_1(y(t_k)) + \frac{h}{2}f_1(y(t_{k+1})) + hf_2(y(t_k)) + O(h^2).$$

If we subtract Eq. 2.46 from this expression, we get

$$\begin{aligned} e^{k+1} &= e^k + \frac{h}{2}(f_1(y(t_k)) - f_1(y^k)) \\ &+ \frac{h}{2}(f_1(y(t_{k+1})) - f_1(y^{k+1})) \\ &+ h(f_2(y(t_k)) - f_2(y^k)) + O(h^2). \end{aligned}$$

Since f_1 and f_2 are Lipschitz continuous, let λ_1 and λ_2 denote the respective Lipschitz constants. Therefore, we can write the above inequality as

$$\begin{aligned} \left|\left|e^{k+1}\right|\right| &\leq \left|\left|e^k\right|\right| + \frac{h\lambda_1}{2}\left|\left|e^k\right|\right| + \frac{h\lambda_1}{2}\left|\left|e^{k+1}\right|\right| + h\lambda_2\left|\left|e^k\right|\right| + O(h^2), \\ &\leq \frac{1 + \frac{h\lambda_1}{2} + h\lambda_2}{1 - \frac{h\lambda_1}{2}}\left|\left|e^k\right|\right| + \frac{ch^2}{1 - \frac{h\lambda_1}{2}} \end{aligned}$$

By induction, we have that

$$\left|\left|e^k\right|\right| \leq \frac{ch}{\lambda_1 + \lambda_2}\left(\left(\frac{2 + h\lambda_1 + 2h\lambda_2}{2 - h\lambda_1}\right)^k - 1\right) \tag{2.47}$$

For sufficiently small h where $0 \leq h\lambda_1 < 2$, note that we can write the following

$$\begin{aligned} \frac{2 + h\lambda_1 + 2h\lambda_2}{2 - h\lambda_1} &= 1 + \frac{2h(\lambda_1 + \lambda_2)}{2 - h\lambda_1} \\ &\leq \sum_{l=0}^{\infty} \frac{1}{l!}\left(\frac{2h(\lambda_1 + \lambda_2)}{(2 - h\lambda_1)}\right)^l \\ &= e^{\frac{2h(\lambda_1+\lambda_2)}{2-h\lambda_1}} \end{aligned}$$

Thus, (2.47) yields

$$\left|\left|e^k\right|\right| \leq \frac{ch}{\lambda_1+\lambda_2}\left(\left(\frac{2+h\lambda_1+2h\lambda_2}{2-h\lambda_1}\right)^k\right)$$

$$\leq \frac{ch}{\lambda_1+\lambda_2}e^{\frac{2kh(\lambda_1+\lambda_2)}{2-h\lambda_1}}$$

Since $kh < t^*$, where t^* is defined as the length of the time interval in Definition 2.1.1,

$$\left|\left|e^{k+1}\right|\right| \leq \frac{ch}{\lambda_1+\lambda_2}e^{\frac{2t^*(\lambda_1+\lambda_2)}{2-h\lambda_1}}.$$

As $h \to 0^+$, $\left|\left|e^{k+1}\right|\right| \to 0$. Therefore, the method converges. □

By this theorem, all of the numerical methods derived for the systems subject to periodic boundary conditions and homogeneous Neumann boundary conditions converge.

2.5 Linear Stability of Semi-Implicit Integration Scheme

To analyze the linear stability of the semi-implicit method, we begin with the system of ODEs given by

$$y' = Ay, \text{ with } y(t_0) = y_0 \in \mathbb{R}^d \tag{2.48}$$

where

$$A = \begin{pmatrix} a_{11} & 0 & \dots & 0 \\ 0 & a_{22} & \dots & 0 \\ \vdots & \vdots & \ddots & \vdots \\ 0 & 0 & \dots & a_{dd} \end{pmatrix}, \ a_{ii} \leq 0 \text{ for } 0 \leq i \leq d, \tag{2.49}$$

(2.50)

with

$$y = (y_1, \ldots, y_d) \in \mathbb{R}^d. \tag{2.51}$$

This system represents a more general form of the linearized system for reaction-diffusion systems subject to periodic boundary conditions and homogeneous Neumann conditions. Application of the semi-implicit method to the linearized system gives

$$\begin{aligned} y^{k+1} - y^k &= \frac{h}{4}\left(Ay^{k+1} + Ay^k\right) + \frac{h}{2}Ay^k \\ y^{k+1} &= \left(I - \frac{h}{4}A\right)^{-1}\left(I + \frac{3h}{4}A\right)y^k. \end{aligned} \tag{2.52}$$

Since the diagonal entries of A are less than or equal to zero, $(I - \frac{h}{2}A)$ is invertible. Explicitly,

$$\left(I - \frac{h}{4}A\right)^{-1} = \begin{pmatrix} \frac{4}{4-ha_{11}} & 0 & \ldots & 0 \\ 0 & \frac{4}{4-ha_{22}} & \ldots & 0 \\ \vdots & \vdots & \ddots & \vdots \\ 0 & 0 & \ldots & \frac{4}{4-ha_{dd}} \end{pmatrix} \tag{2.53}$$

Applying directly to $(I + \frac{3h}{4}A)$ gives

$$(I - \frac{h}{4}A)^{-1}(I + \frac{3h}{4}A) = E, \tag{2.54}$$

where

$$E = \begin{pmatrix} \frac{4+3ha_{11}}{4-ha_{11}} & 0 & \ldots & 0 \\ 0 & \frac{4+3ha_{22}}{4-ha_{22}} & \ldots & 0 \\ \vdots & \vdots & \ddots & \vdots \\ 0 & 0 & \ldots & \frac{4+3ha_{dd}}{4-ha_{dd}} \end{pmatrix}. \tag{2.55}$$

Therefore,

$$y^{k+1} = Ey^k,$$

$$= E^k y^0. \tag{2.56}$$

If $||E||_\infty < 1$, where this norm denotes the maximum absolute row sum of E, then we see that as $k \to \infty$, $y^k \to 0$. This implies that for the ith row, we have that

$$\left| \frac{4 + 3ha_{ii}}{4 - ha_{ii}} \right| < 1. \tag{2.57}$$

Solving this inequality shows that

$$h < -\frac{4}{a_{ii}}, \text{ for each } 1 \leq i \leq dd. \tag{2.58}$$

Therefore, when selecting the time step size, it must be selected sufficiently small so as to achieve convergence.

Chapter 3: Prior Analytical Results

Many of the theoretical results presented in this thesis are built upon the results found in [40, 41, 55]. For local systems subject to homogeneous Neumann boundary conditions like System 1.2, Murray conjectured that the full set of possible nonlinear spatial patterns are not in general predicted by linear analysis if the dominant eigenfunction is two-dimensional [44]. Rather, they depend upon the initial conditions and the nonlinearities in the reaction scheme. However, Sander and Wanner applied the techniques of [40, 41] to show that for a certain initial pattern selection, the early stages of the pattern formation process of System 1.2 can be explained by using the eigenfunctions that correspond to the largest positive eigenvalues [55]. The next chapter extends their work to the more general nonlocal case given by System 1.1. This chapter summarizes the major results of Sander and Wanner, as well as the main supporting definitions, lemmas and propositions.

3.1 Statement of Main Results

The results are given with respect to the following rescaled version of System 1.2. This system was introduced in the Introduction as System 1.13, but it is included here for convenience. By introducing the new time variable $\tilde{t} = \gamma \cdot t$, dropping the tilde after rescaling and using the new parameter $\epsilon = 1/\gamma$, the scaled system is given as

$$\begin{aligned} u_t &= \epsilon \cdot \Delta u + f(u, v), \\ v_t &= d \cdot \epsilon \cdot \Delta v + g(u, v), \end{aligned} \tag{3.1}$$

subject to homogeneous Neumann boundary conditions. For the domainΩ , the following assumption is made.

Assumption 3.1.1. *Assume that $\Omega \subset \mathbb{R}^n$ is a bounded domain with a Lipschitz continuous boundary, where $n \in \{1, 2, 3\}$.*

The following assumption pertains to the smoothness of the nonlinearity.

Assumption 3.1.2. *Let $\delta \in \mathbb{N}$ be arbitrary. Assume that $f, g : \mathbb{R}^2 \to \mathbb{R}$ are $C^{1+\delta}-$functions, and that there exists a point $(\bar{u}_0, \bar{v}_0) \in \mathbb{R}^2$ with $f((\bar{u}_0, \bar{v}_0)) = g((\bar{u}_0, \bar{v}_0)) = 0$. If $\delta \geq 2$, we assume further that all partial derivatives of f and g of order $2, 3, \ldots, \delta$ at $(\bar{u}_0, \bar{v}_0)$ vanish.*

Note that for $\epsilon > 0$, $(\bar{u}_0, \bar{v}_0)$ is an equilibrium solution of System 3.1. Under Assumption 3.1.2, System 3.1 generates a nonlinear semiflow in a suitable phase space $\mathbb{X}^\alpha$ [26,47]. System 3.1 exhibits a Turing instability if $(\bar{u}_0, \bar{v}_0)$ is stable in the absence of diffusion, but unstable otherwise. The following assumption will ensure the presence of Turing instability.

Assumption 3.1.3. *Let f and g be as in Assumption 3.1.2, and assume that for some constant $d > 0$, we have*

$$f_u + g_v < 0, \tag{3.2}$$

$$f_u g_v - f_v g_u > 0, \tag{3.3}$$

$$df_u + g_v > 0, \tag{3.4}$$

$$(df_u + g_v)^2 - 4d(f_u g_v - f_v g_u) > 0, \tag{3.5}$$

$$f_u > 0, \tag{3.6}$$

$$(f_u + g_v)^2 - 4(f_u g_v - f_v g_u) > 0. \tag{3.7}$$

The first four conditions are the standard conditions for Turing instability. Inequalities (3.2) and (3.4) imply that f_u and g_v have opposite signs. If necessary, System 3.1 can always be rescaled so as to satisfy Condition (3.6). The final condition will guarantee that the eigenvalues of the linearization are real.

With the assumptions in place, the first major result of Sander and Wanner describes the pattern formation during the initial stages of the evolution of the solutions. For solutions with initial conditions near the homogeneous equilibrium $(\bar{u}_0, \bar{v}_0)$, the patterns are similar to solutions contained in a particular dominating subspace, $\mathscr{Y}_\epsilon^+$. For the dominating subspace, see Theorem 3.2.1.

Theorem 3.1.1 (Early Pattern Results, [55, Theorem 2.5])**.** *Assume that system 3.1 satisfies Assumptions 3.1.1 - 3.1.3. Choose any constant α with $\dim\Omega/4 < \alpha < 1$, and let $0 < d_0 \ll 1$ be arbitrary, but fixed. Then there exists an $\epsilon_0 > 0$ such that for every $0 < \epsilon \leq \epsilon_0$ there exists a finite-dimensional subspace $\mathscr{Y}_\epsilon^+$, as well as radii $0 < r_\epsilon \leq R_\epsilon$ such that the following is true: In the limit $\epsilon \to 0$ we have*

$$\dim \mathscr{Y}_\epsilon^+ \sim \epsilon^{\dim\Omega/2}, \qquad r_\epsilon \sim \epsilon^{(2\alpha+\dim\Omega)/(2\delta)}, \qquad \text{and} \qquad R_\epsilon \sim \epsilon^{(2\alpha+\dim\Omega)/(2\delta)}.$$

Furthermore, for most initial conditions $(u_0, v_0) \in \mathbb{X}^\alpha$ satisfying

$$||(u_0, v_0) - (\bar{u}_0, \bar{v}_0)||_* < r_\epsilon,$$

the corresponding solution (u, v) of System 3.1 exits a ball around the homogeneous equilibrium $(\bar{u}_0, \bar{v}_0)$ of radius R_ϵ, and upon exiting the ball the distance of (u, v) to the subspace $\mathscr{Y}_\epsilon^+$ is at most $d_0 \cdot R_\epsilon$. In the above estimate, the norm $||\cdot||_*$ denotes the norm of $\mathbb{X}^\alpha$ which is introduced in Definition 3.2.5 and Proposition 3.2.2.

In the previous theorem, the idea of "most initial conditions" can be explained with the concept of probability as defined in [40]. In a small neighborhood of $(\bar{u}_0, \bar{v}_0)$, there exists a finite-dimensional inertial manifold that exponentially attracts all nearby orbits. Rather than observing orbits, we observe the projection of orbits onto the manifold. A standard probability measure is induced by the finite-dimensional Lebesgue measure, giving rise to the meaning of the concept of probability as used in Theorem 3.1.1.

By adapting the techniques of [54], the results in Theorem 3.1.1 can be extended further

beyond $(\bar{u}_0, \bar{v}_0)$. The next theorem shows that the solutions enter into a part of phase space in which their behavior is close to linear.

Theorem 3.1.2 (Almost Linear Behavior, [55, Theorem 2.7])**.** *Consider the reaction-diffusion system 3.1, assume that Assumptions 3.1.1-3.1.3 are satisfied, and let $\rho > 0$ be arbitrarily small, but fixed. Let (u_0, v_0) denote an initial condition close to the homogeneous equilibrium $(\bar{u}_0, \bar{v}_0)$, which is sufficiently close to the dominating subspace $\mathscr{Y}_\epsilon^+$. Finally, let (u, v) and (u_{lin}, v_{lin}) be the solutions to System 3.1 and its affine approximation at $(\bar{u}_0, \bar{v}_0)$, respectively, starting at (u_0, v_0). Then the solution (u, v) remains close to (u_{lin}, v_{lin}) until the distance from (u, v) to the homogeneous equilibrium exceeds a certain threshold. More specifically, as long as*

$$||(u(t), v(t)) - (\bar{u}_0, \bar{v}_0)||_* \leq C \cdot \epsilon^{-(\alpha - \dim\Omega/4) + \alpha/\delta + \rho} \cdot ||(u_0, v_0) - (\bar{u}_0, \bar{v}_0)||_*^\rho ,$$

we have

$$\frac{||(u(t), v(t)) - (u_{lin}(t), v_{lin}(t))||_*}{||(u_{lin}(t), v_{lin}(t)) - (\bar{u}_0, \bar{v}_0)||_*} \leq C \cdot \epsilon^{\alpha - \dim\Omega/4}.$$

3.2 Early Pattern Results

The results presented here use the techniques from dynamical systems. As such, explicit solutions are not sought, but analyzed in terms of nonlinear flows. To use these techniques and apply the theory of [41], System 3.1 must be written of the form

$$U_t = A_\epsilon U + F(U), \tag{3.8}$$

on an appropriate function space $\mathbb{X}$. Furthermore, hypothesis (H1) through (H3) must be verified. They are given as

(H1) The operator $-A_\epsilon$ is a sectoral operator on $\mathbb{X}$.

(H2) There exists a decomposition $\mathbb{X} = \mathbb{X}_\epsilon^{--} \oplus \mathbb{X}_\epsilon^- \oplus \mathbb{X}_\epsilon^+ \oplus \mathbb{X}_\epsilon^{++}$, such that all of these

subspaces are finite-dimensional except $\mathbb{X}_\epsilon^{--}$, and such that the linear semigroup corresponding to $U_t = A_\epsilon U$ satisfies several dichotomy estimates.

(H3) The nonlinearity $F : \mathbb{X}^\alpha \to \mathbb{X}$ is continuously differentiable, and satisfies both $F(\bar{u}_0, \bar{v}_0)$ and $DF(\bar{u}_0, \bar{v}_0)$.

As a reminder, the following definitions for semigroup and sectorial operators are provided.

Definition 3.2.1 (Semigroup)**.** *Let X be a Banach space. A one parameter family $T(t)$, $0 \leq t \leq \infty$, of bounded linear operators from X into X is a semigroup of bounded linear operators on X if*

1. *$T(0) = I$, where I is the identity operator on X*
2. *$T(t+s) = T(t)T(s)$ for every $t, s \geq 0$.*

Definition 3.2.2 (Sectorial Operator)**.** *A linear operator A on a Banach space X is sectorial if A is a closed, densely defined operator such that there exists constants $\phi \in (0, \frac{\pi}{2})$, $M \geq 0$ such that*

$$S_{b,\phi} = \{\lambda \in \mathbb{C} : \phi \leq |arg\lambda - b|, \lambda \neq b\} \subset \rho(A)$$

and

$$\left|(\lambda I - A)^{-1}\right| \leq \frac{M}{|\lambda - b|}$$

for all $\lambda \in S_{b,\phi}$ and where $\rho(A)$ is the resolvent set of A.

For more information about semigroups and sectorial operators, see Appendix A. Returning to the issue of writing System 3.1 as an evolution equation, consider the linearized system of System 3.1 given as

$$\begin{aligned} u_t &= \epsilon \cdot \Delta u + f_u(u,v)u + f_v(u,v)v, \\ v_t &= d \cdot \epsilon \cdot \Delta v + g_u(u,v)u + g_v(u,v)v, \end{aligned} \tag{3.9}$$

More succinctly, the system can be expressed as $U_t = \epsilon D\Delta U + BU$, where

$$D = \begin{pmatrix} 1 & 0 \\ 0 & d \end{pmatrix} \text{ and } B = \begin{pmatrix} f_u & f_v \\ g_u & g_v \end{pmatrix}. \tag{3.10}$$

The following definition describes the linear portion of (3.8).

Definition 3.2.3 (Linear Operator A_ϵ, [55, Definition 3.6])**.** *Let $\mathbb{L}^2(\Omega) = L^2(\Omega) \times L^2(\Omega)$, and for arbitrary $s > 0$, define $\mathbb{H}^s(\Omega) = H^s(\Omega) \times H^s(\Omega)$, where $H^s(\Omega)$ denotes the standard fractional Sobolev space for real-valued functions. Define*

$$\mathbb{X} = \mathbb{L}^2(\Omega), \tag{3.11}$$

and let $A_\epsilon : \mathbb{X} \to \mathbb{X}$ be the linear operator given by the right-hand side of System 3.9 subject to homogeneous Neumann boundary conditions. The domain of A_ϵ is given as $D(A_\epsilon) = \mathbb{H}^2_N(\Omega)$, where $\mathbb{H}^2_N(\Omega)$ denotes the subspace of $\mathbb{H}^2(\Omega)$ which consists of all functions satisfying homogeneous Neumann boundary conditions on $\delta\Omega$.

An important aspect of the linear portion is the eigenvalues of the negative Laplacian. These eigenvalues are used to help determine the eigenvalues of A_ϵ.

Definition 3.2.4 (Eigenvalues of $-\Delta$, [55, Definition 3.1])**.** *Let $\Omega \subset \mathbb{R}^n$ be a domain as in Assumption 3.1.1, and consider the self-adjoint operator $-\Delta : L^2(\Omega) \to L^2(\Omega)$ subject to homogeneous Neumann boundary conditions. We denote by $0 = \tau_1 < \tau_2 < \ldots \to \infty$ the ordered sequence of eigenvalues of $-\Delta$, and the corresponding pairwise orthogonal L^2-normalized real-valued eigenfunctions by ϕ_k for $k \in \mathbb{N}$.*

Their asymptotic growth rate is given as

$$\tau_k \sim k^{2/\dim\Omega}. \tag{3.12}$$

See [15].

As for the nonlinearity F of (3.8), define the function $h : \mathbb{R}^2 \to \mathbb{R}^2$ to be the nonlinear part of (f, g) of System 3.1. Furthermore, let

$$\hat{h}(u, v) = (f(u, v), g(u, v))$$

and

$$h(u, v) = \hat{h}(u, v) - \hat{h}_u(\bar{u}_0, \bar{v}_0) \cdot (u - \bar{u}_0) - \hat{h}_v(\bar{u}_0, \bar{v}_0) \cdot (v - \bar{v}_0). \tag{3.13}$$

Setting $F(U) = h(u, v)$ for $U = (u, v)$ gives the nonlinear portion of (3.8).

Now that System 3.1 has been written in the form of an evolution equation, the hypotheses (H1) - (H3) must be verified. An important key to the verification of the hypotheses involves understanding the spectrum of A_ϵ. The following lemmas and proposition describe the spectrum of A_ϵ and show that this spectrum contains only eigenvalues. Consider the characteristic polynomial given as

$$\det(B - s \cdot D - \lambda I) = \lambda^2 - c_1(s) \cdot \lambda + c_0(s), \tag{3.14}$$

where

$$c_1(s) = (f_u + g_v) - s \cdot (1 + d), \tag{3.15}$$

$$c_0(s) = (f_u g_v - f_v g_u) - (d f_u + g_v) \cdot s + d \cdot s^2. \tag{3.16}$$

Lemma 3.2.1 ([55, Lemma 3.4])**.** *Suppose that Assumption 3.1.3 is satisfied. Then for arbitrary $s \geq 0$ the characteristic polynomial (3.14) has two distinct roots $\lambda^-(s) < \lambda^+(s)$. The function $\lambda^-(\cdot)$ is strictly decreasing with $\lambda^-(s) < 0$ for all $s \geq 0$. Moreover, $\lambda^+(\cdot)$ satisfies $\lambda^+(0) < 0$. It has a unique maximal value $\lambda^+_{max} > 0$ which is attained at some $s_{max} > 0$. It also has two zeros, $s_l < s_r$.*

The asymptotic behavior of the functions $\lambda^{\pm}$ *is given by* $\lim_{s\to\infty}(\lambda^{+}(s)/s) = -1$ *and* $\lim_{s\to\infty}(\lambda^{-}(s)/s) = -d$.

The next lemma describes the eigenfunctions of A_ϵ. Although A_ϵ is not self-adjoint, the lemma shows that the angle between any two of the eigenfunctions is bounded away from 0 or π. This is a critical observation that is used to prove the early pattern formation results.

Lemma 3.2.2 ([55, Lemma 3.5])**.** *Suppose that Assumption 3.1.3 holds. For* $s \geq 0$ *let* $V^{\pm} \in \mathbb{R}^2$ *denote the normalized eigenvectors of the matrix* $B - s \cdot D$ *corresponding to the eigenvalues* $\lambda^{\pm}(s)$*, whose existence is due to Lemma 3.2.1. The angle between* $V^{-}(s)$ *and* $V^{+}(s)$ *is strictly bounded away from both* 0 *and* π *for all* $s \geq 0$*. Moreover, as* s *approaches* ∞ *the angle approaches a right angle.*

The next proposition describes the spectrum of A_ϵ and verifies (H1). Furthermore, it will assist in the verification of the remaining hypotheses by establishing that the eigenfunctions of A_ϵ are a complete set in $\mathbb{X}$.

Proposition 3.2.1 (Spectrum of A_ϵ, [55, Proposition 3.7])**.** *Assume that Assumptions 3.1.1 and 3.1.3 are satisfied. Then* $-A_\epsilon$ *is a sectorial operator, and the spectrum of* A_ϵ *consists of the eigenvalues* $\lambda^{\pm}_{k,\epsilon} = \lambda^{\pm}(\epsilon \cdot \tau_k)$ *for* $k \in \mathbb{N}$*, where* $\lambda^{\pm}$ *is given as in the above Lemma 3.2.1. The eigenfunctions corresponding to* $\lambda^{\pm}_{k,\epsilon}$ *are given by* $\Psi^{\pm}_{k,\epsilon} = \phi_k \cdot V^{\pm}_{k,\epsilon}$*, where* $V^{\pm}_{k,\epsilon} = V^{\pm}(\epsilon \cdot \tau_k)$ *and* $V^{\pm}(\cdot)$ *was defined in Lemma 3.2.2. These eigenfunctions form a complete set in* $\mathbb{X}$*.*

There exists a phase space in which System 3.1 generates a nonlinear semiflow. The main point of the following discussion is to describe the phase space in a meaningful way and provide verification of the final hypotheses. To this end, Proposition 3.2.1 assists in giving a useful description of the phase space and associated norm. First, consider the following space.

Definition 3.2.5 (The space $\mathbb{H}^s_*(\Omega)$, [55, Definition 4.1])**.** *Assume that Assumptions 3.1.1 and 3.1.3 are satisfied and consider the spaces* $\mathbb{H}^s(\Omega) \subset \mathbb{L}^2(\Omega)$ *defined in Definition 3.2.3.*

For $s \in (0,2)$, let $H^s_*(\Omega)$ denote the closure of the span of the set $\{\phi_k : k \in \mathbb{N}\}$ with respect to the norm $||\cdot||_{H^s(\Omega)}$ of the fractional Sobolev space $H^s(\Omega)$, where the functions ϕ_k are the eigenfunctions of Definition 3.2.4. Let $\mathbb{H}^s_*(\Omega) = H^s_*(\Omega \times H^s_*(\Omega)$, equipped with the norm $||\cdot||_{\mathbb{H}^s(\Omega)}$ defined by $||(u,v)||^2_{\mathbb{H}^s(\Omega)} = ||(u)||^2_{\mathbb{H}^s(\Omega)} + ||(v)||^2_{\mathbb{H}^s(\Omega)}$.

Proposition 3.2.1 is used to define $||\cdot||_*$ on $\mathbb{H}^s_*$. For $U \in \mathbb{L}^2(\Omega)$, U can be expressed as

$$U = \sum_{k=1}^{\infty} \left(\alpha_k^+ \cdot V_{k,\epsilon}^+ + \alpha_k^- \cdot V_{k,\epsilon}^- \right) \cdot \phi_k. \tag{3.17}$$

The norm is defined as

$$||U||^2_* = \sum_{k=1}^{\infty} (1+\tau_k)^s \cdot \left(\left(\alpha_k^+\right)^2 + \left(\alpha_k^-\right)^2 \right), \tag{3.18}$$

when the sum on the left hand side is finite. This norm is equivalent to the standard Sobolev norm as indicated in the following lemma.

Lemma 3.2.3 (Characterization of $\mathbb{H}^s_*(\Omega)$, [55, Lemma 4.2])**.** *Assume that Assumptions 3.1.1 and 3.1.3 are satisfied. Then $U \in \mathbb{L}^2(\Omega)$ of the form in (3.17) is contained in the space $\mathbb{H}^s_*(\Omega)$ if and only if $||U||_* < \infty$. Furthermore, the $||\cdot||_*$ norm is equivalent to the standard norm $||\cdot||_{\mathbb{H}^s(\Omega)}$.*

Lemma 3.2.3 is used to help define the fractional power spaces $\mathbb{X}^{\alpha,\epsilon}$ of A_ϵ. These power spaces are given in the next proposition.

Proposition 3.2.2 (Properties of $\mathbb{X}^{\alpha,\epsilon}$, [55, Proposition 4.3])**.** *Assume that Assumptions 3.1.1 and 3.1.3 are satisfied, and consider the linear operator A_ϵ from Proposition 3.2.1. Choose a constant $a > \lambda^+_{max}$, with λ^+_{max} as in Lemma 3.2.1, and for some $\alpha \in (0,1)$ consider the fractional power space $\mathbb{X}^{\alpha,\epsilon} = D((aI - A_\epsilon)^\alpha)$. Let $||\cdot||_{\alpha,\epsilon}$ denote the standard norm on $\mathbb{X}^{\alpha,\epsilon}$ given by $||U||_{\alpha,\epsilon} = ||(aI - A_\epsilon)^\alpha U||_{\mathbb{L}^2(\Omega)}$.*

Then for every $0 < \epsilon \leq 1$ we have $\mathbb{X}^{\alpha,\epsilon} = \mathbb{H}^{2\alpha}_*(\Omega)$, and the norm $||\cdot||_{\alpha,\epsilon}$ is equivalent to the norm $||\cdot||_*$ introduced in Lemma 3.2.3 (with $s = 2\alpha$).

By Proposition 3.2.2, the fractional power space $\mathbb{X}^{\alpha,\epsilon}$ is algebraically and topologically independent of ϵ, so the superscript ϵ is omitted.

The second hypothesis, (H2), can now be verified. To decompose the phase space $\mathbb{X}$, begin with choosing constants

$$\underline{c}^{--} < \bar{c}^{--} \ll 0 \ll \underline{c}^{-} < \bar{c}^{-} < \underline{c}^{+} < \bar{c}^{+} < \lambda^{+}_{max}, \tag{3.19}$$

such that $\bar{c}^{--} - \underline{c}^{--}$, $\bar{c}^{-} - \underline{c}^{-}$, and $\bar{c}^{+} - \underline{c}^{+}$ are small. The following corollary gives the decomposition of the spectrum of A_ϵ.

Corollary 3.2.1 (Decomposition of the Spectrum, [55, Corollary 5.2])**.** *Suppose that both Assumptions 3.1.1 and 3.1.3 are satisfied. Then there exist intervals*

$$J^{--}_\epsilon = [a^{--}_\epsilon, b^{--}_\epsilon] \subset [\underline{c}^{--}, \bar{c}^{--}], \tag{3.20}$$

$$J^{-}_\epsilon = [a^{-}_\epsilon, b^{-}_\epsilon] \subset [\underline{c}^{-}, \bar{c}^{-}], \tag{3.21}$$

$$J^{+}_\epsilon = [a^{+}_\epsilon, b^{+}_\epsilon] \subset [\underline{c}^{+}, \bar{c}^{+}], \tag{3.22}$$

and an $\epsilon-$independent constant $d > 0$ such that for sufficiently small $\epsilon > 0$ the following holds. The intervals J^{--}_ϵ, J^{-}_ϵ, and J^{+}_ϵ are contained in the resolvent set of A_ϵ. Each of them has length at least $d \cdot \epsilon^{\dim\Omega/2}$, and each component of the complement of their union contains at least one eigenvalue of A_ϵ. Finally, the largest eigenvalue of A_ϵ less than a^{--}_ϵ is at least distance $d \cdot \epsilon^{\dim\Omega/2}$ from a^{--}_ϵ.

This corollary leads to the following decomposition of the phase space.

Definition 3.2.6 (Decomposition of Phase Space, [55, Definition 5.3])**.** *Consider the intervals as defined by (3.20) - (3.22). Define the intervals $I^{--}_\epsilon = (-\infty, a^{--}_\epsilon)$, $I^{-}_\epsilon = (b^{--}_\epsilon, a^{-}_\epsilon)$,*

$I_\epsilon^+ = (b_\epsilon^-, a_\epsilon^+)$ *and* $I_\epsilon^{++} = (b_\epsilon^+, \lambda_{max}^+]$. *Denote* $\mathbb{X}_\epsilon^{--}$, $\mathbb{X}_\epsilon^-$, $\mathbb{X}_\epsilon^+$, $\mathbb{X}_\epsilon^{++}$ *as the span of the eigenfunctions whose eigenvalues belong to* I_ϵ^{--}, I_ϵ^-, I_ϵ^+, *and* I_ϵ^{++}, *respectively.*

Proposition 3.2.1 shows that A_ϵ generates an analytic semigroup $S_\epsilon(t)$, $t \geq 0$, on $\mathbb{X}$. The next proposition shows that the semigroup associated with the linear system satisfies several required dichotomy estimates, completing the verification of (H2).

Proposition 3.2.3 (Dichotomy Estimates, [55, Proposition 5.4])**.** *Assume that both Assumptions 3.1.1 and 3.1.3 are satisfied, and let* $A_\epsilon : \mathbb{X} \to \mathbb{X}$ *be as in Definition 3.2.3. Let* $S_\epsilon(t), t \geq 0$, *denote the analytic semigroup on* $\mathbb{X}$ *generated by* A_ϵ, *and let* $\mathbb{X}^\alpha = \mathbb{H}_*^{2\alpha}(\Omega)$ *be the fractional power space of Proposition 3.2.2, equipped with the norm* $||\cdot||_*$.

Then, using the notation and definitions in Corollary 3.2.1 and Definition 3.2.6, for all sufficiently small $\epsilon > 0$ *the following hold:*

(a) The spaces $\mathbb{X}_\epsilon^-$, $\mathbb{X}_\epsilon^+$, *and* $\mathbb{X}_\epsilon^{++}$ *are finite-dimensional subspaces of* $\mathbb{X}^\alpha$ *with dimensions proportional to* $\epsilon^{-\dim\Omega/2}$. *Furthermore, all of the spaces introduced in Definition 3.2.6 are invariant under* $S_\epsilon(t)$, *and we denote the restrictions of the semigroup* $S_\epsilon(t)$ *to these spaces by the appropriate superscripts.*

(b) The following estimates are satisfied for arbitrary $U^{++} \in \mathbb{X}_\epsilon^{++}$, $U^+ \in \mathbb{X}_\epsilon^+$, $U^- \in \mathbb{X}_\epsilon^-$, *and* $U_*^{--} \in \mathbb{X}_\epsilon^{--} \cap \mathbb{X}^\alpha$*:*

$$\left|\left|S_\epsilon^{++}(t)U^{++}\right|\right|_* \leq e^{b_\epsilon^+ t} \cdot \left|\left|U^{++}\right|\right|_*, \text{ for } t \leq 0,$$

$$\left|\left|S_\epsilon^{+}(t)U^{+}\right|\right|_* \leq e^{a_\epsilon^+ t} \cdot \left|\left|U^{+}\right|\right|_*, \text{ for } t \geq 0,$$

$$\left|\left|S_\epsilon^{+}(t)U^{+}\right|\right|_* \leq e^{b_\epsilon^- t} \cdot \left|\left|U^{+}\right|\right|_*, \text{ for } t \leq 0,$$

$$\left|\left|S_\epsilon^{-}(t)U^{-}\right|\right|_* \leq e^{a_\epsilon^- t} \cdot \left|\left|U^{-}\right|\right|_*, \text{ for } t \geq 0,$$

$$\left|\left|S_\epsilon^{-}(t)U^{-}\right|\right|_* \leq e^{b_\epsilon^{--} t} \cdot \left|\left|U^{-}\right|\right|_*, \text{ for } t \leq 0,$$

$$\left|\left|S_\epsilon^{--}(t)U_*^{--}\right|\right|_* \leq e^{a_\epsilon^{--} t} \cdot \left|\left|U_*^{--}\right|\right|_*, \text{ for } t \geq 0,$$

There exists a constant $M_\epsilon^{--} > 0$ *such that for* $U^{--} \in \mathbb{X}_\epsilon^{--}$,

$$\left|\left|S_\epsilon^{--}(t)U^{--}\right|\right|_* \leq M_\epsilon^{--} \cdot t^{-\alpha} \cdot e^{a_\epsilon^{--}t} \cdot \left|\left|U^{--}\right|\right|_{\mathbb{L}^2(\Omega} \text{ for } t > 0. \tag{3.23}$$

Moreover, for some $\epsilon-$*independent constant* $C > 0$ *we have*

$$M_\epsilon^{--} \leq C \cdot \epsilon^{-\alpha\cdot(2+\dim\Omega)/2} \text{ as } \epsilon \to 0.$$

Notice that due to the finite dimensions of $\mathbb{X}_\epsilon^-$, $\mathbb{X}_\epsilon^+$, *and* $\mathbb{X}_\epsilon^{++}$ *the linear semigroups* $S_\epsilon^-(t)$, $S_\epsilon^+(t)$, *and* $S_\epsilon^{++}(t)$ *can be extended to groups.*

(c) There exists a constant $M_{\alpha,\epsilon} \geq 1$ *which is proportional to* $\epsilon^{-\alpha}$ *as* $\epsilon \to 0$, *as well as an* $\epsilon-$*independent constant* $C > 0$ *such that for all* $U \in \mathbb{X}_\epsilon^- \oplus \mathbb{X}_\epsilon^+ \oplus \mathbb{X}_\epsilon^{++}$ *we have*

$$C \cdot ||U||_{\mathbb{L}^2(\Omega)} \leq ||\, U||_* \leq M_{\alpha,\epsilon} \cdot ||U||_{\mathbb{L}^2(\Omega)}.$$

The differentiability of F as required by (H3) is verified with the following lemma.

Lemma 3.2.4 (Properties of F, [55, Lemma 5.5])**.** *Suppose that both Assumptions 3.1.1 - 3.1.3 are satisfied, and let* h *be defined as in (3.13). Furthermore, for arbitrary* $U = (u, v) \in \mathbb{X}^\alpha$ *let* $F(U) = h(u, v)$. *Then for every* α *satisfying* $\dim\Omega/4 < \alpha < 1$, *this defines a nonlinear mapping* $F : \mathbb{X}^\alpha \to \mathbb{X}$ *which is continuously Fréchet differentiable. Furthermore, there exist positive constants* C *and* R_0 *such that for any* $0 < R \leq R_0$ *the following holds. For arbitrary* $U, V \in \mathbb{X}^\alpha$ *with*

$$||U - (\bar{u}_0, \bar{v}_0)||_* \leq R \text{ and } ||V - (\bar{u}_0, \bar{v}_0)||_* \leq R,$$

we have

$$||F(U) - F(V)||_{\mathbb{X}} \leq C \cdot R^\delta \cdot ||U - V||_*.$$

The previous lemma provided the final verification needed for hypotheses (H1) - (H3). The following theorem is a more formal statement of the result given by Theorem 3.1.1. In the proof, Sander and Wanner noted that although the original theory of [41] made use of pairwise orthogonal spaces, the spaces introduced in Definition 3.2.6 are not so. However, inspection of the proofs in [41] revealed that the orthogonality was not necessary. Rather, it is sufficient to assume that the angle between any two subspaces in Definition 3.2.6 is bounded away from 0 for all $0 < \epsilon \leq \epsilon_0$, since this implies the boundedness of the corresponding projection operators. Lemma 3.2.2 ensures that this condition is satisfied.

Theorem 3.2.1 ([55, Theorem 5.7])**.** *Consider the reaction-diffusion system 3.1 and assume that Assumptions 3.1.1 - 3.1.3 are satisfied. Furthermore, assume that* $\dim\Omega/4 < \alpha < 1$*, let* $\mathbb{X}^\alpha$ *be as in Proposition 3.2.2, and choose and fix* $0 < p \ll 1$ *and* $0 < d_0 \ll 1$*. Then there exists a positive constant* ϵ_0*, so that for all* $0 < \epsilon \leq \epsilon_0$ *there exist* $0 < r_\epsilon < R_\epsilon$ *such that with* $\rho_\epsilon = d_0 \cdot R_\epsilon$ *the following is true:*

(a) The constants r_ϵ *and* R_ϵ *are proportional to* $\epsilon^{(2\alpha+\dim\Omega)/(2\delta)}$ *as* $\epsilon \to 0$*.*

(b) The ball $\mathbb{B}_{R_\epsilon}(\bar{u}_0, \bar{v}_0) \subset \mathbb{X}^\alpha$ *contains a finite-dimensional inertial manifold* $\mathcal{N}_\epsilon$ *passing through* $(\bar{u}_0, \bar{v}_0)$ *which exponentially attracts all solutions of System 3.1 originating near the homogeneous equilibrium. Furthermore, the manifold* $\mathcal{N}_\epsilon$ *is of class* C^1*; it is tangent to* $\mathbb{X}_\epsilon^- \oplus \mathbb{X}_\epsilon^+ \oplus \mathbb{X}_\epsilon^{++}$ *at* $(\bar{u}_0, \bar{v}_0)$*, and it carries a natural Lebesgue measure induced by this tangent space.*

(c) Denote the dominating subspace $\mathbb{X}_\epsilon^+ \oplus \mathbb{X}_\epsilon^{++}$ *as* $\mathscr{Y}_\epsilon^+$*. Let* $\mathbb{M}_{r_\epsilon}$ *denote the set of all initial conditions in* $\mathcal{N}_\epsilon \cap \mathbb{B}_{r_\epsilon}(\bar{u}_0, \bar{v}_0)$ *whose corresponding solution of System 3.1 either remains in the larger ball* $\mathbb{B}_{R_\epsilon}(\bar{u}_0, \bar{v}_0)$ *for all positive time, or has distance greater than* ρ_ϵ *from* $(\bar{u}_0, \bar{v}_0) + \mathscr{Y}_\epsilon^+$ *upon exiting* $\mathbb{B}_{R_\epsilon}(\bar{u}_0, \bar{v}_0)$*. Then*

$$\frac{vol(\mathbb{M}_{r_\epsilon})}{vol(\mathbb{B}_{r_\epsilon}(\bar{u}_0, \bar{v}_0) \cap \mathcal{N}_\epsilon)} \leq p,$$

where vol denotes the canonical Lebesgue measure on $\mathcal{N}_\epsilon$.

3.3 Almost Linear Behavior

At the end of the early pattern formation process, most solutions of System 3.1 with initial conditions close to the homogeneous equilibrium will leave the ball $\mathbb{B}_{R_\epsilon}(\bar{u}_0, \bar{v}_0)$ close to the dominating subspace $\mathscr{Y}_\epsilon^+$. The solutions will tend to remain close to the solutions of the linearized system since these solutions enter into a region of phase space in which the nonlinearity has very little effect. For this region, consider

$$\mathscr{Y}_\epsilon^+ = \mathbb{X}_\epsilon^+ \oplus \mathbb{X}_\epsilon^{++} \subset \mathbb{X}^\alpha, \mathscr{Y}_\epsilon^- = (\mathbb{X}_\epsilon^{--} \cap \mathbb{X}^\alpha) \oplus \mathbb{X}_\epsilon^- \subset \mathbb{X}^\alpha, \tag{3.24}$$

and the cones $(\bar{u}_0, \bar{v}_0) + \mathcal{K}_\zeta \subset \mathbb{X}^\alpha$, where

$$\mathcal{K}_\zeta = \{U \in \mathbb{X}^\alpha : ||U_-||_* \leq \zeta \cdot ||U_+||_* , U = U_+ + U_- \in \mathscr{Y}_\epsilon^+ \oplus \mathscr{Y}_\epsilon^-\}, \tag{3.25}$$

for $\zeta > 0$. The following proposition shows that size of F is small on the cones for large distances away from the homogeneous equilibrium. One important assumption needed to prove this result is that the $L^\infty-$norm of the eigenfunctions ϕ_k is uniformly bounded.

Proposition 3.3.1 (Smallness of F, [55, Proposition 6.2])**.** *Suppose that Assumptions 3.1.1 - 3.1.3 are satisfied, and let* h *be defined as in (3.13). For* $U = (u, v) \in \mathbb{X}^\alpha$ *define* $F(U) = h(u, v)$. *Finally, let* $\dim\Omega/4 < \alpha < 1$ *and* $\zeta_0 > 0$ *be arbitrary, and set*

$$\zeta_\epsilon = \zeta_0 \cdot \epsilon^{\alpha - \dim\Omega/4}. \tag{3.26}$$

Then there exist $\epsilon-$*independent constants* $M_1, M_2 > 0$ *such that for every* $0 < \epsilon \leq 1$ *and every* $U \in \mathcal{K}_{\zeta_\epsilon}$ *with*

$$||U||_* \leq M_1 \cdot \epsilon^{-\alpha + \dim\Omega/4} \tag{3.27}$$

we have

$$||F((\bar{u}_0, \bar{v}_0) + U)||_{\mathbb{L}^2(\Omega)} \leq M_2 \cdot \epsilon^{(\alpha - \dim\Omega/4)\cdot(\delta+1)} \cdot ||U||_*^{\delta+1}. \tag{3.28}$$

The constants M_1 and M_2 depend only on h, ζ_0 and Ω.

Using Proposition 3.3.1, the following more formal statement of Theorem 3.1.2 is verified.

Theorem 3.3.1 ([55, Theorem 6.3])**.** *Consider the reaction diffusion system 3.1 and assume that Assumptions 3.1.1 - 3.1.3 are satisfied. Assume that the* $\dim\Omega/4 < \alpha < 1$*, let $\mathbb{X}^\alpha$ be as in Proposition 3.2.2, and choose and fix $\zeta_0 \in (0, \frac{1}{2})$ and $0 < \rho \ll 1$. Then there exist constants $D > 0$ and $0 \ll \underline{c}^- < \bar{c}^- < \lambda_{max}^+$ such that for the splitting of $\mathbb{X}^\alpha$ defined in (3.24) and Definition 3.2.6, and for all $\epsilon \in (0, 1]$ the following is true. If $U_0 \in (\bar{u}_0, \bar{v}_0) + \mathcal{K}_{\zeta_\epsilon}$, with $\zeta_\epsilon = \zeta_0 \cdot \epsilon^{\alpha - \dim\Omega/4}$, is any initial condition satisfying*

$$0 < ||U_0 - (\bar{u}_0, \bar{v}_0)||_* \leq \min\{1, (D \cdot \epsilon^{-(\alpha - \dim\Omega/4) + \alpha/\delta + \rho})^{1/(1-\rho)}\}, \tag{3.29}$$

and if U and U_{lin} denote the solutions of the nonlinear equation (3.1) and the linearized equation (3.9) originating at U_0 and $U_0 - (\bar{u}_0, \bar{v}_0)$, respectively, then there exists a time $T > 0$ such that the following first occurs:

$$||U(T) - (\bar{u}_0, \bar{v}_0)||_* = D \cdot \epsilon^{-(\alpha - \dim\Omega/4) + \alpha/\delta + \rho} \cdot ||U_0 - (\bar{u}_0, \bar{v}_0)||_*^\rho. \tag{3.30}$$

For all $t \in [0, T]$ we have

$$\frac{||U(t) - (\bar{u}_0, \bar{v}_0) - U_{lin}(t)||_*}{||U_{lin}(t)||_*} \leq \frac{\zeta_0}{2} \cdot \epsilon^{\alpha - \dim\Omega/4}. \tag{3.31}$$

Chapter 4: Main Theoretical and Computational Results

The purpose of this chapter is to provide the results describing the almost linear behavior of the scaled system

$$u_t = \epsilon(\beta\Delta u + (1-\beta)(J * u - \hat{J}_0)) + f(u,v),$$

$$v_t = d\epsilon(\beta\Delta v + (1-\beta)(J * v - \hat{J}_0)) + g(u,v), \tag{4.1}$$

subject to periodic boundary conditions [53]. For a kernel J such that $\epsilon^{\theta}\cdot J$ is $\epsilon-$independent, analytic results describing the almost linear behavior for System 4.1 with $0 < \beta \leq 1$ are provided for cases in which $\theta < 1$. For $\theta = 1$ and $0 < \beta <\ 1$, we apply the same techniques that were used for the $\theta < 1$ case. In particular, we show that the nonlinearity no longer possesses an $\epsilon-$dependent bound that ensures its smallness for large distances away from the homogeneous equilibrium. If the nonlinearity does not have a small norm value, then it can greatly influence solutions. We provide numerics that show poor agreement between the solutions and their linearized counterparts, which is a consequence of the increased influence of the nonlinearity.

4.1 Preliminaries

In this section, assumptions are stated about the geometry of the domain, the kernel type, the smoothness of the nonlinearity and the type of instability exhibited by the homogeneous equilibrium. The domain is assumed to be rectangular. Along with periodic boundary conditions, this allows for the spectrum of the local diffusion operator, $-\Delta$ to be explicitly stated. Assumptions of smoothness and periodicity of kernel functions makes it possible to

describe the spectrum of the nonlocal operator, $u \mapsto -\hat{J}_0 u + J * u$. In Section 4.2, the results are combined to describe the spectrum of the linearized right hand side of System 4.1.

Assumption 4.1.1 (Rectangular domain)**.** *Let Ω be a closed rectangular subset of R^n for $n \in \{1, 2, 3\}$.*

Definition 4.1.1 (Spectrum of -Δ)**.** *Suppose that Ω satisfies Assumption 4.1.1. Let $L^2_{per}(\Omega)$ be the space of periodic functions that belong to $L^2(\Omega)$. For $\Delta : L^2_{per}(\Omega) \to L^2_{per}(\Omega)$, denote the ordered sequence of eigenvalues of -Δ as $0 = \kappa_0 < \kappa_1 \leq ... \to \infty$ [2, Section 1.3.1]. Denote the corresponding real-valued L^2-orthonormalized eigenfunctions by ψ_k, for $k \in \mathbb{N}$.*

An important aspect of Definition 4.1.1 is that if $J \in L^2_{per}(\Omega)$, we can define the Fourier series for J as

$$J_N(x) = \sum_{k=0}^{N} \hat{J}_k \psi_k(x), \tag{4.2}$$

where

$$\hat{J}_k = \int_\Omega J(x)\psi_k(x)dx. \tag{4.3}$$

Note that if $J \in C^1(\bar{\Omega})$, then $J_N \to J$ uniformly. See [35].

Definition 4.1.2 (Smoothly periodic onΩ) **.** *Suppose that Ω satisfies Assumption 4.1.1. A function $f : \Omega \to \mathbb{R}$ is said to be smoothly periodic on Ω if it is periodic with respect to the boundary $\partial\Omega$ and can be extended to a smooth function on $\mathbb{R}^n$.*

As an example, $f : \Omega \to \mathbb{R}$ is smoothly periodic on Ω where $\Omega = [a, b] \times [c, d]$, then

$$f(a, y) = f(b, y) \text{ where } y \in [c, d],$$

$$f(x, c) = f(x, d) \text{ where } x \in [a, b],$$

and the extension function $F : \mathbb{R}^2 \to \mathbb{R}$ such that $F(x, y) = f(x, y)$ on $\Omega$and

$$F(x, y) = F(x + (b - a), y) = F(x, y + (d - c)).$$

is smooth.

Assumption 4.1.2 (Kernel)**.** *Suppose that Ω satisfies Assumption 4.1.1. Let the kernel $J \in C^1(\bar{\Omega})$ be such that $\epsilon^\theta \cdot J$ is $\epsilon-$independent, where $\theta \in \mathbb{R}$, and $\epsilon^\theta \cdot J$ is smoothly periodic on Ω. Furthermore, $\hat{J}_0 > \hat{J}_k$ for all $k > 0$.*

Assumption 4.1.2 establishes a kernel J such $\epsilon^\theta \cdot J$ remains fixed with respect to ϵ^θ. The presence of the θ allows us to explore the almost linear behavior for the following three cases: $\theta < 1$, $\theta = 1$ and $\theta > 1$. The analysis proceeds by first describing the case $\theta < 1$ in its entirety. For the remainder of the section, continuing through to Section 4.3, we shall only look at this case. However, as some of the initial framework can be applied to other θ values, we indicate which results are true for larger θ values when relevant.

The convolution operator of a whole-space function on the whole space is well defined, whereas the convolution of functions on Ω are not. In the following definition, the convolution of J on Ω is specified to be the convolution with respect to the periodic extension of J.

Definition 4.1.3. *Suppose that J satisfies Assumption 4.1.2 with $\theta \in \mathbb{R}$ and that the periodic extension of J is given as J_{per}. The convolution of J and u is defined as*

$$J_c(u) = J * u = \int_\Omega J_{per}(x - y)u(y)dy,$$

where $J_c : L^2_{per}(\Omega) \to L^2_{per}(\Omega)$.

We now compute the adjoint of J_c. This will be used in Section 4.2 to describe the spectrum of the linearization of System 4.1. Let J_{per} be the smooth periodic extension of

J. We begin by defining A_{per} such that

$$A_{per}(x) = J_{per}(-x). \tag{4.4}$$

The convolution of A with u is given by

$$A_c(u) = A * u = \int_\Omega A_{per}(y-x)u(x)dx. \tag{4.5}$$

The following lemma shows that the adjoint of J_c is equal to A_c.

Lemma 4.1.1. *Suppose that Assumptions 4.1.1 - 4.1.2 are satisfied with $\theta \in \mathbb{R}$ and A_c is defined as in (4.5). The adjoint of J_c is A_c.*

Proof. Let $u, v \in L^2_{per}(\Omega)$. Computing the inner product directly gives

$$\begin{aligned}(J_c(u), v) &= \int_\Omega J_c(u(x)) \cdot v(y)\ dy, \\ &= \int_\Omega \int_\Omega J_{per}(y-x) \cdot u(x) \cdot v(y)\ dx\ dy.\end{aligned}$$

Switching the order of integration, we have

$$\begin{aligned}(J_c(u), v) &= \int_\Omega \int_\Omega J_{per}(y-x) \cdot u(x) \cdot v(y)\ dy\ dx, \\ &= \int_\Omega u(x) \left(\int_\Omega J_{per}(y-x) \cdot v(y)\ dy \right)\ dx, \\ &= \int_\Omega u(x) \left(\int_\Omega A_{per}(x-y) \cdot v(y)\ dy \right)\ dx, \\ &= (u, A_c(v)).\end{aligned}$$

□

By Lemma 4.1.1, in order to guarantee that J_c is self-adjoint, we must use an even kernel function. The following definition describes what it means for functions mapping from $\mathbb{R}^n$ to $\mathbb{R}$ to be even.

Definition 4.1.4. *Let $T : \mathbb{R}^n \to \mathbb{R}$ and $x = (x_1, x_2, ..., x_n) \in \mathbb{R}^n$. The function T is even if for each $x_i < 0$, $0 \leq i \leq n$,*

$$T(x_1, x_2, ..., x_i, ..., x_n) = T(-x_1, -x_2, ..., -x_i, ..., -x_n).$$

Assumption 4.1.3. *Suppose that J_{per} is even.*

Lemma 4.1.2. *Suppose that Assumptions 4.1.1 - 4.1.3 are satisfied with $\theta \in \mathbb{R}$ and A_c is defined as in (4.5). J_c is a self-adjoint operator.*

Proof. By Lemma 4.1.1, A_c is the adjoint operator of J_c. Since J is such that J_{per} satisfies Assumption 4.1.3, $J_{per}(x) = J_{per}(-x)$. Thus $A_c = J_c$ and J_c is self-adjoint. □

Note that Lemma 4.1.2 implies that $\hat{J}_k \in \mathbb{R}$. Furthermore, as pointed out in [25], the convolution of J with u has the same eigenfunctions as $-\Delta$. The next lemma gives the full spectrum of J_c.

Lemma 4.1.3 (Spectrum of J_c)**.** *Suppose that Ω satisfies Assumption 4.1.1, and that J satisfies Assumptions 4.1.2 - 4.1.3 with $\theta \in \mathbb{R}$. Then the following statements are true:*

1) $\hat{J}_k \to 0$ as $k \to \infty$.

2) The spectrum of J_c contains only the $\hat{J}_k$ and 0, where 0 is a limit point of the $\hat{J}_k$.

Proof. For part 1, $J \in C^1(\bar{\Omega})$ implies that $\hat{J}_k \to 0$ as $k \to \infty$. See [35, Chapter 1, Section 4.3]. We have that J_c is a compact operator on a Banach space [52, Theorem 8.3]. Therefore, the spectrum of J_c contains only the eigenvalues J_k and its limit point 0 [1, Theorem 7.3]. □

Lemma 4.1.3 shows that the spectrum of J_c only contains 0 and $\hat{J}_k$. However, we need to understand how the spectrum of J_c is affected by the addition of the term $-\hat{J}_0$. Before we give the spectrum of $J_c - \hat{J}_0$, we need to prove one more lemma that helps to characterize the residual spectrum of an operator in terms of the eigenvalues of its adjoint.

Lemma 4.1.4. *Let X be a Hilbert space and $H : X \to X$ a linear operator. The residual spectrum of H contains only eigenvalues of the adjoint of H if and only if H and its adjoint H^* do not have the same set of eigenvalues.*

Proof. Suppose that the residual spectrum of H is nonempty. For λ in the residual spectrum, there exists an $f \in (R(H - \lambda I))^\perp$ such that $0 = ((H - \lambda I)g, f)$ for all $g \in X$. By definition of the adjoint, we have that $0 = (g, (H^* - \lambda I)f)$ for all $g \in X$. Thus, λ is an eigenvalue of H^*, but not an eigenvalue of H.

Now suppose that λ^* is an eigenvalue of H^*, but not an eigenvalue of H. Let E^* be the corresponding eigenfunction of H^*. For any $f \in X$, we have that $0 = (f, (H^* - \lambda^* I)E^*) = ((\mathcal{H}_\epsilon - \lambda_k^* I) \cdot f, E_k^*)$. This shows that $E_k^* \in R((\mathcal{H}_\epsilon - \lambda^*))^\perp$, which shows that the range of $H - \lambda^*$ is not dense in X. Thus, λ^* is in the residual spectrum of H. □

The next lemma shows that although we shift 0 and $\hat{J}_k$ by $-\hat{J}_0$, there is no qualitative change to the spectrum of J_c. Specifically, the residual spectrum of $J_c - \hat{J}_0$ remains empty.

Lemma 4.1.5 (Spectrum of $J_c - \hat{J}_0$)**.** *Suppose that Ω satisfies Assumption 4.1.1, and that J satisfies Assumptions 4.1.2 - 4.1.3 with $\theta \in \mathbb{R}$. The spectrum of $J_c - \hat{J}_0$ contains the eigenvalues $\hat{J}_k - \hat{J}_0$ and the limit point $-\hat{J}_0$.*

Proof. Observe that we obtain the point and continuous spectra of $\hat{J}_c - \hat{J}_0$ by shifting the point and continuous spectra of J_c by $-\hat{J}_0$. Since $J_c - \hat{J}_0$ is self-adjoint, $J_c - \hat{J}_0$ and its adjoint have the same eigenvalues. Lemma 4.1.4 shows that the residual spectrum of $J_c - \hat{J}_0$ is empty. □

Assumption 4.1.4 (Smoothness of the nonlinearity and a homogeneous equilibrium)**.** *Let $\chi \in \mathbb{N}$ be arbitrary. Assume that $f, g : \mathbb{R}^2 \to \mathbb{R}$ are $C^{1+\chi}$-functions, and that there exists a point $(\bar{u}_0, \bar{v}_0) \in \mathbb{R}^2$ with $f(\bar{u}_0, \bar{v}_0) = g(\bar{u}_0, \bar{v}_0) = 0$. If $\chi \geq 2$, assume further that the partial derivatives of f and g of order $2, 3, ..., \chi$ at the $(\bar{u}_0, \bar{v}_0)$ vanish.*

Assumption 4.1.4 implies that $(\bar{u}_0, \bar{v}_0)$ is a homogeneous equilibrium for System 4.1.

Assumption 4.1.5 (Turing instability)**.** *Suppose that f and g satisfy Assumption 4.1.4 and that the homogeneous equilibrium of System 4.1 exhibits Turing instability. That is, in the absence of nonlocal and local diffusion terms, the homogeneous equilibrium is stable, but in the presence of the nonlocal and local diffusion terms, it is stable.*

The following lemma gives necessary and sufficient conditions for Turing instability. For proof, see [44].

Lemma 4.1.6 (Turing Instability Conditions)**.** *The homogeneous equilibrium of System 4.1 exhibits Turing instability. This is true if and only there exists $d > 0$ be such that*

1) $f_u + g_v < 0$,

2) $f_u g_v - f_v g_u > 0$,

3) $df_u + g_v > 0$,

4) $(df_u + g_v)^2 - 4d(f_u g_v - f_v g_u) > 0$,

where the partials are evaluated at the homogeneous equilibrium $(\bar{u}_0, \bar{v}_0)$.

The first two conditions in this lemma ensure the stability of the homogeneous equilibrium in the absence of diffusion. The next two conditions ensure that the homogeneous equilibrium is unstable when diffusion is present. Note that the first and third conditions show that $d > 1$. We make one more assumption about the eigenvalues of the linearization to guarantee that the eigenvalues are real.

Assumption 4.1.6 (Real eigenvalues for the nonlinearity)**.** *Suppose that f and g satisfy Assumption 4.1.4. Suppose that*

$$(f_u + g_v)^2 - 4(f_u g_v - f_v g_u) > 0.$$

This section is concluded with definitions of the function spaces that provide the context for the results of this chapter.

Definition 4.1.5 (Function Spaces)**.** *Let $L^2(\Omega)$ be the space of smoothly periodic functions on Ω that belong to $L^2(\Omega)$ as defined by Definition 4.1.1. Let*

$$\mathbb{L}^2_{per}(\Omega) = L^2_{per}(\Omega) \times L^2_{per}(\Omega). \tag{4.6}$$

For $s > 0$, let $H^s(\Omega)$ be the standard fractional Sobolev space for real-valued functions. Let

$$\mathbb{H}^s_{per}(\Omega) = H^s_{per}(\Omega) \times H^s_{per}(\Omega). \tag{4.7}$$

4.2 Properties of the linearization

In this section, we state and derive explicit representations for the eigenvalues and eigenfunctions of the linearized right hand side of System 4.1. For $0 < \beta \leq 1$ and $\theta < 1$, we show that if Assumptions 4.1.1 - 4.1.6 are satisfied, then there exists an ϵ_0 such that for $0 < \epsilon \leq \epsilon_0$, the homogeneous equilibrium will be unstable.

The following system is the linearized form of System 4.1:

$$U' = \epsilon D \mathcal{J} U + BU, \tag{4.8}$$

where

$$D = \begin{pmatrix} 1 & 0 \\ 0 & d \end{pmatrix}, \tag{4.9}$$

$$\mathcal{J} = \mathcal{J}_1 + \mathcal{J}_2 \tag{4.10}$$

$$\mathcal{J}_1 = \beta \begin{pmatrix} \Delta & 0 \\ 0 & \Delta \end{pmatrix} \tag{4.11}$$

$$\mathcal{J}_2 = (1-\beta) \begin{pmatrix} J_c & 0 \\ 0 & J_c \end{pmatrix}, \tag{4.12}$$

$$B = \begin{pmatrix} f_u(\bar{u}_0, \bar{v}_0) & f_v(\bar{u}_0, \bar{v}_0) \\ g_u(\bar{u}_0, \bar{v}_0) & g_v(\bar{u}_0, \bar{v}_0) \end{pmatrix}, \tag{4.13}$$

for $U = (u, v)^T$. For the sake of notation, we shall denote this operator as

$$\mathcal{H}_\epsilon = \epsilon D\mathcal{J} + B, \tag{4.14}$$

where $\mathcal{H}_\epsilon : \mathbb{L}^2_{per}(\Omega) \to \mathbb{L}^2_{per}(\Omega)$. The domains for the local and nonlocal operators are given respectively as $D(\Delta) = H^2_{per}(\Omega)$ and $D(J_c) = L^2_{per}(\Omega)$. Thus, for $0 < \beta \leq 1$, the domain of $\mathcal{H}_\epsilon$ is given as $D(\mathcal{H}_\epsilon) = H^2_{per}(\Omega)$ and for $\beta = 0$, $D(\mathcal{H}_\epsilon) = \mathbb{L}^2_{per}(\Omega)$.

The asymptotic growth of the eigenvalues of the negative Laplacian and J_c is important for our results. Since both the negative Laplacian and J_c have the same set of eigenfunctions,

the eigenvalues of $-\beta\Delta - (1-\beta)(J_c - \hat{J}_0)$ are given as

$$\nu_k = \beta\kappa_k + (1-\beta)(\hat{J}_0 - \hat{J}_k), \tag{4.15}$$

where $k \in \mathbb{N}$. Here, the κ_k are the eigenvalues of $-\Delta$ as defined in Definition 4.1.1 and the $\hat{J}_k$ are the eigenvalues of J_c as defined by Equation 4.3. Note that ν_k is real since κ_k and $\hat{J}_k$ are real. For rectangular domains, the growth of eigenvalues of the negative Laplacian are given as

$$\kappa_k \sim k^{2/n}, \tag{4.16}$$

where $n = \dim \Omega$ [13]. Since $J \in C^1(\bar{\Omega})$, application of Lemma 4.1.3 shows that

$$\hat{J}_0 - \hat{J}_k \sim \hat{J}_0. \tag{4.17}$$

Thus, we see that if $\beta > 0$,

$$\nu_k \sim k^{2/n}, \tag{4.18}$$

and if $\beta = 0$,

$$\nu_k \sim \hat{J}_0. \tag{4.19}$$

Lemma 4.2.1 (Eigenvalues of $\mathcal{H}_\epsilon$)**.** *Suppose that Assumptions 4.1.1 - 4.1.6 are satisfied with $\theta \in \mathbb{R}$. The eigenvalues of $\mathcal{H}_\epsilon$ are*

$$\lambda_k^{\pm} = \lambda^{\pm}(\epsilon\nu_k) = \frac{b_k(\epsilon\nu_k) \pm \sqrt{(b_k(\epsilon\nu_k)^2 - 4c_k(\epsilon\nu_k)}}{2}, \tag{4.20}$$

where $\lambda_k^{\pm} \in \mathbb{R}$ *and*

$$b_k = b(\epsilon\nu_k) = (f_u + g_v) - (d+1)(\epsilon\nu_k) \tag{4.21}$$

$$c_k = c(\epsilon\nu_k) = (f_u g_v - g_u f_v) - (df_u + g_v)(\epsilon\nu_k) + d(\epsilon\nu_k)^2, \tag{4.22}$$

and ν_k *are the eigenvalues* $-\beta\Delta - (1-\beta)(J_c - \hat{J}_0)$*. The eigenfunctions of* $\mathcal{H}_\epsilon$ *are the given as* $\Psi_{k,\epsilon}^{\pm} = E^{\pm}(\epsilon\nu_k) \cdot \psi_k$*, where* $E^{\pm}(\epsilon\nu_k)$ *are eigenfunctions of* $B - \epsilon\nu_k D$*. If* $\beta = 0$*, then* $\lambda^{\pm}(\epsilon \cdot \nu_k) \to \lambda^{\pm}(\epsilon \cdot \hat{J}_0)$ *as* $k \to \infty$*.*

Proof. We begin by showing that any eigenvalue of $\mathcal{H}_\epsilon$ is expressible as $\lambda_k^{\pm}$ for some k. Let λ and U be an eigenvalue and corresponding eigenfunction of $\mathcal{H}_\epsilon$, respectively, where $U \in \mathbb{L}^2_{per}(\Omega)$ and $U \neq (0,0)$. We can write $U \in \mathbb{L}^2_{per}(\Omega)$ as

$$U = \sum_{j=0}^{\infty} \psi_j r_j,$$

where $r_j = (s_j, t_j)^T$ and $s_j, t_j \in \mathbb{R}$. Since U is nontrivial, then for $j = k$, $r_j \neq (0,0)^T$. Since λ is an eigenvalue of $\mathcal{H}_\epsilon$, and U is the corresponding eigenfunction,

$$\mathcal{H}_\epsilon U - \lambda U = 0.$$

Using Equation 4.14, we evaluate the left hand side as

$$\begin{aligned}\mathcal{H}_\epsilon U - \lambda U &= \sum_{j=0}^{\infty} \psi_j (\epsilon D\mathcal{J} + B - \lambda I) r_j \\ &= \sum_{j=0}^{\infty} \psi_j (-\epsilon\nu_j D + B - \lambda I) r_j.\end{aligned}$$

Since the ψ_j are linearly independent,

$$(-\epsilon\nu_j D + B - \lambda I)r_j = 0,$$

for all j. For $j = k$, we see that r_k is nontrivial, which implies that $-\epsilon\nu_k D + B - \lambda I$ must be singular. Therefore, we have that

$$|-\epsilon\nu_k D + B - \lambda I| = 0.$$

Solving for λ gives the result.

Let $\lambda_k^{\pm}$ be as given by Equation 4.20 and $E^{\pm}(\epsilon\nu_k)$ be the associated eigenfunction of $B - \epsilon\nu_k D$. To show that $\lambda_k^{\pm}$ is an eigenvalue of $\mathcal{H}_\epsilon$ and$\Psi\ {}^{\pm}_{k,\epsilon}$ is an eigenvector of $\mathcal{H}_\epsilon$, we compute

$$\begin{aligned}\mathcal{H}_\epsilon \Psi^{\pm}_{k,\epsilon} &= \epsilon D\mathcal{J}\Psi^{\pm}_{k,\epsilon} + B\Psi^{\pm}_{k,\epsilon} \\ &= \lambda^{\pm}_{k,\epsilon} E^{\pm}_{k,\epsilon}\psi_k \\ &= \lambda^{\pm}_{k,\epsilon}\Psi^{\pm}_{k,\epsilon}\end{aligned}$$

As $k \to \infty$, Lemma 4.1.3 shows that $\hat{J}_k \to 0$. Thus, $\lambda^{\pm}(\epsilon\nu_k) \to \lambda^{\pm}(\hat{J}_0)$. Assumption 4.1.6 implies that $\lambda_k^{\pm} \in \mathbb{R}$. □

Remark 4.2.1. *We need to understand how the $\hat{J}_0 - \hat{J}_k$ are affecting the κ_k. Figure 4.1 shows exactly what is happening to the eigenvalues of the pure nonlocal case. Notice that as $\epsilon \to 0$, we see that the $\epsilon \cdot \hat{J}_k \to 0$. Now consider the ν_k given in (4.15) for another fixed β where $0 < \beta \leq 1$. The $\epsilon(\hat{J}_0 - \hat{J}_k)$ form a bounded sequence, while the $\epsilon\kappa_k$ form an unbounded sequence. As ϵ is decreased, we are adding the increasingly negligible $\epsilon(\hat{J}_0 - \hat{J}_k)$ to the $\epsilon\kappa_k$ to form the sequence $\epsilon\nu_k$. We know this is true since $\theta < 1$, meaning that the $\epsilon(\hat{J}_0 - \hat{J}_k)$ must move to the right toward 0. We see that for $\theta < 1$, the eigenvalues of the mixed*

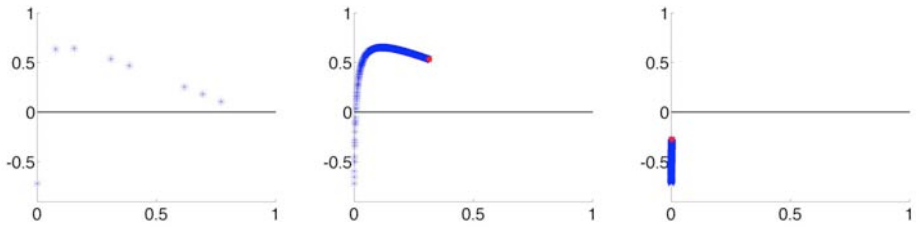

(a) Large ϵ (b) Medium ϵ (c) Small ϵ

Figure 4.1: The eigenvalues lie on a dispersion curve as a function of $\epsilon\nu_k$, where the ν_k are the eigenvalues of the nonlocal diffusion operator and $\theta < 1$. For θ, see Assumption 4.1.2. These eigenvalues are given as black asterisks and $\lambda^+(\epsilon\hat{J}_0)$ is given as a red asterisk. In Subfigure (a), the eigenvalues are sparsely distributed on the curve when ϵ is large. In Subfigure (b), as ϵ grows, the eigenvalues are more closely spaced. Since $\beta = 0$, the values limit on the point $\lambda^+(\epsilon \cdot \hat{J}_0)$. As $\epsilon \to 0$ in Subfigure (c), the eigenvalues lie on the leftmost part of the curve where all of the eigenvalues are negative.

diffusion operator become more like the eigenvalues of the pure local diffusion operator. In other words, as $\epsilon \to 0$, $\epsilon\nu_k$ behave asymptotically like $\epsilon\kappa_k$ for $0 < \beta \leq 1$. We will use this similarity to establish the main result for $\theta < 1$.

For the analysis of $\lambda_k^{\pm}$, we replace $\epsilon\nu_k$ in Equation 4.20 with the continuous variable $s \in \mathbb{R}_0$. If d is such that Assumption 4.1.5 and 4.1.6 are valid, then the $\lambda^{\pm}(s)$ have particular algebraic properties that we describe with the following lemma.

Lemma 4.2.2. *Suppose that Assumptions 4.1.5 and 4.1.6 are satisfied. The following properties of $\lambda^{\pm}(s)$ are true for $s \geq 0$:*

- $\lambda^-(s) < \lambda^+(s)$.
- $\lambda^+(0) < 0$.
- $\lambda^+(s)$ *has a unique maximum* λ^+_{max}.
- $\lambda^+(s)$ *has two real roots,* s_l *and* s_r.
- $\lambda^-(s)$ *is strictly decreasing with* $\lambda^-(s) < 0$.
- $\lim_{s\to\infty}(\lambda^+(s)/s) = -1$.

- $\lim_{s\to\infty}(\lambda^-(s)/s) = -d.$

Proof. The proof follows exactly as that given in Lemma 3.2.1. Application of Inequalities (1), (3) of Lemma 4.1.6 and Assumption 4.1.6 give that $b_k^2 - 4c_k > 0$ for every $s \geq 0$. Part (1) of Lemma 4.1.6 shows that $b_k(s) < 0$ for all $s \geq 0$, and therefore, $\lambda^-(s) < 0$. For $\lambda^+(s) > 0$, then $c_k(s) < 0$. Parts (2) - (4) of Lemma 4.1.6 show that $c_k(s) < 0$ is equivalent to $s_l < s < s_r$, where

$$s_{l/r} = \frac{1}{2d}((df_u + g_v) \mp \sqrt{(df_u + g_v)^2 - 4d(f_u g_v - f_v g_u)})$$

Computing the asymptotic limits for $\lambda^{\pm}(s)/s$ gives the final part of the lemma. □

The next lemma shows that for $0 \leq \beta \leq 1$, the eigenfunctions$\Psi^{\pm}_{k,\epsilon}$ defined in Lemma 4.2.1 form a complete set for $\mathbb{X} = \mathbb{L}^2_{per}(\Omega) \times \mathbb{L}^2_{per}(\Omega)$. Furthermore, the angle between the the eigenfunctions are bounded away from π and 0.

Lemma 4.2.3. *Suppose that Assumptions 4.1.1 - 4.1.6 are satisfied with $\theta \in \mathbb{R}$. For $0 \leq \beta \leq 1$, the eigenfunctions of $\mathcal{H}_\epsilon$ form a complete set for $\mathbb{X}$. The angle between $E^{\pm}_{k,\epsilon}$ is bounded away from π and 0.*

Proof. The eigenfunctions are given by$\Psi^{\pm}_{k,\epsilon} = E^{\pm}_{k,\epsilon} \cdot \psi_k$, where $E^{\pm}_{k,\epsilon} = E^{\pm}(\epsilon \cdot \nu_k)$ and $E^{\pm}(\cdot)$ is defined by Lemma 4.2.1. By Lemma 4.2.2, we see that for each $s \geq 0$, $\lambda^+(s) < \lambda^-(s)$. Thus, the eigenvectors $E^{\pm}(s)$ are linearly independent for all $s \geq 0$. However, we are only interested in the discrete points of s in which $s = \epsilon \cdot \nu_k$. All that is left to show is that $\epsilon \cdot \nu_k \geq 0$ for all $k \geq 0$. By Assumption 4.1.2, $\epsilon(1-\beta)(\hat{J}_0 - \hat{J}_k) \geq 0$ for $0 \leq \beta \leq 1$. Definition 4.1.1 shows that $\kappa_k > 0$ for all $k \geq 0$. Since $\nu_k = \beta\kappa_k + (1-\beta)(\hat{J}_0 - \hat{J}_k) \geq 0$, we have shown the first part of this lemma. The$\Psi^{\pm}_{k,\epsilon}$ form a complete set in $\mathbb{X}$ since the ψ_k form a complete set for $L^2(\Omega)$ and the $E^{\pm}_{k,\epsilon}$ are linearly independent.

Since the eigenfunctions of $B - sD$ are the same as $s^{-1}B - D$, we see that as $s \to \infty$,

$s^{-1}B - D$ approaches a diagonal matrix. Hence, the eigenfunctions become orthogonal as $s \to \infty$ and are bounded away from 0 and π. □

We now use these properties to show that System 4.1 with $0 < \beta \leq 1$ is unstable for $0 < \epsilon \leq \epsilon_0$. The details follow the proof given in [55, Lemma 5.1].

Lemma 4.2.4. *Suppose that Assumptions 4.1.2 with $\theta < 1$, 4.1.5 and 4.1.6 are satisfied. For $0 < \beta \leq 1$, there exists $\epsilon_0 > 0$, such that for all $\epsilon \leq \epsilon_0$, the homogeneous equilibrium of System 4.1 is unstable.*

Proof. Let $0 < \beta \leq 1$, $\theta < 1$, and choose $0 < c_1 < c_2 < \lambda^+_{max}$, where λ^+_{max} is given in Lemma 4.2.2. By Lemma 4.2.2 and Lemma 4.2.3, there exists a compact interval I such that $\lambda^+_{k,\epsilon} \in [c_1, c_2]$ if and only if $\epsilon \cdot \nu_k \epsilon^{-1} I$. The interval I is the union of two compact sets. Using the asymptotic distribution of eigenvalues ν_k given in (4.18), we see that as $\epsilon \to 0$, the number of eigenvalues of $\mathcal{H}_\epsilon$ in $[c_1, c_2]$ is of the order $\epsilon^{-\dim\Omega/2}$. Thus, for some ϵ_0, we have that the homogeneous equilibrium is unstable for $0 < \epsilon \leq \epsilon_0$. □

4.2.1 Spectrum of the linear operator

The results presented in the following sections depend upon the spectrum of $\mathcal{H}_\epsilon$ and its associated spectral gaps. For this reason, we describe the full spectrum of $\mathcal{H}_\epsilon$ for all $0 \leq \beta \leq 1$. We begin with a theorem describing the spectrum of $\mathcal{H}_\epsilon$, followed by useful lemmas used in proving the theorem and finally the proof.

Theorem 4.2.1 (Spectrum of $\mathcal{H}_\epsilon$)**.** *Suppose that Assumptions 4.1.1 - 4.1.6 are satisfied with $\theta \in \mathbb{R}$. Let $\mathcal{H}_\epsilon$ be as defined in (4.14). If $0 < \beta \leq 1$, the spectrum contains only the eigenvalues of $\mathcal{H}_\epsilon$. If $\beta = 0$, then the spectrum of $\mathcal{H}_\epsilon$ consists of the eigenvalues $\mathcal{H}_\epsilon$ and the points $\lambda^{\pm}(\epsilon \hat{J}_0)$.*

Theorem 4.2.1 shows that for $\beta = 0$, the spectrum of $\mathcal{H}_\epsilon$ contains only eigenvalues of $\mathcal{H}_\epsilon$ and two points in the continuous spectrum. In [30], a sufficient condition is given that states for certain self-adjoint operators defined on Hilbert spaces, all points of the spectrum

are expressible as limit points of eigenvalues. Theorem 4.2.1 shows that in general, it is not necessary for an operator to be self-adjoint. Theorem 4.2.1 also shows a fundamental difference between the spectrum of $\mathcal{H}_\epsilon$ for $0 < \beta \leq 1$ and $\beta = 0$. For $0 < \beta \leq 1$, only eigenvalues are present in the spectrum. However, for $\beta = 0$, $\mathcal{H}_\epsilon$ contains a nonempty continuous spectrum.

We introduce a norm that will be useful for the spectrum computation. As we show in the next lemma, the equivalence the $\mathbb{L}^2$-norm and this new norm is possible since the angle between the $E^{\pm}_{k,\epsilon}$ are bounded away from both 0 and π.

Definition 4.2.1. *Let $\epsilon > 0$. For $U \in \mathbb{L}^2_{per}(\Omega)$, Lemma 4.2.3 implies that U may be written as*

$$U = \sum_{k=0}^{\infty} \left((\alpha^+_{k,\epsilon}) E^+_{k,\epsilon} + (\alpha^-_{k,\epsilon}) E^-_{k,\epsilon} \right) \cdot \psi_k. \tag{4.23}$$

When the following is finite, define the $||\cdot||_{\#}-$norm is defined as

$$||U||^2_{\#} = \sum_{k=0}^{\infty} \left((\alpha^+_{k,\epsilon})^2 + (\alpha^-_{k,\epsilon})^2 \right). \tag{4.24}$$

Lemma 4.2.5. *Suppose that Assumptions 4.1.1 - 4.1.6 are satisfied with $\theta \in \mathbb{R}$. Let $||\cdot||_{\#}$ be as defined in Definition 4.2.1. For $U \in \mathbb{L}^2_{per}(\Omega)$,*

$$\sqrt{1-r}\, ||U||_{\#} \leq || U||_{\mathbb{L}^2_{per}(\Omega)} \leq \sqrt{1+r}\, ||U||_{\#},$$

where $\left| \left(E^+_{k,\epsilon}, E^-_{k,\epsilon} \right)_{\mathbb{R}^2} \right| \leq r < 1$ for all $k \in \mathbb{Z}$.

Proof. Let $\epsilon > 0$. For $U \in \mathbb{L}^2_{per}(\Omega)$, we write U as

$$U = \sum_{k=0}^{\infty} \left((\alpha^+_{k,\epsilon}) E^+_{k,\epsilon} + (\alpha^-_{k,\epsilon}) E^-_{k,\epsilon} \right) \cdot \psi_k.$$

Note that r exists by Lemma 4.2.3. Computing the square of the $\mathbb{L}^2_{per}(\Omega)$-norm of U yields

$$\begin{aligned}
||U||^2_{\mathbb{L}^2_{per}(\Omega)} &= \sum_{k=0}^{\infty}((\alpha^+_{k,\epsilon})^2 + (\alpha^-_{k,\epsilon})^2 + 2\alpha^+_{k,\epsilon}\alpha^-_{k,\epsilon}(E^+_{k,\epsilon}, E^-_{k,\epsilon})), \\
&\leq \sum_{k=0}^{\infty}((\alpha^+_{k,\epsilon})^2 + (\alpha^-_{k,\epsilon})^2) + 2\left|\alpha^+_{k,\epsilon}\alpha^-_{k,\epsilon}\right| r, \\
&\leq \sum_{k=0}^{\infty}(\alpha^+_{k,\epsilon})^2 + (\alpha^-_{k,\epsilon})^2 + r((\alpha^+_{k,\epsilon})^2 + (\alpha^-_{k,\epsilon})^2) \\
&= (1+r)\sum_{k=0}^{\infty}(\alpha^+_{k,\epsilon})^2 + (\alpha^-_{k,\epsilon})^2, \\
&= (1+r)\,||U||^2_{\#}\,.
\end{aligned}$$

Taking square roots gives the right hand inequality. For the other direction, we compute

$$\begin{aligned}
||U||^2_{\mathbb{L}^2(\Omega)} &\geq \sum_{k=0}^{\infty}(\alpha^+_{k,\epsilon})^2 + (\alpha^-_{k,\epsilon})^2 - \left((\alpha^+_{k,\epsilon})^2 + (\alpha^-_{k,\epsilon})^2\right)(E^+_{k,\epsilon}, E^-_{k,\epsilon})), \\
&\geq (1-r)\,||U||^2_{\#}\,.
\end{aligned}$$

Again, taking square roots gives the left hand inequality. □

The following lemma gives the adjoint of $\mathcal{H}_\epsilon$, which will allow us to describe the full spectrum of $\mathcal{H}_\epsilon$ for $\beta = 0$.

Lemma 4.2.6. *Suppose that Assumptions 4.1.1 - 4.1.2 are satisfied with $\theta \in \mathbb{R}$. Let $\mathcal{H}_\epsilon$ be as defined in (4.14). The adjoint of $\mathcal{H}_\epsilon$ is given as $\mathcal{H}^*_\epsilon = \epsilon D\mathcal{A} + B^T$, where*

$$\mathcal{A} = \begin{pmatrix} A_c & 0 \\ 0 & A_c \end{pmatrix},$$

and A_c is as defined in (4.5). If the periodic extension of J satisfies Assumption 4.1.3, then the adjoint of $\mathcal{H}_\epsilon$ is given as $\mathcal{H}_\epsilon^* = \epsilon D\mathcal{J} + B^T$.

Proof. Let $\epsilon > 0$. Application of Lemma 4.1.1 shows that the adjoint of $\epsilon D\mathcal{J}$ is $\epsilon D\mathcal{A}$. Since the adjoint of B is B^T, the adjoint of $\mathcal{H}_\epsilon$ is given as $\mathcal{H}_\epsilon^* = \epsilon D\mathcal{A} + B^T$. On the other hand if J_{per} satisfies Assumption 4.1.3, then J_c is self-adjoint by Lemma 4.1.1 and the adjoint of $\mathcal{H}_\epsilon$ is given as $\mathcal{H}_\epsilon^* = \epsilon D\mathcal{J} + B^T$. □

We are now ready to prove Theorem 4.2.1 that describes the full spectrum of $\mathcal{H}_\epsilon$ for all $0 \leq \beta \leq 1$.

Proof of Theorem 4.2.1. Let $0 < \beta \leq 1$. Recall that $\mathcal{J} = \mathcal{J}_1 + \mathcal{J}_2$ as defined in Equations (4.10) - (5.5). Since $\epsilon D\mathcal{J}_1 + B$ has a compact resolvent, its spectrum contains only eigenvalues [47]. The operator $\epsilon D\mathcal{J} + B$ also has a compact resolvent, since $\epsilon D\mathcal{J}_1 + B$ has a compact resolvent and $\epsilon D\mathcal{J}_2$ is a bounded operator. See [16, pg. 120]. Since the resolvent is compact, then for $0 < \beta \leq 1$, the spectrum of $\mathcal{H}_\epsilon$ contains only eigenvalues [34, pg. 187]. For the remainder of this proof, we focus on the case $\beta = 0$.

A value λ is in the spectrum of $\mathcal{H}_\epsilon$ is either in the point spectrum, continuous spectrum or residual spectrum. We have already computed the eigenvalues of $\mathcal{H}_\epsilon$, which implies that the point spectrum of $\mathcal{H}_\epsilon$ is nonempty. We now show that the residual spectrum must be empty. Since $\mathcal{J}$ is self-adjoint, then by similar reasoning used in the proof of the eigenvalues of $\mathcal{H}_\epsilon$, we have that the eigenvalues of $\mathcal{H}_\epsilon^*$ are given as the roots of

$$det(B^T - (\epsilon\hat{J}_k)D - \lambda_k^{*\pm} I) = 0. \tag{4.25}$$

Since the determinant of a matrix is the same as the determinant of the transpose of that matrix, we have

$$det(B^T - (\epsilon\hat{J}_k)D - \lambda_k^{*\pm} I) = det(B - (\epsilon\hat{J}_k)D - \lambda_k^{\pm} I). \tag{4.26}$$

Thus, the eigenvalues of $\mathcal{H}_\epsilon^*$ are the same as those of $\mathcal{H}_\epsilon$. By Lemma 4.1.4, the residual spectrum of $\mathcal{H}_\epsilon$ is empty.

The last portion of the spectrum to check is the continuous spectrum. We now show that both $\lambda^{\pm}(\epsilon\hat{J}_0)$ are contained in the continuous spectrum. The proof for $\lambda^{-}(\epsilon\hat{J}_0)$ follows in the same manner as the proof for $\lambda^{+}(\epsilon\hat{J}_0)$, so we only give proof for $\lambda^{+}(\epsilon\hat{J}_0)$. Consider $\lambda^{+}(\epsilon\hat{J}_0)I - \mathcal{H}_\epsilon$ and let $f_k = \Psi^{+}_{k,\epsilon} / \left|\left|\Psi^{+}_{k,\epsilon}\right|\right|_{\mathbb{L}^2_{per}(\Omega)}$ where the$\Psi^{+}_{k,\epsilon}$ are eigenfunctions of $\mathcal{H}_\epsilon$. Since $\lambda^{+}(\epsilon\hat{J}_0)$ is not an eigenvalue of $\mathcal{H}_\epsilon$, we have that $\lambda^{+}(\epsilon\hat{J}_0)I - \mathcal{H}_\epsilon$ is one-to-one. Thus,

$$\begin{aligned}\left|\left|(\lambda^{+}(\epsilon\hat{J}_0)I - \mathcal{H}_\epsilon)f_k\right|\right|_{\mathbb{L}^2_{per}(\Omega)} &= \left|\left|(\lambda^{+}(\epsilon\hat{J}_0) - \lambda^{+}_{k,\epsilon})f_k\right|\right|_{\mathbb{L}^2_{per}(\Omega)} \\ &\leq \left|\lambda^{+}(\epsilon\hat{J}_0) - \lambda^{+}_{k,\epsilon}\right|\end{aligned}$$

As $k \to \infty$, $\lambda^{+}_{k,\epsilon} \to \lambda^{+}(\epsilon\hat{J}_0)$ and

$$\left|\left|(\lambda^{+}(\epsilon\hat{J}_0)I - \mathcal{H}_\epsilon)f_k\right|\right|_{\mathbb{L}^2_{per}(\Omega)} \to 0.$$

Since $||f_k||_{\mathbb{L}^2_{per}(\Omega)} = 1$ for all k and $\left|\left|(\lambda^{+}(\epsilon\hat{J}_0)I - \mathcal{H}_\epsilon)f_k\right|\right|_{\mathbb{L}^2_{per}(\Omega)} \to 0$, we see that $(\lambda^{+}(\epsilon\hat{J}_0)I - \mathcal{H}_\epsilon)^{-1}$ is unbounded. Thus, $\lambda^{\pm}(\epsilon\hat{J}_0)$ is in the continuous spectrum of $\mathcal{H}_\epsilon$.

For the continuous spectrum, we have shown that the limit points of the eigenvalues are elements of this set. We now show that the points in the continuous spectrum must be limit points of the eigenvalues. To do this, we will argue by contradiction. Suppose that λ is in the continuous spectrum, but that it is not a limit point of eigenvalues of $\mathcal{H}_\epsilon$. Since the $||\cdot||_{\#}$ is equivalent to the $\mathbb{L}^2-$norm by Lemma 4.2.5, we have that for some sequence of $f_n \in \mathbb{L}^2_{per}(\Omega)$ with $||f_n||_{\#} = 1$ for all n, $||(\lambda I - \mathcal{H}_\epsilon)f_n||_{\#} \to 0$ as $n \to \infty$. Since $f_n \in \mathbb{L}^2_{per}(\Omega)$,

we can write f_n as

$$f_n = \sum_{k=0}^{\infty}((\alpha^+_{n,k,\epsilon})E^+_{k,\epsilon} + (\alpha^-_{n,k,\epsilon})E^-_{k,\epsilon}) \cdot \psi_k.$$

By definition of the continuous spectrum, λ can not be an eigenvalue. Since we assumed that it is also not a limit point of eigenvalues, there exists $M > 0$ such that $M \leq \left|\lambda - \lambda^{\pm}_{k,\epsilon}\right|$ for all k. Computing the following estimate gives

$$\begin{aligned}
||(\lambda I - \mathcal{H}_\epsilon)f_n||^2_{\#} &= \sum_{k=0}^{\infty}(\lambda - \lambda^+_{k,\epsilon})^2(\alpha^+_{n,k,\epsilon})^2 + (\lambda - \lambda^-_{k,\epsilon})^2(\alpha^-_{n,k,\epsilon})^2, \\
&\geq M^2 \sum_{k=0}^{\infty}((\alpha^+_{n,k,\epsilon})^2 + (\alpha^-_{n,k,\epsilon})^2), \\
&= M^2 \, ||f_n||^2_{\#} = M^2 > 0.
\end{aligned}$$

However, this is a contradiction, since $||(\lambda I - \mathcal{H}_\epsilon)f_n||_{\#} \to 0$. Therefore, the continuous spectrum of $\mathcal{H}_\epsilon$ contains only $\lambda^{\pm}(\epsilon\hat{J}_0)$. □

4.3 Almost linear behavior for the mixed case with $\theta < 1$

We show how the linearization is used to describe the behavior of solutions. Again, these results will first be given with respect to $\theta < 1$, where θ is given in Assumption 4.1.2. The major result is proven by two theorems, one for early pattern selection and another for later pattern selection. The first theorem uses the linearization of System 4.1 to describe the process of early pattern selection in the following way. See also Figure 4.2. If solutions (u, v) have initial conditions (u_0, v_0) that are contained within an initial ϵ neighborhood of the homogeneous equilibrium $(\bar{u}_0, \bar{v}_0)$, then with a high probability, they will exit a larger ϵ neighborhood very close to a highly unstable space. This subspace consists of those eigenfunctions of the linearization corresponding to the most unstable eigenvalues.

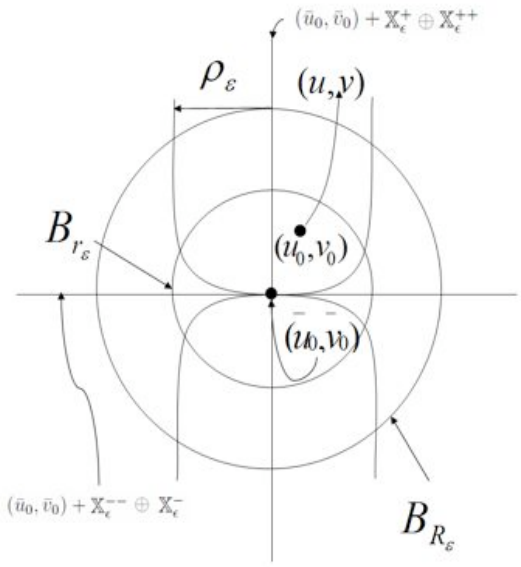

Figure 4.2: Schematic depicting early pattern formation as described in Theorem 4.3.1. The initial condition (u_0, v_0) of the solution (u, v) is within a parabolic region surrounding the unstable subspace spanned by the eigenfunctions of the most unstable eigenvalues. For most solutions with this type of initial conditions, the solutions remain close to the unstable space during the early stage of pattern formation.

At the end of the early pattern formation stage, solutions that satisfy a particular cone condition will enter into a region of phase space in which the nonlinear effects are negligible. With the nonlinearity diminished, solutions for large distances away from the homogeneous equilibrium can be described reasonably well with the linearization. This behavior of solutions during this stage of pattern development is referred to as almost linear.

To prove these results, we use the abstract theory and techniques developed for the Cahn-Hilliard equation found in [40,41]. The theory requires an abstract evolution equation of the form

$$U_t = \mathcal{H}_\epsilon U + F(U), \tag{4.27}$$

on some appropriate function space $\mathbb{X}$ that satisfies the following assumptions.

(H1) The operator $-\mathcal{H}_\epsilon$ is a sectorial operator on $\mathbb{X}$.

(H2) There exists a decomposition $\mathbb{X} = \mathbb{X}^{--} \oplus \mathbb{X}^{-} \oplus \mathbb{X}^{+} \oplus \mathbb{X}^{++}$, such that all of these subspaces are finite except $\mathbb{X}^{--}$, and such that the linear semigroup corresponding to $U_t = \mathcal{H}_\epsilon U$ satisfies several dichotomy estimates.

(H3) The nonlinearity $F : \mathbb{X}^\alpha \to \mathbb{X}$ is continuously differentiable, and satisfies both $F(\bar{u}_0, \bar{v}_0) = 0$ and $DF(\bar{u}_0, \bar{v}_0) = 0$.

In light of how $\mathcal{H}_\epsilon$ is defined in (4.14), we define the nonlinearity of the evolution equation given by 4.27 in the following way. Define the function $h : \mathbb{R}^2 \to \mathbb{R}^2$ to be the nonlinear part of (f, g) of System 4.1. Furthermore, let

$$\hat{h}(u, v) = (f(u, v), g(u, v))$$

and

$$h(u, v) = \hat{h}(u, v) - \hat{h}_u(\bar{u}_0, \bar{v}_0) \cdot (u - \bar{u}_0) - \hat{h}_v(\bar{u}_0, \bar{v}_0) \cdot (v - \bar{v}_0). \tag{4.28}$$

Setting

$$F(U) = h(u, v) \text{ for } U = (u, v) \tag{4.29}$$

gives the nonlinear portion of (4.27). Note that this is also how the nonlinearity was defined in the local setting given by (3.13).

We now briefly describe the implications of the three hypotheses. If the first hypothesis is true, $\mathcal{H}_\epsilon$ is sectorial which implies the existence of an analytic semigroup $S : X \to X$. Using this analytic semigroup, we analyze the behavior of the solutions of the evolution equation given in (4.27). The next hypothesis, (H2), acts to partition $\mathbb{X}$ into subspaces that are are characterized as the most unstable and stable subspaces of $\mathbb{X}$, given as $\mathbb{X}^{--} \oplus \mathbb{X}^{-}$ and $\mathbb{X}^{+} \oplus \mathbb{X}^{++}$, respectively. The behavior of S is described by restricting S to each of the subspaces and verifying dichotomy estimates. If (H3) is satisfied, then $(\bar{u}_0, \bar{v}_0)$ is

the homogeneous equilibrium of the evolution equation. Most importantly, a bound on a global Lipschitz constant of F is established that is necessary to describe certain invariant manifolds that are tangent to $\mathbb{X}^- \oplus \mathbb{X}^+ \oplus \mathbb{X}^{++}$. In fact, if all three hypotheses are true, then by [41, Lemma 2.1], we are guaranteed the existence of such a manifold $\mathcal{N} \subset \mathbb{X}^\alpha$ such that orbits of the evolution equation are exponentially attracted to the orbits in $\mathcal{N}$. Furthermore, this manifold is tangent to the space $\mathbb{X}^- \oplus \mathbb{X}^+ \oplus \mathbb{X}^{++}$. After some transient time, the dynamics of the evolution equation can be described by examining the orbits of this manifold. Using this manifold, Wanner and Maier-Paape showed that with a high probability, solutions beginning in a $r_\epsilon-$neighborhood that leave a larger $R_\epsilon-$neighborhood of the homogeneous equilibrium are contained in a parabolic-shaped region [41, Theorem 2.1]. Furthermore, the solutions do so close to a strongly stable subspace, given by $(\bar{u}_0, \bar{v}_0) + \mathbb{X}^+ \oplus \mathbb{X}^{++}$. Therefore, by verifying that (H1) - (H3) are valid for System 4.1 with $0 \leq \beta < 1$, we show that the early pattern formation process is accurately described in terms of the linearization.

As we have stated, the three hypotheses H1 - H3 are critical to proving the early pattern results, and consequently the later pattern results. The next three lemmas are designed to verify hypotheses H1 - H3.

Lemma 4.3.1. *For System 4.1, suppose that Assumptions 4.1.1 - 4.1.6 are satisfied with $\theta \in \mathbb{R}$ and that $0 < \beta \leq 1$. Let $\mathcal{H}_\epsilon$ be as defined in (4.14). $\mathcal{H}_\epsilon$ is a sectorial operator.*

Proof. For $0 < \beta \leq 1$, again we note that the operator $\epsilon D\mathcal{J}_2$ is a bounded perturbation of $\epsilon D\mathcal{J}_1 + B$, which is a sectorial operator [26]. Thus, $\mathcal{H}_\epsilon$ is sectorial [25, 47]. □

We now seek to verify (H2). To accomplish this, we first need to decompose the phase space $\mathbb{X}$, choose constants

$$\underline{c}^{--} < \bar{c}^{--} \ll 0 \ll \underline{c}^{-} < \bar{c}^{-} < \underline{c}^{+} < \bar{c}^{+} < \lambda^{+}_{max}, \tag{4.30}$$

such that $\bar{c}^{--} - \underline{c}^{--}$, $\bar{c}^{-} - \underline{c}^{-}$, and $\bar{c}^{+} - \underline{c}^{+}$ are small. For fixed $0 < \beta \leq 1$, Equation (4.18) and Lemma 4.2.1 show that the distribution of eigenvalues of $\mathcal{H}_\epsilon$ is asymptotically

the same as that of the local operator considered in [55]. This fact coupled with the validity of Assumptions 4.1.1 - 4.1.6 allows us to apply Corollary 3.2.1 to show the existence of well defined spectral gaps. These gaps are given as

$$J_\epsilon^{--} = [a_\epsilon^{--}, b_\epsilon^{--}] \subset [\underline{c}^{--}, \bar{c}^{--}], \tag{4.31}$$

$$J_\epsilon^{-} = [a_\epsilon^{-}, b_\epsilon^{-}] \subset [\underline{c}^{-}, \bar{c}^{-}], \tag{4.32}$$

$$J_\epsilon^{+} = [a_\epsilon^{+}, b_\epsilon^{+}] \subset [\underline{c}^{+}, \bar{c}^{+}], \tag{4.33}$$

where J_ϵ^{--}, J_ϵ^{-}, and J_ϵ^{+} are contained in the resolvent of $\mathcal{H}_\epsilon$ for sufficiently small ϵ. Furthermore, the length of each of these intervals is at least $d\epsilon^{\dim\Omega/2}$ for some $\epsilon-$independent constant $d > 0$. We now define the decomposition of the phase space. Note that the following decomposition is the same as the decomposition used for the local system subject to homogeneous Neumann boundary conditions. See Definition 3.2.6.

Definition 4.3.1. *Consider the intervals as defined by (4.31) - (4.33). Define the intervals* $I_\epsilon^{--} = (-\infty, a_\epsilon^{--})$, $I_\epsilon^{-} = (b_\epsilon^{--}, a_\epsilon^{-})$, $I_\epsilon^{+} = (b_\epsilon^{-}, a_\epsilon^{+})$ *and* $I_\epsilon^{++} = (b_\epsilon^{+}, \lambda_{max}^{+}]$. *Denote* $\mathbb{X}_\epsilon^{--}$, $\mathbb{X}_\epsilon^{-}$, $\mathbb{X}_\epsilon^{+}$, $\mathbb{X}_\epsilon^{++}$ *as the span of the eigenfunctions whose eigenvalues belong to* I_ϵ^{--}, I_ϵ^{-}, I_ϵ^{+}, *and* I_ϵ^{++}, *respectively.*

Since the theory that we are applying makes use of fractional power spaces of $\mathcal{H}_\epsilon$, we need to discuss these spaces, as well as the norm used. The fractional power spaces are given as $\mathbb{X}^\alpha = D((aI - \mathcal{H}_\epsilon)^\alpha)$ subject to the norm $||U||_\alpha = ||(aI - \mathcal{H}_\epsilon)^\alpha U||_{\mathbb{L}^2(\Omega)}$ for $U \in \mathbb{X}^\alpha$. As pointed out in [25], the fractional power spaces of $\mathcal{H}_\epsilon$ are given as

$$\mathbb{X}^\alpha = \mathbb{H}_{per}^{2\alpha}(\Omega), \tag{4.34}$$

where $H_{per}^{2\alpha}(\Omega)$ are the Sobolev spaces of smoothly periodic functions on Ω and $0 < \alpha < 1$

as defined by Definition 4.1.5. By Lemma 4.2.3, $U \in \mathbb{L}^2_{per}(\Omega)$ is written as

$$U = \sum_{k=0}^{\infty} (\alpha_k^+ E_{k,\epsilon}^+ + \alpha_k^- E_{k,\epsilon}^-)\psi_k.$$

When the following is finite, define $||\cdot||_{**}$ as

$$||U||_{**}^2 = \sum_{k=0}^{\infty} (1+\kappa_k)^s \left((\alpha_k^+)^2 + (\alpha_k^-)^2\right). \tag{4.35}$$

Note that this norm is very similar to the norm defined in (3.18) for the pure local case. If Assumptions 4.1.1 - 4.1.6 are satisfied, then for $0 < \epsilon \leq 1$, $||U||_{**}$ is equivalent to both $||U||_{\mathbb{H}^{2\alpha}_{per}}$ and $||U||_{\alpha}$. Inspection of the proofs of Lemma 3.2.3 and Proposition 3.2.2 respectively, show that the same techniques can be applied to achieve these equivalences in norm. Since $\mathbb{H}^{2\alpha}_{per}(\Omega) \subset \mathbb{H}^{2\alpha}(\Omega)$ and Lemma 3.2.3 in the local case shows that $||\cdot||_*$ is equivalent to $||\cdot||_{\mathbb{H}^{2\alpha}(\Omega)}$, then the norm for the local case $||\cdot||_*$ is also equivalent to the $||\cdot||_{**}$ −norm for the nonlocal case.

We have now established a suitable decomposition of the phase space. We now give the dichotomy estimates and show that they are similarly satisfied as with the local case analyzed in [55].

Lemma 4.3.2. *Let $0 < \beta \leq 1$. Assume that Assumptions 4.1.1, 4.1.2 with $\theta < 1$, 4.1.5, and 4.1.6 are satisfied and let $\mathcal{H}_\epsilon$ be as defined in (4.14). Let $S_\epsilon(t), t \geq 0$ denote the analytic semigroup on $\mathbb{X}$ generated by $\mathcal{H}_\epsilon$. Consider the decomposition as given by Definition 4.3.1 and let $\mathbb{X}^\alpha = \mathbb{H}^{2\alpha}_{per}(\Omega)$ be the fractional power spaces of $\mathcal{H}_\epsilon$.*

(a) The spaces $\mathbb{X}_\epsilon^-$, $\mathbb{X}_\epsilon^+$, and $\mathbb{X}_\epsilon^{++}$ are finite-dimensional subspaces of $\mathbb{X}^\alpha$ with dimensions proportional to $\epsilon^{-\dim\Omega/2}$. Furthermore, all of the spaces introduced in Definition 4.3.1 are invariant under $S_\epsilon(t)$, and we denote the restrictions of the semigroup $S_\epsilon(t)$ to these spaces by the appropriate superscripts.

(b) *The following estimates are satisfied for arbitrary* $U^{++} \in \mathbb{X}_\epsilon^{++}$, $U^{+} \in \mathbb{X}_\epsilon^{+}$, $U^{-} \in \mathbb{X}_\epsilon^{-}$, *and* $U_{**}^{--} \in \mathbb{X}_\epsilon^{--} \cap \mathbb{X}^\alpha$*:*

$$\left|\left|S_\epsilon^{++}(t)U^{++}\right|\right|_{**} \leq e^{b_\epsilon^{+}t} \cdot \left|\left|U^{++}\right|\right|_{**}, \text{ for } t \leq 0,$$

$$\left|\left|S_\epsilon^{+}(t)U^{+}\right|\right|_{**} \leq e^{a_\epsilon^{+}t} \cdot \left|\left|U^{+}\right|\right|_{**}, \text{ for } t \geq 0,$$

$$\left|\left|S_\epsilon^{+}(t)U^{+}\right|\right|_{**} \leq e^{b_\epsilon^{-}t} \cdot \left|\left|U^{+}\right|\right|_{**}, \text{ for } t \leq 0,$$

$$\left|\left|S_\epsilon^{-}(t)U^{-}\right|\right|_{**} \leq e^{a_\epsilon^{-}t} \cdot \left|\left|U^{-}\right|\right|_{**}, \text{ for } t \geq 0,$$

$$\left|\left|S_\epsilon^{-}(t)U^{-}\right|\right|_{**} \leq e^{b_\epsilon^{--}t} \cdot \left|\left|U^{-}\right|\right|_{**}, \text{ for } t \leq 0,$$

$$\left|\left|S_\epsilon^{--}(t)U_{**}^{--}\right|\right|_{**} \leq e^{a_\epsilon^{--}t} \cdot \left|\left|U_{**}^{--}\right|\right|_{**}, \text{ for } t \geq 0,$$

There exists a constant $M_\epsilon^{--} > 0$ *such that for* $U^{--} \in \mathbb{X}_\epsilon^{--}$,

$$\left|\left|S_\epsilon^{--}(t)U^{--}\right|\right|_{**} \leq M_\epsilon^{--} \cdot t^{-\alpha} \cdot e^{a_\epsilon^{--}t} \cdot \left|\left|U^{--}\right|\right|_{\mathbb{L}^2(\Omega} \text{ for } t > 0. \tag{4.36}$$

Moreover, for some $\epsilon-$*independent constant* $C > 0$ *we have*

$$M_\epsilon^{--} \leq C \cdot \epsilon^{-\alpha \cdot (2+\dim\Omega)/2} \text{ as } \epsilon \to 0.$$

(c) *There exists a constant* $M_{\alpha,\epsilon} \geq 1$ *which is proportional to* $\epsilon^{-\alpha}$ *as* $\epsilon \to 0$*, as well as an* $\epsilon-$*independent constant* $C > 0$ *such that for al* $U \in \mathbb{X}_\epsilon^{-} \oplus \mathbb{X}_\epsilon^{+} \oplus \mathbb{X}_\epsilon^{++}$ *we have*

$$C \cdot ||U||_{\mathbb{L}^2(\Omega)} \leq || U||_{**} \leq M_{\alpha,\epsilon} \cdot ||U||_{\mathbb{L}^2(\Omega)}.$$

Proof. Application of Lemma 4.2.2, Definition 4.3.1, and the lower bound estimate of the spectral gaps as $d \cdot \epsilon^{\dim\Omega/2}$ gives the results of part (a). Note that the size of the dimension

of $\mathbb{X}_\epsilon^-$, $\mathbb{X}_\epsilon^+$, and $\mathbb{X}_\epsilon^{++}$ are the same as those of the local case given in Proposition 3.2.3. We attribute this to the similar asymptotic growth rates of the $\Delta$and $\beta\Delta + (1-\beta)\cdot(J_c - \hat{J}_0)$ given by (4.18).

For parts (b) and (c), inspection of the proofs given in Proposition 3.2.3 shows that the results also hold for our situation. Their proofs depend upon knowledge of the asymptotic growth of the eigenvalues of the linearization. Again, since the eigenvalues of the linearization for our case with $0 < \beta \leq 1$ are asymptotically the same as the eigenvalues in their local case, we achieve the same results for the mixed system considered here. □

The final lemma shows that the nonlinearity of the evolution equation is differentiable in the Banach setting. Furthermore, the Lipschitz constant is polynomially bounded.

Lemma 4.3.3 (Properties of F, Lemma 3.2.4)**.** *Let $0 < \beta \leq 1$. Suppose that Assumptions 4.1.1 - 4.1.6 are satisfied with $\theta \in \mathbb{R}$, and let h be defined as in (4.28). Furthermore, for arbitrary $U = (u, v) \in \mathbb{X}^\alpha$ let $F(U) = h(u, v)$. Then for every α satisfying $\dim\Omega/4 < \alpha < 1$ this defines a nonlinear mapping $F : \mathbb{X}^\alpha \to \mathbb{X}$ which is continuously Fréchet differentiable. Furthermore, there exist positive constants C and R_0 such that for any $0 < R \leq R_0$ the following holds. For arbitrary $U, V \in \mathbb{X}^\alpha$ with*

$$||U - (\bar{u}_0, \bar{v}_0)||_{**} \leq R \text{ and } ||V - (\bar{u}_0, \bar{v}_0)||_{**} \leq R,$$

we have

$$||F(U) - F(V)||_{\mathbb{X}} \leq C \cdot R^\chi \cdot ||U - V||_{**}.$$

Proof. The result follows directly from Lemma 3.2.4. Note that χ describes the smoothness of (f, g) as given by Assumption 4.1.4. □

We now have everything that we need to prove the result for early pattern formation.

Theorem 4.3.1 (Early Pattern Formation)**.** *For System 4.1, suppose that Assumptions 4.1.1 - 4.1.6 are satisfied with $\theta < 1$ and that $0 < \beta \leq 1$. Choose α such that $\dim\Omega/4 <$*

$\alpha < 1$ where $\mathbb{X}^\alpha = \mathbb{H}^{2\alpha}_{per}(\Omega)$. For fixed $0 < p \ll 1$ and $0 < d_0 \ll 1$, there exists ϵ_0 such that for $\epsilon \leq \epsilon_0$, there exists $0 < r_\epsilon < R_\epsilon$ with $\rho_\epsilon = d_0 R_\epsilon$ and $0 < r_\epsilon < R_\epsilon \sim \epsilon^{(2\alpha+\dim\Omega)/(2\chi)}$. Furthermore, there exists an invariant manifold $\mathcal{N}_\epsilon$ in which the following is true. Solutions with initial conditions contained in $\mathcal{N}_\epsilon \cap B_{r_\epsilon}(\bar{u}_0, \bar{v}_0)$ leave the ball B_{R_ϵ} with a probability of $1 - p$ and at a distance from $(\bar{u}_0, \bar{v}_0) + \mathbb{X}^+_\epsilon \oplus \mathbb{X}^{++}_\epsilon$ no larger than ρ_ϵ.

Proof of Theorem 4.3.1. Lemmas 4.3.1 - 4.3.3, show that hypotheses H1 - H3 are valid. As pointed out in Theorem 3.2.1, pairwise orthogonality is not required to apply the theory in [41], as long as the angle between any two spaces is bounded away from 0 and π. Since Lemma 4.2.3 shows this to be true, we have verified everything except for the size of r_ϵ and R_ϵ.

Using [41, Remark 3.1, Lemma 3.6], the estimates for $r_\epsilon, R_\epsilon \sim L$, where L is a global Lipschitz constant of the nonlinearity F. By Lemma 4.3.3, we have that the global Lipschitz constant is given as $L = C \cdot R^\chi$, where C, R are constants. As $\epsilon \to 0$, [41, Remark 2.5] gives

$$C \cdot R^\chi \leq \frac{C^{--}_\epsilon C^+_\epsilon}{2C^+_\epsilon + M_{\alpha,\epsilon} C^{--}_\epsilon}, \tag{4.37}$$

where

$$C^+_\epsilon = \frac{\min\left(b^-_\epsilon - a^-_\epsilon, b^+_\epsilon - a^+_\epsilon\right)}{6 + \chi + 1/\chi},$$

and

$$C^{--}_\epsilon = \frac{b^{--}_\epsilon - a^{--}_\epsilon}{2 \cdot M_{\alpha,\epsilon} + 3\sqrt{2} \cdot M^{--}_\epsilon \cdot (b^{--}_\epsilon - a^{--}_\epsilon)^\alpha}.$$

Using Lemma 4.3.2, we have that as $\epsilon \to 0$, $M_{\alpha,\epsilon} = C_1 \cdot \epsilon^{-\alpha}$ and $M^{--}_\epsilon \leq C_2 \cdot \epsilon^{-\alpha - \alpha \dim\Omega/2}$. This implies that

$$C^{--}_\epsilon \geq C_3 \cdot \epsilon^{2\alpha + \dim\Omega/2}, \tag{4.38}$$

and

$$C_\epsilon^+ \geq d \cdot \epsilon^{\dim\Omega/2}. \tag{4.39}$$

Combining Estimates (4.38) and (4.39) with Estimate 4.37, we have

$$R^\chi \leq K \cdot \epsilon^{(2\alpha+\dim\Omega)/2}. \tag{4.40}$$

Since $r_\epsilon, R_\epsilon \sim R^\chi$, we get that $r_\epsilon, R_\epsilon \sim \epsilon^{(2\alpha+\dim\Omega)/(2\chi)}$.

□

Theorem 4.3.1 shows that the addition of the nonlocal term to local diffusion produces similar early pattern results when compared to the pure local case considered in [55]. Lemma 3.2.4 provides an initial estimate for the size of the nonlinearity F. However, this bound is improved in Proposition 3.3.1 and we now discuss the improved estimate as it is essential for the almost linear result. Consider the regions that are given in terms cones $(\bar{u}_0, \bar{v}_0) + \mathcal{K}_\delta$, where

$$\mathcal{K}_\delta = \{U \in \mathbb{X}^\alpha : ||U_-||_{**} \leq \delta \, ||U_+||_{**}, U = U_+ + U_- \in \mathcal{Y}_\epsilon^+ \oplus \mathcal{Y}_\epsilon^-\} \tag{4.41}$$

and

$$\mathcal{Y}_\epsilon^+ = \mathbb{X}_\epsilon^+ \oplus \mathbb{X}_\epsilon^{++} \subset \mathbb{X}^\alpha, \mathcal{Y}_\epsilon^- = \left(\mathbb{X}_\epsilon^{--} \cap \mathbb{X}^\alpha\right) \oplus \mathbb{X}_\epsilon^- \subset \mathbb{X}^\alpha. \tag{4.42}$$

Using these cone regions, the improved bound is given by the following lemma that follows immediately from Proposition 3.3.1.

Lemma 4.3.4. *Suppose that Assumptions 4.1.1 - 4.1.6 are satisfied with $\theta < 1$ and let F*

be as defined in (4.29). For $\dim\Omega/4 < \alpha < 1$ *and* $\delta_0 > 0$*, denote*

$$\delta_\epsilon = \delta_0 \cdot \epsilon^{\alpha - \dim\Omega/4}. \tag{4.43}$$

Then there exists $\epsilon-$*independent constants* M_1*,* $M_2 > 0$ *such that for every* $0 < \epsilon \leq 1$ *and* $U \in \mathcal{K}_{\delta_\epsilon}$*, with*

$$||U||_{**} \leq M_1 \cdot \epsilon^{-\alpha + \dim\Omega/4}, \tag{4.44}$$

we have

$$||F((\bar{u}_0, \bar{v}_0) + U)||_{\mathbb{L}^2(\Omega)} \leq M_2 \epsilon^{(\alpha - \dim\Omega/4)\cdot(\chi+1)}. ||U||_{**}^{\chi+1} \tag{4.45}$$

The order of the zero $(\bar{u}_0, \bar{v}_0)$ *of* F *is given by* χ *in Assumption 4.1.4.*

In other words, if a solution U with initial condition $U_0 \in (\bar{u}_0, \bar{v}_0) + \mathcal{K}_{\delta_\epsilon}$, with $\delta_\epsilon = \delta_0 \cdot \epsilon^{\alpha - \dim\Omega}$, then it is possible for the solution to remain close to $\mathbb{X}_\epsilon^+ \oplus \mathbb{X}_\epsilon^{++}$ for larger distances away from the homogeneous equilibrium compared to the early pattern results. As with the early pattern result, we now give a result that shows the addition of the nonlocal operator does not change the results for the pure local case.

Theorem 4.3.2 (Later Pattern Formation)**.** *Suppose that Assumptions 4.1.1 - 4.1.6 are satisfied with* $\theta < 1$*and choose and fix* $\delta_0 \in (0, \frac{1}{2})$ *and* $0 < \xi \ll 1$*. Let* $\epsilon \in (0, 1]$ *and* $0 < \beta \leq 1$*. Choose* α *such that* $\dim\Omega/4 < \alpha < 1$ *where* $\mathbb{X}^\alpha = \mathbb{H}^{2\alpha}_{per}(\Omega)$*. There exists a constant* D *and splitting of* $\mathbb{X}^\alpha$ *such that the following is true. If* $U_0 \in (\bar{u}_0, \bar{v}_0) + \mathcal{K}_{\delta_\epsilon}$*, with* $\delta_\epsilon = \delta_0 \cdot \epsilon^{\alpha - \dim\Omega}$ *whose initial condition satisfies*

$$0 < ||U_0 - (\bar{u}_0, \bar{v}_0)||_{**} < \min(1, (D\epsilon^{-(\alpha - \dim\Omega/4) + \alpha/\chi + \xi})^{1/(1-\xi)}), \tag{4.46}$$

then for

$$||U(t) - (\bar{u}_0, \bar{v}_0)||_{**} \leq D\epsilon^{-(\alpha - \dim\Omega/4) + \alpha/\chi + \xi} \cdot ||U_0 - (\bar{u}_0, \bar{v}_0)||_{**}^{\xi},$$

then the relative distance of the (u, v) *and* (u_{lin}, v_{lin}) *is bounded by*

$$\frac{||U(t) - (\bar{u}_0, \bar{v}_0) - U_{lin}(t)||_{**}}{||U_{lin}(t)||_{**}} \leq \frac{\delta_0}{2} \cdot \epsilon^{\alpha - \dim\Omega/4} \tag{4.47}$$

Proof of Theorem 4.3.2. Fix $0 < \beta \leq 1$. Lemmas 4.3.1 - 4.3.3 are used to provide the early pattern results given by Theorem 4.3.1 and show that for solutions that are initially close to the unstable subspace $(\bar{u}_0, \bar{v}_0) + \mathbb{X}_\epsilon^+ \oplus \mathbb{X}_\epsilon^{++}$ remain close to this space. These lemmas show that the decomposition of the phase space for the local case is also achievable for the mixed system. Furthermore, the fractional power space used for the nonlocal case is a subset of the fractional power space used in the local case. Theorem 3.3.1 is directly applied, thus giving the result. □

4.4 Behavior for $\theta \geq 1$

For $\theta = 1$, we use the same techniques of the previous section to show that $R_\epsilon \sim \epsilon^{\alpha/\chi}$. Furthermore, we show that we lose the $\epsilon-$dependency in the nonlinear estimate that is crucial for verifying almost linear behavior. As a result, the nonlinearity is not forced to be arbitrarily small as in the the $\theta < 1$ case. We now impose the following assumption, which establishes the case in which we consider for $\theta = 1$.

Assumption 4.4.1. *Suppose that* $\theta = 1$, $\epsilon(1-\beta)\hat{J}_0 > s_r$ *so that at least one* $\epsilon(1-\beta)(\hat{J}_0 - \hat{J}_k) \in (s_l, s_r)$.

As $\epsilon \to 0$, $\epsilon\nu_k \to \epsilon(1-\beta)(\hat{J}_0 - \hat{J}_k)$. Figure 4.3 demonstrates the limiting behavior of the eigenvalues. Using the distribution of $\epsilon(1-\beta)(\hat{J}_0 - \hat{J}_k)$, we define the following decomposition of $\mathbb{X}$.

Definition 4.4.1 (Decomposition of the spectrum)**.** *Choose the constants*

$$\lambda^+(\epsilon(1-\beta)\hat{J}_0) \ll a^{--} < b^{--} < 0 < a^- < b^- < a^+ < b^+ < \lambda^+_{max}, \tag{4.48}$$

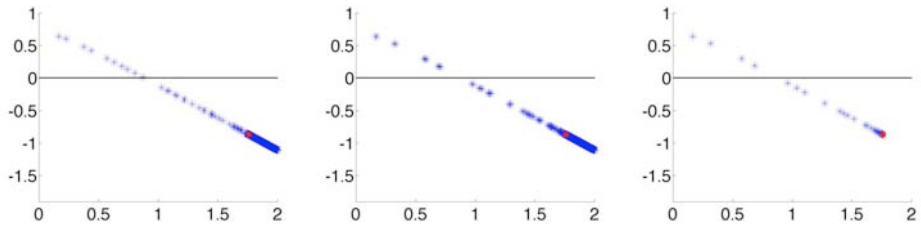

(a) Large ϵ (b) Medium ϵ (c) Small ϵ

Figure 4.3: The positive eigenvalues of the linearized right hand side of System 4.1. The eigenvalues of the linearization are given as blue asterisks and $\lambda^+(\epsilon \cdot \hat{J}_0)$ given by the red dot. As ϵ decreases, the $\epsilon\hat{J}_0$ acts to block or prevent all but a finite few eigenvalues from moving to the left of $\epsilon\hat{J}_0$ as ϵ decreases. The value $\hat{J}_0$ is $\epsilon-$dependent and is described further in Section 4.5.

in the following way. The intervals $[a^{--}, b^{--}]$, $[a^-, b^-]$ *and* $[a^+, b^+]$ *lie completely within the resolvent of* $\mathcal{H}_\epsilon$ *such that the number of eigenvalues within*

$$I^{++} = (b^+, \lambda^+_{max}), \tag{4.49}$$

$$I^{+} = (b^-, a^+), \tag{4.50}$$

$$I^{-} = (b^{--}, a^-), \tag{4.51}$$

have approximately the same number of eigenvalues, denoted as N*. Furthermore, denote the distance from* a^{--} *to the largest* $\lambda^{\pm}_k(\epsilon(1-\beta)(\hat{J}_0 - \hat{J}_k))$ *as* d_a*.*

Definition 4.4.2. *Consider the intervals defined by (4.49) - (4.51). For* $0 < \beta < 1$*, denote* $\mathbb{Y}^{++}_\epsilon$, $\mathbb{Y}^{+}_\epsilon$, $\mathbb{Y}^{-}_\epsilon$ *and* $\mathbb{Y}^{--}_\epsilon$ *as the span of the eigenfunctions whose eigenvalues belong to* I^{++}, I^+, I^- *and* I^{--}*, respectively.*

Before verifying the dichotomy estimates we consider $T_\epsilon : \mathbb{L}^2(\Omega) \to \mathbb{L}^2(\Omega)$, where for any $U \in \mathbb{L}^2(\Omega)$,

$$T_\epsilon U = \sum_{k=1}^{\infty} \left(\alpha^+_k \cdot e_1 + \alpha^-_k \cdot e_2\right) \cdot \psi_k, \tag{4.52}$$

where e_1 and e_2 denote the standard unit vectors in $\mathbb{R}^2$. As observed in [55], Lemma 4.2.3 is used to show that T_ϵ is a bounded and invertible linear operator with

$$c_1 \cdot ||U||_{\mathbb{L}^2(\Omega)} \leq || \, T_\epsilon U||_{\mathbb{L}^2(\Omega)} \leq c_2 \, ||U||_{\mathbb{L}^2,(\Omega)} \tag{4.53}$$

for all $U \in \mathbb{L}^2(\Omega)$ with $\epsilon-$independent constants c_1 and c_2.

By Assumption 4.4.1, there are only a finite number of $\epsilon(1-\beta)(\hat{J}_0 - \hat{J}_k) \in (s_l, s_r)$, which is the unstable interval. Denote the indices corresponding to these $\epsilon(1-\beta)(\hat{J}_0 - \hat{J}_k)$ as

$$K_1 \leq k \leq K_2. \tag{4.54}$$

The following lemma shows that for sufficiently small $\epsilon > 0$, the indices of the unstable eigenvalues remain fixed as $\epsilon \to 0$.

Lemma 4.4.1. *For System 4.1 with $0 \leq \beta < 1$, suppose that Assumptions 4.1.1 - 4.1.6 and 4.4.1 are satisfied with $\theta = 1$. Let $K_1 \leq K_2$ be as given in (4.54). There exists an ϵ_1 such that for $0 < \epsilon \leq \epsilon_1$ the indices of the $\epsilon\nu_k \in (s_l, s_r)$ are given by $K_1 \leq k \leq K_2$.*

Proof. This results follows immediately from Assumption 4.4.1 and that as $\epsilon \to 0$, $\epsilon\nu_k \to \epsilon(1-\beta)(\hat{J}_0 - \hat{J}_k)$. □

We now show that the values for r_ϵ and R_ϵ corresponding to the early pattern formation depend polynomially upon α and are smaller than those obtained for the $\theta < 1$ case.

Lemma 4.4.2. *Let $0 < \beta < 1$, $\theta = 1$. Assume that Assumptions 4.1.1, 4.1.2, 4.1.5, 4.1.6 and 4.4.1 are satisfied and let $\mathcal{H}_\epsilon$ be as defined in (4.14). Let $S_\epsilon(t), t \geq 0$ denote the analytic semigroup on $\mathbb{X}$ generated by $\mathcal{H}_\epsilon$. Consider the decomposition as given by Definition 4.4.2 and let $\mathbb{X}^\alpha = \mathbb{H}^{2\alpha}_{per}(\Omega)$ be the fractional power spaces of $\mathcal{H}_\epsilon$.*

(a) There exists a constant $M_\epsilon^{--} > 0$ such that for $U^{--} \in \mathbb{Y}_\epsilon^{--}$,

$$\left|\left|S_\epsilon^{--}(t)U^{--}\right|\right|_{**} \leq M_\epsilon^{--} \cdot t^{-\alpha} \cdot e^{a^{--}t} \cdot \left|\left|U^{--}\right|\right|_{\mathbb{L}^2(\Omega} \text{ for } t > 0. \tag{4.55}$$

As $\epsilon \to 0$, there exists an $\epsilon-$independent constant $C > 0$ such that

$$M_\epsilon^{--} \leq C \cdot \epsilon^{-\alpha}.$$

(b) There exists a constant $M_{\alpha,\epsilon} \geq 1$ which is proportional to an $\epsilon-$independent constant as $\epsilon \to 0$. Furthermore, there exists an $\epsilon-$independent constant $C > 0$ such that for al $U \in \mathbb{Y}_\epsilon^- \oplus \mathbb{Y}_\epsilon^+ \oplus \mathbb{Y}_\epsilon^{++}$ we have

$$C \cdot ||U||_{\mathbb{L}^2(\Omega)} \leq || U||_{**} \leq M_{\alpha,\epsilon} \cdot ||U||_{\mathbb{L}^2(\Omega)}.$$

(c) $r_\epsilon, R_\epsilon \sim \epsilon^{\alpha/\chi}$ as $\epsilon \to 0$.

Proof. The proof for this lemma is a variation of the proof given for [55, Proposition 5.4]. For $\eta > 0$,

$$e^{-\eta t} \leq \frac{\eta^{-2\alpha} \cdot (2\alpha)^{2\alpha}}{e^{2\alpha} t^{2\alpha}}.$$

Since $U \in \mathbb{Y}^{--}$, then whenever $\alpha_{k,\epsilon}^{\pm} \neq 0$, $a^{--} - \lambda_{k,\epsilon}^{\pm} > 0$. Applying the inequality with $\eta = 2(a^{--} - \lambda_{k,\epsilon}^{\pm})$ gives for all $t > 0$ that

$$\begin{aligned}
\left|\left|S_\epsilon^{--}(t)U\right|\right|_{**}^2 &= \sum_{k=1}^{\infty} (1+\kappa_k)^{2\alpha} \cdot \left(e^{2\lambda_{k,\epsilon}^+ t} \cdot (\alpha_k^+)^2 + e^{2\lambda_{k,\epsilon}^- t} \cdot (\alpha_k^-)^2 \right), \\
&\leq \sum_{k=1}^{\infty} \left(\frac{((1+\kappa_k)^{2\alpha} \cdot (\alpha_k^+)^2}{(a^{--} - \lambda_{k,\epsilon}^+)^{2\alpha}} + \frac{((1+\kappa_k)^{2\alpha} \cdot (\alpha_k^-)^2}{(a^{--} - \lambda_{k,\epsilon}^-)^{2\alpha}} \right) \\
&\cdot \frac{\alpha^{2\alpha}}{e^{2\alpha} \cdot t^{2\alpha}} e^{2a^{--} \cdot t}
\end{aligned}$$

If we assume that there exists a $\epsilon-$independent constant $C > 0$ such that

$$\frac{1+\kappa_k}{a^{--} - \lambda_{k,\epsilon}^{\pm}} \leq C \cdot \epsilon^{-1}, \text{ whenever } \lambda_{k,\epsilon}^+ < a^{--}, \tag{4.56}$$

then the previous estimate yields

$$\begin{aligned}
\left|\left|S_{\epsilon}^{--}(t)U\right|\right|_{**}^{2} &\leq \left(\frac{C\alpha}{e}\right)^{2\alpha} \cdot \epsilon^{-2\alpha} \cdot t^{-2\alpha} \cdot e^{2a^{--}\cdot t} \cdot \sum_{k=1}^{\infty} \left((\alpha_{k,\epsilon}^{+})^{2} + (\alpha_{k,\epsilon}^{-})^{2}\right), \\
&\leq \left(\frac{C\alpha}{e}\right)^{2\alpha} \cdot \epsilon^{-2\alpha} \cdot t^{-2\alpha} \cdot e^{2a^{--}\cdot t} \cdot ||T_{\epsilon}U||_{\mathbb{L}^{2}(\Omega)}^{2}, \\
&\leq c_{2}^{2}\left(\frac{C\alpha}{e}\right)^{2\alpha} \cdot \epsilon^{-2\alpha} \cdot t^{-2\alpha} \cdot e^{2a^{--}\cdot t} \cdot ||U||_{\mathbb{L}^{2}(\Omega)}^{2}
\end{aligned}$$

Choosing $M_{\epsilon}^{--} = c_2(C\alpha/e)^{\alpha} \cdot \epsilon^{-\alpha}$ provides the estimate. By Lemma 4.2.2, there exists an $\epsilon-$independent constant C such that

$$0 < \frac{1+s}{a^{--} + \lambda^{\pm}(s)} \leq C, \text{ for all } s \geq \epsilon(1-\beta)\hat{J}_0.$$

For $\epsilon\nu_k \geq \epsilon(1-\beta)\hat{J}_0$, we have

$$\begin{aligned}
\frac{1+\kappa_k}{a^{--} - \lambda_{k,\epsilon}^{\pm}} &= \frac{1+\epsilon\nu_k}{a^{--} - \lambda_{k,\epsilon}^{+}} \cdot \frac{1+\kappa_k}{1+\epsilon\nu_k}, \\
&\leq C\frac{1+\kappa_k}{1+\epsilon\beta\kappa_k + \epsilon(1-\beta)(\hat{J}_0 - \hat{J}_k)}, \\
&\leq C\frac{1+\kappa_k}{1+\epsilon\beta\kappa_k}, \\
&\leq C\beta^{-1}\epsilon^{-1}.
\end{aligned}$$

Now assume that $\epsilon\nu_k < \epsilon(1-\beta)\hat{J}_0$. By Definition 4.4.1, we have that for sufficiently small $\epsilon > 0$, we get $a^{--} - \lambda_{k,\epsilon}^{+} > d_a$. This gives

$$\frac{1+\kappa_k}{a^{--} - \lambda_{k,\epsilon}^{\pm}} = \frac{1+\epsilon\nu_k}{a^{--} - \lambda_{k,\epsilon}^{\pm}} \cdot \frac{1+\kappa_k}{1+\epsilon\nu_k} \leq \frac{1+\epsilon(1-\beta)\hat{J}_0}{d_a} \cdot \beta^{-1}\epsilon^{-1}.$$

For part (b), let $U \in \mathbb{Y}_\epsilon^- \oplus \mathbb{Y}_\epsilon^+ \oplus \mathbb{Y}_\epsilon^{++}$. By (4.53), we have that

$$c_1^2 \, ||U||^2_{\mathbb{L}^2(\Omega)} \leq || \, T_\epsilon U||^2_{\mathbb{L}^2(\Omega)} \leq || \, U||^2_{**} \, .$$

As $\epsilon \to 0$, only a finite number of the terms of the Fourier series for U are nonzero. Furthermore, the corresponding indices remained fixed. For sufficiently small ϵ, we can write U as

$$U = \sum_{k=k_1}^{k_2} \left(\alpha_k^+\right) E_{k,\epsilon}^+ \psi_k + \left(\alpha_k^-\right) E_{k,\epsilon}^- \psi_k.$$

Therefore, we have the following

$$\begin{aligned} ||U||^2_{**} &= \sum_{k=k_1}^{k_2} (1+\kappa_k)^{2\alpha} \left(\left(\alpha_k^+\right)^2 + \left(\alpha_k^-\right)^2 \right), \\ &\leq (1+\kappa_{k_2})^{2\alpha} \, ||T_\epsilon U||^2_{\mathbb{L}^2(\Omega)} \, , \\ &\leq c_2^2 (1+\kappa_{k_2})^{2\alpha} \, ||U||^2_{\mathbb{L}^2(\Omega)} \, . \end{aligned}$$

Choosing $M_{\alpha,\epsilon} = c_2(1+\kappa_{k_2})^\alpha$ gives the final result.

Using [41, Remark 3.1, Lemma 3.6], the estimates for $r_\epsilon, R_\epsilon \sim L$, where L is a global Lipschitz constant of the nonlinearity F. By Lemma 4.3.3, we have that the global Lipschitz constant is given as $L = C \cdot R^\chi$, where C, R are constants. As $\epsilon \to 0$, [41, Remark 2.5] gives

$$C \cdot R^\chi \leq \frac{C_\epsilon^{--} C_\epsilon^+}{2C_\epsilon^+ + M_{\alpha,\epsilon} C_\epsilon^{--}}, \tag{4.57}$$

where

$$C_\epsilon^+ = \frac{\min\left(b^- - a^-, b^+ - a^+\right)}{6 + \chi + 1/\chi},$$

and

$$C_\epsilon^{--} = \frac{b^{--} - a^{--}}{2 \cdot M_{\alpha,\epsilon} + 3\sqrt{2} \cdot M_\epsilon^{--} \cdot (b^{--} - a^{--})^\alpha}.$$

Using Lemma 4.4.2, we have that as $\epsilon \to 0$, $M_{\alpha,\epsilon} = c_2(1+\kappa_{k_2})^\alpha$ and $M_\epsilon^{--} \leq C_2 \cdot \epsilon^{-\alpha}$. This with (4.57) implies that r_ϵ, $R_\epsilon \sim \epsilon^{\alpha/\chi}$. □

We now consider the case in which $\epsilon \ll 1$ is fixed and $\theta \to 1$. We begin by considering how the $\epsilon\nu_k$ fill the unstable interval (s_l, s_r) for fixed $\theta < 1$.

$$\epsilon\nu_k = \epsilon\beta\kappa_k + \epsilon^{1-\theta}(1-\beta)\epsilon^\theta(\hat{J}_0 - \hat{J}_k),$$

$$\leq \epsilon^{1-\theta}\left(\beta\kappa_k + (1-\beta)\epsilon^\theta(\hat{J}_0 - \hat{J}_k)\right).$$

Since the $\beta\kappa_k + (1-\beta)\epsilon^\theta(\hat{J}_0 - \hat{J}_k) \sim k^{2/\dim\Omega}$, we get that the lower bound of the number of $\epsilon\nu_k \in (s_l, s_r)$ is $\sim \epsilon^{-(1-\theta)\dim/\Omega/2}$. Thus, the spectral gaps are bounded above by $\epsilon^{(1-\theta)\dim\Omega/2}$. We have that $M_{\alpha,\epsilon}$ is proportional to $\epsilon^{-\alpha}$, and $M_\epsilon^{--} \leq C \cdot \epsilon^{-\alpha(2+(1-\theta)\dim\Omega)/2}$. Again following [41, Remark 3.1, Lemma 3.6], we get that r_ϵ and $R_\epsilon \sim \epsilon^{(2\alpha+(1-\theta)\dim\Omega)/(2\chi)}$. As $\theta \to 1$, we get that $r_\epsilon, R_\epsilon \sim \epsilon^{\alpha/\chi}$.

We now begin to show how the nonlinearity loses its $\epsilon-$dependent bound that was critical for the almost linear behavior results for $\theta < 1$. First, we show the following bound.

Lemma 4.4.3. *Suppose that Assumptions 4.1.1 - 4.1.6 and 4.4.1 are satisfied with $\theta = 1$. Let $\dim\Omega/4 < \alpha < 1$ and for $\delta_0 > 0$,*

$$\delta = \delta_0 \cdot (K_1 - 1)^{1-4\alpha/\dim\Omega}, \tag{4.58}$$

where K_1 is given by 4.54. For $U \in \mathcal{K}_\delta$ and constant C,

$$||U||_{C(\bar{\Omega})} \leq C \cdot (K_1 - 1)^{1-4\alpha/\dim\Omega} \cdot ||U||_{**}. \tag{4.59}$$

Proof. This proof is a modification of part of the proof given in [55, Proposition 6.2]. Let $U \in \mathcal{K}_\delta$, where $U = U_+ + U_- \in \mathcal{Y}^+_\epsilon \oplus \mathcal{Y}^-_\epsilon$ and $\mathcal{Y}^+_\epsilon = \mathbb{Y}^+_\epsilon \oplus \mathbb{Y}^{++}_\epsilon$ and $\mathbb{Y}^-_\epsilon = (\mathbb{Y}^{--}_\epsilon \cap \mathbb{Y}^\alpha) \oplus \mathbb{Y}^-_\epsilon \subset \mathbb{X}^\alpha$. For U_+, we therefore have

$$U_+ = \sum_{k=k_1}^{k_2} \alpha_k^+ \cdot E^+_{k,\epsilon} \cdot \psi_k,$$

where $E^+_{k,\epsilon} \in \mathbb{R}^2$ and $\psi_k \in L^2(\Omega)$ with $||\psi_k||_{L^2(\Omega)} = 1$. We assume that the maximum norms of the $L^2(\Omega)-$normalized eigenfunctions of the Laplacian are uniformly bounded. Using Hölder's inequality, we have

$$\begin{aligned} ||U_+||_{C(\bar{\Omega})} &\leq C \cdot \left(\sum_{k=k_1}^{k_2} (1+\kappa_k)^{2\alpha} \cdot (\alpha_k^+)^2 \right)^{1/2} \cdot \left(\sum_{k=k_1}^{k_2} \frac{1}{(1+\kappa_k)^{2\alpha}} \right)^{1/2}, \\ &= ||U_+||_{**} \cdot \left(\sum_{k=k_1}^{k_2} \frac{1}{(1+\kappa_k)^{2\alpha}} \right)^{1/2}. \end{aligned} \tag{4.60}$$

For the remainder of the proof, we use C to represent constants, although not all C's represent the same constant. By Lemma 4.4.1, we can choose $\epsilon \leq \epsilon_1$, such that if $\epsilon\nu_k \in (s_l, s_r)$, then the $\epsilon\nu_k$ will remain in the unstable interval. Therefore, we have

$$\begin{aligned} \sum_{k=K_1}^{K_2} \frac{1}{(1+\kappa_k)^{2\alpha}} &\leq C \cdot \sum_{k=k_1}^{k_2} k^{-4\alpha/\dim\Omega}, \\ &\leq C \cdot \int_{K_1-1}^{K_2} \tau^{-4\alpha/\dim\Omega} \, d\tau, \\ &\leq C \cdot (K_1 - 1)^{1-4\alpha/\dim\Omega}. \end{aligned}$$

With (4.60), we now have

$$||U_+||_{C(\bar{\Omega})} \leq C \cdot (K_1 - 1)^{1-4\alpha/\dim\Omega} \cdot ||U_+||_{**} . \tag{4.61}$$

It is worth noting that this estimate, unlike the estimate given in the proof of [55, Proposition 6.2], has no dependency upon ϵ. By Sobolev's embedding theorem for fractional power spaces [57] and $U \in \mathcal{K}_\delta$, there exists a $\epsilon-$independent constant C such that $||U_-||_{C(\bar{\Omega})} \leq ||U_-||_{**} \leq C \cdot \delta \cdot ||U_+||_{**}$. Combining this with (4.61) gives

$$\begin{aligned} ||U||_{C(\bar{\Omega})} \leq & || U_+||_{C(\bar{\Omega})} + ||U_-||_{C(\bar{\Omega})} , \\ & \leq C \cdot (K_1 - 1)^{1-4\alpha/\dim\Omega} \cdot ||U_+||_{**} , \\ & \leq C \cdot (K_1 - 1)^{1-4\alpha/\dim\Omega} \cdot ||U||_{**} \end{aligned}$$

□

Using the previous result, we show the main result of this section. Due to this main result, the almost linear behavior is no longer ensured, since the nonlinearity is not longer bounded above by a decreasing $\epsilon-$dependent bound.

Theorem 4.4.1 (Largeness of F)**.** *Suppose that Assumptions 4.1.1 - 4.1.6 and 4.4.1 are satisfied with $\theta = 1$ and let F be as defined in (4.29). Let $\dim\Omega/4 < \alpha < 1$ and $\delta_0 > 0$ be arbitrary and set*

$$\delta = \delta_0 \cdot (K_1 - 1)^{1-4\alpha/\dim\Omega}. \tag{4.62}$$

Then for $0 < \epsilon \leq \epsilon_1$, where ϵ_1 is defined in Lemma 4.4.1, there exists $\epsilon-$independent constants M_1, $M_2 > 0$ such that for $U \in \mathcal{K}_\delta$, with

$$||U||_{**} \leq M_1 \cdot (K_1 - 1)^{4\alpha/\dim\Omega - 1}, \tag{4.63}$$

we have

$$||F((\bar{u}_0, \bar{v}_0) + U)||_{\mathbb{L}^2(\Omega)} \leq M_2 \cdot (K_1 - 1)^{(1-4\alpha/\dim\Omega)\cdot(\chi+1)} . ||U||_{**}^{\chi+1} . \tag{4.64}$$

The order of the zero $(\bar{u}_0, \bar{v}_0)$ *of* F *is given by* χ *in Assumption 4.1.4.*

Proof. This proof follows that of [55, Proposition 6.2], except that we use the new estimate determined by Lemma 4.4.3. By Assumption 4.1.4 and the definition of F in (4.29), we have

$$||F(U_0 + U)||_{\mathbb{R}^2} \leq \tilde{M}_1 \cdot ||U||_{\mathbb{R}^2}^{\chi+1} \text{ for all } ||U||_{\mathbb{R}^2} \leq \tilde{M}_2. \tag{4.65}$$

By Lemma 4.4.3, we have

$$||U||_{C(\bar{\Omega})} \leq C \cdot (K_1 - 1)^{1-4\alpha/\dim\Omega} \cdot ||U||_{**} . \tag{4.66}$$

If we let $M_1 = \tilde{M}_2/C$, then for $U \in \mathcal{K}_\delta$ we have that $||U||_{C(\bar{\Omega})} \leq \tilde{M}_2$. Therefore, we get the following estimate

$$\begin{aligned} ||F(U_0 + U)||_{C(\bar{\Omega})} &\leq \tilde{M}_1 \cdot ||U||_{C(\bar{\Omega})}^{\chi+1} , \\ &\leq \tilde{M}_1 C^{\chi+1} \cdot (K_1 - 1)^{(1-4\alpha/\dim\Omega)\cdot(\chi+1)} \cdot ||U||_{**}^{\chi+1} . \end{aligned}$$

□

Theorem 4.4.1 shows that unlike the case for $\theta < 1$, the norm of F is not forced to be arbitrarily small on the cone $\mathcal{K}_\delta$. How this cone condition affects the agreement between the solutions and the solutions of the linearized system is now described. The proof of the almost linear behavior given in [55] is modified to show that for $\theta = 1$, (u, v) and (u_{lin}, v_{lin})

reach a distance from the homogeneous equilibrium that is bounded above by

$$R_\epsilon = \left(\frac{2^{\alpha-1} \left((m+1) \cdot a^- - \lambda_{\max}^+ \right)^{1-\alpha}}{K_\epsilon \cdot M \cdot \Gamma(1-\alpha)} \right)^{1/\chi}, \tag{4.67}$$

where

$$K_\epsilon = C\epsilon^{-\alpha},$$

$$M = M_2 \cdot (K_1 - 1)^{1-4\alpha/\dim\Omega},$$

$$\frac{\lambda_{\max}^+}{m+1} < a^- < \lambda_{\max}^+,$$

and the separation of (u, v) and (u_{lin}, v_{lin}) is given as

$$\frac{||(u(t), v(t)) - (\bar{u}_0, \bar{v}_0) - (u_{lin}(t), v_{lin}(t))||_{**}}{||(u_{lin}(t), v_{lin}(t))||_{**}} \leq \frac{\delta_0}{2} \cdot (K_1 - 1)^{1-4\alpha/\dim\Omega}. \tag{4.68}$$

Note that the bounds for our cone condition are used to define M. In the $\theta < 1$ case, this constant is $\epsilon-$dependent, unlike our current situation. As $\epsilon \to 0$,

$$R_\epsilon \sim \epsilon^{\alpha/\chi}. \tag{4.69}$$

We see no improvement upon the R_ϵ obtained for the early pattern behavior for $\theta = 1$. Note that in the previous case where $\theta < 1$, R_ϵ is proportional to $\epsilon^{-(\alpha-\dim\Omega/4)+\dim\Omega/4}$. For $\theta = 1$, the solutions will not separate for large distances away from the homogeneous equilibrium. When the $\theta = 1$ case is compared to the $\theta < 1$ case, we see that the cone condition is affecting this dramatic change in separation distance. Lemma 4.4.3 establishes the cone condition in which we are using. In this lemma, we are unable to place a bound upon $||U_+||_{C(\bar{\Omega})} / ||U_+||_{**}$ in a way that drives this ratio to 0 as $\epsilon \to 0$. We can not do this, as the eigenfunctions in the unstable space $\mathbb{Y}_\epsilon^+ \oplus \mathbb{Y}_\epsilon^{++}$ remain fixed for arbitrarily small ϵ. These eigenfunctions correspond to the initial modes of the Fourier series. If we consider the

Fourier series of F, we see that the lower order modes have much higher amplitude than the higher order modes. In this sense, F will be much more nonlinear for our current situation than when compared to the $\theta < 1$ case. In the $\theta < 1$ case, the unstable space consists of eigenfunctions that are comprised of increasingly less nonlinear Fourier basis functions as $\epsilon \to 0$. However, in the $\theta = 1$ situation, this is not true. As a consequence for $\theta = 1$, we expect greater influence of the nonlinearity as $\epsilon \to 0$. This implies an increasingly poor agreement between the solutions and their linearized counterparts. In the next section, we provide numerics that support this claim.

For $\theta > 1$, we again examine the $\epsilon\nu_k$ and see that for each k, as $\epsilon \to 0$, the $\epsilon(\hat{J}_0 - \hat{J}_k) \to \infty$. Since for each k we have that $\epsilon\kappa_k \to 0$, we see that $\epsilon\nu_k \to \infty$. Thus, there exists some small ϵ_0, such that for all $\epsilon \leq \epsilon_0$, $\epsilon\nu_k \notin (s_l, s_r)$ for all k. In other words, the homogeneous is stable for arbitrarily small ϵ.

4.5 Numerical experiments

In this section, we begin with solutions whose initial conditions are contained within $r_\epsilon \sim \epsilon^p$ for $\theta = 1$. For our numerics, $r_\epsilon = \epsilon^{0.5}$. Theorem 4.3.2 shows that $R_\epsilon \sim \epsilon^{-q}, q \geq 0$, and $q = -(\alpha - \dim\Omega/4) + \alpha/\chi +$ *some small constant* as $\epsilon \to 0$. For our numerics, we choose $\alpha = 3/4$. When R_ϵ is reached, the relative distance between the solutions and their linearized counterparts is bounded above by $C \cdot \epsilon^{\alpha - \dim\Omega/4}$. Our goal is to test how the constant C in front of the bound on the relative distance varies with β. In all simulations, we use a Galerkin spectral method with a semi-implicit integration scheme that was discussed in Chapter 2. For each set of parameters, multiple initial conditions are chosen as random perturbations of the homogeneous equilibrium so that these initial conditions lie within $r_\epsilon = \epsilon^{0.5}$ of the homogeneous equilibrium. The random numbers are generated using a random number generator that samples from a uniform probability distribution between 0 and 1. In the notation of the previous section, we measure the relative distance between $((u, v) - (\bar{u}_0, \bar{v}_0))$ and (u_{lin}, v_{lin}). Distances are measured in the $||\cdot||_{**}$ given in (4.35).

Calculating this norm is straightforward, since it corresponds to calculating the standard Euclidean norm of the spectral coefficients. The linear and nonlinear solutions evolve until they are at a fixed ϵ-dependent relative distance

$$tol = \frac{1}{4}\epsilon^{1/4}, \text{ (from (4.47))}, \tag{4.70}$$

where this value is obtained by using Equation 4.46. The distance R_ϵ from the homogeneous equilibrium is measured and plotted. The other parameter values are chosen as $\delta_0 = .25$, $\xi = .001$, $\dim \Omega = 2$, $\Omega = [0,1]^2$, and $D = 1$. The results are depicted in Figures 1.2 and 4.4.

Remark 4.5.1. *An alternative approach would be to allow the simulation to run until the distance of the solution to the homogeneous equilibrium reaches a certain tolerance, and then compute the relative distance of the solution to its linearized counterpart. However, the approach that we used allows for a longer simulation time before stopping. If the almost linear behavior for the nonlocal system were present, then we would have a higher probability of seeing the effect by using the way outlined.*

For our numerics, the Thomas nonlinearities for f and g are used. The Thomas nonlinearities are chosen since they satisfy conditions necessary for Turing instability. The nonlinearities are given as

$$\begin{aligned} f(u,v) &= a - u - \frac{\rho u v}{1 + u + K u^2}, \\ g(u,v) &= A(b - v) - \frac{\rho u v}{1 + u + K u^2}, \end{aligned} \tag{4.71}$$

where a, b, ρ, A, and K are positive constants that depend upon reaction kinetics. We choose $a = 150$, $b = 100$, $\rho = 13$, $A = 1.5$, and $K = .05$. With $\delta = 1$, the Thomas system satisfies Assumption 4.1.4.

We consider a kernel that is similar to the kernel used in [25]. Let the Gaussian kernel

G_0 be defined as

$$\mathcal{G}(x,y) = \frac{C}{\epsilon} \cdot exp\left(\frac{-x^2-y^2}{\sigma^2}\right) \cdot \eta(x,y), \tag{4.72}$$

where $\eta(x,y)$ is a smooth cutoff function. The function η is 1 on $B_{1/3}(0,0)$, but vanishes outside of $B_{1/2}(0,0)$. On the domain $\Omega = [0,1]^2$, the kernel G is given as

$$G(x,y) = \frac{C}{\epsilon} \cdot \left(\mathcal{G}(x,y) + \mathcal{G}(x+1,y) + \mathcal{G}(x,y+1) + \mathcal{G}(x+1,y+1)\right). \tag{4.73}$$

Outside of $\Omega = [0,1]^2$, $J(x,y)$ is given as the smooth periodic extension of $G(x,y)$, denoted as

$$J(x,y) = G_{per}(x,y). \tag{4.74}$$

Note that $\hat{J}_0 = \frac{C}{\epsilon} \cdot \hat{\mathcal{G}}_0$. We perform numerics for two cases, one in which the $\epsilon\hat{J}_0$ lies just to the right of (s_l, s_r) and the other in which $\epsilon\hat{J}_0$ lies within (s_l, s_r). For the first case, we choose $\frac{C}{\epsilon}$ so that the infinitely many eigenvalues of the linearized right hand side are not all positive. The condition

$$\begin{aligned} \frac{\epsilon \cdot \frac{C}{\epsilon}\hat{\mathcal{G}}_0}{s_r} &> 1, \\ \frac{C\hat{\mathcal{G}}_0}{s_r} &> 1, \end{aligned} \tag{4.75}$$

where s_r is the rightmost root of $\lambda^+(s)$ permits a finite number of positive eigenvalues. Note that the integral of the kernel J over $[0,1]^2$ is given as the first Fourier coefficient denoted as $\hat{J}_0$. For small σ, a good approximation for this integral is the volume of G over all $\mathbb{R}^2$. To understand why, observe that most of the support for G occurs within 3σ of each corner

of $[0,1]^2$ for $\sigma \ll 1$. Thus, we can compute $\hat{J}_0$ as

$$\hat{\mathcal{G}}_0 = \int_\Omega \mathcal{G}(x)dx,$$

$$\approx \sigma^2\pi.$$

For $\sigma \ll 1$,

$$C = \frac{2s_r}{\sigma^2\pi}. \tag{4.76}$$

Choosing $\sigma = .1$ is sufficient for our purposes. Thus from (4.76),

$$C = 200 \cdot \frac{s_r}{\pi}. \tag{4.77}$$

Note that

$$\lim_{\epsilon \to 0} \epsilon \cdot \hat{J}_0 = 2s_r > 0.$$

Using this kernel, the following numerical experiment was performed to determine how well the linearization describes the actual solutions of System 4.1 using $\beta \in \{0.0, 0.125, .5, .875, 1.0\}$. The values of ϵ are 70 logarithmically spaced points between 10^{-6} and 10^{-4}. For each ϵ and β pair, 20 random initial conditions were used. See Figure 4.4.

For $\beta = 1.0$, we see that the distance from the solutions to the homogeneous equilibrium upon separation becomes very large as ϵ decreases. For $\beta = .875$, this trend continues, although not as pronounced as the pure local case. However, for $\beta = 0, .125, .5$, we see that quite the opposite is true. As ϵ decreases, we see that the separation of the solution and its linearized counterpart occurs much closer to the homogeneous equilibrium when compared to the case of $\beta = 1.0$ and $\beta = .875$. The results indicate that for this value of σ, the linearization does not accurately describe the solutions of System 4.1. For this value of σ, the solutions are more influenced by the effects of the nonlinearity rather than the linear

features of the system. Thus, the solution behavior is much more nonlinear, causing the early separation shown in Figure 4.4.

Similarly, Figure 1.2 shows the result of the same experiment, but with fixed β and varying ϵ values. For part (a), we see that for the pure local case, the deviation between the solution and the linearized solutions dramatically increases as $\epsilon \to 0$. For part (b), we see that the mixed local and nonlocal diffusion case shows a less pronounced deviation for the solution and its linearized counterpart. For parts (c) - (d), we see that as $\beta \to 0$, the deviation is very small, indicating the increasing influence of the nonlinearity of the nonlocal system.

We now move $\epsilon\hat{J}_0$ to be inside of (s_l, s_r). For this numerical experiment, we choose

$$C = \frac{.9s_r}{\sigma^2\pi}, \tag{4.78}$$

which moves $\epsilon\hat{J}_0$ to be slightly to the left of s_r. Figure 4.5 shows the results. Comparison of Figure 4.5 to Figure 4.4 reveals very interesting results. First, observe that for $\beta = .875$, the almost linear behavior seems more pronounced for the case in which $\epsilon\hat{J}_0 \in (s_l, s_r)$. For $\beta = .5$, we see evidence of almost linear behavior for $\epsilon\hat{J}_0 \in (s_l, s_r)$. However, for the case in which $\epsilon\hat{J}_0 \notin (s_l, s_r)$, we see no evidence of almost linear behavior with $\beta = .5$. These results suggest that moving $\epsilon\hat{J}_0$ to the left increases almost linear behavior for smaller β values. This is consistent with our theoretical view, which is precisely what is occurring in the case of $\theta < 1$.

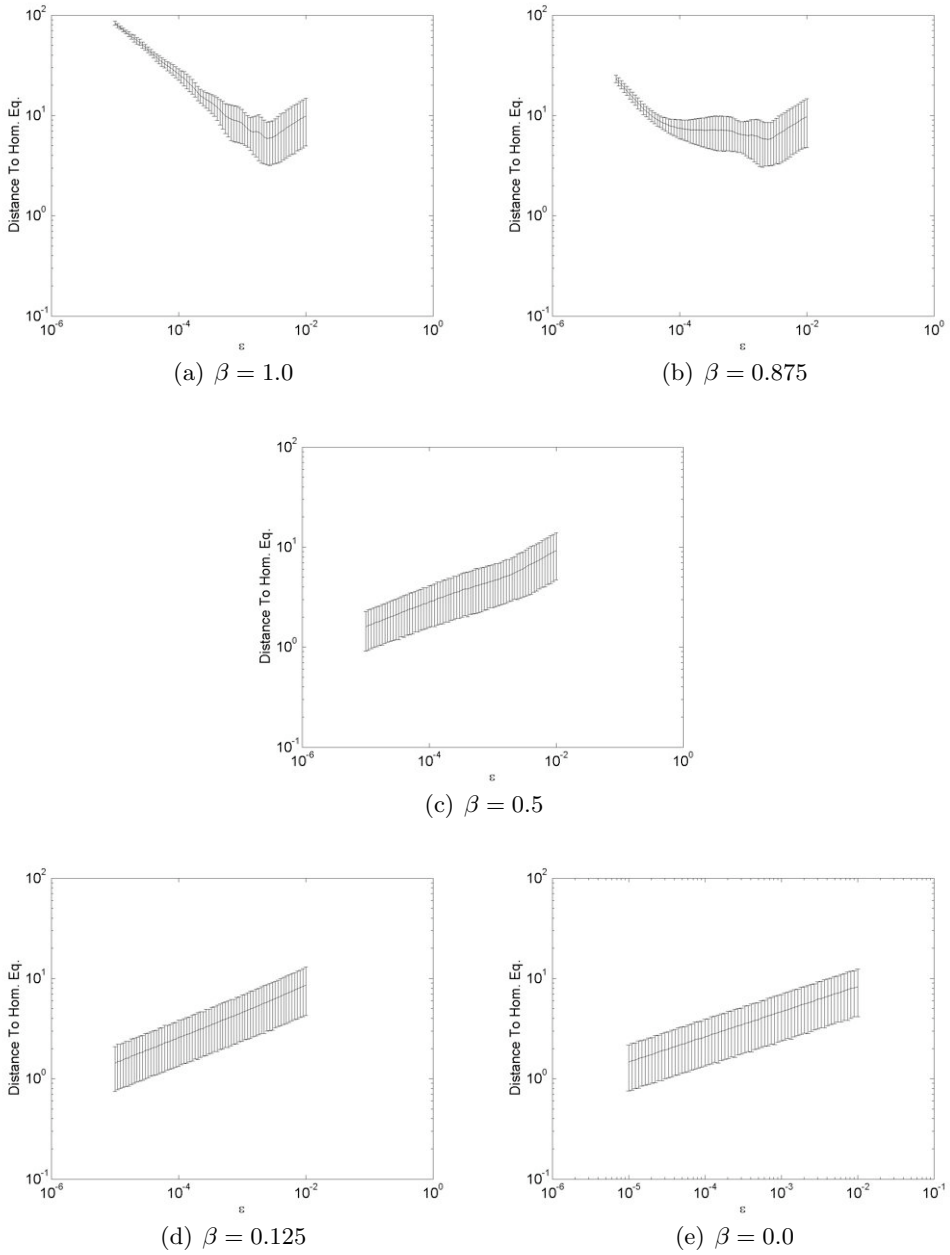

(a) $\beta = 1.0$ (b) $\beta = 0.875$

(c) $\beta = 0.5$

(d) $\beta = 0.125$ (e) $\beta = 0.0$

Figure 4.4: For small β values, the separation between the solution and the linear solution is much smaller for small values of ϵ, suggesting a more nonlinear influence from the nonlocal term. For each ϵ and β pair, 20 random initial conditions were used. The values of ϵ are 70 logarithmically spaced points between 10^{-5} and 10^{-2}. $C = 2s_r/(\sigma^2\pi)$.

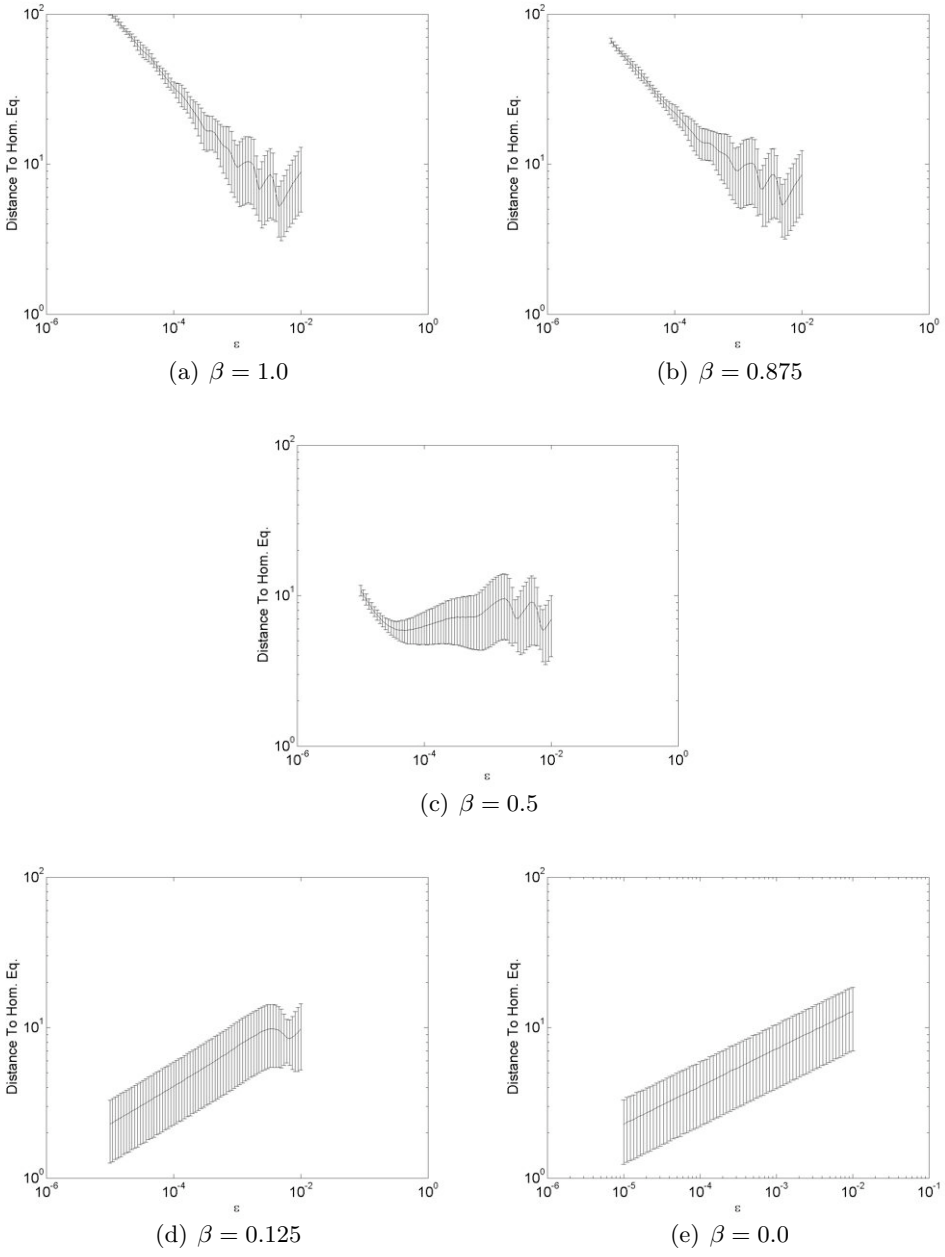

(a) $\beta = 1.0$ (b) $\beta = 0.875$

(c) $\beta = 0.5$

(d) $\beta = 0.125$ (e) $\beta = 0.0$

Figure 4.5: For small β values, the separation between the solution and the linear solution is much smaller for small values of ϵ, suggesting a more nonlinear influence from the nonlocal term. However, comparison with Figure 4.4 shows more evidence of almost linear behavior in this particular case for $\beta = .875$ and $\beta = .5$. For each ϵ and β pair, 20 random initial conditions were used. The values of ϵ are 70 logarithmically spaced points between 10^{-5} and 10^{-2}. $C = .9s_r/(\sigma^2\pi)$

4.6 Summary

In this thesis, reaction-diffusion systems with mixed nonlocal and local diffusion terms are considered where $\epsilon^\theta J$ is an $\epsilon-$independent kernel. For $\theta < 1$, the initial pattern selection is dominated by linear behavior. The methods can be applied to other related mixed local-nonlocal models. For example, such behavior has previously been observed numerically for phase field models with local and nonlocal diffusion terms, and we believe similar results can be obtained with only minor adjustments to the proofs presented here. For further results on the current model, it should be possible to apply the probabilistic methods found in [14, 61] to show that later stages of pattern formation are governed by linear effects. As a conjecture, these results are attainable on certain nonrectangular domains, as long as it is possible to define the nonlocal kernel to have even symmetry. For example, it should be possible to extend these results to the disk. If $\theta = 1$, and $\epsilon(1-\beta)\hat{J}_0$ is sufficiently larger than s_r, we show how the nonlinearity is bounded above by a constant, and not an $\epsilon-$dependent bound as for $\theta < 1$. As $\epsilon \to 0$, the deviation of the solutions from the linearized solutions reaches an $\epsilon-$independent amount so that the distance from the solution to the homogeneous equilibrium is proportional to $\epsilon^{\alpha/\chi}$. Furthermore, the numerics show that initial pattern selection for $\beta \ll 1$ is dominated by nonlinear effects.

Chapter 5: Further Numerical Pattern Studies

We continue the study of reaction-diffusion systems with numerical pattern studies of Systems 1.1 and 1.2. For the first study, we begin by choosing a set of parameter values for (d,γ) associated with System 1.1. We numerically demonstrate that if the positive portion of the dispersion relations of both the local and nonlocal periodic systems are similar, then the solutions for System 1.1 will also be very similar for all $0 \leq \beta \leq 1$. To accomplish this, we first fix the local dispersion relation for each (d,γ) pair and then choose the kernel parameters. These kernel parameters are chosen so as to minimize the least squares difference between the positive portion of the local and nonlocal dispersion relations. With the kernel parameters determined, next we use the implemented spectral methods of Chapter 2 to evolve the same set of initial conditions using various β values. The results show that if the initial conditions are the same, then the pattern is the same for all β values considered in this study. Therefore, for the purpose of studying the patterns of System 1.1, it is sufficient to study the patterns of only one β value. Thus, we examine the patterns that occur in the local case ($\beta = 0$) for System 1.1. We conclude this study with a description of these patterns and show that System 1.1 can generate striped, spotted and irregular snakelike patterns that are typical for reaction-diffusion systems with Turing instability.

For the remaining pattern study, we compare the solutions of System 1.1 with $\beta = 1$ and System 1.2 using similar dispersion relations. Using the (d,γ) values in the previous study, we fix the d and γ values for the Neumann system and then determine the d and γ values for the periodic system with $\beta = 1$. As before, the parameters are chosen so that the least squares difference between the two dispersion relations is minimum. However, as the eigenfunctions for both cases are not the same, we use different subsets of the positive dispersion relation associated with the Neumann system to see if agreement between the solutions improves. See Section 5.4 for more details. As before, the corresponding solutions

of both systems are evolved for a specific period of time and compared. Although the eigenfunctions associated with the eigenvalues of the dispersion relations for both systems are different, we numerically demonstrate that for some cases, the solutions for both systems can be similar.

5.1 Kernels

The kernels are defined in the same manner as in Section 2.2, but they are included here for convenience. Let the Gaussian kernel g_1 be defined as

$$g_1(x) = A \cdot exp\left(\frac{-x^2}{\sigma^2}\right) \cdot \eta(x), \tag{5.1}$$

where $A > 0$ and $\eta(x)$ is a smooth cutoff function. The function η is 1 on $B_{1/3}(0)$, but vanishes outside of $B_{1/2}(0)$. On the domain $\Omega = [0, 1]$, the kernel G_1 is given as

$$G_1(x) = g_1(x) + g_1(x + 1). \tag{5.2}$$

Outside of $\Omega = [0, 1]^2$, $J_1(x)$ is given as the smooth periodic extension of $G_1(x)$, denoted as

$$J_1(x) = G_{1,per}(x). \tag{5.3}$$

The 2d kernel is defined analogously. For this case, we begin with the 2d Gaussian function given as

$$g_2(x, y) = A \cdot exp\left(\frac{-x^2 - y^2}{\sigma^2}\right) \cdot \eta(x, y), \tag{5.4}$$

where $A > 0$ and $\eta(x, y)$ is a smooth cutoff function. The function η is 1 on $B_{1/3}(0, 0)$, but vanishes outside of $B_{1/2}(0, 0)$. On the domain $\Omega = [0, 1]^2$, the kernel G_2 is given as

$$G_2(x, y) = g_2(x, y) + g_2(x + 1, y) + g_2(x, y + 1) + g_2(x + 1, y + 1). \tag{5.5}$$

Outside of $\Omega = [0, 1]^2$, $J_2(x, y)$ is given as the smooth periodic extension of $G_2(x, y)$, denoted as

$$J_2(x, y) = G_{2,per}(x, y). \tag{5.6}$$

5.2 Linear Analysis

The eigenvalues of the linearization can reveal stability information about the solutions that are very close to the homogeneous equilibrium. For example, if we know that an eigenvalue is less than 0, then as time progresses, the contribution of the corresponding eigenfunction will approach 0. For those eigenvalues that are greater than 0, the corresponding eigenfunction will have some contribution to the overall solution as time continues.

In Chapter 4, analysis of the eigenvalues of the linearized right hand side of $\mathcal{H}_\epsilon$ has been provided. In this section, we analyze System 1.1 without scaling by $1/\gamma$. Although scaling changes the order of magnitude of the time scale, it has no effect upon the patterns that are produced. The linearization of System 1.1 is given as

$$U' = D\mathcal{J}U + \gamma BU, \tag{5.7}$$

where D, $\mathcal{J}$, and B are defined by Equations (4.9), (4.10), and (4.13), respectively. For the sake of notation, we shall denote this operator as

$$\mathcal{H}_\gamma = D\mathcal{J} + \gamma B. \tag{5.8}$$

As discussed in Section 4.2, the eigenfunctions for $\Delta$and $\mathcal{J}$ are the same. Furthermore, the

eigenvalues for the convolution operator are in fact the Fourier coefficients $\hat{J}_k$ of the kernel J. Therefore, we recognize that the eigenvalues of $\mathcal{J}$ as

$$\rho_{\beta,k} = \beta\kappa_k + (1-\beta)(\hat{J}_0 - \hat{J}_k). \tag{5.9}$$

The following lemma gives the eigenvalues for (5.8).

Lemma 5.2.1. *For $\rho_{\beta,k}$ defined in (5.9), the eigenvalues of the right-hand operator of Eq. (5.7) are given as*

$$\xi^{\pm}_{\beta,k} = \frac{-b_{\beta,k} \pm \sqrt{b^2_{\beta,k} - 4c_{\beta,k}}}{2},$$

where

$$b_{\beta,k} = (d+1)\rho_{\beta,k} - \gamma(g_v + f_u),$$

$$c_{\beta,k} = \gamma^2(f_u g_v - g_u f_v) - \gamma(df_u + g_v)\rho_{\beta,k} + d\rho^2_{\beta,k}.$$

Proof. The proof of this lemma follows the same reasoning as that presented in Lemma 4.2.1. □

5.3 Similar Dispersions for Local and Nonlocal Systems

For a d, γ, and $0 \leq \beta \leq 1$, Lemma 5.2.1 gives us the eigenvalues for the linearized right hand side of System 1.1. Since the eigenfunctions for both $\Delta$and $\mathcal{J}$ are the same, the solutions for $\beta = 0$ and $\beta = 1$ should be close when the positive eigenvalues are close. It is this finite set of positive eigenvalues that is responsible for pattern formation [45]. Consider the 1d example using the kernel $J_1(x)$ in which the positive eigenvalues of the local and nonlocal system are similar for $(d,\gamma) = (500, 3500)$. The eigenvalues of the right hand side of the local and nonlocal linearized System 1.1 are shown in Figure 5.1. To produce the similar dispersion relations, the parameters $A = 11^6, \sigma = .0078$ were chosen for J_1. For $\beta = 0$ and $\beta = 1$, the dispersion relations show that the eigenvalues for modes $1 \leq k \leq 10$ are very

close. Therefore, we expect that the resulting patterns should be very close for both values of β. Figure 5.2 confirms this. This figure shows solutions that are the result of using 128 modes and executing code that is based upon the spectral algorithm derived in Chapter 2. The code was implemented and verified in Matlab. The source code, as well as the results of a few simple test cases have been included in Appendix D.

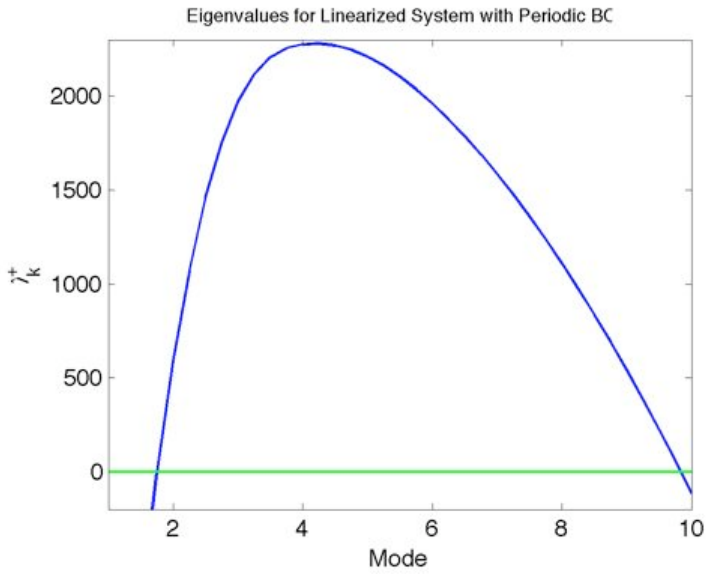

(a) $\xi_{1,k}^+$ for local diffusion

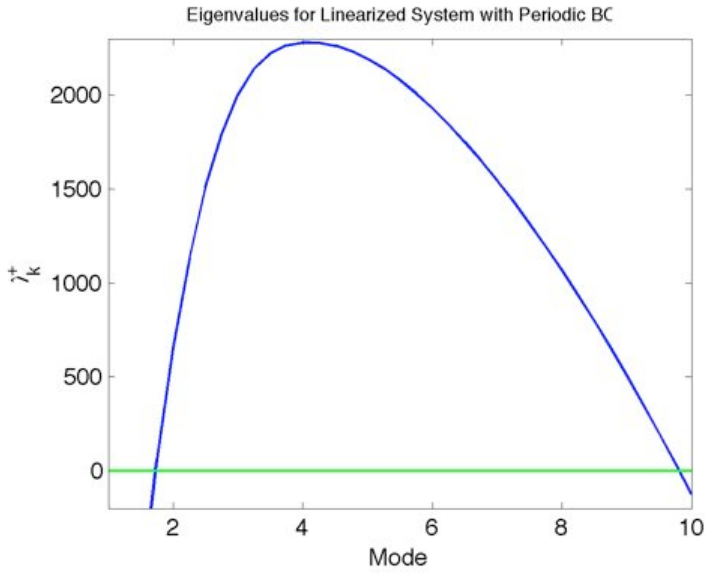

(b) $\xi_{0,k}^+$ for nonlocal diffusion

Figure 5.1: Similar positive eigenvalues for both local and nonlocal diffusion, using $(d,\gamma) = (500, 3500)$.

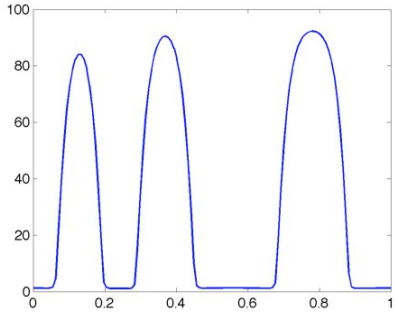

(a) $\beta = 0.00$

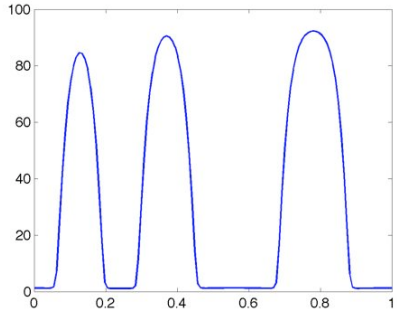

(b) $\beta = 0.25$

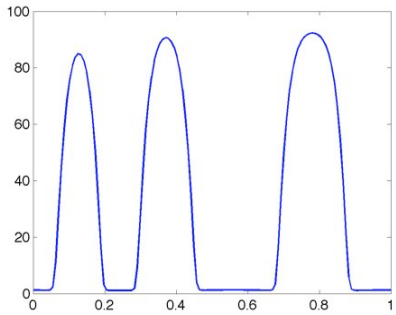

(c) $\beta = 0.50$

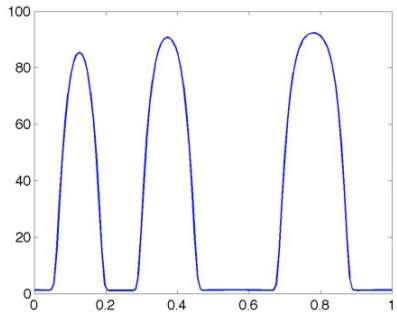

(d) $\beta = 0.75$

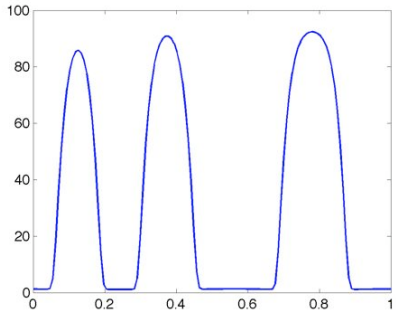

(e) $\beta = 1.00$

Figure 5.2: Similar patterns occur for $0 \leq \beta \leq 1$, when the linearized right hand sides of the local and nonlocal systems have positive eigenvalues that are very close. See Figure 5.1 for the positive dispersion relations. The simulation that produced these solutions was stopped at $time = .01$, and the same random initial conditions were used for each β.

Table 5.1: Values for $||u||_2$ and $||v||_2$ for the sample run described in Figure 5.2. For each β, the same random initial conditions were used. For a fixed β, the norms of u and v are similar to the norms of corresponding solutions of other β values. This is expected since the positive dispersion relations for the local and nonlocal systems are similar.

β	$\|\|u\|\|_2$	$\|\|v\|\|_2$
1.00	566.5886340029	254.1897514141
0.75	566.5090275642	254.2089822436
0.50	566.4197862710	254.2800503218
0.25	566.3728375571	254.2753654840
0.00	566.4085306740	254.3038483792

This example shows that as β is changed from 1 to 0, the same pattern persists. Table 5.1 shows that the norms of the solutions remain close as β changes. By choosing parameters for the kernel associated with $\mathcal{J}$, the positive portion of the local and nonlocal dispersion curves can be made very close. In doing this, the patterns found for all $0 \leq \beta \leq 1$ should be very similar. The next section gives a more systematic approach for discovering the correct (A,σ)-pair that result in similar positive dispersion curves and solutions for $0 \leq \beta \leq 1$.

5.3.1 Description of Numerical Experiment and Results

In this subsection, we describe a systematic approach for determining the kernel parameters such that for all $0 \leq \beta \leq 1$, System 1.1 generates similar solutions when the same initial conditions are used. In the previous chapter, we gave an example in which the nonlinearity greatly influenced the nonlocal system, but not the local system. However, Bates and Chen [4] point out that the Laplacian is considered as a first-order approximation for pure nonlocal systems for a single space dimension. See also [5,6]. Furthermore, it is possible to approximate the nonlocal heat equation subject to Dirichlet boundary conditions [11] and the heat equation subject to Neumann boundary conditions [12] with local diffusion. The relevant perspective from these results for our situation is that as σ gets smaller, the local and nonlocal systems should produce similar solutions. Thus, we expect small σ values so that the dispersion relations of the local and nonlocal systems match. By small, we mean in comparison to $\sigma = .1$ that was used Section 4.5.

With the kernel parameters are selected, we conclude this subsection by evolving the same set of random initial conditions for each

$$\beta \in \{0.00, 0.25, 0.50, 0.75, 1.00\}, \tag{5.10}$$

a constant amount of time so that the relative L^2-difference between the solutions can be computed. If the kernel choices are reasonable, then the L^2 differences between the local solution and the other solutions for each β should be small. The results given in this section show this to be the case. In the next section, we therefore only look at patterns for one β value, since we have numerically demonstrated that it is possible for all considered β values to give rise to the same solution.

The simulation is stopped when the simulation time is T_{max}. The values are given in Table 5.2. Heuristically, these time values are based upon observations in which the solutions appeared to not change very much.

For parameter selection, we proceed by selecting (d,γ) pairs that allow for pattern

Table 5.2: Stopping times for 1d and 2d simulations.

γ	$1d$	$2d$
100	0.50	1
1000	0.05	.1
5000	0.05	.1

formation in System 1.1 with periodic boundary conditions and $\beta = 1$. In [45, p. 112], Murray uses various parameter values for (d,γ) in an attempt to classify the types of patterns encountered for the local reaction-diffusion system with homogeneous Neumann boundary conditions. We use a variation of these parameters. To understand the effects of higher values of the domain size, we have chosen to use a somewhat higher set of γ values than Murray. Furthermore, the d values that we have used have a much finer granularity than those of Murray. The parameters that we have used for our numerical experiments are given as

$$\gamma_{local} \in \{100, 1000, 5000\}, \tag{5.11}$$

$$d_{local} \in \{50, 100, 200, ..., 2000\}. \tag{5.12}$$

For fixed $(d_{local}, \gamma_{local})$, we compute the corresponding dispersion relation. With the fixed dispersion relation for local diffusion, we select kernel parameters (A,σ) such that the positive eigenvalues of the dispersion relation for the nonlocal case are close to the positive eigenvalues of the dispersion relation for the local case. We achieve this if we make the least square difference between the two dispersion relations small. For this numerical experiment, the function

$$f_{obj} = \sum_{k=M}^{N} (\xi_{1,k} - \xi_{0,k})^2, \tag{5.13}$$

is minimized where $\xi_{k,1}$ and $\xi_{k,0}$ are the eigenvalues of the linearized local and nonlocal systems, respectively, and $M \leq k \leq N$ describes the range of positive eigenvalues of $\xi_{k,1}$.

The Discrete Fourier Transform (DFT) is used to estimate the coefficients $\xi_{k,0}$. For small σ, the objective function f_{obj} can seem to change abruptly for small perturbations in σ. This effect is directly attributed to the discretization used to estimate the Fourier coefficients. For one dimension, the particular implementation of the DFT used for the numerics uses the discretization of

$$d_x = \{0, \frac{1}{\mathrm{P}}, ..., \frac{\mathrm{P}}{2}, -\frac{\mathrm{P}+1}{2}, ..., -\frac{1}{\mathrm{P}}\},$$

where P represents the number of points used in the discretization. For the kernel J_1 with a small $\sigma \leq .1$, observe that J_1 is very close to 0, except for when J_1 is evaluated over the intervals $[0, 3 \cdot \sigma]$ and $[1 - 3 \cdot \sigma, 1]$. Heuristically, we need $\mathrm{P} \geq \frac{1}{\sigma}$ to obtain a reasonable estimate of J and its Fourier coefficients. For sufficiently small σ, the DFT will be unusable, since it will require more points than can be afforded on a finite precision machine. As such, this will affect f_{obj} by creating erroneous discontinuities in f_{obj}. A minimization technique such as the steepest descent method is useless, since it requires knowledge of the gradient of the function over the region the function is minimized.

To overcome the difficulty introduced, we begin by discretizing σ into a uniform grid over values $[\sigma_{min}, \sigma_{max}]$ such that the DFT accurately estimates J. Denote this grid as

$$G_d = \{\sigma_j : \sigma_j = \sigma_{min} + j \cdot (\sigma_{max} - \sigma_{min})/N_\sigma), 0 \leq j \leq N_\sigma\},$$

where $N_\sigma + 1$ is the number of uniformly distributed points on $[\sigma_{min}, \sigma_{max}]$. For each fixed σ_j in the discretized grid G_d, we then use a robust method such as the golden search method to estimate the value A_j that minimizes f_{obj} for the fixed value of σ_j. We then select A such that

$$A = \min_{0 \leq j \leq N_\sigma} A_j. \tag{5.14}$$

Note that we can get better estimates for the minimum by selecting smaller grids for σ, as long as the DFT can accommodate such values of σ.

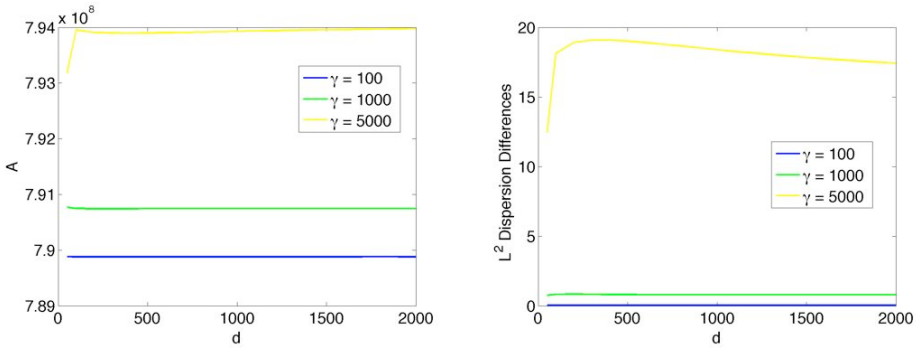

(a) A values that minimize Eq. (5.13) (b) Minimization error of Eq. 5.13

Figure 5.3: The minimizing values of Eq. (5.13) and corresponding minimization error using the 1d kernel J_1 defined in Eq. (5.2).

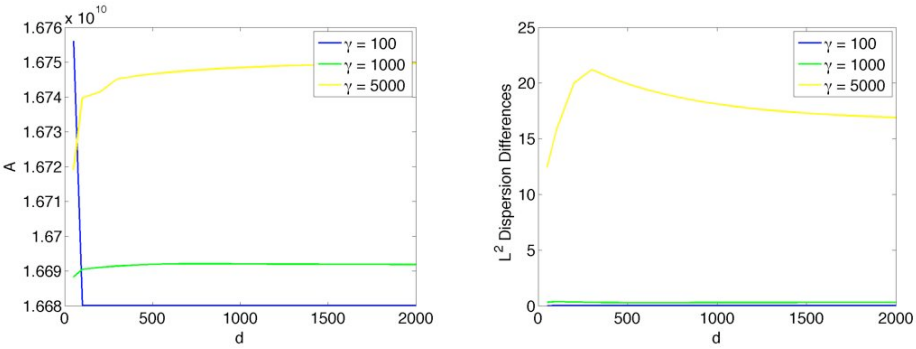

(a) A values that minimize Eq. (5.13) (b) Minimization error of Eq. 5.13

Figure 5.4: The minimizing values of Eq. (5.13) and corresponding minimization error using the 2d kernel J_2 defined in Eq. (5.5).

The actual grid used for this numerical experiment is the grid containing 100 points that are uniformly spaced over the interval $[.001, .1]$. Using the minimization technique described and the parameters d and γ specified above, values of σ and A corresponding to each value of d and γ are determined. Figures 5.3 and 5.4 give the results. For both the 1d and 2d cases, the values of σ remain constant over the values of d and γ. For the 1d case, $\sigma = 0.002$ and for the 2d case, $\sigma = 0.003$. This gives a verification that smaller σ values tend to result in nonlocal solutions that are similar to the local solutions. Again, we mean smaller in comparison to $\sigma = .1$ of Section 4.5. Note that for fixed γ values, the dispersion errors seem to approach asymptotes as indicated in Figures 5.3 and 5.4. The reason for this is because the $\xi_{1,k}^{+}$ and $\xi_{0,k}^{+}$ do not change significantly for large d, thus explaining this

behavior. The interval in which the eigenvalues $\xi^{+}_{\beta,k}$ are positive is given by $[s_{\gamma,l}, s_{\gamma,r}]$, where

$$s_{\gamma,l} = \frac{\gamma(df_u + g_v) + \sqrt{\gamma^2(df_u + g_v)^2 - 4d\gamma^2(f_u g_v - f_v g_u)}}{2d}, \tag{5.15}$$

$$s_{\gamma,r} = \frac{\gamma(df_u + g_v) - \sqrt{\gamma^2(df_u + g_v)^2 - 4d\gamma^2(f_u g_v - f_v g_u)}}{2d}, \tag{5.16}$$

and are found as the roots of the equation defining the eigenvalues in Lemma 5.2.1. For fixed γ with $d \to \infty$, we see that the positive interval converges to the interval given by $[0, \gamma \cdot f_u]$. This means that as d increases, the positive eigenvalues of the linearization also approach constant values for $\beta = 0$ and $\beta = 1$. Thus, the L^2 differences that compare the positive eigenvalues of the local and nonlocal linearization also approach an asymptote as d increases.

With the parameters for (A,σ) determined, we now compare solutions of System 1.1 with $\beta = 1$ to solutions of the same system using the values of β given in (5.10). For each β, we compare corresponding solutions to the solutions of the local system using the relative norm

$$||(u_\beta, v_\beta)||_r = \frac{||(u_1 - u_\beta, v_1 - v_\beta)||_{L^2}}{||(u_1, v_1)||_{L^2}}, \tag{5.17}$$

where (u_1, v_1) is the solution of the local system, (u_β, v_β) is the solution of the system with $0 \leq \beta < 1$, and $||(u,v)||^2_{L^2} = ||u||^2_{L^2} + ||v||^2_{L^2}$. Figures 5.5 and 5.6 contain the relative norm results for the 1d and 2d cases, respectively. Further information about the solutions such as the norm values of the u and v component can be found in Appendices B - C. Again, the values of T_{max} can be found in Table 5.2. Figure 5.5 shows that for most solutions, as β changes, there is agreement with the local solutions with relative errors less than 2%. For the 2d case, Figure 5.6 shows similar agreement, except for the case of (d,γ) = $(200, 5000)$. This can be attributed to the method producing an A value for the kernel that was close to the optimal A value, but not close enough to produce very similar solutions. See Figure 5.7.

The solutions do have very similar features in spite of the relatively higher minimization error.

Collectively, the data generated suggests that for the values of (d,γ) considered in this study, the local and nonlocal system can produce similar patterns. Furthermore, similar dispersion relations for both the local and nonlocal system will give rise to similar solutions for intermediate β values. We now focus on exploring the same parameter range of β and γ for only pure local diffusion and provide the types of patterns that may be possible for System 1.1.

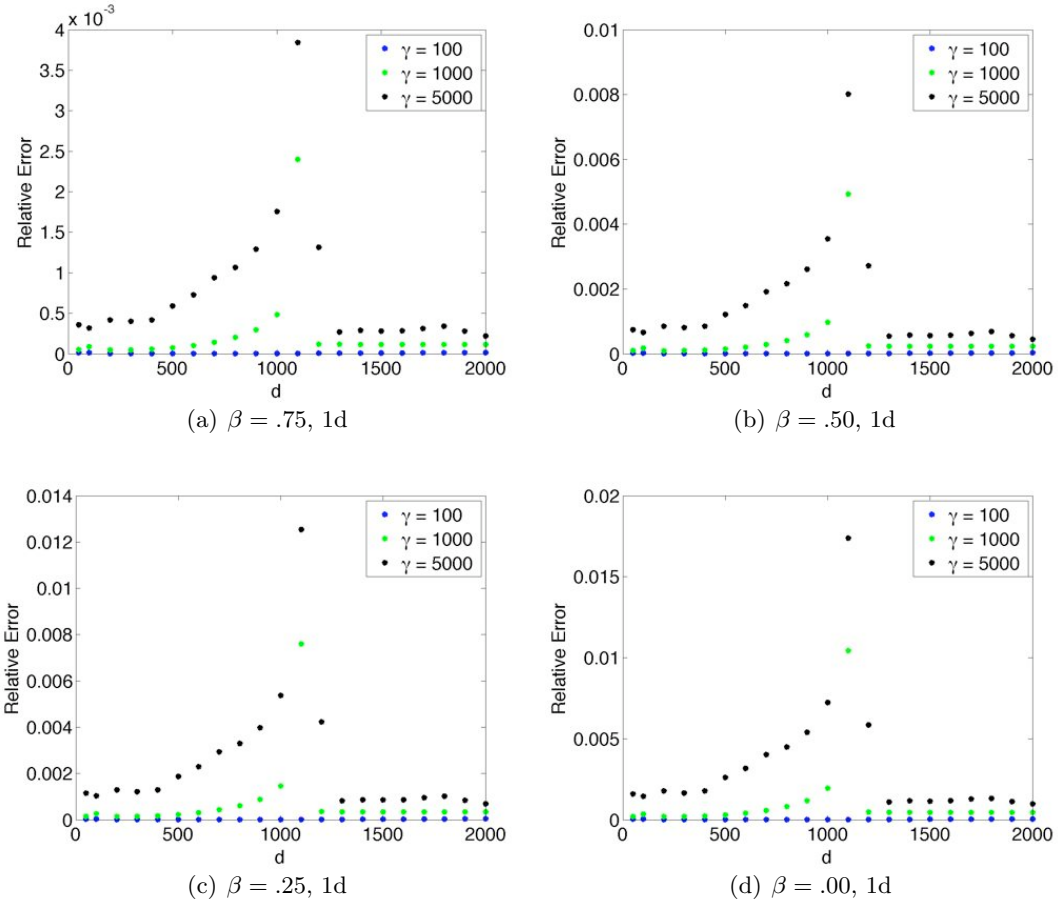

(a) $\beta = .75$, 1d (b) $\beta = .50$, 1d

(c) $\beta = .25$, 1d (d) $\beta = .00$, 1d

Figure 5.5: The $y-$axis represents the values of $||(u_\beta, v_\beta)||_r$, where $||\cdot||_r$ is given by (5.17). For each (d,γ) and β value, the same random initial condition was evolved until $time = T_{max}$. See Table 5.2 for the time values. The relative difference between the local solution and the solution associated with $0 \leq \beta < 1$ was computed and plotted for each (d,γ). The small relative difference between these solutions confirms that similar solutions can be generated for the 1d version of System 1.1 when the appropriate kernel parameters are selected.

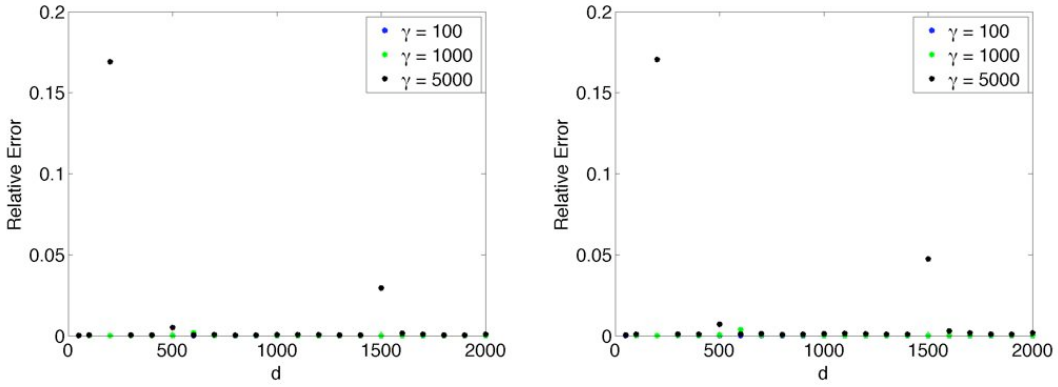

(a) $||(u,v)_{.75}||_r$, 2d (b) $||(u,v)_{.50}||_r$, 2d

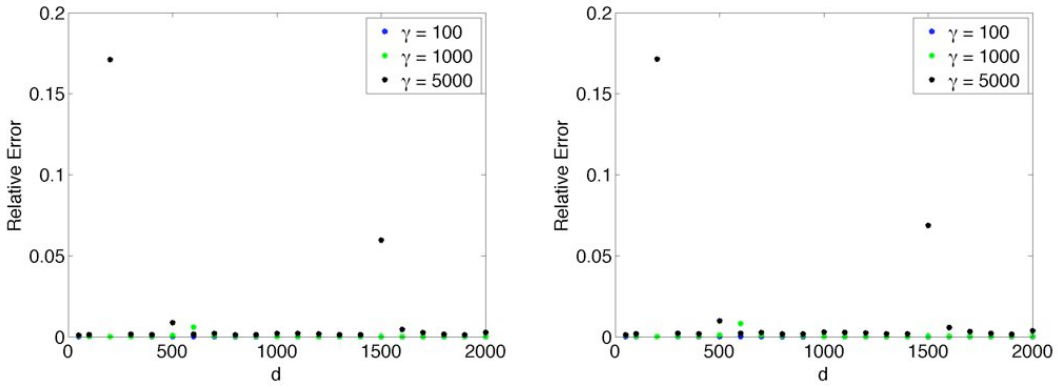

(c) $||(u,v)_{.25}||_r$, 2d (d) $||(u,v)_0||_r$, 2d

Figure 5.6: The $y-$axis represents the values of $||(u_\beta, v_\beta)||_r$, where $||\cdot||_r$ is given by (5.17). For each (d,γ) and β value, the same random initial condition was evolved until $time = T_{max}$. See Table 5.2 for the time values. The relative difference between the local solution and the solution associated with $0 \leq \beta < 1$ was computed and plotted for each (d,γ). For most cases, there is a small relative difference between the solutions. This confirms that similar solutions can be generated for the 2d version of System 1.1 when the appropriate kernel parameters are selected. However, the error for $(d,\gamma) = (200, 5000)$ is larger compared to the other (d,γ)-pairs. This can be attributed to a shortcoming of the method.

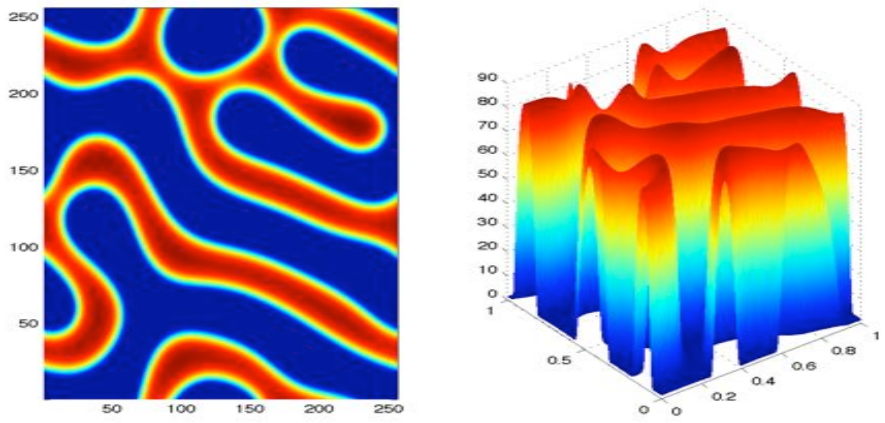

(a) Local solution

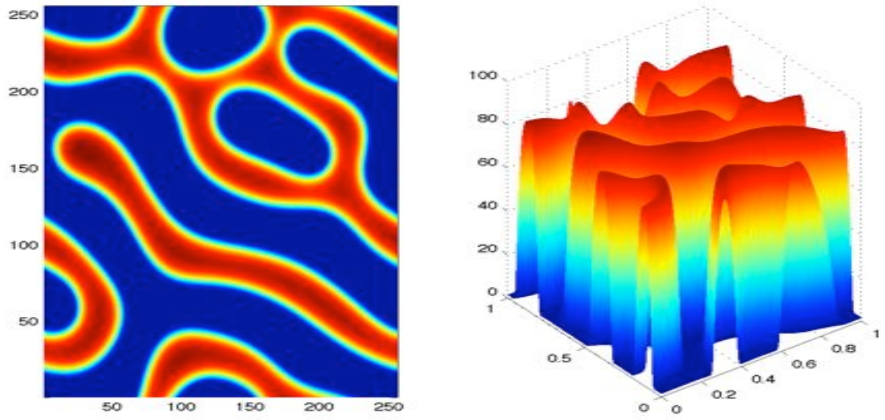

(b) Nonlocal solution

Figure 5.7: Comparison of local and nonlocal solutions for $(d,\gamma) = (200, 5000)$, $time = .1$. The nonlocal solution is produced using the kernel parameters that were determined by the minimization method presented in this section. In this particular case, the method produced an A value that was smaller than the optimal A value for kernel J_2 given by (5.5). The result is that although the solutions produced using the same initial conditions are distinct, the two solutions share several common features.

5.3.2 Patterns for the Local System Subject to Periodic Boundary Conditions

In this section, we present a more qualitative description of the types of patterns that are generated when applying the spectral method described by Equations (2.29) - (2.30) to System 1.1 with pure local diffusion. If Turing instability is present, then for slight perturbations of the homogeneous equilibrium, we expect the initial conditions to evolve into nontrivial solutions. Patterns such as spots or stripes have been experimentally observed in the CIMA reaction in a gel reactor [9], [46], the CDIMA reaction [23] and more recently the BZ reaction dispersed in a water-in-oil microemulsion system [60]. Models for the CIMA reaction [32], CDIMA reaction [62] and BZ reaction [33] have all been shown to produce both spots and stripes. Using the 2d form of System 1.1 with $\beta = 1$, we present results showing that these types of patterns can be found in System 1.1 when using the Thomas nonlinearities. As before, we use the same values of the parameters for β and γ given in 5.11 and 5.12, respectively. The patterns are observed when the resulting simulation reaches the stopping time of T_{max}, which is specified in Table 5.2. The same set of initial conditions was used to generate solutions for all values of d and γ considered. The patterns are grouped according to their associated γ values. For fixed γ, we observe how the complexity of the pattern geometry changes as d increases.

For $\gamma = 100$, we get the striped pattern as shown in Figure 5.8. For all d values considered in this study, we were only able to find the striped patterns. For $\gamma = 1000$, we get the patterns shown in Figure 5.9. Figure 5.9 shows that as d increases, the complexity of the patterns decreases for $\gamma = 1000$. In fact, we see that as d increases we transition from a complex geometrical pattern to a circle.

For $\gamma = 5000$, we get the patterns shown in Figure 5.10. All of the patterns generated for the corresponding d values produced snakelike patterns. These solutions, although well-defined, lack any kind of recognizable geometry as in comparison to the patterns corresponding to lower values of γ. However, as with $\gamma = 1000$, the patterns associated with $\gamma = 5000$ decrease in complexity as d increases.

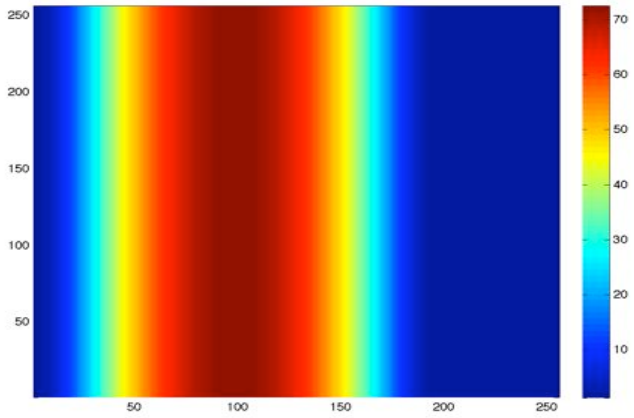

Figure 5.8: Patterns for the local system with $\gamma = 100$ and $time = 1$. For all of the d values considered, only striped patterns are found.

These solutions were generated using the same initial condition for each run of the simulation. Using multiple initial conditions, we now demonstrate that for the values of d and γ in Figures 5.8 - 5.10, we can produce the same types of patterns, but with some exceptions. We also tripled the stopping time listed in Table 5.2 so as to better see more longer term behavior. Again, we examine the pattern complexity for each γ as d increases to determine if the increased stopping time has any effect on the generated solutions. Figure 5.11 shows the results for $\gamma = 100$. For this case, all of the solutions have a single stripe.

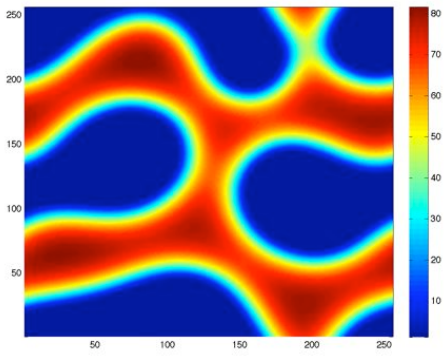

(a) $(d,\gamma) = (100, 1000)$

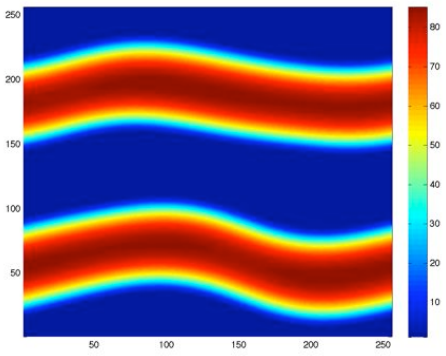

(b) $(d,\gamma) = (200, 1000)$

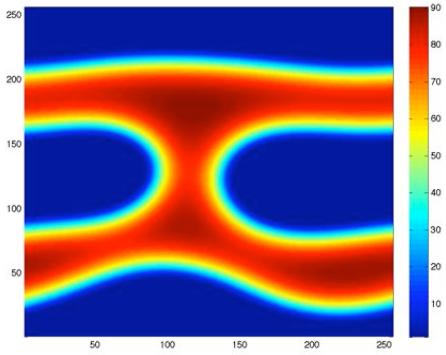

(c) $(d,\gamma) = (400, 1000)$

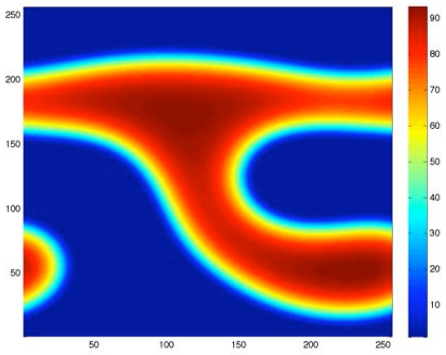

(d) $(d,\gamma) = (500, 1000)$

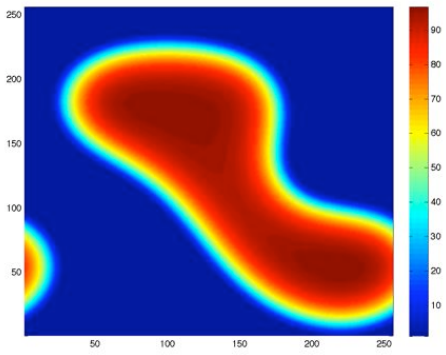

(e) $(d,\gamma) = (700, 1000)$

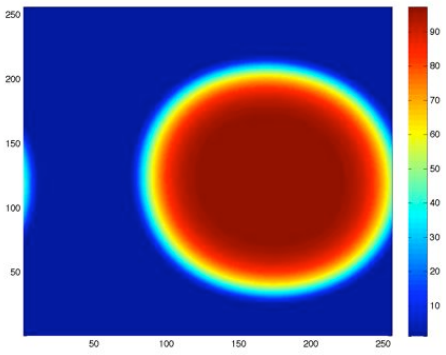

(f) $(d,\gamma) = (1000, 1000)$

Figure 5.9: Patterns for the local system with $\gamma = 1000$ and $time = .1$. These patterns were generated using the same initial conditions for all d and γ. Increasing d tends to decrease the complexity of the patterns. Part (a), in comparison to Parts (b) - (f), shows a less organized structure. As we move to Part (b), we see a set of wavy lines emerge. Transitioning from Part (b) to (c), we see the wavy lines become attached in the center. Transitioning from Parts (c) - (e), we see a change from the connected lines to more of an unfamiliar shape. The final transition from (e) - (d) shows the formation of a circle.

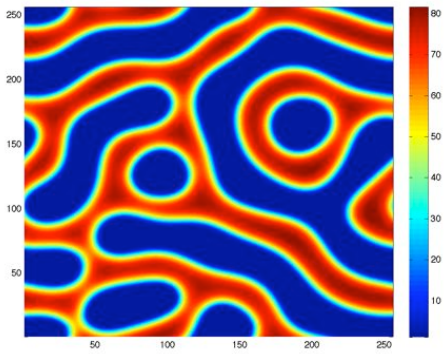

(a) $(d,\gamma) = (100, 5000)$

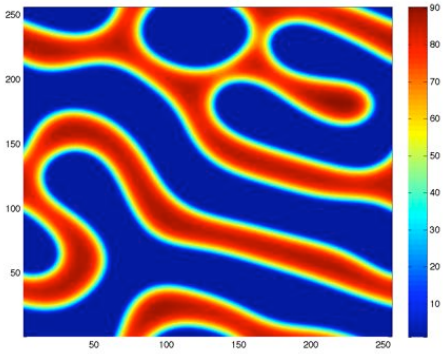

(b) $(d,\gamma) = (200, 5000)$

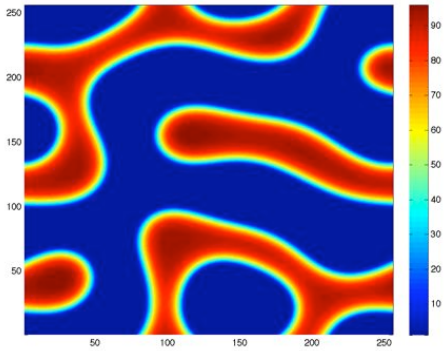

(c) $(d,\gamma) = (500, 5000)$

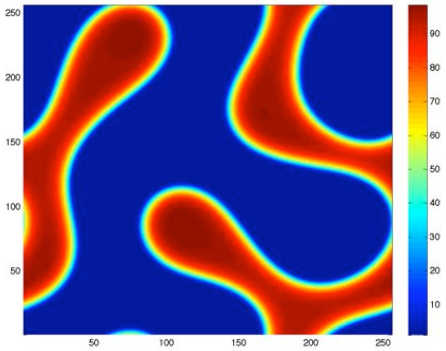

(d) $(d,\gamma) = (1100, 5000)$

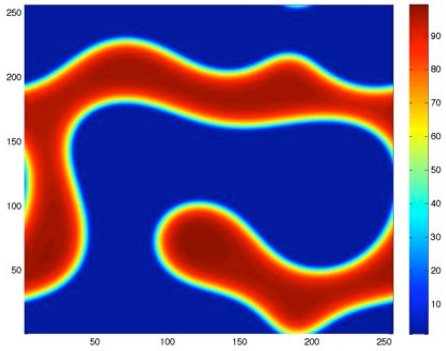

(e) $(d,\gamma) = (1500, 5000)$

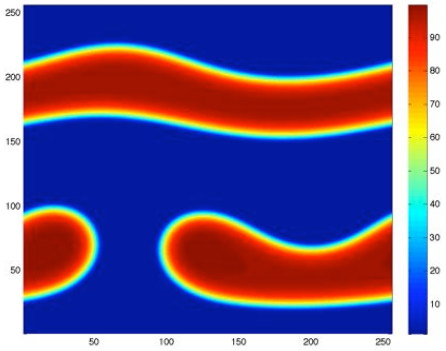

(f) $(d,\gamma) = (2000, 5000)$

Figure 5.10: Patterns for the local system with $\gamma = 5000$ and $time = .1$. As with $\gamma = 1000$, we see that the pattern organization increase as d increases. For Parts (a) and (b), we see a group of snakelike structures. As d increases, Parts (c) and (d) show a decrease in pattern complexity. Transitioning to Parts (d) - (f), we see a dramatic decrease in pattern complexity to what appears to be two lines, one connected and the other disconnected.

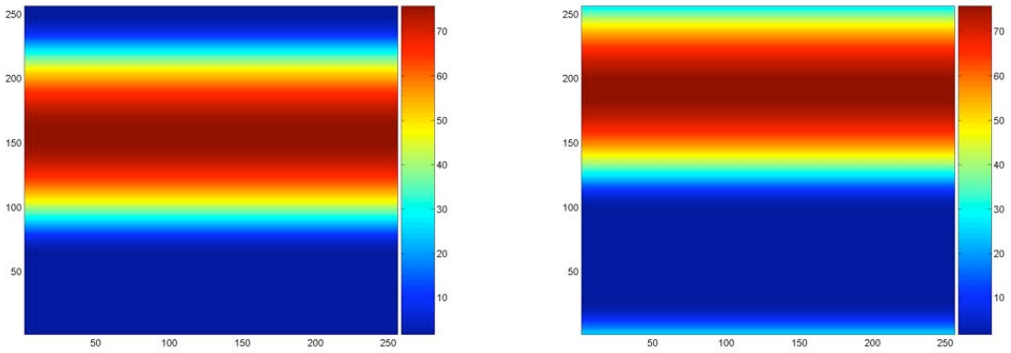

(a) Iteration 1

(b) Iteration 2

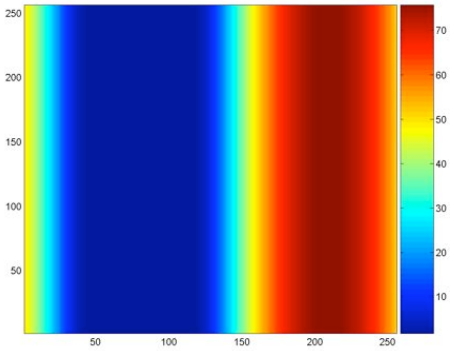

(c) Iteration 3

Figure 5.11: Patterns for the local system with $d = 2000$ and $\gamma = 100$, each using a different set of random initial conditions. The stopping time is $time = 3$. Only the single stripe seems available for this γ value.

For $\gamma = 1000$, the patterns are slightly more complicated. For $d = 100$, Figure 5.12 shows a striped pattern for the first and second iteration. However, for the third iteration, the set of initial conditions used produces a pattern that contains hexagonally arranged spots. For $d = 200$, Figure 5.13 shows again the presence of stripes in the second iteration. However, the first and third iteration show solutions that are slightly more irregular when compared to the second iteration. The third iteration also contains holes in the stripes. For $d = \{400, 500, 700\}$, Figures 5.14 - 5.16 show the striped patterns. For $d = 1000$, Figure 5.17 shows larger spots for iteration 1 and stripes for the other iterations.

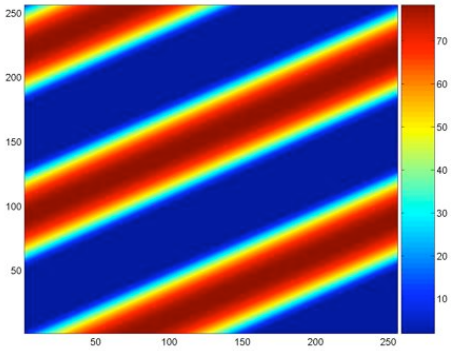

(a) Iteration 1

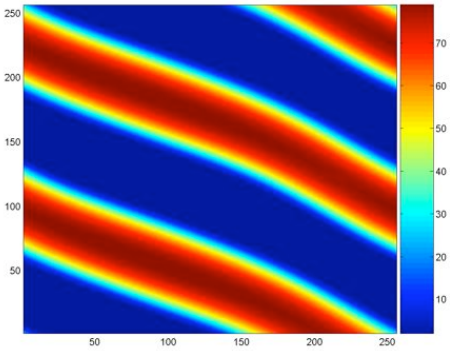

(b) Iteration 2

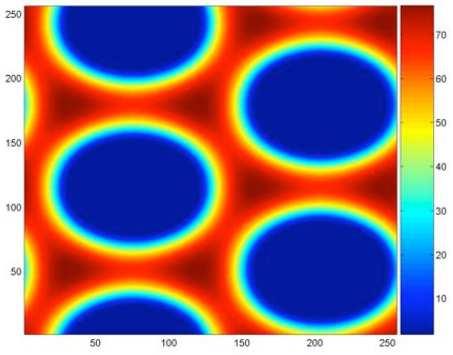

(c) Iteration 3

Figure 5.12: Patterns for the local system with $d = 100$, $\gamma = 1000$ and $time = .3$. Using three distinct sets of random initial conditions, these patterns were generated. For two of the iterations, we see that we generated striped patterns. Note, however, we did get a hexagonal array of spots depicted in Part (c). Figures 5.13 - 5.17 show some of the remaining results for $\gamma = 1000$.

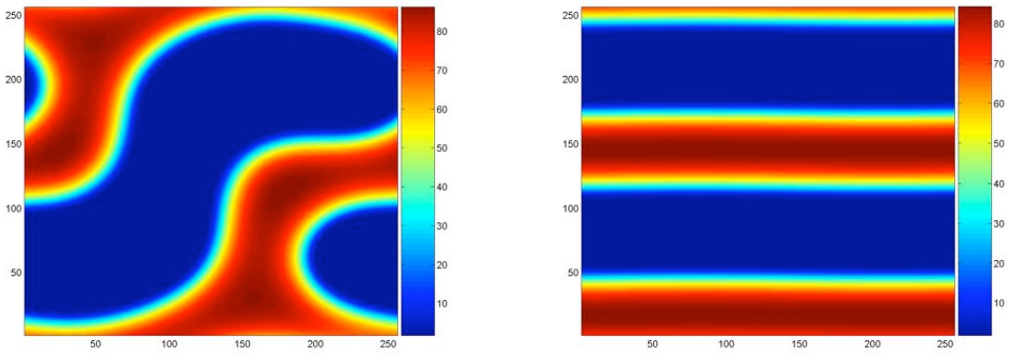

(a) Iteration 1

(b) Iteration 2

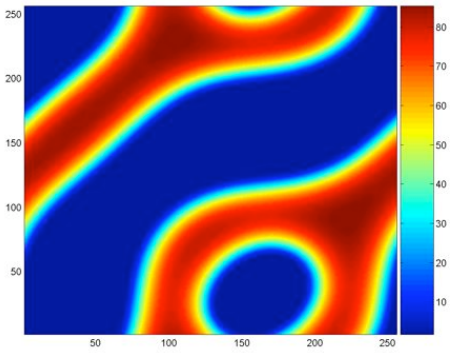

(c) Iteration 3

Figure 5.13: Patterns for the local system with $d = 200$, $\gamma = 1000$ and $time = .3$. Using three distinct sets of random initial conditions, these patterns were generated.

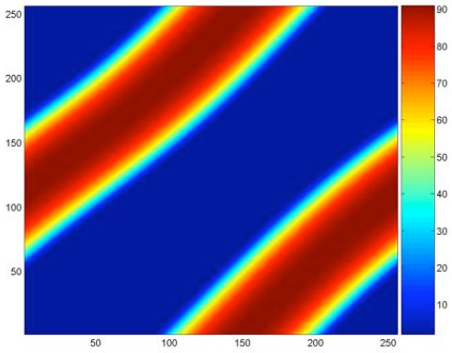

(a) Iteration 1

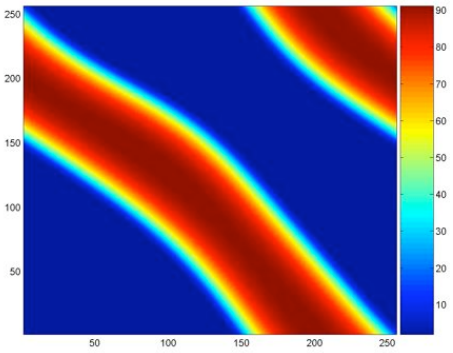

(b) Iteration 2

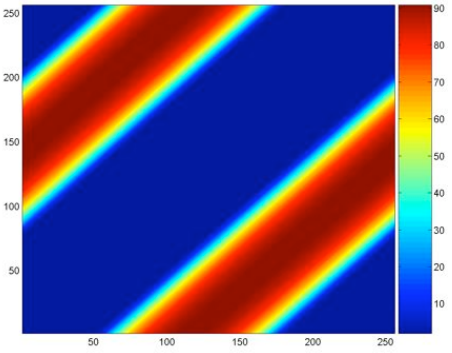

(c) Iteration 3

Figure 5.14: Patterns for the local system with $d = 400$, $\gamma = 1000$ and $time = .3$.

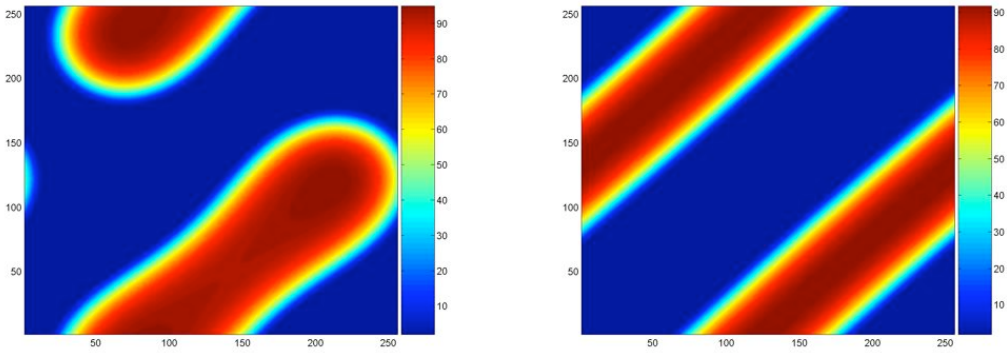

(a) Iteration 1

(b) Iteration 2

(c) Iteration 3

Figure 5.15: Patterns for the local system with $d = 500$, $\gamma = 1000$ and $time = .3$.

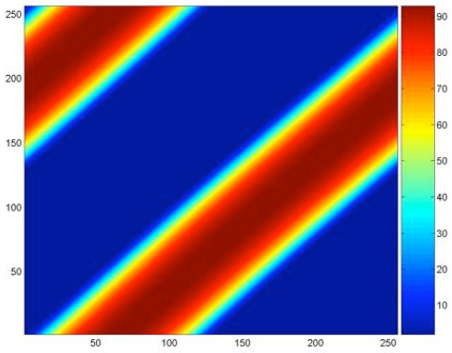

(a) Iteration 1

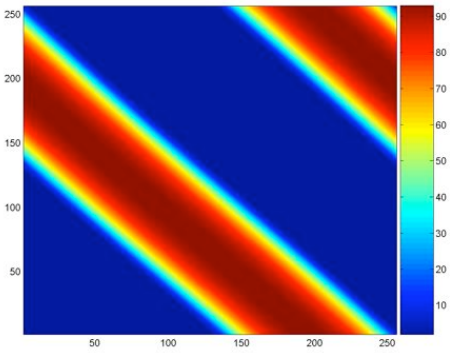

(b) Iteration 2

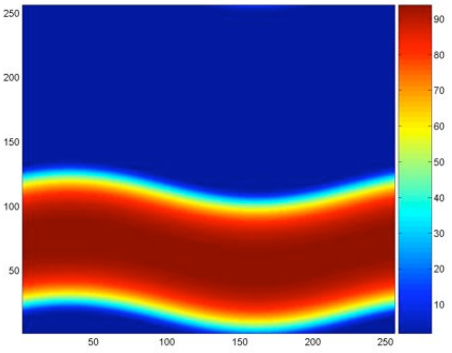

(c) Iteration 3

Figure 5.16: Patterns for the local system with $d = 700$, $\gamma = 1000$ and $time = .3$.

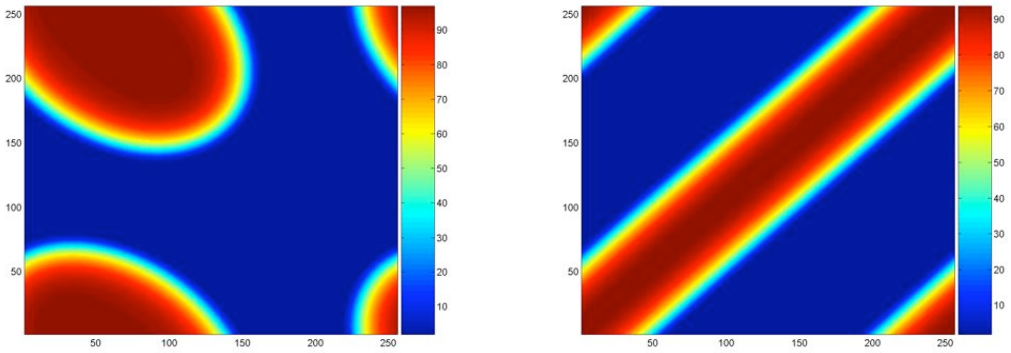

(a) Iteration 1

(b) Iteration 2

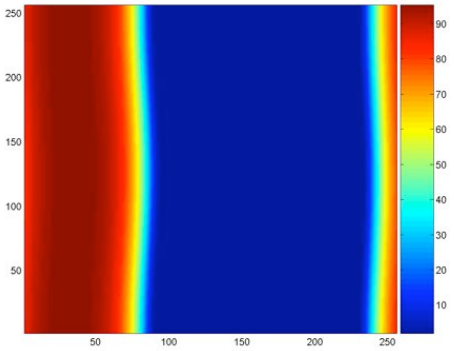

(c) Iteration 3

Figure 5.17: Patterns for the local system with $d = 1000$, $\gamma = 1000$ and $time = .3$. If we compare these solutions to the other solutions corresponding to the lower d values in Figures 5.12 - 5.16, we observe that the pattern complexity does not increase substantially.

For $\gamma = 5000$, we see a wavy striped pattern given by the second iteration for $d = 100$ as shown in Figure 5.18. The other two iterations show much more intricate, snakelike patterns. Figures 5.19-5.20 show more irregular patterns for $d = 200$ and $d = 500$, respectively. In Figure 5.21, for $d = 1100$, we see that the first iteration shows a striped pattern that we have seen for the lower values of γ. However, Figures 5.22 - 5.23 show much more symmetrical patterns that have not been previously observed.

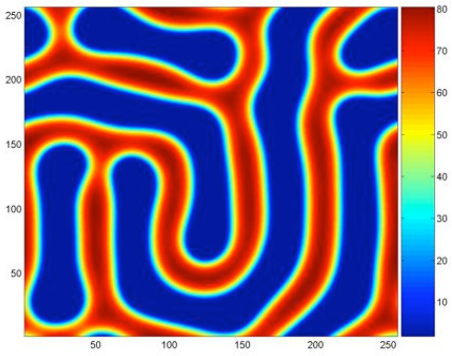

(a) Iteration 1

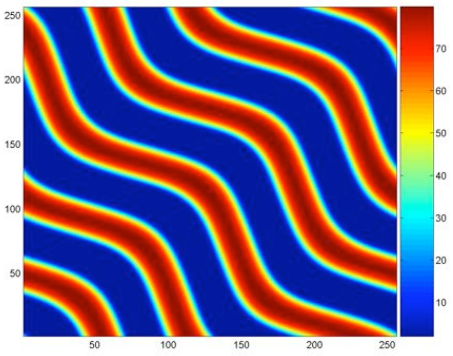

(b) Iteration 2

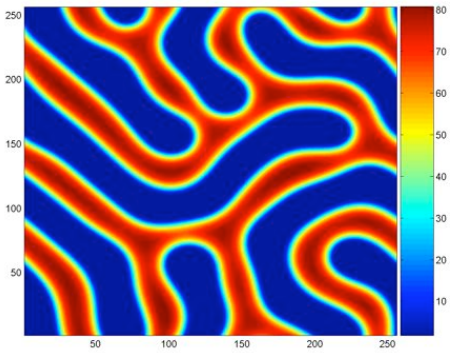

(c) Iteration 3

Figure 5.18: Patterns for the local system with $d = 100$, $\gamma = 5000$ and $time = .3$. If we compare the solutions of this figure to the solutions of Figures 5.19 - 5.23, we see that increasing the d value seems to decrease the pattern complexity.

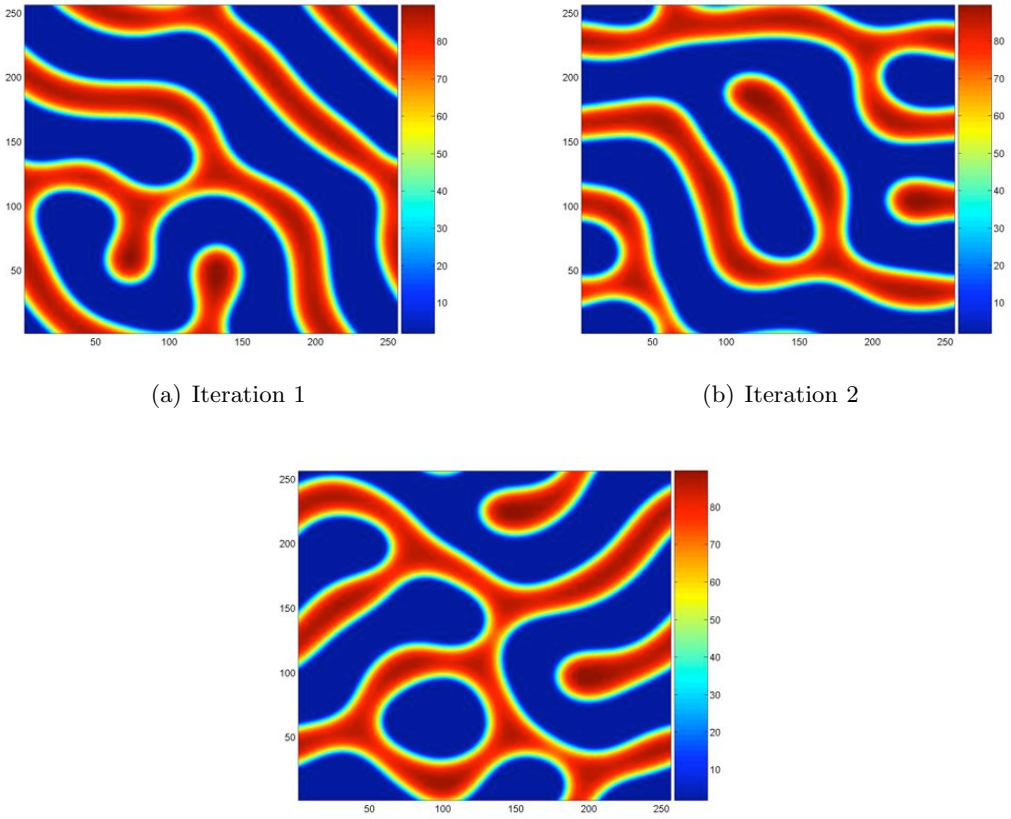

(a) Iteration 1

(b) Iteration 2

(c) Iteration 3

Figure 5.19: Patterns for the local system with $d = 200$, $\gamma = 5000$ and $time = .3$.

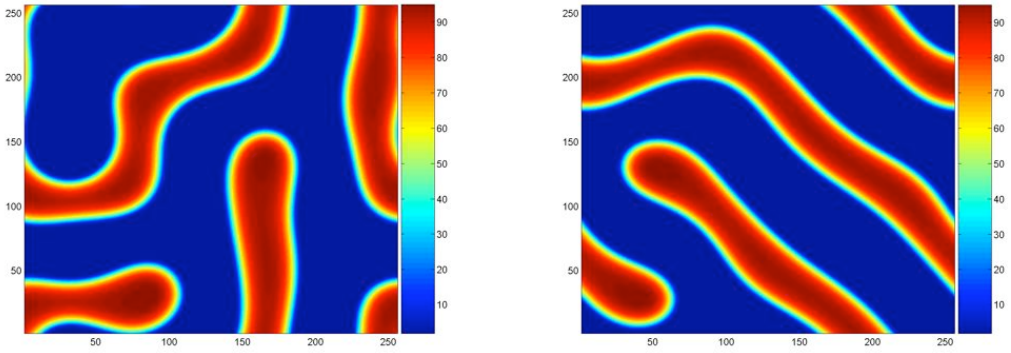

(a) Iteration 1

(b) Iteration 2

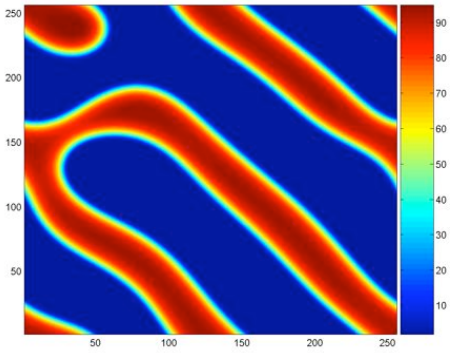

(c) Iteration 3

Figure 5.20: Patterns for the local system with $d = 500$, $\gamma = 5000$ and $time = .3$.

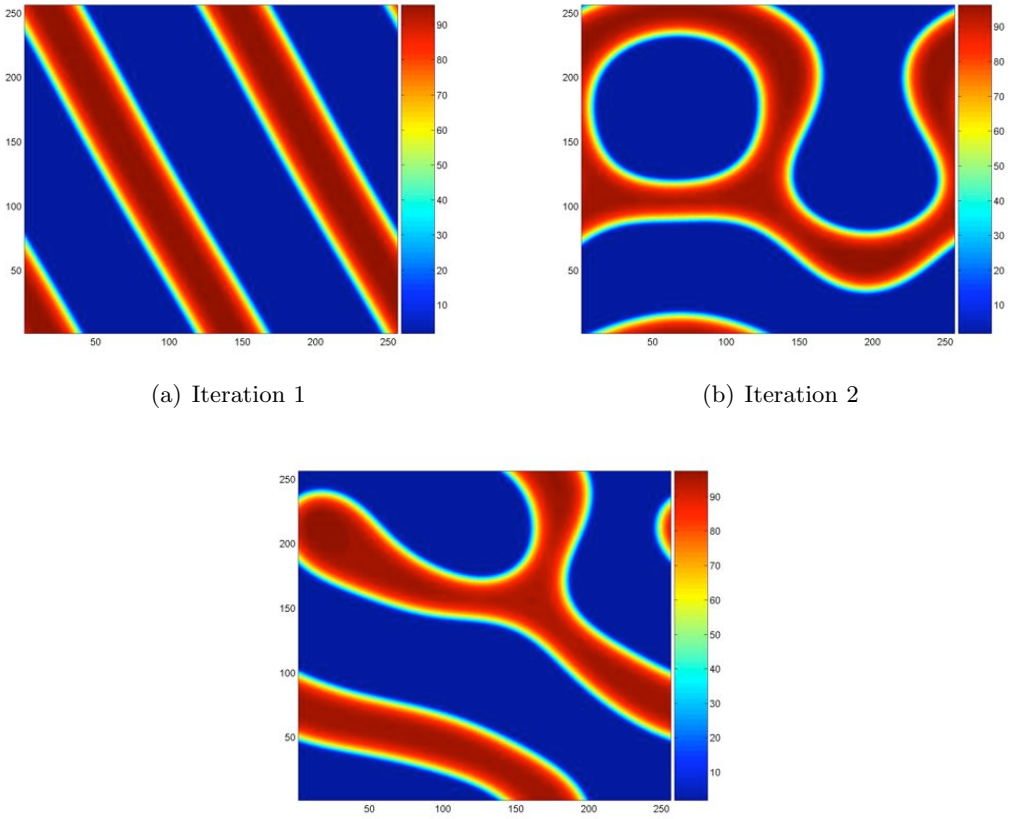

(a) Iteration 1

(b) Iteration 2

(c) Iteration 3

Figure 5.21: Patterns for the local system with $d = 1100$, $\gamma = 5000$ and $time = .3$.

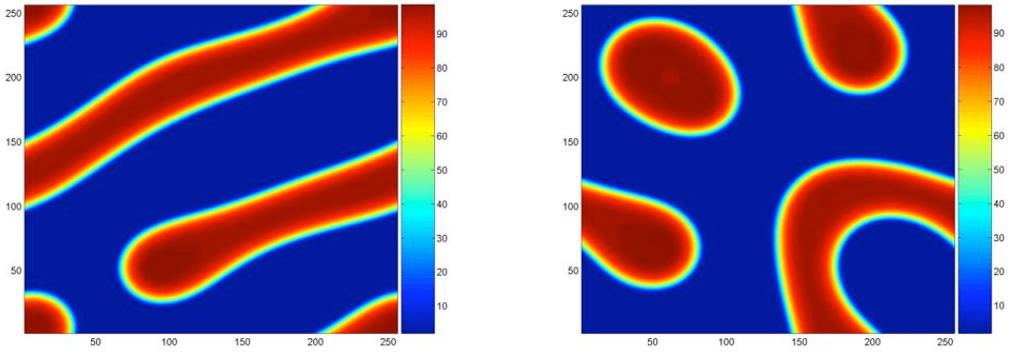

(a) Iteration 1

(b) Iteration 2

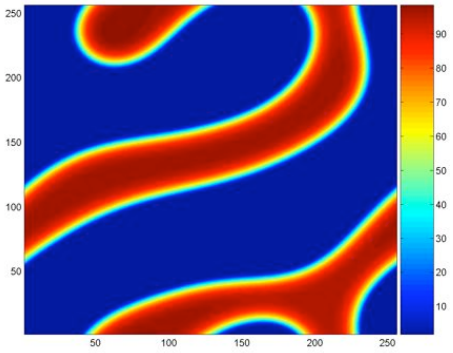

(c) Iteration 3

Figure 5.22: Patterns for the local system with $d = 1500$, $\gamma = 5000$ and $time = .3$.

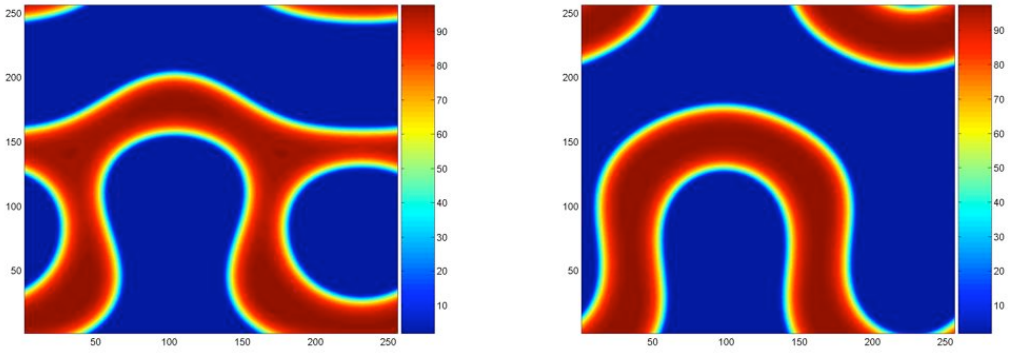

(a) Iteration 1

(b) Iteration 2

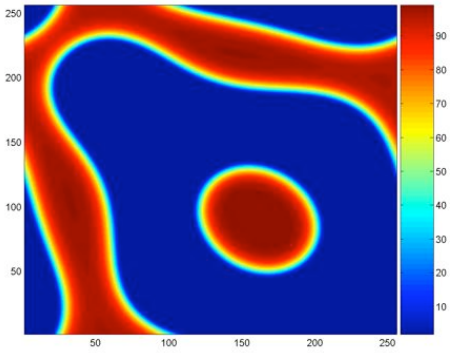

(c) Iteration 3

Figure 5.23: Patterns for the local system with $d = 2000$, $\gamma = 5000$ and $time = .3$.

Table 5.3: The supremum norm of the right hand side of the local periodic system, $\gamma = 100, time = 3$. The large values indicate that the solutions are far away from any equilibria.

iteration	$d = 2000$
1	5861.10
2	5861.08
3	5861.10

Table 5.4: The supremum norm of the right hand side of the local periodic system, $\gamma = 1000, time = .3$. The large values indicate that the solutions are far away from any equilibria.

iteration	$d = 100$	$d = 200$	$d = 400$	$d = 500$	$d = 700$	$d = 1000$
1	49581.31	56979.95	59755.15	65295.98	62770.76	66210.38
2	49841.65	56139.62	59841.45	61135.91	62771.34	64007.92
3	47205.31	56662.88	59718.91	59912.27	61443.44	63023.97

Tables 5.3 - 5.5 show that these patterns are more intermediate patterns and still remain far away from any equilibria of System 1.1 with pure local diffusion. As Figure 5.24, Part (a) shows, some portions of the approximated u do appear to be close to equilibrium. These pieces correspond to the dark red and dark blue regions of Part (b). However, Part (a) shows that the solution in Part (b) has regions that remain far away from any equilibria of the local periodic system.

Table 5.5: The supremum norm of the right hand side of the local periodic system, $\gamma = 5000, time = .3$. The large values indicate that the solutions are far away from any equilibria.

iteration	$d = 100$	$d = 200$	$d = 500$	$d = 1100$	$d = 1500$	$d = 2000$
1	258442.78	307433.18	325399.19	317492.15	340949.26	332016.14
2	245377.01	306033.32	326323.11	324279.23	337714.49	328811.84
3	260102.08	303988.82	325979.14	334928.73	340757.27	341323.83

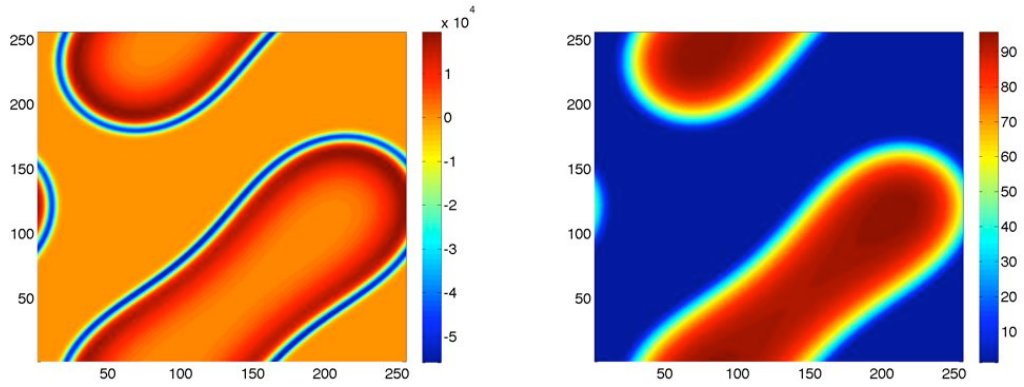

(a) Right hand side of local periodic system

(b) u portion of solution

Figure 5.24: Example of the right hand side of the local periodic system and associated u solution with $d = 500$, $\gamma = 1000$, $time = .3$. This solution corresponds to iteration 1 of Figure 5.15. Note that in Part (a), the orange color indicates some of the solution is close to equilibrium. This corresponds to the dark red and dark blue regions of the pattern formed in Part (b). However, the blue and red borders of Part (a) indicate that the solution remains far away from any equilibria of the local periodic system.

The results of the previous subsection showed that given the appropriate kernel parameters, it is possible to generate the same type of solutions for intermediate values of β for System 1.1. In this subsection, we then analyzed the patterns for $\beta = 1$ and showed that as d increases for each γ, the complexity of the solutions tend to decrease. The results of this section show that we can achieve spots, stripes and irregularly shaped patterns for the local reaction-diffusion system subject to periodic boundary conditions. However, these patterns still remain large distances away from the true equilibria of the local periodic system. For future work, a robust software package like AUTO should be used to find the equilibria for comparison to the intermediate solutions in this study. For documentation about AUTO, see **http://indy.cs.concordia.ca/auto/.**

5.4 Periodic vs. Neumann Boundary Conditions

In this section, we perform a more speculative numerical investigation in which we compare the solutions of the local system subject to homogeneous Neumann boundary conditions to the solutions of the system with periodic boundary conditions. As we are considering local diffusion subject to both homogeneous Neumann and periodic boundary conditions, a natural question is to ask if the boundary conditions make a difference in the solutions. Let (d_n, γ_n) and (d_p, γ_p) denote the d and γ values for the homogeneous Neumann and local periodic ($\beta = 1$) systems, respectively. For both dispersion relations, we sort the eigenvalues in ascending order. If we fix the positive dispersion relation for the Neumann system and choose (d_p, γ_p) so as to minimize the least square error between the first positive eigenvalue of each dispersion relation, we want to know how well the solutions for both systems agree. Using the same initial conditions, the solutions can sometimes be similar, as shown in Figures 5.25 and 5.26.

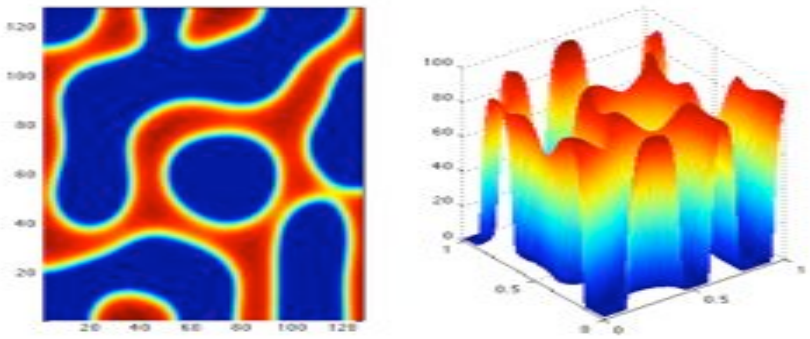

Figure 5.25: u Solution of System 1.2 , $(d,\gamma) = (500, 3500)$ and $time = .1$.

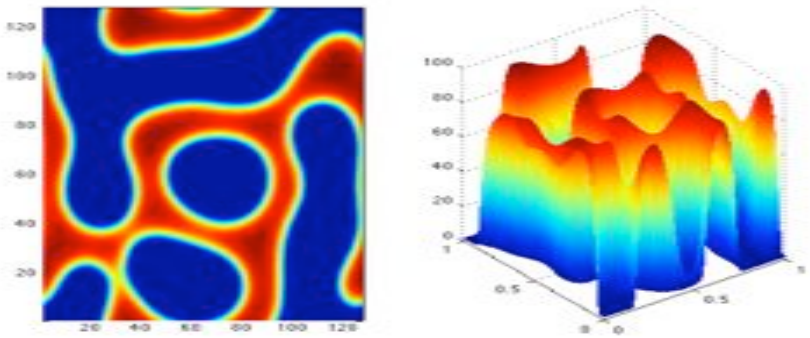

Figure 5.26: u Solution of System 1.1 with $\beta = 1$, $(d,\gamma) = (520, 3500)$, $time = .1$ and same initial conditions as Figure 5.25. Although the boundary conditions are different, we see that there are similarities of the two solutions, notably in the interior of the domain.

We want to see if there is any improvement to the solutions by using different subsets of the positive dispersion relation associated with the Neumann system. We now describe what is meant by different subsets. For fixed (d_n, γ_n), let $K \in [K_{min}, K_{max}]$, where $[K_{min}, K_{max}]$ is the range of indices of the positive eigenvalues in the dispersion relation associated with the Neumann system. For $k \in [K_{min}, K]$, where $K \in [K_{min}, K_{max}]$, let λ_k and $\xi_{1,k}$ be the eigenvalues associated with the Neumann and periodic systems, respectively. We use the steepest descent method to minimize

$$E^2 = \sum_{k=K_{min}}^{K} (\lambda_k - \xi_{1,k})^2, \tag{5.18}$$

for different values of $K \in [K_{min}, K_{max}]$. As an example, we choose $(d_n, \gamma_n) = (500, 3500)$ and compute (d_p, γ_p) using $1 \leq K \leq 19$, which is the range of positive eigenvalues of the dispersion relation of the Neumann system. For each pair (d_n, γ_n) and (d_p, γ_p), we use the spectral methods already discussed to evolve the solutions using the same set of initial conditions until $T_{max} = .1$ is reached. Once the time reaches T_{max}, the difference of the solutions are computed using the Euclidean norm. The results of this numerical experiment can be found in Table 5.4.

Table 5.6: Comparison of solutions of periodic and Neumann systems. The dispersion relation of the Neumann system for $(d_n, \gamma_n) = (500, 3500)$ has positive eigenvalues whose indices are in the interval $[1, 19]$. For each $K \in [1, 19]$, values of (d_p, γ_p) are selected so as to minimize (5.18). Once the time reaches $T_{max} = .1$, the solutions for both systems are compared using the Euclidean norm of their differences. Note that the best comparison occurs when only the first eigenvalue of the dispersion relation associated with the Neumann system is used.

K	$\|\|u_n - u_p\|\|_2$	$\|\|v_n - v_p\|\|_2$
1	1301.3039765662	38.5504753980
2	1998.7080751395	150.6099172609
3	1991.1606648768	142.2888127142
4	1987.4522957485	151.1561413771
5	2001.6932957400	96.3386675137
6	2067.7544636865	76.6435871372
7	2141.2552277902	78.5952085637
8	2199.4348834694	88.0778646274
9	2193.8487452515	98.1504512061
10	2246.8219027077	110.4192086313
11	2305.9220074609	115.5491423856
12	2340.5458655518	116.0211272887
13	2338.6971350831	117.4304459774
14	2357.9425425534	112.7716082149
15	2374.0249270290	111.8279533545
16	2432.0235605047	116.6245654973
17	2469.5287195159	127.0147251571
18	2481.5352044401	129.9782413353
19	2557.6979609753	131.2242979218

The value of $K = 1$ corresponds to the case where $(d_p, \gamma_p) = (520, 3500)$ and it has the least error. For all other values of K, the errors are substantially larger. For $2 \leq K \leq 19$, the best occurs when $K = 4$. Using this procedure and the values of (d_n, γ_n) found in (5.11) and (5.12), we examined the 1d and 2d systems. We found that the first eigenvalue always produced the best estimate using the outlined procedure. The next section shows the results.

5.4.1 Comparison of the Solutions of the Local Systems

To get a better idea of the solution agreement, we present a series of plots that show how the solutions for the Neumann and periodic boundary cases agree. Figures 5.27 - 5.29 show the solutions for $d = \{100, 500, 1000, 1500, 2000\}$. For $\gamma_n = 100$, Figure 5.27 shows that the solutions do not agree with each other. Contrasting Figure 5.27 with Figure 5.28, we see that there is better agreement. In fact, as d increases, we see that the solutions become closer. Figure 5.29 visually seems to have the best agreement for the 1d cases. Note that for $\gamma_n = 1000$ and $\gamma_n = 5000$, the interior pieces of the solutions are close, although the boundary conditions do produce slight variations at the edges.

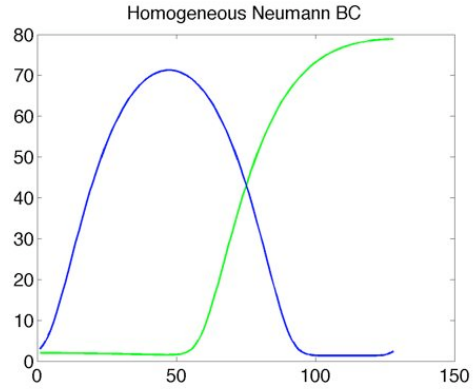

(a) $(d_n, \gamma_n) = (100, 100)$, $(d_p, \gamma_p) = (120, 100)$

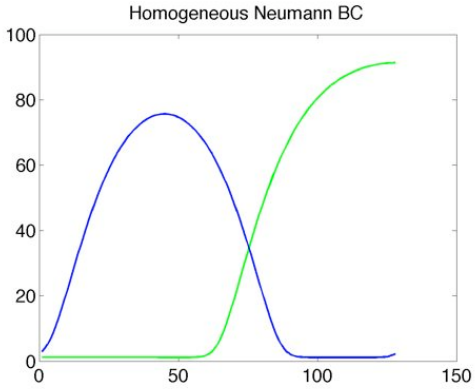

(b) $(d_n, \gamma_n) = (500, 100)$,$(d_p, \gamma_p) = (520, 100)$

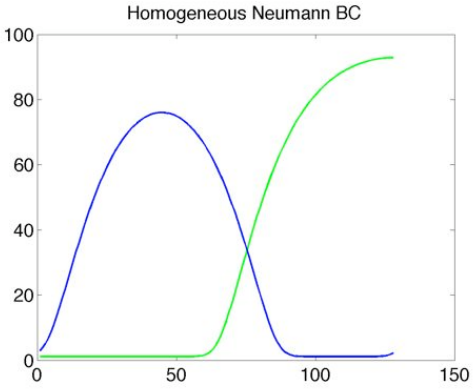

(c) $(d_n, \gamma_n) = (1000, 100)$,$(d_p, \gamma_p) = (1020, 100)$

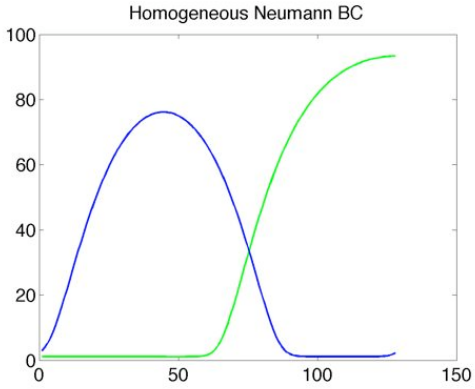

(d) $(d_n, \gamma_n) = (1500, 100)$,$(d_p, \gamma_p) = (1520, 100)$

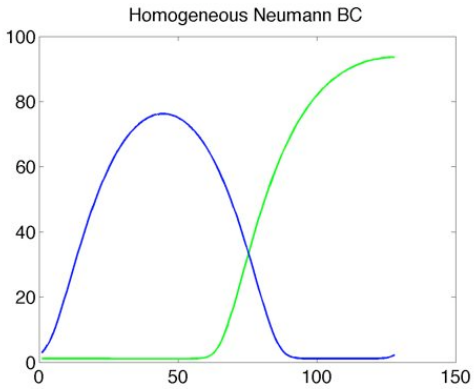

(e) $(d_n, \gamma_n) = (2000, 100)$,$(d_p, \gamma_p) = (2020, 100)$

Figure 5.27: Comparison of the 1d periodic and homogeneous Neumann solutions for $\gamma_n = 100$ and $time = .5$. Here blue represents the solution of the periodic solution and green represents the homogeneous Neumann system. There is very little agreement for this case.

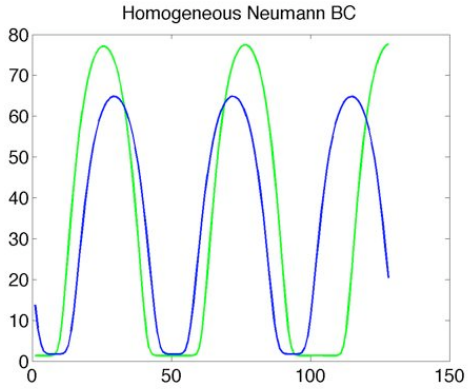

(a) $(d_n, \gamma_n) = (100, 1000)$, $(d_p, \gamma_p) = (120, 1000)$

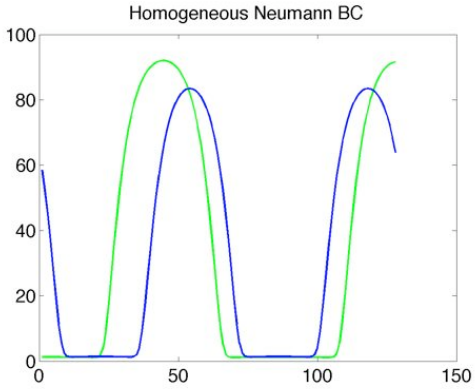

(b) $(d_n, \gamma_n) = (500, 1000)$, $(d_p, \gamma_p) = (520, 1000)$

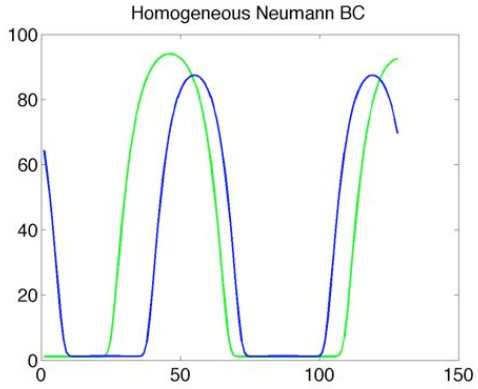

(c) $(d_n, \gamma_n) = (1000, 1000)$, $(d_p, \gamma_p) = (1020, 1000)$

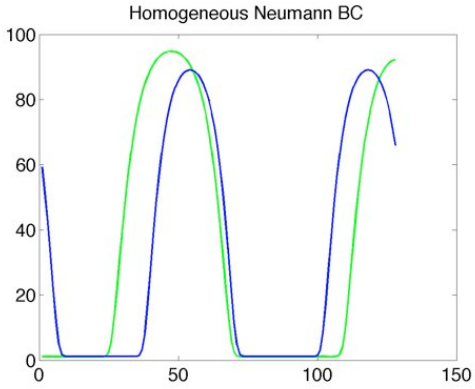

(d) $(d_n, \gamma_n) = (1500, 1000)$,$(d_p, \gamma_p) = (1520, 1000)$

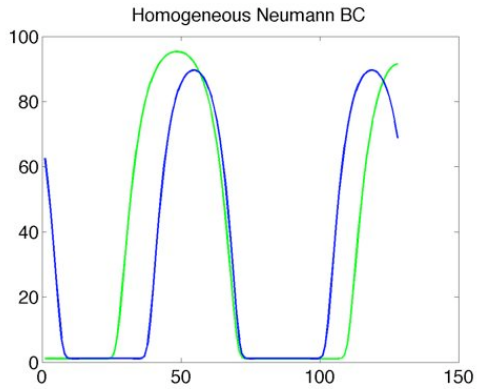

(e) $(d_n, \gamma_n) = (2000, 1000)$, $(d_p, \gamma_p) = (2020, 1000)$

Figure 5.28: Comparison of the 1d periodic and homogeneous Neumann solutions for $\gamma_n = 1000$ and $time = .05$. Here blue represents the solution of the periodic solution and green represents the homogeneous Neumann system. Note that although the boundary values are different, the interior of the solutions are similar.

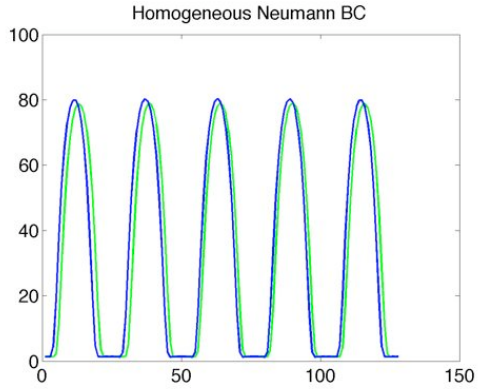

(a) $(d_n, \gamma_n) = (100, 5000)$,$(d_p, \gamma_p) = (120, 5000)$

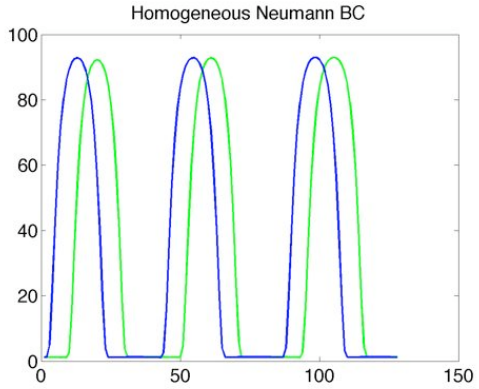

(b) $(d_n, \gamma_n) = (500, 5000)$,$(d_p, \gamma_p) = (520, 5000)$

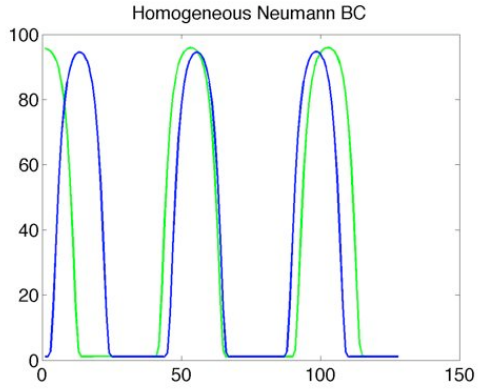

(c) $(d_n, \gamma_n) = (1000, 5000)$, ,$(d_p, \gamma_p) = (1020, 5000)$

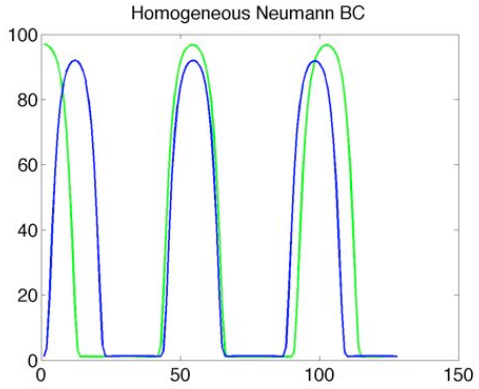

(d) $(d_n, \gamma_n) = (1500, 5000)$,$(d_p, \gamma_p) = (1520, 5000)$

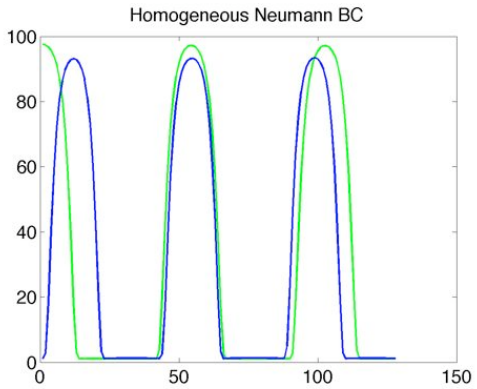

(e) $(d_n, \gamma_n) = (2000, 5000)$,$(d_p, \gamma_p) = (2020, 5000)$

Figure 5.29: Comparison of 1d periodic and homogeneous Neumann solutions for $\gamma_n = 5000$ and $time = .05$. Here blue represents the solution of the periodic solution and green represents the homogeneous Neumann system. As with the $\gamma_n = 1000$, the interior of the solutions are similar.

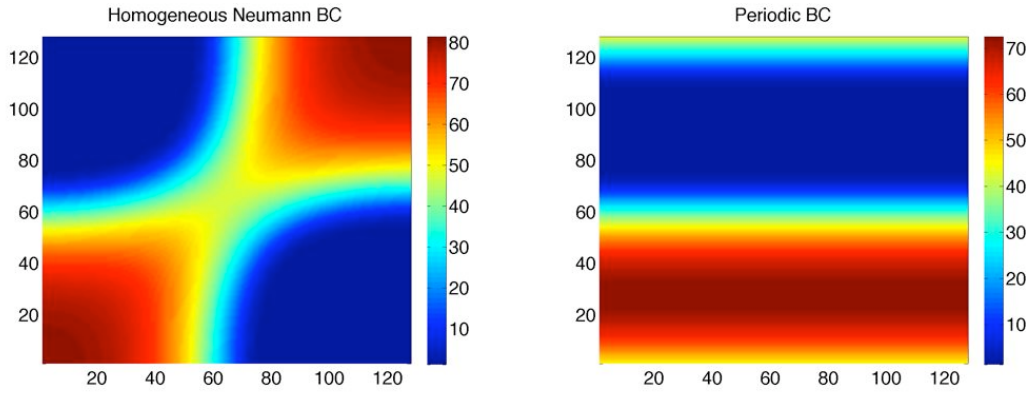

(a) $(d_n, \gamma_n) = (100, 100)$ (b) $(d_p, \gamma_p) = (113.9, 99.6)$

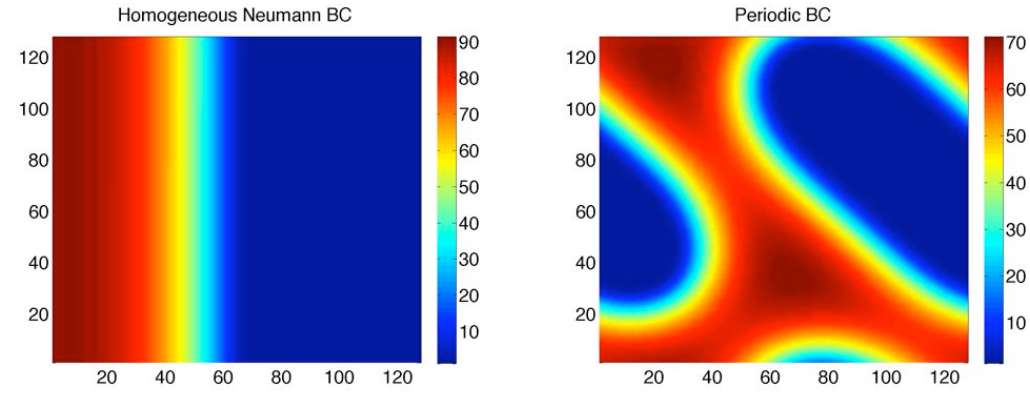

(c) $(d_n, \gamma_n) = (500, 100)$ (d) $(d_p, \gamma_p) = (519.8, 99.8)$

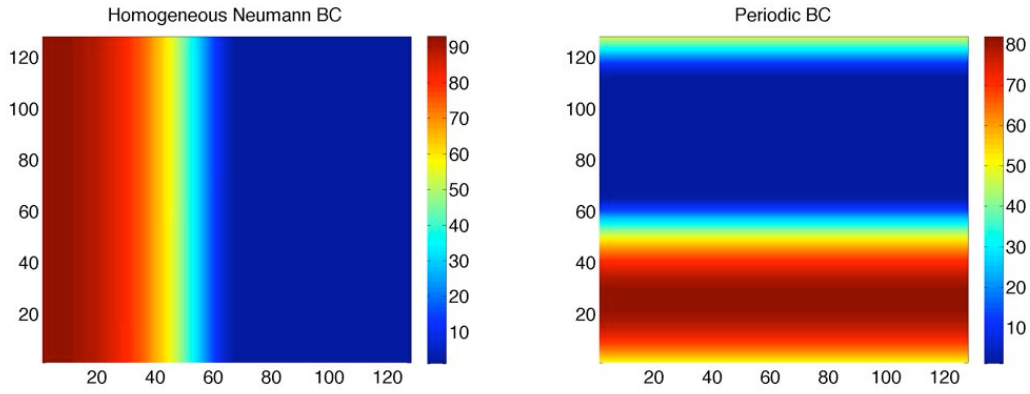

(e) $(d_n, \gamma_n) = (1000, 100)$ (f) $(d_p, \gamma_p) = (1019.9, 100)$

Figure 5.30: Comparison of the 2d periodic and homogeneous Neumann solutions for $\gamma_n = 100$ and $time = 1$. For these d values, there seems to be very little agreement between the solutions.

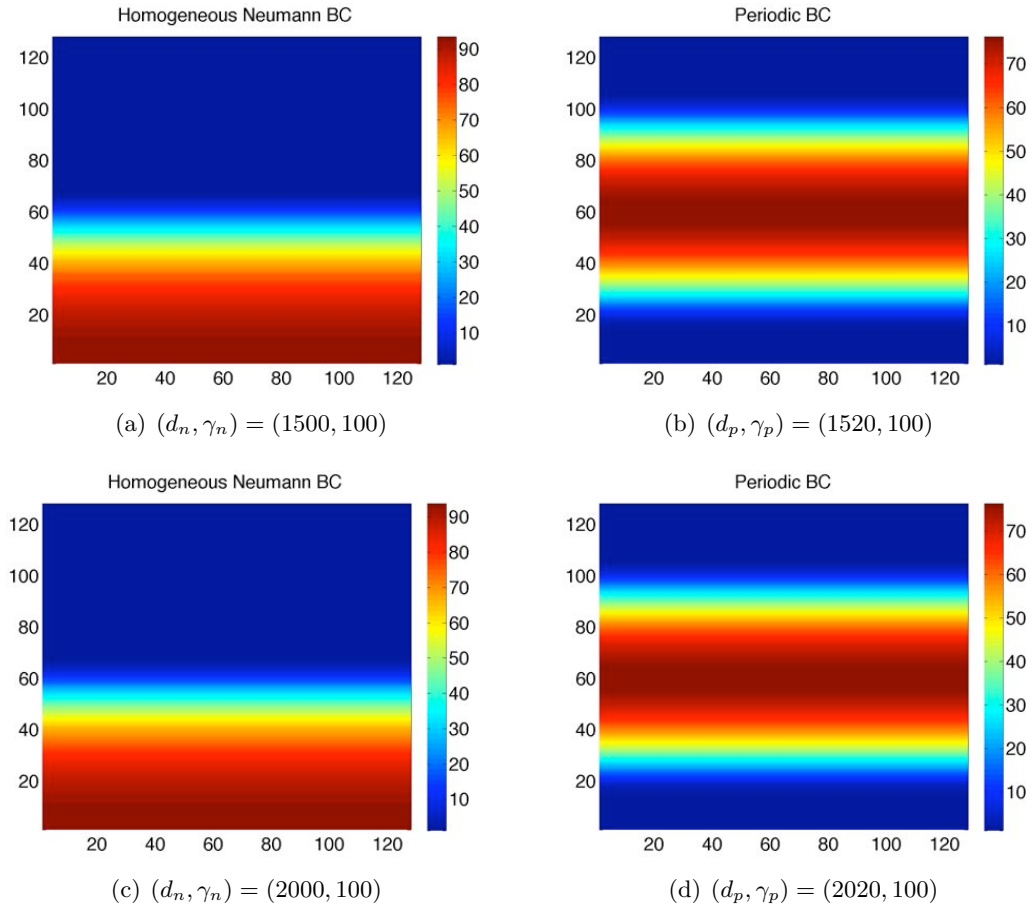

(a) $(d_n, \gamma_n) = (1500, 100)$ (b) $(d_p, \gamma_p) = (1520, 100)$

(c) $(d_n, \gamma_n) = (2000, 100)$ (d) $(d_p, \gamma_p) = (2020, 100)$

Figure 5.31: Comparison of the 2d periodic and homogeneous Neumann solutions for $\gamma_n = 100$ and $time = .1$. For these d values, there is more agreement between the solutions when compared to the agreement of the solutions presented in Figure 5.30.

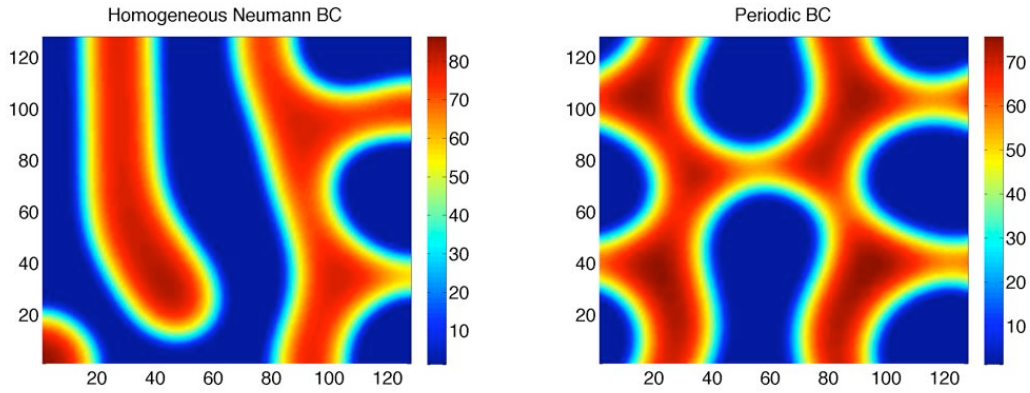

(a) $(d_n, \gamma_n) = (100, 1000)$ (b) $(d_p, \gamma_p) = (101.9, 1021.5)$

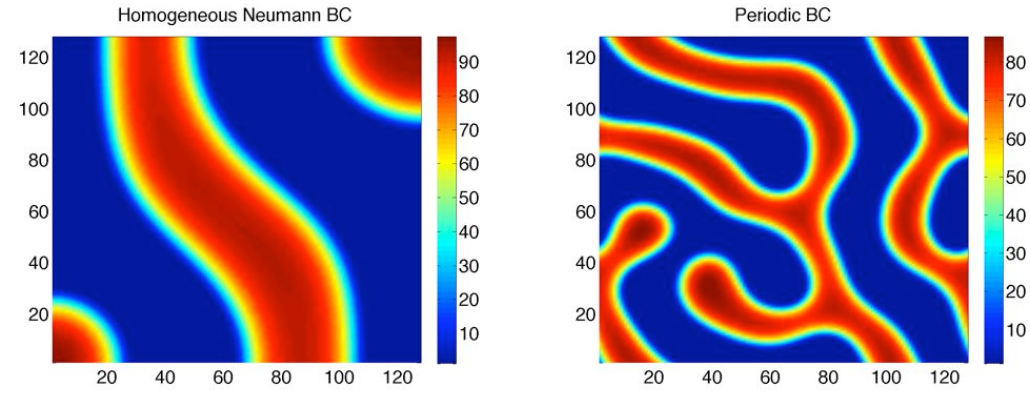

(c) $(d_n, \gamma_n) = (500, 1000)$ (d) $(d_p, \gamma_p) = (497.2, 1004.2)$

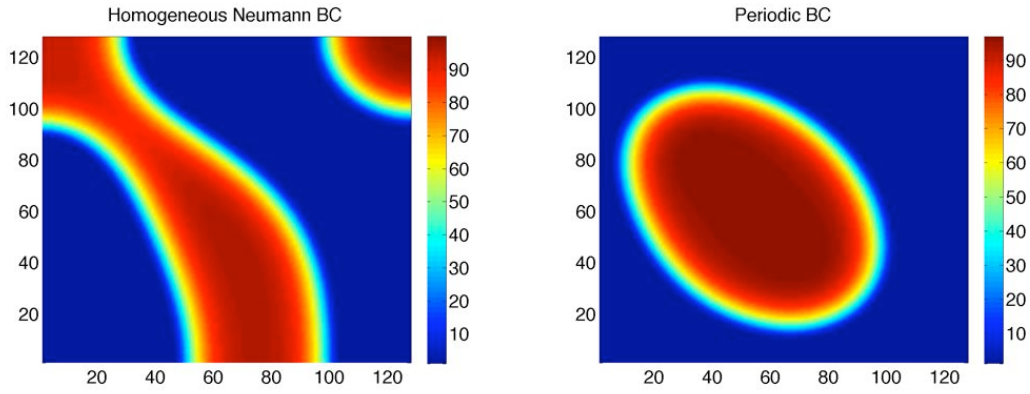

(e) $(d_n, \gamma_n) = (1000, 1000)$ (f) $(d_p, \gamma_p) = (1013.4, 996.3)$

Figure 5.32: Comparison of the 2d periodic and homogeneous Neumann solutions for $\gamma_n = 1000$ and $time = .1$. The agreement between the solutions for these d values is small.

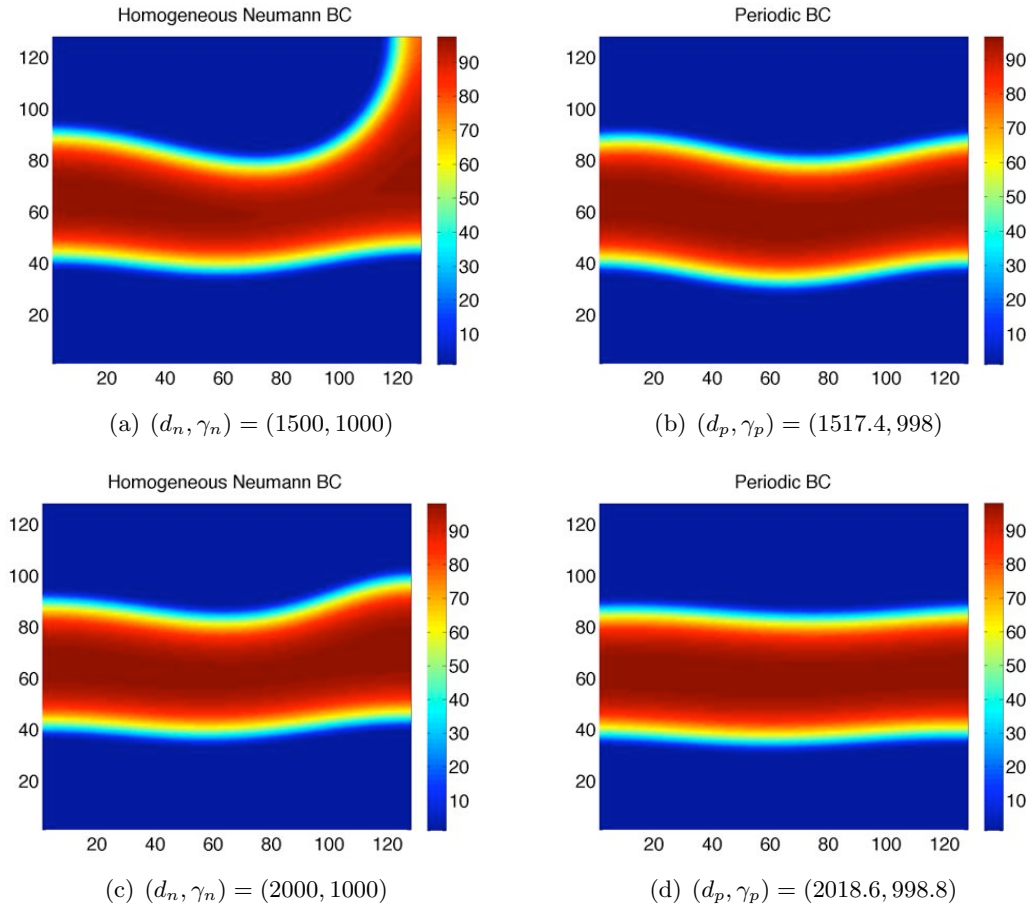

(a) $(d_n, \gamma_n) = (1500, 1000)$ (b) $(d_p, \gamma_p) = (1517.4, 998)$

(c) $(d_n, \gamma_n) = (2000, 1000)$ (d) $(d_p, \gamma_p) = (2018.6, 998.8)$

Figure 5.33: Continuation of the comparison of the 2d periodic and homogeneous Neumann solutions for $\gamma_n = 1000$ and $time = .1$. The agreement between the solutions for these d values is significantly better than the agreement for the lower d values.

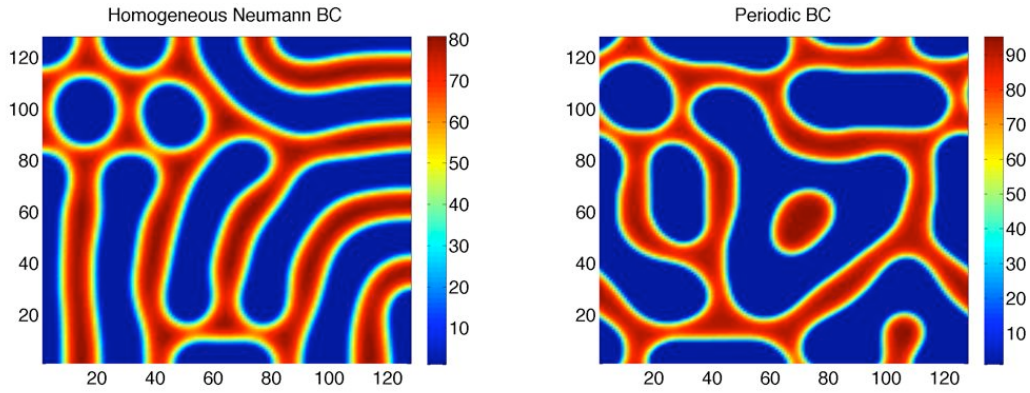

(a) $(d_n, \gamma_n) = (100, 5000)$ (b) $(d_p, \gamma_p) = (40.2, 5019.6)$

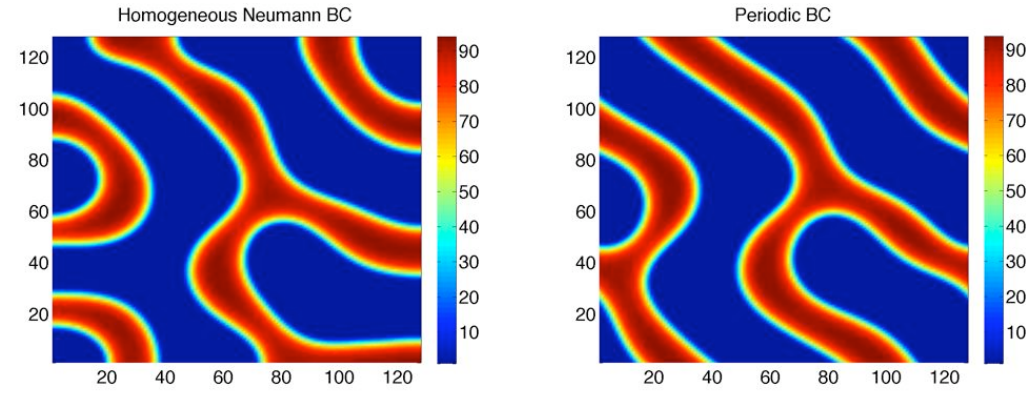

(c) $(d_n, \gamma_n) = (500, 5000)$ (d) $(d_p, \gamma_p) = (501.9, 5021.6)$

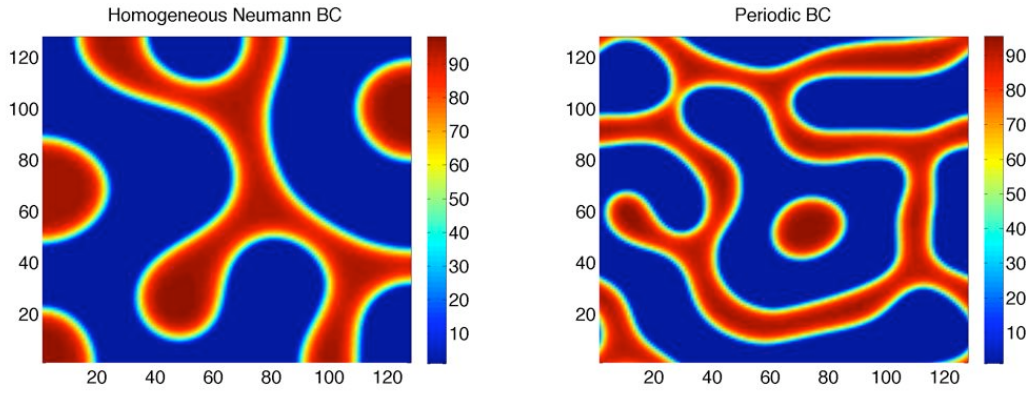

(e) $(d_n, \gamma_n) = (1000, 5000)$ (f) $(d_p, \gamma_p) = (1000.6, 5020.5)$

Figure 5.34: Comparison of the 2d periodic and homogeneous Neumann solutions for $\gamma_n = 5000$ and $time = .1$. There is very little agreement between the solutions for these d values.

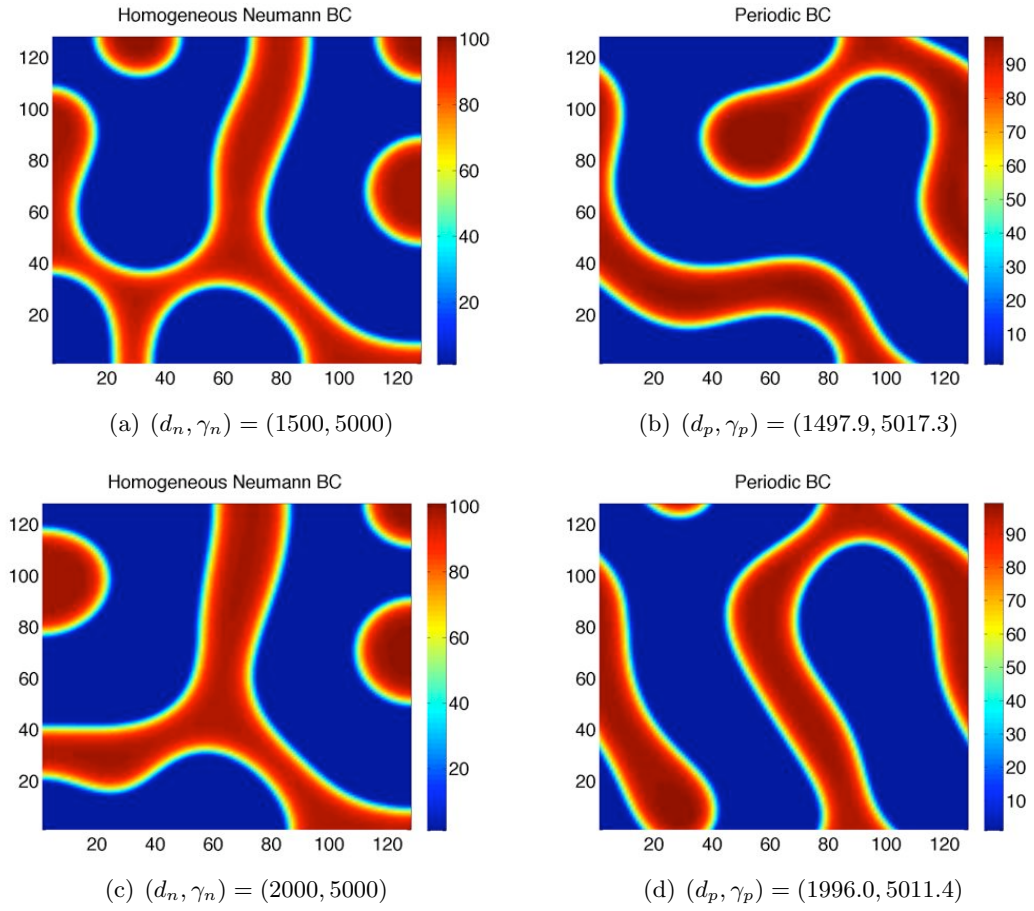

(a) $(d_n, \gamma_n) = (1500, 5000)$ (b) $(d_p, \gamma_p) = (1497.9, 5017.3)$

(c) $(d_n, \gamma_n) = (2000, 5000)$ (d) $(d_p, \gamma_p) = (1996.0, 5011.4)$

Figure 5.35: Continuation of comparison of the 2d periodic and homogeneous Neumann solutions for $\gamma_n = 5000$ and $time = .1$. Unlike for $\gamma = 1000$, the agreement for the solutions remains small as d increases.

For the 2d cases, we see a much different behavior for the solutions. For $\gamma_n = 100$, Figure 5.30 shows that for smaller values of d, solutions have very little in common with each other. However, the larger d values tend to produce patterns that although are shifted for the Neumann and periodic cases, seem to be much more similar. Figure 5.32 shows a similar behavior for the case when $\gamma_n = 1000$. In this case, we have the best agreement between the periodic and Neumann solutions of all γ_n when d is larger. For $\gamma_n = 5000$, examination of Figure 5.34 shows that the solutions are quite different for all of the values of d considered.

This numerical investigation is speculative in nature. For the 1d case, our method

for selecting the (d_p, γ_p) seems to choose parameters that yield similar solutions in both the homogeneous Neumann and periodic cases. For the 2d case, our method was not as successful. However, we did see some examples for the 2d case in which the periodic and Neumann solutions were similar. Although there are perhaps better methods to compare the two systems, the method presented for this study at least gives rise to cases in which the two systems produce similar solutions.

Chapter 6: Conclusion

In this thesis, reaction-diffusion systems with mixed nonlocal and local diffusion terms are considered where $\epsilon^\theta J$ is an $\epsilon-$independent kernel. For $\theta < 1$, the initial pattern selection is dominated by linear behavior. If $\theta = 1$ and $\epsilon(1-\beta)\hat{J}_0$ is sufficiently larger than the right endpoint of the unstable interval (s_l, s_r), the situation is different. When the techniques used for $\theta < 1$ are applied to the $\theta = 1$ case, the critical estimates used in the proof of the almost linear behavior for $\theta < 1$ are not attainable in the $\theta = 1$ case. In particular, the nonlinearity is no longer bounded by an $\epsilon-$dependent bound that forces F to be small for large distances away from the homogeneous equilibrium. Also, the distance from the homogeneous equilibrium to the solution is bounded above by an $\epsilon-$independent constant when the solution and its linearized counterpart separate by an $\epsilon-$independent amount. Furthermore, the numerics show that initial pattern selection for small $\beta > 0$ is dominated by nonlinear effects.

The numerical pattern studies, although speculative, examined more intermediate patterns for the local periodic system and made comparisons between the local periodic and Neumann systems. For the intermediate patterns of the local periodic system, we showed that for fixed γ values, the geometric complexity of the patterns tends to decrease as d increases. We also showed that spotted, striped and irregular patterns are possible. As future work, we noted that a software package such as AUTO could be used to find equilibria for comparison to the intermediate patterns that were generated for the local system. We also demonstrated that for the 1d system, similar solutions for the local periodic and homogeneous Neumann system can be generated using the outlined procedure in Section 5.4.1. However, this method was not as successful for the 2d systems.

Appendix A: Semigroups

The purpose of this appendix is to provide a brief introduction to semigroups relevant to this thesis. This is an overview of chapters 1 and 2 found in [47].

Definition A.0.1 (Semigroup)**.** *Let X be a Banach space. A one parameter family $T(t)$, $0 \leq t \leq \infty$, of bounded linear operators from X into X is a semigroup of bounded linear operators on X if*

1. *$T(0) = I$, where I is the identity operator on X*
2. *$T(t+s) = T(t)T(s)$ for every $t, s \geq 0$.*

Definition A.0.2 (Uniform Continuity)**.** *A semigroup of bounded linear operators, $T(t)$, is uniformly continuous if*

$$\lim_{t \to 0^+} ||T(t) - I|| = 0,$$

Theorem A.0.1. *A linear operator A is the infinitesimal generator of a uniformly continuous semigroup if and only if A is a bounded linear operator.*

Definition A.0.3 (Infinitesimal Generator)**.** *Let $D(A)$ be the domain of of the linear operator A. The infinitesimal generator of the semigroup $T(t)$ is defined as*

$$Ax = \lim_{t \to 0^+} \frac{T(t)x - x}{t},$$

where $x \in D(A)$ and the limit exists.

Definition A.0.4 (Strongly Continuous Semigroup)**.** *A semigroup $T(t)$, $0 \leq t \leq \infty$, of bounded linear operators on X is a strongly continuous semigroup of bounded linear operators if*

$$\lim_{t \to 0^+} T(t)x = x,$$

for every $x \in X$.

A strongly continuous semigroup of bounded linear operators on X will be called a semigroup of class C_0 or a C_0 semigroup.

Definition A.0.5. *A linear operator A on a Banach space X is sectorial if A is a closed, densely defined operator such that there exists constants $\phi \in (0, \frac{\pi}{2})$, $M \geq 0$ such that*

$$S_{b,\phi} = \{\lambda \in \mathbb{C} : \phi \leq |arg\lambda - b|, \lambda \neq b\} \subset \rho(A)$$

and

$$\left|(\lambda I - A)^{-1}\right| \leq \frac{M}{|\lambda - b|}$$

for all $\lambda \in S_{b,\phi}$ and where $\rho(A)$ is the resolvent set of A.

Remark A.0.1. *It is known that if A is sectorial, then the semigroup e^{-At} generated by A is analytic.*

Appendix B: Tables Comparing Solutions of Local and Nonlocal Systems, 1d

Table B.1: Values of $||u||_2, \beta = 0.00$, 1d

d	$\|\|u\|\|_2, \gamma = 100$	$\|\|u\|\|_2, \gamma = 1000$	$\|\|u\|\|_2, \gamma = 5000$
50.0000000000	678.5179810698	683.8852768239	693.3360465888
100.0000000000	696.4230459281	740.9044630335	734.9306225694
200.0000000000	601.4530800976	764.6335223536	754.1124991908
300.0000000000	601.4531109164	773.0883261721	783.0973148650
400.0000000000	601.4531310455	777.4245209273	788.5000168959
500.0000000000	601.4531450476	780.0509712035	791.7941636267
600.0000000000	601.4531553047	781.7934354542	794.0016544316
700.0000000000	601.4531631264	783.0086959605	795.5802606170
800.0000000000	601.4531692817	783.8724094453	796.7695972060
900.0000000000	601.4531742490	784.4718040322	797.6982280970
1000.0000000000	601.4531783406	784.8217254945	798.4606094440
1100.0000000000	601.4531817685	784.5222121326	799.1655174556
1200.0000000000	601.4531846818	841.5371316060	826.1566310277
1300.0000000000	601.4531871881	842.9596505358	845.9673136098
1400.0000000000	601.4531893669	844.1848632171	847.4793641524
1500.0000000000	601.4531912784	845.2511363455	848.8005739719
1600.0000000000	601.4531929690	846.1875089557	849.9596058932
1700.0000000000	601.4531944750	847.0163563736	850.9820382749
1800.0000000000	601.4531958249	847.7551941457	851.8952907625
1900.0000000000	601.4531970419	848.4179295961	852.7167203304
2000.0000000000	601.4531981448	849.0157452786	853.4582333214

Table B.2: Values of $||v||_2, \beta = 0.00$, 1d

d	$\|\|u\|\|_2, \gamma = 100$	$\|\|u\|\|_2, \gamma = 1000$	$\|\|u\|\|_2, \gamma = 5000$
50.0000000000	357.2960876513	357.7235819973	358.8468709067
100.0000000000	355.7589210968	356.6314386397	357.1925852946
200.0000000000	400.9670478998	357.8269737708	358.1786276393
300.0000000000	400.9670038973	358.8699513689	358.3072376041
400.0000000000	400.9669753501	359.5167309599	359.1586939864
500.0000000000	400.9669555634	359.9391973237	359.7370659838
600.0000000000	400.9669411016	360.2241467969	360.1387822207
700.0000000000	400.9669300908	360.4143014449	360.4257879361
800.0000000000	400.9669214359	360.5300831796	360.6315026679
900.0000000000	400.9669144576	360.5759262455	360.7785915702
1000.0000000000	400.9669087139	360.5299248247	360.8831330722
1100.0000000000	400.9669039048	360.1226850767	360.8639905490
1200.0000000000	400.9668998201	358.1037496386	360.5479126214
1300.0000000000	400.9668963084	358.4715649182	357.1369105863
1400.0000000000	400.9668932578	358.7925600280	357.5355418983
1500.0000000000	400.9668905842	359.0750144487	357.8936605735
1600.0000000000	400.9668882234	359.3254157335	358.2095029782
1700.0000000000	400.9668861255	359.5488898294	358.4842306819
1800.0000000000	400.9668842518	359.7495347564	358.7337782522
1900.0000000000	400.9668825715	359.9306623397	358.9627676894
2000.0000000000	400.9668810602	360.0949763412	359.1709908527

Table B.3: Values of $||u||_2, \beta = 0.25$, 1d

d	$\|\|u\|\|_2, \gamma = 100$	$\|\|u\|\|_2, \gamma = 1000$	$\|\|u\|\|_2, \gamma = 5000$
50.0000000000	678.5216170436	683.8857317350	693.2964752572
100.0000000000	696.4282399021	740.8993484286	734.9012169811
200.0000000000	601.4530801262	764.6340046467	754.0935457103
300.0000000000	601.4531109580	773.0909775812	783.0791892966
400.0000000000	601.4531310960	777.4283533570	788.4868163879
500.0000000000	601.4531451045	780.0555812281	791.7827151898
600.0000000000	601.4531553665	781.7986453569	793.9928751459
700.0000000000	601.4531631919	783.0144447865	795.5743336136
800.0000000000	601.4531693503	783.8787248303	796.7633707865
900.0000000000	601.4531743202	784.4788625699	797.6927914925
1000.0000000000	601.4531784141	784.8302587229	798.4547180426
1100.0000000000	601.4531818440	784.5513564085	799.1538464618
1200.0000000000	601.4531847591	841.5353661459	826.1518635729
1300.0000000000	601.4531872670	842.9583598335	845.9456872675
1400.0000000000	601.4531894474	844.1839839048	847.4597828009
1500.0000000000	601.4531913605	845.2506162143	848.7803253547
1600.0000000000	601.4531930526	846.1873053561	849.9403754135
1700.0000000000	601.4531945600	847.0164336546	850.9657486362
1800.0000000000	601.4531959114	847.7555223403	851.8806271835
1900.0000000000	601.4531971299	848.4184833085	852.7027860268
2000.0000000000	601.4531982344	849.0165028119	853.4450048060

Table B.4: Values of $||v||_2, \beta = 0.25$, 1d

d	$\|\|u\|\|_2, \gamma = 100$	$\|\|u\|\|_2, \gamma = 1000$	$\|\|u\|\|_2, \gamma = 5000$
50.0000000000	357.2963679463	357.7265332245	358.8568489115
100.0000000000	355.7596358164	356.6316618280	357.1973308170
200.0000000000	400.9670478667	357.8269923439	358.1824221729
300.0000000000	400.9670038487	358.8702354062	358.3065531637
400.0000000000	400.9669752909	359.5172243114	359.1604269032
500.0000000000	400.9669554966	359.9398634625	359.7355034782
600.0000000000	400.9669410292	360.2249800324	360.1385048583
700.0000000000	400.9669300141	360.4153234934	360.4283623781
800.0000000000	400.9669213558	360.5313539228	360.6319883422
900.0000000000	400.9669143750	360.5775940007	360.7804034687
1000.0000000000	400.9669086296	360.5324932710	360.8842438857
1100.0000000000	400.9669038201	360.1380442020	360.8786041709
1200.0000000000	400.9668997373	358.1019697788	360.5461693227
1300.0000000000	400.9668962309	358.4698954757	357.1322367118
1400.0000000000	400.9668931909	358.7909900224	357.5320139975
1500.0000000000	400.9668905354	359.0735335180	357.8845058704
1600.0000000000	400.9668882024	359.3240149465	358.1994107825
1700.0000000000	400.9668861446	359.5475616077	358.4789377507
1800.0000000000	400.9668843253	359.7482723234	358.7302346644
1900.0000000000	400.9668827159	359.9294597785	358.9587106522
2000.0000000000	400.9668812940	360.0938286050	359.1665451496

Table B.5: Values of $||u||_2, \beta = 0.50$, 1d

d	$\|\|u\|\|_2, \gamma = 100$	$\|\|u\|\|_2, \gamma = 1000$	$\|\|u\|\|_2, \gamma = 5000$
50.0000000000	678.5252531598	683.8862320286	693.2582286527
100.0000000000	696.4334343369	740.8942641037	734.8732096370
200.0000000000	601.4530801549	764.6345298830	754.0764360386
300.0000000000	601.4531109995	773.0936768264	783.0622861423
400.0000000000	601.4531311464	777.4322361571	788.4750376440
500.0000000000	601.4531451614	780.0602430827	791.7730089266
600.0000000000	601.4531554282	781.8039079234	793.9856827461
700.0000000000	601.4531632576	783.0202466674	795.5695616182
800.0000000000	601.4531694191	783.8850931750	796.7588097526
900.0000000000	601.4531743917	784.4859727332	797.6891065301
1000.0000000000	601.4531784879	784.8388343519	798.4506000174
1100.0000000000	601.4531819199	784.5790201793	799.1441400708
1200.0000000000	601.4531848370	841.5336217909	826.1483417625
1300.0000000000	601.4531873467	842.9570907110	845.9243627835
1400.0000000000	601.4531895289	844.1831265814	847.4405529786
1500.0000000000	601.4531914437	845.2501184506	848.7611301572
1600.0000000000	601.4531931376	846.1871244539	849.9222283588
1700.0000000000	601.4531946467	847.0165339184	850.9500517958
1800.0000000000	601.4531960000	847.7558737825	851.8665242932
1900.0000000000	601.4531972203	848.4190605120	852.6895057185
2000.0000000000	601.4531983266	849.0172840524	853.4324758428

Table B.6: Values of $||v||_2, \beta = 0.50$, 1d

d	$\|\|u\|\|_2, \gamma = 100$	$\|\|u\|\|_2, \gamma = 1000$	$\|\|u\|\|_2, \gamma = 5000$
50.0000000000	357.2966494837	357.7294837638	358.8667447151
100.0000000000	355.7603505224	356.6318802718	357.2020187240
200.0000000000	400.9670478335	357.8270075620	358.1865183617
300.0000000000	400.9670038001	358.8705171134	358.3055982190
400.0000000000	400.9669752317	359.5177159173	359.1617891039
500.0000000000	400.9669554299	359.9405281870	359.7348396586
600.0000000000	400.9669409569	360.2258119849	360.1385593107
700.0000000000	400.9669299375	360.4163442082	360.4301506856
800.0000000000	400.9669212763	360.5326229800	360.6331006235
900.0000000000	400.9669142942	360.5792588847	360.7827258521
1000.0000000000	400.9669085506	360.5350524849	360.8861858486
1100.0000000000	400.9669037479	360.1524547561	360.8894877645
1200.0000000000	400.9668996796	358.1001872330	360.5450403681
1300.0000000000	400.9668961988	358.4682235337	357.1264316746
1400.0000000000	400.9668931987	358.7894176719	357.5274017310
1500.0000000000	400.9668906006	359.0720504510	357.8763859817
1600.0000000000	400.9668883453	359.3226122141	358.1905108789
1700.0000000000	400.9668863877	359.5462316014	358.4732608179
1800.0000000000	400.9668846929	359.7470082955	358.7261079323
1900.0000000000	400.9668832333	359.9282558293	358.9543436823
2000.0000000000	400.9668819867	360.0926796703	359.1619155184

Table B.7: Values of $||u||_2, \beta = 0.75$, 1d

d	$\|\|u\|\|_2, \gamma = 100$	$\|\|u\|\|_2, \gamma = 1000$	$\|\|u\|\|_2, \gamma = 5000$
50.0000000000	678.5288894202	683.8867766653	693.2211576080
100.0000000000	696.4386292314	740.8892091635	734.8464016586
200.0000000000	601.4530801835	764.6350968055	754.0608815092
300.0000000000	601.4531110411	773.0964224989	783.0464845225
400.0000000000	601.4531311969	777.4361678351	788.4644512934
500.0000000000	601.4531452184	780.0649552109	791.7647761059
600.0000000000	601.4531554901	781.8092215307	793.9798480364
700.0000000000	601.4531633233	783.0260998900	795.5658817548
800.0000000000	601.4531694881	783.8915126242	796.7557250074
900.0000000000	601.4531744634	784.4931324137	797.6869271702
1000.0000000000	601.4531785621	784.8474497437	798.4481088952
1100.0000000000	601.4531819964	784.6054014811	799.1363236962
1200.0000000000	601.4531849155	841.5318977851	826.1457960624
1300.0000000000	601.4531874273	842.9558424042	845.9033511478
1400.0000000000	601.4531896115	844.1822904808	847.4216562541
1500.0000000000	601.4531915283	845.2496422811	848.7427574845
1600.0000000000	601.4531932242	846.1869654715	849.9049523591
1700.0000000000	601.4531947354	847.0166563857	850.9348556481
1800.0000000000	601.4531960907	847.7562476885	851.8528972255
1900.0000000000	601.4531973132	848.4196604179	852.6767824227
2000.0000000000	601.4531984215	849.0180882081	853.4205247108

Table B.8: Values of $||v||_2, \beta = 0.75$, 1d

d	$\|\|u\|\|_2, \gamma = 100$	$\|\|u\|\|_2, \gamma = 1000$	$\|\|u\|\|_2, \gamma = 5000$
50.0000000000	357.2969322619	357.7324336443	358.8765689010
100.0000000000	355.7610652149	356.6320940777	357.2066241960
200.0000000000	400.9670478003	357.8270194913	358.1907760948
300.0000000000	400.9670037514	358.8707965343	358.3045512596
400.0000000000	400.9669751724	359.5182058089	359.1628587236
500.0000000000	400.9669553631	359.9411915099	359.7347888828
600.0000000000	400.9669408846	360.2266426431	360.1388964422
700.0000000000	400.9669298616	360.4173635375	360.4315855361
800.0000000000	400.9669211995	360.5338902300	360.6347450322
900.0000000000	400.9669142214	360.5809206335	360.7854409465
1000.0000000000	400.9669084900	360.5376019098	360.8889496349
1100.0000000000	400.9669037121	360.1660397083	360.8983072678
1200.0000000000	400.9668996855	358.0984020942	360.5441623338
1300.0000000000	400.9668962675	358.4665491962	357.1198952716
1400.0000000000	400.9668933547	358.7878431100	357.5220405489
1500.0000000000	400.9668908709	359.0705653900	357.8689189390
1600.0000000000	400.9668887585	359.3212076914	358.1824450913
1700.0000000000	400.9668869729	359.5448999816	358.4673105209
1800.0000000000	400.9668854790	359.7457428441	358.7215492155
1900.0000000000	400.9668842482	359.9270506528	358.9497660192
2000.0000000000	400.9668832568	360.0915296841	359.1571371431

Table B.9: Values of $||u||_2, \beta = 1.00$, 1d

d	$\|\|u\|\|_2, \gamma = 100$	$\|\|u\|\|_2, \gamma = 1000$	$\|\|u\|\|_2, \gamma = 5000$
50.0000000000	678.5325258259	683.8873646625	693.1851491077
100.0000000000	696.4438245844	740.8841827674	734.8206511723
200.0000000000	601.4530802122	764.6357042454	754.0466805066
300.0000000000	601.4531110827	773.0992132946	783.0316811468
400.0000000000	601.4531312474	777.4401470123	788.4549055016
500.0000000000	601.4531452754	780.0697161806	791.7578161211
600.0000000000	601.4531555520	781.8145846961	793.9752120907
700.0000000000	601.4531633892	783.0320029109	795.5632306355
800.0000000000	601.4531695573	783.8979815459	796.7539561787
900.0000000000	601.4531745355	784.5003398304	797.6860763603
1000.0000000000	601.4531786368	784.8561028580	798.4471027813
1100.0000000000	601.4531820735	784.6306632237	799.1303481511
1200.0000000000	601.4531849950	841.5301934319	826.1440494514
1300.0000000000	601.4531875090	842.9546142092	845.8826510715
1400.0000000000	601.4531896955	844.1814748964	847.4030735585
1500.0000000000	601.4531916145	845.2491869930	848.7250511231
1600.0000000000	601.4531933126	846.1868276915	849.8883961489
1700.0000000000	601.4531948260	847.0168003365	850.9201077975
1800.0000000000	601.4531961835	847.7566433343	851.8396816622
1900.0000000000	601.4531974082	848.4202822977	852.6645384655
2000.0000000000	601.4531985187	849.0189145469	853.4090706694

Table B.10: Values of $||v||_2, \beta = 1.00$, 1d

d	$\|\|u\|\|_2, \gamma = 100$	$\|\|u\|\|_2, \gamma = 1000$	$\|\|u\|\|_2, \gamma = 5000$
50.0000000000	357.2972162783	357.7353828938	358.8863293102
100.0000000000	355.7617798936	356.6323033455	357.2111420655
200.0000000000	400.9670477671	357.8270281941	358.1951160403
300.0000000000	400.9670037027	358.8710737096	358.3034879096
400.0000000000	400.9669751131	359.5186940147	359.1636993967
500.0000000000	400.9669552964	359.9418534457	359.7351539139
600.0000000000	400.9669408129	360.2274720056	360.1394780927
700.0000000000	400.9669297884	360.4183814561	360.4328856210
800.0000000000	400.9669211310	360.5351556099	360.6368068515
900.0000000000	400.9669141687	360.5825791094	360.7884641042
1000.0000000000	400.9669084697	360.5401412786	360.8924242088
1100.0000000000	400.9669037464	360.1789003337	360.9063397128
1200.0000000000	400.9668998012	358.0966144589	360.5433457343
1300.0000000000	400.9668964948	358.4648725649	357.1128668455
1400.0000000000	400.9668937257	358.7862664513	357.5161328231
1500.0000000000	400.9668914183	359.0690784461	357.8618681032
1600.0000000000	400.9668895142	359.3198014839	358.1749721236
1700.0000000000	400.9668879673	359.5435668476	358.4611839501
1800.0000000000	400.9668867402	359.7444760506	358.7166421634
1900.0000000000	400.9668858017	359.9258443037	358.9450126086
2000.0000000000	400.9668851253	360.0903786731	359.1522379201

Appendix C: Tables Comparing Solutions of Local and Nonlocal Systems, 2d

Table C.1: Values of $||u||_2, \beta = 0.00$, 2d

d	$\|\|u\|\|_2, \gamma = 100$	$\|\|u\|\|_2, \gamma = 1000$	$\|\|u\|\|_2, \gamma = 5000$
50.0000000000	9590.9013107642	8929.9837793255	8877.7171813319
100.0000000000	9660.9831956052	9744.7627407345	8924.1745109748
200.0000000000	9660.9831998316	11694.7169140339	8977.8658109626
300.0000000000	9660.9832028048	12042.4103690340	9344.0844855950
400.0000000000	9660.9832048372	11427.9967775323	9674.5128147238
500.0000000000	9660.9832062920	11028.5534661122	9760.8258072821
600.0000000000	9660.9832073819	10806.3025877683	10115.7482910257
700.0000000000	9660.9832082301	10523.6417981405	9651.4941145020
800.0000000000	9660.9832089113	10556.7826088011	9531.7810797260
900.0000000000	9660.9832094729	10953.3249250015	9502.0641327692
1000.0000000000	11469.7386874780	13174.9479640583	9495.8238885188
1100.0000000000	9660.9832103544	11950.4315919329	9397.3160150966
1200.0000000000	9660.9832107114	12046.3055235534	10424.3852696250
1300.0000000000	9660.9832110293	12132.3810628448	10493.0617291371
1400.0000000000	9660.9832113168	12209.0760048367	10540.3311964157
1500.0000000000	9660.9832115805	12277.5789889288	11353.0334504402
1600.0000000000	9660.9832118256	12338.9962157460	11596.7399560615
1700.0000000000	9660.9832120562	12394.2738882622	11680.6117711944
1800.0000000000	9660.9832122757	12444.2108599430	11737.0184758827
1900.0000000000	9660.9832124867	12489.4822813476	11782.6490340490
2000.0000000000	9660.9832126915	12530.6610857594	12504.2746147934

Table C.2: Values of $||v||_2, \beta = 0.00$, 2d

d	$\|\|u\|\|_2, \gamma = 100$	$\|\|u\|\|_2, \gamma = 1000$	$\|\|u\|\|_2, \gamma = 5000$
50.0000000000	6379.6227696960	5806.2740000174	5850.6157480149
100.0000000000	6440.6550844840	5775.7963461259	5755.4437391525
200.0000000000	6440.6550773528	5748.1993065116	5736.2686475908
300.0000000000	6440.6550726803	5763.9526168927	5717.7468044314
400.0000000000	6440.6550695783	5818.5041053910	5726.2973885284
500.0000000000	6440.6550674020	5763.5186331275	5736.0892213449
600.0000000000	6440.6550658006	5739.4546197508	5749.4381673130
700.0000000000	6440.6550645770	5688.3730955078	5737.9060557532
800.0000000000	6440.6550636142	5686.7132927784	5744.7673422690
900.0000000000	6440.6550628384	5680.5231701194	5751.9936405703
1000.0000000000	5724.3643572577	5653.7247578116	5757.9048069581
1100.0000000000	6440.6550616706	5674.0577523087	5747.3382928797
1200.0000000000	6440.6550612224	5675.3055014916	5741.2764847178
1300.0000000000	6440.6550608405	5676.4126660665	5743.6183620356
1400.0000000000	6440.6550605126	5677.4093952795	5745.8424950004
1500.0000000000	6440.6550602296	5678.3112395324	5753.4093510464
1600.0000000000	6440.6550599846	5679.1305401897	5756.9294175266
1700.0000000000	6440.6550597722	5679.8778068466	5759.6104906455
1800.0000000000	6440.6550595885	5680.5620439197	5761.8496983098
1900.0000000000	6440.6550594301	5681.1909459724	5763.7721255399
2000.0000000000	6440.6550592947	5681.7710805440	5745.4162402982

Table C.3: Values of $||u||_2, \beta = 0.25$, 2d

d	$\|\|u\|\|_2, \gamma = 100$	$\|\|u\|\|_2, \gamma = 1000$	$\|\|u\|\|_2, \gamma = 5000$
50.0000000000	9590.9013123466	8930.0834486136	8877.9805388606
100.0000000000	9660.9831956059	9744.4599997543	8923.9585756272
200.0000000000	9660.9831998392	11694.6634779043	8976.3607013788
300.0000000000	9660.9832028203	12042.4770055556	9342.9511724403
400.0000000000	9660.9832048617	11428.2908577086	9673.9591942699
500.0000000000	9660.9832063269	11028.8716007269	9757.2879421247
600.0000000000	9660.9832074286	10810.2316970012	10115.5474510008
700.0000000000	9660.9832082906	10524.3357672559	9651.0499808733
800.0000000000	9660.9832089879	10557.3916469846	9530.6599272471
900.0000000000	9660.9832095686	10953.2246610186	9500.9331745828
1000.0000000000	11469.7227246200	13174.8688274470	9495.0165322092
1100.0000000000	9660.9832104988	11950.6310345409	9395.4673039152
1200.0000000000	9660.9832108865	12046.5084754435	10422.5003883769
1300.0000000000	9660.9832112397	12132.5928865323	10491.6956802464
1400.0000000000	9660.9832115673	12209.2942063318	10539.0021346664
1500.0000000000	9660.9832118758	12277.8009863034	11333.3238812427
1600.0000000000	9660.9832121704	12339.2200062831	11594.5896275734
1700.0000000000	9660.9832124550	12394.4980249218	11679.6018514788
1800.0000000000	9660.9832127327	12444.4343257809	11736.2202992656
1900.0000000000	9660.9832130057	12489.7043714788	11781.7684643204
2000.0000000000	9660.9832132759	12530.8813267999	12506.2474724765

Table C.4: Values of $||v||_2, \beta = 0.25$, 2d

d	$\|\|u\|\|_2, \gamma = 100$	$\|\|u\|\|_2, \gamma = 1000$	$\|\|u\|\|_2, \gamma = 5000$
50.0000000000	6379.6227857413	5806.3147512353	5850.8761564691
100.0000000000	6440.6550844841	5775.8318369587	5755.5565559407
200.0000000000	6440.6550773552	5748.2097189359	5736.3180873027
300.0000000000	6440.6550726852	5763.9639612024	5717.7608645726
400.0000000000	6440.6550695864	5818.5224595086	5726.2872826293
500.0000000000	6440.6550674137	5763.5531777566	5736.1110957855
600.0000000000	6440.6550658165	5740.3830238640	5749.4511588987
700.0000000000	6440.6550645979	5688.3840212966	5737.8835955080
800.0000000000	6440.6550636411	5686.7153015300	5744.7297492184
900.0000000000	6440.6550628727	5680.5210539442	5751.9575527777
1000.0000000000	5724.3679980054	5653.7179668336	5757.8755039272
1100.0000000000	6440.6550617254	5674.0478686216	5747.3092059048
1200.0000000000	6440.6550612916	5675.2954149414	5741.2462856738
1300.0000000000	6440.6550609274	5676.4023630608	5743.5829464226
1400.0000000000	6440.6550606211	5677.3989525019	5745.7982861420
1500.0000000000	6440.6550603642	5678.3007232091	5753.3144948420
1600.0000000000	6440.6550601500	5679.1200003757	5756.8776017979
1700.0000000000	6440.6550599737	5679.8672797568	5759.5645953366
1800.0000000000	6440.6550598314	5680.5515552590	5761.8062712669
1900.0000000000	6440.6550597200	5681.1805138846	5763.7319289894
2000.0000000000	6440.6550596371	5681.7607171933	5745.3761562205

Table C.5: Values of $||u||_2, \beta = 0.50$, 2d

d	$\|\|u\|\|_2, \gamma = 100$	$\|\|u\|\|_2, \gamma = 1000$	$\|\|u\|\|_2, \gamma = 5000$
50.0000000000	9590.9013137791	8930.1838811073	8878.2419349102
100.0000000000	9660.9831956052	9744.1558454390	8923.7548779659
200.0000000000	9660.9831998459	11694.6087670655	8974.5038796295
300.0000000000	9660.9832028357	12042.5426099537	9341.8112654404
400.0000000000	9660.9832048875	11428.5853273971	9673.3980453837
500.0000000000	9660.9832063650	11029.1903452666	9753.0339190913
600.0000000000	9660.9832074819	10814.0069721677	10115.3194666483
700.0000000000	9660.9832083627	10525.0285822247	9650.7059399623
800.0000000000	9660.9832090832	10557.9967825444	9529.6165924383
900.0000000000	9660.9832096922	10953.1233220291	9499.8673109699
1000.0000000000	11469.7067779411	13174.7900812205	9494.2514575307
1100.0000000000	9660.9832106960	11950.8257768167	9393.6976477367
1200.0000000000	9660.9832111292	12046.7066572746	10420.5763756404
1300.0000000000	9660.9832115335	12132.7999592422	10490.3554570830
1400.0000000000	9660.9832119171	12209.5077084380	10537.7170048044
1500.0000000000	9660.9832122863	12278.0183559560	11307.9176436131
1600.0000000000	9660.9832126454	12339.4392529666	11592.2924580804
1700.0000000000	9660.9832129978	12394.7177085846	11678.5447358246
1800.0000000000	9660.9832133459	12444.6534329426	11735.4143159466
1900.0000000000	9660.9832136914	12489.9221983406	11780.9047183062
2000.0000000000	9660.9832140356	12531.0973995349	12507.8763821821

Table C.6: Values of $||v||_2, \beta = 0.50$, 2d

d	$\|\|u\|\|_2, \gamma = 100$	$\|\|u\|\|_2, \gamma = 1000$	$\|\|u\|\|_2, \gamma = 5000$
50.0000000000	6379.6228021129	5806.3553974043	5851.1322840348
100.0000000000	6440.6550844838	5775.8672075928	5755.6670138190
200.0000000000	6440.6550773572	5748.2200847458	5736.3663368471
300.0000000000	6440.6550726902	5763.9752709252	5717.7743861845
400.0000000000	6440.6550695949	5818.5407151772	5726.2764209493
500.0000000000	6440.6550674266	5763.5879283376	5736.1356004605
600.0000000000	6440.6550658350	5741.2425113859	5749.4644254660
700.0000000000	6440.6550646237	5688.3950897306	5737.8628472730
800.0000000000	6440.6550636765	5686.7173713433	5744.6920226275
900.0000000000	6440.6550629209	5680.5189882079	5751.9208367781
1000.0000000000	5724.3716392954	5653.7112043544	5757.8454887081
1100.0000000000	6440.6550618118	5674.0380796761	5747.2799912991
1200.0000000000	6440.6550614047	5675.2854271169	5741.2182808188
1300.0000000000	6440.6550610731	5676.3921612643	5743.5477995271
1400.0000000000	6440.6550608057	5677.3886126687	5745.7555410694
1500.0000000000	6440.6550605940	5678.2903110094	5753.2124504359
1600.0000000000	6440.6550604315	5679.1095654573	5756.8238779179
1700.0000000000	6440.6550603133	5679.8568580292	5759.5185851798
1800.0000000000	6440.6550602352	5680.5411721956	5761.7639168542
1900.0000000000	6440.6550601940	5681.1701874465	5763.6924960983
2000.0000000000	6440.6550601867	5681.7504593986	5745.3356191939

Table C.7: Values of $||u||_2, \beta = 0.75$, 2d

d	$\|\|u\|\|_2, \gamma = 100$	$\|\|u\|\|_2, \gamma = 1000$	$\|\|u\|\|_2, \gamma = 5000$
50.0000000000	9590.9013151525	8930.2850598699	8878.5013986513
100.0000000000	9660.9831956038	9743.8504402811	8923.5606002239
200.0000000000	9660.9831998524	11694.5529014579	8970.8615875164
300.0000000000	9660.9832028518	12042.6073108626	9340.6658220637
400.0000000000	9660.9832049155	11428.8806082727	9672.8310950451
500.0000000000	9660.9832064084	11029.5097760238	9747.1990358389
600.0000000000	9660.9832075453	10817.6379239213	10115.0693234356
700.0000000000	9660.9832084515	10525.7202894173	9650.4477609976
800.0000000000	9660.9832092041	10558.5980486293	9528.6402318936
900.0000000000	9660.9832098520	10953.0174315190	9498.8550911198
1000.0000000000	11469.6908473961	13174.7117130766	9493.5219642740
1100.0000000000	9660.9832109534	11951.0167246651	9391.9935259962
1200.0000000000	9660.9832114440	12046.9009176112	10418.6091487329
1300.0000000000	9660.9832119105	12133.0031028206	10489.0352337424
1400.0000000000	9660.9832123601	12209.7173113866	10536.4616818362
1500.0000000000	9660.9832127981	12278.2318781205	11273.2280640498
1600.0000000000	9660.9832132283	12339.6547168454	11589.8580018761
1700.0000000000	9660.9832136531	12394.9336816933	11677.4455017426
1800.0000000000	9660.9832140743	12444.8689057799	11734.5958365108
1900.0000000000	9660.9832144929	12490.1364686990	11780.0525745723
2000.0000000000	9660.9832149098	12531.3099936255	12509.1824422715

Table C.8: Values of $||v||_2, \beta = 0.75$, 2d

d	$\|\|u\|\|_2, \gamma = 100$	$\|\|u\|\|_2, \gamma = 1000$	$\|\|u\|\|_2, \gamma = 5000$
50.0000000000	6379.6228186114	5806.3959404252	5851.3845174670
100.0000000000	6440.6550844831	5775.9024672138	5755.7752525092
200.0000000000	6440.6550773591	5748.2304053078	5736.4157719370
300.0000000000	6440.6550726954	5763.9865476079	5717.7874110734
400.0000000000	6440.6550696043	5818.5588717174	5726.2649891378
500.0000000000	6440.6550674417	5763.6228790827	5736.1653086912
600.0000000000	6440.6550658580	5742.0404146057	5749.4779385129
700.0000000000	6440.6550646578	5688.4062948333	5737.8435355854
800.0000000000	6440.6550637261	5686.7195150100	5744.6539762487
900.0000000000	6440.6550629914	5680.5170361179	5751.8836021182
1000.0000000000	5724.3752811261	5653.7044698986	5757.8147980446
1100.0000000000	6440.6550619432	5674.0283743935	5747.2507842513
1200.0000000000	6440.6550615772	5675.2755274948	5741.1920747355
1300.0000000000	6440.6550612941	5676.3820502882	5743.5128011293
1400.0000000000	6440.6550610825	5677.3783654539	5745.7139857468
1500.0000000000	6440.6550609336	5678.2799926506	5753.0996974454
1600.0000000000	6440.6550608405	5679.0992251888	5756.7684593950
1700.0000000000	6440.6550607976	5679.8465314530	5759.4725150527
1800.0000000000	6440.6550608002	5680.5308845528	5761.7222066236
1900.0000000000	6440.6550608443	5681.1599565176	5763.6537591473
2000.0000000000	6440.6550609263	5681.7402970603	5745.2954956771

Table C.9: Values of $||u||_2, \beta = 1.00$, 2d

d	$\|\|u\|\|_2, \gamma = 100$	$\|\|u\|\|_2, \gamma = 1000$	$\|\|u\|\|_2, \gamma = 5000$
50.0000000000	9590.9013164976	8930.3869860354	8878.7590183057
100.0000000000	9660.9831956021	9743.5438918611	8923.3740957164
200.0000000000	9660.9831998590	11694.4959497106	8836.4732873131
300.0000000000	9660.9832028690	12042.6711653316	9339.5155087487
400.0000000000	9660.9832049468	11429.1767974369	9672.2592607313
500.0000000000	9660.9832064588	11029.8299376233	9734.6910596082
600.0000000000	9660.9832076214	10821.1353602668	10114.8002023263
700.0000000000	9660.9832085610	10526.4112838885	9650.2656146870
800.0000000000	9660.9832093548	10559.1960628371	9527.7231602887
900.0000000000	9660.9832100514	10952.9060442658	9497.8886742046
1000.0000000000	11469.6749329402	13174.6337120095	9492.8232156805
1100.0000000000	9660.9832112686	11951.2043642515	9390.3453859855
1200.0000000000	9660.9832118242	12047.0917205828	10416.5936237142
1300.0000000000	9660.9832123587	12133.2027699302	10487.7311034219
1400.0000000000	9660.9832128785	12209.9234566717	10535.2283311228
1500.0000000000	9660.9832133877	12278.4419827164	11221.1999769206
1600.0000000000	9660.9832138894	12339.8668160347	11587.2949954067
1700.0000000000	9660.9832143853	12395.1463505553	11676.3029066790
1800.0000000000	9660.9832148766	12445.0811389697	11733.7611173684
1900.0000000000	9660.9832153641	12490.3475658919	11779.2076221121
2000.0000000000	9660.9832158481	12531.5194814214	12510.1758615289

Table C.10: Values of $||v||_2, \beta = 1.00$, 2d

d	$\|\|u\|\|_2, \gamma = 100$	$\|\|u\|\|_2, \gamma = 1000$	$\|\|u\|\|_2, \gamma = 5000$
50.0000000000	6379.6228351689	5806.4363824082	5851.6331674648
100.0000000000	6440.6550844824	5775.9376227117	5755.8814098545
200.0000000000	6440.6550773611	5748.2406818333	5738.0143668958
300.0000000000	6440.6550727010	5763.9977921324	5717.7999553336
400.0000000000	6440.6550696150	5818.5769310318	5726.2531037314
500.0000000000	6440.6550674599	5763.6580333183	5736.2154413673
600.0000000000	6440.6550658875	5742.7835162552	5749.4916449055
700.0000000000	6440.6550647039	5688.4176364394	5737.8255153815
800.0000000000	6440.6550637952	5686.7217350465	5744.6155185949
900.0000000000	6440.6550630908	5680.5152166449	5751.8459092104
1000.0000000000	5724.3789234966	5653.6977630056	5757.7834799121
1100.0000000000	6440.6550621278	5674.0187462822	5747.2217254199
1200.0000000000	6440.6550618168	5675.2657096846	5741.1674712422
1300.0000000000	6440.6550615964	5676.3720237149	5743.4779280927
1400.0000000000	6440.6550614547	5677.3682044229	5745.6734553723
1500.0000000000	6440.6550613820	5678.2697617013	5752.9886992057
1600.0000000000	6440.6550613707	5679.0889731565	5756.7117317518
1700.0000000000	6440.6550614141	5679.8362936416	5759.4263958225
1800.0000000000	6440.6550615068	5680.5206859779	5761.6809044184
1900.0000000000	6440.6550616439	5681.1498147853	5763.6156275537
2000.0000000000	6440.6550618210	5681.7302239117	5745.2563014843

Appendix D: Source Code

D.1 Spectral Code for 1d Periodic System

```
function [u,v] = spectral1d_periodic( registry, ...
initialConditions_fun, varargin )
%
% This function computes the time-evolved solution
% for the 1d mixed local and nonlocal
% reaction-diffusion equation.  The user must
% specify the following fields in the registry struct:
%
%   dim - # of modes
%   d - Ratio of diffusivity of u & v
%   gamma - Regulates the effect of the reaction
%           model
%   beta - Scalar value between 0 & 1.
%          1 = pure local, 0 = pure nonlocal
%   deltaTime - Step size
%   tMax - Stopping time
%   showPlot - Will show the plot as time evolves
%   showTime - Will show the time on the xaxis
%   a, b, K, rho, alpha - positive parameters
%                         corresponding to the
%                         Thomas system
%
% This function uses pseudospectral
%  methods to solve the mixed
```

```
% local-nolocal reaction-diffusion system.
% When complete, it returns
% the value of u and v at tMax.

time = 0;
validateRegistry( registry, 'dim', 'd', ...
'gamma', 'beta',  ...
'deltaTime', 'tMax',...
'showPlot', 'showTime',...
'a', 'b', 'K', 'rho', 'alpha' );

dim = registry.dim;
d = registry.d;
gamma = registry.gamma;
beta = registry.beta;
deltaTime = registry.deltaTime;
tMax = registry.tMax;
showPlot = registry.showPlot;
showTime = registry.showTime;
color = registry.color;
tMax = registry.tMax;
a = registry.a;
b = registry.b;
K = registry.K;
rho = registry.rho;
```

```
alpha = registry.alpha;



% Compute the eigenvalues of the laplacian
n = [0:dim/2 -dim/2+1:-1];
kappa = 4*pi^2*(n.^2 );

% Compute the eigenvalues of the
% convolution operator.  This may
% seem a bit more complicated, but
% it is necessary.  We do this so
% that we can compute with arbitrarily
% specified kernels, which has
% happened on more than one occasion.
Jhat = 0;
if ( beta < 1 )
    assert( max( size( varargin ) ) >= 2,...
      'Missing parameters' );
    eigenvalues = varargin{1};
    kernel = varargin{2};
    Jhat = eigenvalues( registry, kernel );
end;

den   =   2 + beta*deltaTime*kappa -...
 (1-beta)*deltaTime*Jhat;
```

```
diffU = ( 2 - beta*deltaTime*kappa + ...
(1-beta)*deltaTime*Jhat) ./ den;
reacU = ( 2 * gamma * deltaTime )./ den;

kappa = kappa*d;
den   =   2 + beta*deltaTime*kappa -...
 (1-beta)*d*deltaTime*Jhat;
diffV = ( 2 - beta*deltaTime*kappa + ...
(1-beta)*d*deltaTime*Jhat) ./ den;
reacV = ( 2 * gamma * deltaTime )./ den;

% Note that this allows us to specify
% any set of inital conditions that
% we want, including the end of a previous run.
[u,v] = initialConditions_fun( registry );
uHat = fft(u)/dim;
vHat = fft(v)/dim;

if ( showPlot )
    x = linspace(0,1,dim);
    handle = [];
    hold on;
end

iter = 1;
```

```
% A word on plotting.  We save the handle
% so that we can delete the
% plot before the next plot event occurs.
% Matlab would do this for us
% anyway, except we are using "hold on."
% This allows us to plot
% the current plot over a previous run -
% useful for comparison purposes.
while( time < tMax )

    % Convert from Fourier space to real space
    u = dim*real(ifft( uHat));
    v = dim*real(ifft( vHat));

    % Show the plot & time if the user wants them
    if ( showPlot )
        if (ishandle( handle ) )
            delete(handle);
            handle = plot( x, real(u),...
                        color, 'linewidth', 2);
        else
            handle = plot( x, real(u), ...
                        color, 'linewidth', 2 );
        end
```

```
    if ( showTime )
        xlabel( sprintf( 'Time = %d', time ) );
    end

    drawnow();
end

h = rho * u.*v./( 1 + u + K*u.*u );
f = a - u - h;
g = alpha*( b - v ) - h;

fHat = fft(f)/dim;
gHat = fft(g)/dim;

% Update next solution
uHatNext = diffU'.*uHat + reacU'.*fHat;
vHatNext = diffV'.*vHat + reacV'.*gHat;

% Error computation
uDiff = uHatNext - uHat;
vDiff = vHatNext - vHat;

uHat = uHatNext;
vHat = vHatNext;
time = time + deltaTime;
```

```
    iter = iter + 1;
end
```

```
function Jhat = eigenvalues_Convolution1d(...
 registry, kernel_fun )
%
% This function accepts a reference to
% kernel_fun and computes the
% eigenvalues of kernel_fun.  Before
% returning the values, it subtracts
% the largest eigenvalue from all of
% the eigenvalues of kernel_fun.

validateRegistry( registry, 'dim' );
J = kernel_fun( registry );
Jhat = real( fft( J )/registry.dim );
Jhat = Jhat - Jhat(1);
```

The 1d code was tested to see if the method would converge to the equilibrium solution, given by $(u_0, v_0) \approx (37.738, 25.158)$. For this test, $\gamma = 2$ and $d = 2$. For $\beta \in \{0.00, 0.25, 0.50, 0.75, 1.00\}$, initial conditions were randomly selected to be within .1 of the homogeneous equilibrium. A dimension of 128 and$\Delta\ t = .001$ was used. The simulation was stopped once the Euclidean norm of the difference between the homogeneous equilibrium and the approximated solution reached 1×10^{-5}. For each β, the method successfully produced solutions close to the homogeneous equilibrium within the tolerance specified.

D.2 Spectral Code for 2d Periodic System

```
function [u,v]= spectral2d_periodic(registry, ...
initialConditions_fun, varargin )
%
% This function computes the time-evolved solution
% for the 2d mixed
% local and nonlocal reaction-diffusion equation.
% The user must specify the following fields in
% the registry struct:
%
%   dim - # of modes
%   d - Ratio of diffusivity of u & v
%   gamma - Regulates the effect of the reaction
%           model
%   beta - Scalar value between 0 & 1.
%          1 = pure local, 0 = pure nonlocal
%   deltaTime - Step size
%   tMax - Stopping time
%   showPlot - Will show the plot as time evolves
%   showTime - Will show the time on the xaxis
%   a, b, K, rho, alpha - positive parameters
%                         corresponding to the
%                         Thomas system
%
% This function uses pseudospectral methods
```

```
% to solve the mixed local-nolocal reaction-diffusion
% system.  When complete, it returns
% the value of u and v at tMax.

time = 0;
validateRegistry( registry, 'dim', 'd', ...
'gamma', 'beta',  ...
'deltaTime', 'tMax',...
'showPlot', ...
'showTime',...
'a', 'b', 'K',...
'rho', 'alpha' );

dim = registry.dim;
d = registry.d;
gamma = registry.gamma;
beta = registry.beta;
deltaTime = registry.deltaTime;
tMax = registry.tMax;
showPlot = registry.showPlot;
showTime = registry.showTime;
color = registry.color;
tMax = registry.tMax;
a = registry.a;
b = registry.b;
```

```
K = registry.K;
rho = registry.rho;
alpha = registry.alpha;

n = [0:dim/2 -dim/2+1:-1];
m = [0:dim/2 -dim/2+1:-1];
x = linspace(0,1,dim);
y = x;
[xx,yy] = meshgrid(x,y);

% Compute the eigenvalues of the convolution
% operator.  This may seem a bit more complicated,
% but it is necessary.  We do this so
% that we can compute with arbitrarily
% specified kernels, which has
% happened on more than one occasion.
Jhat = 0;
if ( beta < 1 )
    assert( max( size( varargin ) ) >= 2, ...
        'Missing parameters' );
    eigenvalues = varargin{1};
    kernel = varargin{2};
    Jhat = eigenvalues( registry, kernel );
end;
```

```
% Compute the coefficients for the semi-
%  implicit midpoint method
[mm,nn] = meshgrid( m, n );
kappa = 4*pi^2*(mm.^2 + nn.^2 );


den    =    2 + beta*deltaTime*kappa - ...
(1-beta)*deltaTime*Jhat;
diffU = ( 2 - beta*deltaTime*kappa + ...
(1-beta)*deltaTime*Jhat) ./ den;
reacU = ( 2 * deltaTime*gamma )./ den;

kappa = kappa*d;
den    =    2 + beta*deltaTime*kappa - ...
(1-beta)*d*deltaTime*Jhat;
diffV = ( 2 - beta*deltaTime*kappa + ...
(1-beta)*d*deltaTime*Jhat) ./ den;
reacV = ( 2 * deltaTime*gamma )./ den;

% Note that this allows us to specify
% any set of inital conditions that
% we want, including the end of a previous run.
[u,v] = initialConditions_fun( registry );
uHat = fft2(u)/(dim*dim);
vHat = fft2(v)/(dim*dim);
```

```
while( time < tMax )

    % Convert from Fourier space to real space
    u = real( dim*dim*ifft2( uHat ) );
    v = real( dim*dim*ifft2( vHat ) );

    % Show the plot & time if the user wants them
    if ( showPlot )

        subplot(1,2,1);
        pcolor(u), shading interp;
        colorbar;
        if ( showTime )
            xlabel( sprintf( 'Time = %d', time ) );
        end

        subplot(1,2,2);
        surf(xx,yy,u),shading interp;
        drawnow();

    end

    h = rho * u.*v./( 1 + u + K*u.*u );
    f = a - u - h;
```

```
    g = alpha*( b - v ) - h;

    fHat = fft2(f)/(dim*dim);
    gHat = fft2(g)/(dim*dim);

    % Update next solution
    uHatNext = diffU'.*uHat + reacU'.*fHat;
    vHatNext = diffV'.*vHat + reacV'.*gHat;

    uHat = uHatNext;
    vHat = vHatNext;

    time = time + deltaTime;

end
```

```
function Jhat = eigenvalues_Convolution2d(...
 registry, kernel_fun )
%
% This function accepts a reference
% to kernel_fun and computes the
% eigenvalues of kernel_fun.
% Before returning the values, it subtracts
% the largest eigenvalue from all
% of the eigenvalues of kernel_fun. The
% parameters index1( optional )
% and index2( optional )
% are based upon sorting the eigenvalues
% of the Laplacian and removing
% redundant eigenvalues (Ex. e_i_j is the
% same as e_j_i).

validateRegistry( registry, 'dim' );
dim = registry.dim;

J = kernel_fun( registry );
Jhat = real( fft2( J )/( dim*dim ) );
Jhat = Jhat - Jhat(1);
```

The 2d code was tested to see if the method would converge to the equilibrium solution, given by $(u_0, v_0) \approx (37.738, 25.158)$. For this test, $\gamma = 2$ and $d = 2$. For $\beta \in \{0.00, 0.25, 0.50, 0.75, 1.00\}$, initial conditions were randomly selected to be within .1 of the homogeneous equilibrium. A dimension of 128 and$\Delta\ t = .01$ was used. The simulation was stopped once the Euclidean norm of the difference between the homogeneous equilibrium and the approximated solution reached 1×10^{-5}. For each β, the method successfully produced solutions close to the homogeneous equilibrium within the tolerance specified.

D.3 Spectral Code for 1d Neumann System

```
function [u,v] = spectral1d_neumann(...
registry, initialConditions_fun )

dim = registry.dim;
deltaTime = registry.deltaTime;
gamma = registry.gamma;
d = registry.d;
tMax = registry.tMax;
a = registry.a;
b = registry.b;
K = registry.K;
rho = registry.rho;
alpha = registry.alpha;

%Thomas system constants
if ( registry.useSeed ) rand( 'seed', ...
registry.seed ); end
time = 0;

% Compute the coefficients for the
% semi-implicit midpoint method

n = 0:dim-1;
kappa = pi^2*n.^2;
```

```
den    =    2 + deltaTime*kappa;
diffU = ( 2 - deltaTime*kappa ) ./ den;
reacU = ( 2 * deltaTime*gamma )./ den;

kappa = kappa*d;
den    =    2 + deltaTime*kappa;
diffV = ( 2 - deltaTime*kappa ) ./ den;
reacV = ( 2 * deltaTime*gamma )./ den;

% DCT weights
w = [sqrt(1/dim); sqrt(2/dim)*ones(dim-1,1)];

[u,v] = initialConditions_fun( registry );
uHat = dct(u)./w;
vHat = dct(v)./w;

if ( registry.showPlot )
    axis([0,1, 0, 90] );
    x = linspace(0,1,dim);
end

while( time < tMax )

    % Convert from Fourier space
```

```
    % to real space
u = idct( uHat.*w );
v = idct( vHat.*w );

if ( registry.showPlot )
    plot(x,u,registry.color, ...
            'linewidth', 2 );

    if ( registry.showTime )
        xlabel( sprintf( 'Time = %d',...
                    time ) );
    end

    drawnow();
end

h = rho * u.*v./( 1 + u + K*u.*u );
f = a - u - h;
g = alpha*( b - v ) - h;

fHat = dct(f)./w;
gHat = dct(g)./w;

% Update next solution
uHatNext = diffU'.*uHat + reacU'.*fHat;
```

```
    vHatNext = diffV'.*vHat + reacV'.*gHat;

    % Error computation
    uDiff = uHatNext - uHat;
    vDiff = vHatNext - vHat;

    uHat = uHatNext;
    vHat = vHatNext;

    time = time + deltaTime;
end
```

The 1d code was tested to see if the method would converge to the equilibrium solution, given by $(u_0, v_0) \approx (37.738, 25.158)$. For this test, $\gamma = 2$ and $d = 2$. Initial conditions were randomly selected to be within .1 of the homogeneous equilibrium. A dimension of 128 and $\Delta t = .001$ was used. The simulation was stopped once the Euclidean norm of the difference between the homogeneous equilibrium and the approximated solution reached 1×10^{-5}. For the initial conditions selected, the method successfully produced solutions close to the homogeneous equilibrium within the tolerance specified.

D.4 Spectral Code for 2d Neumann System

```
function [u,v] = spectral2d_neumann(...
registry, initialConditions_fun)

dim = registry.dim;
d = registry.d;
gamma = registry.gamma;
deltaTime = registry.deltaTime;
tMax = registry.tMax;

%Thomas system constants
a = registry.a;
b = registry.b;
alpha = registry.alpha;
rho = registry.rho;
K = registry.K;

if ( registry.useSeed ) rand('seed', ...
registry.seed); end

time = 0;

% Compute the coefficients for the ...
semi-implicit midpoint method
n = 0:(dim-1);
```

```
m = 0:(dim-1);

[mm,nn] = meshgrid( m, n );
kappa = pi^2*(mm.^2 + nn.^2 );

den   =   2 + deltaTime*kappa;
diffU = ( 2 - deltaTime*kappa ) ./ den;
reacU = ( 2 * deltaTime*gamma )./ den;

kappa = kappa*d;
den   =   2 + deltaTime*kappa;
diffV = ( 2 - deltaTime*kappa ) ./ den;
reacV = ( 2 * deltaTime*gamma )./ den;

% DCT weights
w = dim*ones( dim, dim );
w(1,2:end) = w(1,2:end)/sqrt(2);
w(2:end,1) = w(2:end,1)/sqrt(2);
w(2:end,2:end) = w(2:end,2:end)/2;

[u,v] = initialConditions_fun(registry);
uHat = dct2(u)./w;
vHat = dct2(v)./w;

if ( registry.showPlot )
```

```
    axis([0,1, 0, 90] );
    x = linspace(0,1,dim);
    [xx,yy] = meshgrid(x,x);
end

while( time < tMax )

    % Convert from Fourier space
        % to real space
    u = idct2( uHat .* w );
    v = idct2( vHat .* w );

    if ( registry.showPlot )
        subplot(1,2,1);
        pcolor(u), shading interp;
        if ( registry.showTime )
            xlabel( sprintf( 'Time = %d',...
                        time ) );
        end

        subplot(1,2,2);
        surf(xx,yy,u),shading interp;
        drawnow();
    end
```

```
    h = rho * u.*v./( 1 + u + K*u.*u );
    f = a - u - h;
    g = alpha*( b - v ) - h;

    fHat = dct2(f)./w;
    gHat = dct2(g)./w;

    % Update next solution
    uHatNext = diffU'.*uHat + reacU'.*fHat;
    vHatNext = diffV'.*vHat + reacV'.*gHat;

    % Error computation
    uDiff = uHatNext - uHat;
    vDiff = vHatNext - vHat;

    uHat = uHatNext;
    vHat = vHatNext;

    time = time + deltaTime;
end
```

The 2d code was tested to see if the method would converge to the equilibrium solution, given by $(u_0, v_0) \approx (37.738, 25.158)$. For this test, $\gamma = 2$ and $d = 2$. Initial conditions were randomly selected to be within .1 of the homogeneous equilibrium. A dimension of 128 and $\Delta t = .001$ was used. The simulation was stopped once the Euclidean norm of the difference between the homogeneous equilibrium and the approximated solution reached 1×10^{-5}. For the initial conditions selected, the method successfully produced solutions close to the homogeneous equilibrium within the tolerance specified.

Bibliography

Bibliography

[1] Y. A. Abramovich and C. D. Aliprantis. *An invitation to operator Theory*. American Mathematical Society, Providence RI, 2002.

[2] W. Arendt and W. P. Schleich. *Mathematical Analysis of Evolution, Information and Complexity*. Wiley-VCH, Germany, 2009.

[3] G. Bachman, L. Narici, and E. Beckenstein. *Fourier and wavelet analysis*. Springer-Verlag, NewYork, 2000. 413 pp.

[4] P. Bates and F. Chen. Spectral analysis and multidimensional stability of traveling waves for nonlocal Allen-Cahn equation. *J. Math. Anal. Appl.*, 273:45–57, 2001.

[5] P. Bates, F. Chen, and J. Wang. *Global existence and uniqueness of solutions to a nonlocal phase-field system: in P.W. Bates, S.-.N Chow, K. Lu, X. Pan (Eds)*. International Press, Cambridge, MA, 1997. 14-21 pp.

[6] P. Bates, P. Fife, R. Gardner, and C. Jones. The existence of traveling wave solutions of a generalized phase-field model. *SIAM J. Math. Anal.*, 28:60–93, 1997.

[7] J. Billingham. Dynamics of a strongly nonlocal reaction-diffusion population model. *Nonlinearity*, 17:313–346, 2004.

[8] V. Capasso and L. Maddalena. Convergence to equilibrium states for a reaction-diffusion system modeling the spatial spread of a class of bacterial and viral diseases. *Journal of Mathematical Biology*, 13:173–184, 1981.

[9] V. Castets, J. Boissonade, and P. D. Kepper. Experimental evidence of a sustained standing Turing-type nonequilibrium chemical pattern. *Phys. Rev. Lett.*, 64:2953–2956, 1990.

[10] J. W. Cooley and J. Tukey. An algorithm for the machine computation of complex Fourier series. *Mathematics of Computation*, 19(90):297–301, 1965.

[11] C. Cortazar, M. Elgueta, and J. Rossi. Nonlocal diffusion problems that approximate the heat equation with Dirichlet boundary conditions. *Israel Journal of Mathematics*, 170(1):53–60, 2009.

[12] C. Cortazar, M. Elgueta, J. Rossi, and N. Wolanski. How to approximate the heat equation with Neumann boundary conditions by nonlocal diffusion problems. *Archive for Rational Mechanics and Analysis*, 187(1):137–156, 2008.

[13] R. Courant and D. Hilbert. *Methods of Mathematical Physics*. Interscience Publishers, Inc., New York, 1989.

[14] J. P. Desi, E. Sander, and T. Wanner. Complex transient patterns on the disk. *Discrete and Continuous Dynamical Systems*, 15(4):1049–1078, 2006.

[15] D. E. Edmunds and W. D. Evans. *Spectral Theory and Differential Operators*. Oxford University Press, New York, 1987.

[16] K. Engel and R. Nagel. *One-Parameter Semigroups for Linear Evolution Equations*. Springer-Verlag, New York, 2000.

[17] I. R. Epstein, I. B. Berenstein, M. Dolnik, V. K. Vanag, L. Yang, and A. M. Zhabotinsky. Coupled and forced patterns in reaction-diffusion systems. *Phil. Trans. R. Soc A*, 366:397–408, 2008.

[18] R. J. Field and R. M. Noyes. Oscillations in chemical systems. IV. Limit cycle behaviour in a model of a real chemical reaction. *J. Chem. Phys.*, 60:1877–1884, 1974.

[19] B. Fornberg. *A Practical Guide to Pseudospectral Methods*. Cambridge University Press, Cambridge, 1998.

[20] A. Friedman. *Partial Differential Equations of Parabolic Type*. Prentice Hall, Englewood, 1964.

[21] D. Gottlieb and S. Orszag. *Numerical analysis of spectral methods*. SIAM, Philadelphia, 1977.

[22] S. A. Gourley and N. F. Britton. A predator-prey reaction-diffusion system with nonlocal effects. *Journal of Mathematical Biology*, 34(3):297–333, 1996.

[23] G. H. Gunarantne, Q. Ouyang, and H. L. Swinney. Pattern formation in the presence of symmetries. *Phys. Rev. E*, 50:2802–2820, 1994.

[24] T. Hartley. An analysis of phase separation processes for stochastic and nonlocal extensions of the classical phase field model. GMU, 2008.

[25] T. Hartley and T. Wanner. A semi-implicit spectral method for stochastic nonlocal phase-field models. *Discrete and Continuous Dynamical Systems, A*, 25:399–429, 2009.

[26] D. Henry. *Geometric Theory of Semilinear Parabolic Equations*. Springer–Verlag, New York, 1981.

[27] M. Hildebrand, H. Skødt, and K. Showalter. Spatial symmetry breaking in the Belousov-Zhabotinksy reaction with light-induced remote communication. *Phys. Rev. Lett.*, 87(8):1–4, 2001.

[28] A. Hutt. Generalization of the reactin-diffusion, Swift-Hohenberg, and Kuramoto-Sivashinksy equations and effects of finite propagation speeds. *Phys. Rev. E*, 75:026214, 1–8, 2007.

[29] A. Hutt and F. M. Atay. Analysis of nonlocal neural fields for both general and gamma-distributed connectivities. *Physica D*, 203:30–54, 2005.

[30] E. K. Infantis and P. N. Panagopoulos. Limit points of eigenvalues of truncated tridiagonal operators. *J. Comp. and Appl. Math.*, 133:413–422, 2001.

[31] A. Iserles. *A First Course in the Numerical Analysis of Differential Equations*. Cambridge University Press, New York, 1996.

[32] O. Jensen, V. Pannbacker, G. Dewel, and P. Borckmans. Subcritical transitions to turing structures. *Phys. Letters A*, 179:91–96, 1993.

[33] A. Kaminaga, V. Vanag, and I. Epstein. "black spots" in a surfactant-rich belousov-zhabotinsky reaction dispersed in a water-in-oil microemulsion system. *J. of Chem. Phys.*, 122, 2005.

[34] T. Kato. *Perturbation Theory for Linear Operators*. Springer-Verlag, Heidelberg, 1976.

[35] Y. Katznelson. *Introduction to Harmonic Analysis*. Cambridge University Press, United Kingdom, 2004.

[36] S. Kouachi. Existence of global solutions to reaction-diffusion systems with nonhomogeneous boundary condtions via a Lyapunov functional. *Electronic Journal of Differential Equations*, 2002(88):1–13, 2002.

[37] I. Lengyel and I. R. Epstein. Modeling of Turing structures in the chlorite-iodide-malonic acid-starch reaction system. *Science*, 251:650–652, 1991.

[38] I. Lengyel and I. R. Epstein. A chemical approach to designing Turing patterns in reaction-diffusion systems. *Proc. Natl. Acad. Sci., USA*, 89:3977–3979, 1992.

[39] D. Lima, A. D. wit, G. Dewel, and P. Borckmans. Chaotic spatially subharmonic oscillations. *Phys. Rev. E*, 53(2):1305–1308, 1995.

[40] S. Maier-Paape and T. Wanner. Spinodal decomposition of the Cahn-Hilliard equation in higher dimensions. part I: probability and wavelength estimate. *Comm. Math. Phys.*, 195(2):435–464, 1998.

[41] S. Maier-Paape and T. Wanner. Spinodal decomposition for the Cahn-Hilliard equations in higher dimensions: nonlinear dynamics. *Arch. Rational Mech. Anal.*, 151(3): 187–219, 2000.

[42] A. S. Mikhailov and K. Showalter. Control of waves, patterns and turbulence in chemical systems. *Physics Reports*, pages 79–194, 2006.

[43] A. P. Munuzuri, M. Dolnik, A. M. Zhabotinsky, and I. R. Epstein. Control of the chlorine dioxide-iodine-malonic acid oscillating reaction by illumination. *J. Am. Chem. Soc*, 121(35):8065–8069, 1999.

[44] J. Murray. A prepattern formation mechanism for animal coat markings. *Journal of Theoretical Biology*, 88:161–199, 1981.

[45] J. D. Murray. *Mathematical Biology, Vol. I, An Introduction*. Springer–Verlag, New York, third edition, 1993.

[46] Q. Ouyang and H. Swinney. Transition from a uniform state to hexagonal and striped turing patterns. *Nature*, 352:610–612, 1991.

[47] A. Pazy. *Semigroups of Linear Operators and Applications to Partial Differential Equations. Applied Mathematical Sciences*, volume 44. Springer–Verlag, New York, 1983.

[48] D. Pelinovsky and M. Grasselli. *Numerical Mathematics*. Jones and Bartlett Publishers, Sudbury, MA, first edition, 2008.

[49] J.-J. Perraud, A. D. Wit, E. dulos, P. D. Kepper, G. Dewel, and P. Borckmans. One-dimensional spirals: novel asynchronous chemical wave sources. *Phys. Rev. Lett.*, 71 (8):1272–1274, 1992.

[50] V. Petrov, S. Metens, P. Borckmans, G. Dewel, and K. Showalter. Tracking unstable Turing patterns through mixed-mode spatiotemporal chaos. *Phys. Rev. Lett.*, 75(15): 2895–2898, 1995.

[51] G. Rábai and K. M. Kovács. Photoinduced reaction between chlorine dioxide and iodine in acidic aqueous solutioin. *J. Phys. Chem. A*, 105:6167–6170, 2001.

[52] M. Renardy and R. C. Rogers. *An Introduction to Partial Differential Equations*. Springer–Verlag, New York, second edition, 2004.

[53] E. Sander and R. Tatum. Pattern formation in a mixed local and nonlocal reaction-diffusion system. *In Preparation*, 2010.

[54] E. Sander and T. Wanner. Unexpectedly linear behavior for the Cahn-Hilliard equation. *SIAM Journal of Applied Mathematics*, 60(6):925–948, 2000.

[55] E. Sander and T. Wanner. Pattern formation in a nonlinear model for animal coats. *Journal of Differential Equations*, 191:143–174, 2003.

[56] E. M. Stein and R. Shakarchi. *Fourier Analysis: An Introduction*. Princeton University Press, Princeton, New Jersey, first edition, 2003.

[57] R. Temam. *Infinite-Dimensional Dynamical Systems in Mechanics and Physics*. Springer-Verlag, New York, second edition, 1997.

[58] L. N. Trefethen. *Spectral Methods in Matlab*. SIAM, Philadelphia, first edition, 2000.

[59] A. Turing. The chemical basis of morphogenesis. *Philosophical Transactions of the Royal Society of London. Series B, Biological Sciences*, 237:37–72, 1952.

[60] V. K. Vanag and I. R. Epstein. Pattern formation in a tunable reaction-diffusion medium: the BZ reaction in an aerosol OT microemulsion. *Phys. Rev. Lett.*, 87:1–4, 2001.

[61] T. Wanner. Maximum norms of random sums and transient pattern formation. *Transactions of the American Mathematical Society*, 356(6):2251–2279, 2004.

[62] D. J. Wollkind and L. E. Stephenson. Chemical Turing pattern formation analyses: comparison of theory with experiment. *SIAM J. Appl. Math*, 61(2):387–431, 2000.

[63] D. Xu and X. Zhao. Asymptotic speed of spread and traveling waves for a nonlocal epidemic model. *Discrete and Continuous Dynamical Systems-Series B*, 5(4):1043–1056, 2005.

Curriculum Vitae

Richard Tatum earned his bachelor of arts degree in Mathematic from Albany State University in 1996. Soon after, he attended the University of Georgia whereupon he received is masters of applied mathematical sciences degree in 1999. Since then, he has worked at the Naval Surface Warfare Center performing mostly computer science tasks. Upon completing his doctoral degree, he plans to continue working at the Naval Surface Warfare Center performing more research oriented tasks related to the field of computational mathematics.